N$_2$ Splitting and Functionalization in the Coordination Sphere of Rhenium

Dissertation

Zur Erlangung des mathematisch-naturwissenschaftlichen Doktorgrades

"DOCTOR RERUM NATURALIUM"

der Georg-August-Universität Göttingen

im Promotionsprogramm der Georg-August University School of Science (GAUSS)

vorgelegt von

M. Sc. Isabel Klopsch

aus Erlangen

Göttingen, 2016

Betreuungsausschuss

PROF. DR. SVEN SCHNEIDER,

PROF. DR. FRANC MEYER,

Institut für Anorganische Chemie der Georg-August-Universität-Göttingen.

Mitglieder der Prüfungskommission

Referent:

PROF. DR. SVEN SCHNEIDER

Co-Referent:

PROF. DR. FRANC MEYER

Weitere Mitglieder der Prüfungskommission:

DR. INKE SIEWERT

PROF. DR. MANUEL ALCARAZO

PROF. DR. THOMAS WAITZ

JUN.-PROF. DR. SELVAN DEMIR

Tag der mündlichen Prüfung: 16.12.2016

A great time.

This thesis originated in the time between January 2013 and October 2016 at the Institute for Inorganic Chemistry of the Georg August Universität Göttingen.

I am deeply indebted to my supervisor

Prof. Dr. Sven Schneider

Thank you for offering me this fascinating research project, for your help, continual support and motivation also in hard times, for your trust in me and my skills, the many opportunities to meet researchers on conferences all over the world, the very good research equipment and the many inspiring discussions.

I also want to express my gratitude to

Prof. Dr. Franc Meyer

For taking the part of my second supervisor and being referee for my thesis.

Content

I   Introduction

Parts of this chapter were submitted as a review article for publication in "**Topics in Organometallic Chemistry**" of the *Springer* publishing company.

1 Nitrogenase, Haber Bosch and heterogeneous N_2-Splitting

Nitrogen is next to oxygen, hydrogen and carbon one of the main elements found in organic compounds. For thousands of years, there was basically only one way to convert the relatively inert atmospheric N_2, which constitutes about 80% in air, into organic molecules. Certain microbial organisms are able to transform N_2 into ammonia via the enzyme nitrogenase. The most active form of this enzyme, the Fe-Mo nitrogenase has been intensively studied and the active site (FeMo-co) for N_2 fixation was structurally characterized in 1992,[1] as a cluster of seven iron and one molybdenum atom bridged by ten sulfurs. In the center, one light atom was found (C, N or O) [2] whose identity was revealed as interstitial carbide not before 2011.[3,4] There exist two proposed mechanisms for N_2 reduction by nitrogenase: The alternating pathway, entailing subsequent protonation and reduction of both nitrogen atoms until the N-N bond is split and the distal pathway, comprising first full reduction and protonation of the β-nitrogen to yield NH_3 and an intermediate metal nitride M≡N.[5,6]

$$N_2 \ + \ 6\,e^- \ + \ 6\,H^+ \ \xrightarrow{\text{[cat]}} \ 2\,NH_3$$
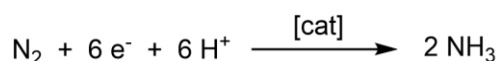
As the world´s population was growing, the interest in synthetic nitrogen fixation for production of artificial fertilizers led to the development of one of the most important technical applications. In 1910, *Fritz Haber* discovered a synthesis for NH_3 out of its elements[7], which was brought on an industrial scale by *Carl Bosch* only a few years later and which is now called the *Haber-Bosch* process.[8]

$$N_2 \ + \ 3\,H_2 \ \xrightarrow{\text{[cat]}} \ 2\,NH_3$$
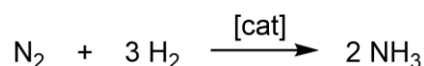
Magnetite Fe_3O_4 with additives of aluminum, potassium and calcium oxides is commonly used as heterogeneous catalyst in this reaction. The accepted mechanism proceeds over initial dissociative chemisorption of N_2 on the catalyst surface into nitrides, which also represents the rate limiting step of the reaction. These surface bound nitrides react with adsorbed H atoms to form stepwise three N-H bonds and release ammonia. As chemisorption of N_2 is very slow, high temperatures and

pressures (300-500°C, 200-300 bar) are needed in this process to obtain good yields, although the actual transformation of N_2 to NH_3 is exothermic.[9] The tremendous demand of NH_3 for the agricultural and chemical industry, about 200 million tons are produced annually, as well as the harsh reaction conditions lead to a global energy consumption of about 1-3%. Besides, the process is responsible for 1.6% of the global CO_2 emissions, especially attributed to the steam reforming for H_2 production.[10] Alternative nitrogen fixation systems are therefore of high interest. Especially electrochemical approaches are intensively studied, but suffer from comparatively low selectivities (H_2 evolution) and energy efficiency.[9,10]

About 20% of ammonia produced by the *Haber-Bosch* process is converted into organic molecules including amino acids, nitriles, amides, and ureas.[11,12] Another approach in N_2 chemistry is trying to circumvent NH_3 (and therefore H_2 production) but directly produce these molecules by nitrogen functionalization in homogenous systems. Examples for such reaction are still scarce though.[13,14]

The functionalization of N_2 thus represents a major challenge for today´s chemistry. This work will focus on initial N_2 cleavage in homogenous systems in analogy to the *Haber-Bosch* process in order to transform nitrogen in chemically and biologically more valuable compounds.

2   The beginnings of molecular N_2 chemistry

Vol´pin and *Shur* were the first to study nitrogen fixation with transition metals under mild conditions in the mid 1960s.[15] Inspired by the nitrogenase, which is fixing dinitrogen rapidly under ambient conditions under participation of transition metals - even though the characteristics of the active site and its mode of action were completely unclear to that time - the authors stated, activation of N_2 may be possible due to coordination of dinitrogen to a metal center. π-Transition metal complexes with olefins or acetylene were known, so in the presence of a coordinatively unsaturated metal complex, also complexation by N_2 was thought to be possible. To test their assumption, they reacted metal halide salts ($TiCl_4$, $FeCl_3$, WCl_6 and $MoCl_5$) with hydrogen delivering reducing agents such as $LiAlH_4$, grignard reagents, lithium or aluminum alkyls under N_2 pressure (150 atm) and observed ammonia formation in

9-25% yield after workup with dilute acids. Yields of 70% are reported even under atmospheric N_2 pressure for the reaction of Cp_2TiCl_2 (Cp = cyclopentadienyl) with ethylmagnesium bromide, illustrating the huge influence of the ligand sphere. However, these systems remain ill-defined and no intermediate could be structurally characterized. [16–18]

The first isolated transition metal complex containing coordinated N_2 was reported in 1965 by *Allen* and *Senoff* (Figure 1) and stimulated the discovery of hundreds of other dinitrogen complexes.[19] Usually the coordinated dinitrogen is not bound very strongly to the metal center and is easily replaced by several other ligands. This is why the discoverers of the first N_2 complex brought into question whether such N_2 complexes even play a part
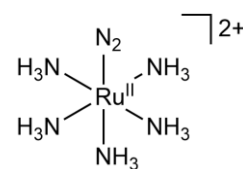
Figure 1: First isolated N2-complex.

in the enzymatic nitrogen fixation observed for the nitrogenase.[20,21] Hope sparked again, when the first successful functionalization of N_2 with a well-defined metal complex was carried out by the group of *Chatt* in 1972. Protonation of *trans*-$[M(N_2)_2(dppe)_2]$ (M = Mo or W, dppe = $Ph_2PCH_2CH_2PPh_2$) with hydrochloric acid yields $[MX_2(N_2H_2)(dppe)_2]$, where one N_2 ligand is reduced to N_2H_2.[22] Additionally, *Chatt* observed the first nitrogen-carbon bond formation with N_2 derived nitrogen by addition of acyl chlorides to N_2 complexes in which however the N-N bond in the resulting M(Cl)(-N=N-COR) complex is still intact.[23,24] Stoichiometric conversion of coordinated N_2 into ammonia and/or hydrazine under mild reaction conditions could be accomplished in molybdenum and tungsten based complexes bearing phosphines as ligands. This reaction has been intensively studied and led to the formulation of the so called "*Chatt cycle*" for a proposed catalytic nitrogen fixation reaction (Scheme 1).[25–30] However, it took more than 20 years for the development of a defined homogenous and well-characterized catalytic system for N_2 reduction to ammonia.

Scheme 1: Chatt cycle for catalytic NH3 production.

3   Catalytic systems for ammonia formation

In 2003, the group of *Schrock* reported the first homogenous catalyst, which fulfilled the whole six electron - six proton reduction of N_2 to NH_3 (Scheme 2).[31] The triamidoamine Mo complex coordinates N_2 and cleaves the NN bond upon alternating steps of protonation and reduction, similar to the *Chatt cycle*. Decamethylchromocene (CrCp*$_2$) acts as reducing agent together with lutidinium tetrakis[3,5-bis(trifluoromethyl)phenylborate] ([LutH]Bar$^F_4$) as proton source. The system is able to generate 8 equivalents of ammonia based on the catalyst. An impressive number of

intermediates in the catalytic cycle has been isolated and characterized, giving detailed insights into the mechanism of the catalytic nitrogen fixation, which is also supported by theoretical investigations.[30–35] In contrast to the *Chatt cycle*, where Mo(0) to Mo(IV) oxidation states are assumed, in the *Schrock cycle* the physiologically more relevant oxidation states Mo(III) to Mo(VI) are passed through. This is also related to the enzyme nitrogenase, where a similar mechanism is proposed for nitrogen fixation.

Scheme 2: Schrock´s catalyst and reaction conditions for NH$_3$ production.

In 2011, the group of *Nishibayashi* published a homogenous catalyst, which initially evolved 23 equivalents of ammonia (Scheme 3).[36,37] The dinitrogen bridged dimolybdenum complex with PNP´-pincer ligand (PNP´ = 2,6-bis(di-*tert*-butylphosphinomethyl)pyridine] is reduced with cobaltocene as reducing agent and lutidinium triflate ([LutH]OTf) as proton source. Modifications of the pincer ligand strongly affected the catalytic reactivity of the complex.
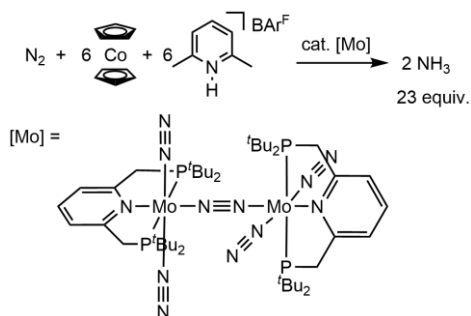
Scheme 3: Nishibayashi´s catalyst and reactions conditions for NH$_3$ production.

Smaller substituents on the PNP ligand gave only an about stoichiometric amount of NH_3. Furthermore, electron donating groups in the pyridyl ring were found to facilitate the most difficult step according to DFT calculations, the first protonation of N_2 to a -NNH unit.[38] The proposed mechanism does not involve the fragmentation of the molybdenum dimer into monomers as it has been suggested formerly.[39,40] Instead, the μ-N_2 bridged dimolybdenum core is believed to play an important role. Similar to the *Schrock cycle*, the terminal nitrogen is then reduced and protonated to

release one molecule of ammonia under formation of a terminal nitrido complex. Subsequent protonation and reduction then converts the nitrido moiety into the second equivalent of ammonia.[41,42] In an attempt to enhance the stability of the catalyst towards protonation, a new triphosphine PPP pincer ligand (PPP = bis(di-*tert*-butyl-phosphinoethyl)phenylphosphine) has been developed recently.[43] Unexpectedly, already the starting compound [(PPP)MoCl$_3$] showed catalytic activity for nitrogen fixation, which is not the case in the PNP system. The cationic nitrido complex [(PPP)Mo(N)Cl]$^+$ generated under improved reaction conditions 63 equivalents of ammonia, the so far highest catalytic activity ever observed for a defined homogenous catalyst system. A similar mechanism as for the PNP system is proposed, but no intermediates could be observed so far.[43]

Besides molybdenum, iron is one of the most studied transition metals related to nitrogen fixation. In the Haber Bosch process as well as in the nitrogenase, iron centers are involved in the NN splitting process. First attempts to nitrogen fixation with iron reach back into the 1960s, when *Vol´pin* and *Shur*, reported ammonia formation in 9% yield.[15] The first well-defined catalytic system for nitrogen fixation using iron has been developed by the group of *Peters* in 2013 (Scheme 4).[44] The complex [(TPB)Fe]BAr$^F_4$ (TPB = tris[2-(di-*iso*-propyl-phosphanyl)phenyl]borane) can be reduced with excess Na/Hg and crown-ether under N$_2$ atmosphere to the iron(-1) compound [Na(12-C-4)$_2$][(TPB)Fe(N$_2$)]. Both complexes turned out to be catalytically active, with the latter achieving slightly higher turn overs. Catalysis experiments are performed by sequential addition of an excess amount of HBAr$^F_4$ as proton source and an excess amount of KC$_8$ as reductant to the catalyst solution at -78°C and generated 6.2 and 8.5 equivalents of NH$_3$, respectively, based on the aforementioned amount of catalyst. The major side reaction is formation of H$_2$ from the proton source under the highly reducing conditions. Dihydrogen acts as catalyst poison, as it reacts with neutral [(TPB)Fe(N$_2$)] to the adduct [(TPB)(μ-H)Fe(N$_2$)(H)], which is only little active in nitrogen fixation.[44,45]. Although some other Fe systems have been found to catalyze the reduction of N$_2$ into ammonia, *Peters´* complex is still the most active.[37,46]
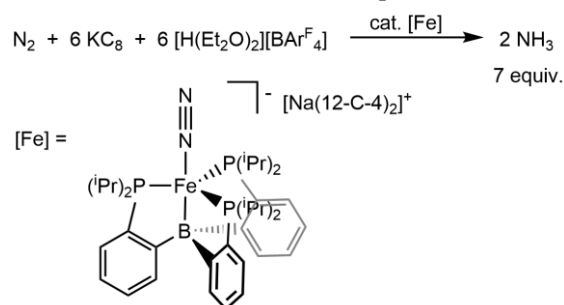
Scheme 4: Peter´s catalyst and reaction conditions for NH$_3$ production.

All catalytic systems until now have in common that they rely on strong reducing agents and acids as proton source.

4 Towards N-N-bond cleavage: Bonding in N_2-complexes

4.1 General considerations

The lacking dipole moment and the high bond dissociation energy (941 kJ mol^{-1}) account for dinitrogen as a kinetically and thermodynamically very stable molecule. The reason for its exceptional stability lies in the effective overlap of the s- and p-orbitals of the two nitrogen atoms to form very low lying, completely filled σ- and π-molecular orbitals. The energy gap from the HOMO (highest occupied molecular orbital) to the LUMO (lowest unoccupied molecular orbital) is substantial, leading to both difficult reduction and oxidation. Hence, the ionization energy of N_2 is approximately the same as for argon (15.58 eV and 15.75 eV respectively). In addition, also the proton and electron affinities are low (5.1 eV and -1.9 eV respectively).[21,47,48] Considering the cleavage of the NN bond, dissociation of the first of the three bonds in dinitrogen is the most difficult, requiring about half of the total triple bond energy (410 kJ mol^{-1}) and resulting in a high kinetic barrier. This is in contrast to acetylene for example, which first bond is a lot more easy to brake (222 kJ mol^{-1}), although the total triple bond energy (962 kJ mol^{-1}) is even stronger than for N_2.[49]

The way N_2 is bound to a metal center strongly depends on the metal, its oxidation state and the ligand environment. In principle, there have been observed 4 coordination modes: (1) mononuclear end-on, (2) Dinuclear end-on, (3) Dinuclear side-on and (4) Dinuclear side-on-end-on (Figure 2).
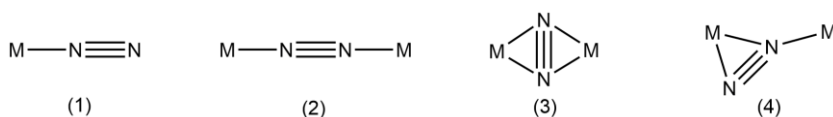
Figure 2: Different bonding motifs in N_2 complexes.

The different coordination modes generally show a different kind of activation of the N-N bond. The term "activation" herein describes the degree of elongation of the N-N bond length combined with the reduction of its stretching frequency compared to free N_2 (1.10 Å and 2331 cm^{-1}).[50,51] In general, activation in mononuclear end-on N_2 complexes (η^1-N_2) turned out to be rather low. The vast majority of such metal complexes, especially for the later transition metals, belongs to this type. The metal dinitrogen bond can be described as a combination of overlap of the filled σ-orbitals

of dinitrogen with suitably empty metal d-orbitals forming a σ-bond and π-backbonding from filled metal d-orbitals into empty π*-orbitals of dinitrogen (Figure 3). In consequence, the N-N bond becomes weaker upon coordination to a metal center and activation increases similar to isoelectronic CO complexes. But compared to the latter, N_2 is both a much poorer σ-donor and π-acceptor, mainly because the energy of HOMO and LUMO orbitals usually simply does not match very well the energy of the metal´s d-orbitals.[21] These reduced interactions decrease the stability of N_2 complexes and lead to the main reaction observed for this kind of complexes: dissociation and replacement of the N_2 ligand.
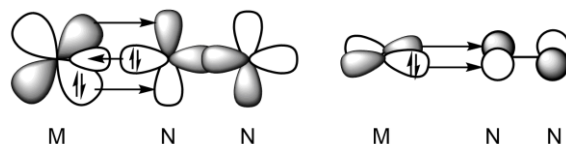
Figure 3: End-on metal-N_2 bonding: σ-bonding from N_2 to the metal and two π-bonding interactions from the metal to N_2.

In dinuclear complexes, where the N_2 moiety is bridging two metal centers, activation can become higher. As π-backbonding from the metal to dinitrogen accounts mostly for increased M-N strength, the metal must be in a low oxidation state and possess a rather high electron density. Highly reducing early transition metals can donate their electrons more easily into the empty π*-orbitals of N_2, resulting in stronger activation. Concerning, the splitting of the NN-bond forming nitrides, the metal center must be capable of donating enough electrons to provide all 6 electrons required for complete nitrogen reduction. An initial low oxidation state of the metal is therefore beneficial and the use of multiple metal centers, where the electron count is distributed on all metals, seems reasonable. As dinuclear coordination is also essential for the metal mediated cleavage of the NN-bond into nitrido complexes, bonding in these complexes will therefore be discussed in more detail in the following sections.

4.2 End-on bridging N_2

N_2 end-on bridging, M-(μ-η^1-η^1-N_2)-M, is the most frequently observed coordination mode for dinuclear N_2 complexes. The M-N≡N-M unit is more or less linear to allow for efficient orbital overlap. In general, N_2 gets activated upon η^1-coordination to the first metal center, so electron density in the π^* orbitals increases, rendering the coordinated molecule a better base for another metal center. Thermodynamics also play a role, as formation of strong multiple M-N-bonds is facilitated by further reduction from the other metal, creating electron delocalization over the whole M-N-N-M unit.[52] In principle, such a complex can be represented in three different resonance structures, with differing modes of activation: (1) N_2 is only coordinatively bound to both metals centers, showing only minor activation. (2) Formal two electron reduction of N_2 to a diazene unit $(N_2)^{2-}$ and (3) formation of a hydrazine derivative $(N_2)^{4-}$, if the metals are capable of donating two electrons each to the N_2 moiety, leading to simultaneous cleavage of both π-bonds of N_2 (Figure 4). Following this approach, further reduction would then lead to N-N-bond cleavage and form metal nitrides.[53]
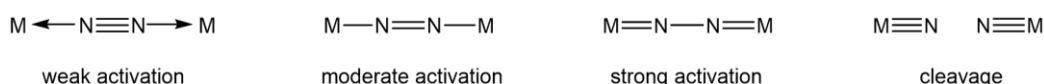
Figure 4: Different types of N_2 activation in end-on coordinated dinuclear complexes.

In this very simplistic view, one might think, the more electrons, the more the NN bond is weakened and the easier N_2 is split. This expectation is however only in parts true. For example, the complex $[(NH_3)_5Ru-N_2-Ru(NH_3)_5]^{4+}$ with a d^6 electron configuration for both metal centers, shows only little activation of the N_2 unit (Figure 5) and only minor differences compared to the mononuclear analogue $[(NH_3)_5RuN_2]^{2+}$, although two metals are involved in bonding. Moreover, a rather strong activation is observed for complex $[(PMe_2Ph)_4ClRe-N_2-MoCl_4(OMe)]$ with a d^6 and d^1 electron configuration for Re and Mo respectively.
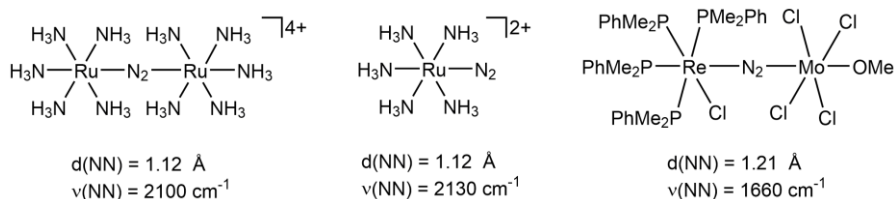
Figure 5: Different degree of activation in N_2 complexes.[21]

This observation can be rationalized by considering the molecular orbitals of a M-N-N-M moiety, as first stated by Gray[54] and Chatt[55] and reviewed by Sellmann.[21] In a qualitative scheme, four center molecular orbitals are obtained by linear combination

9
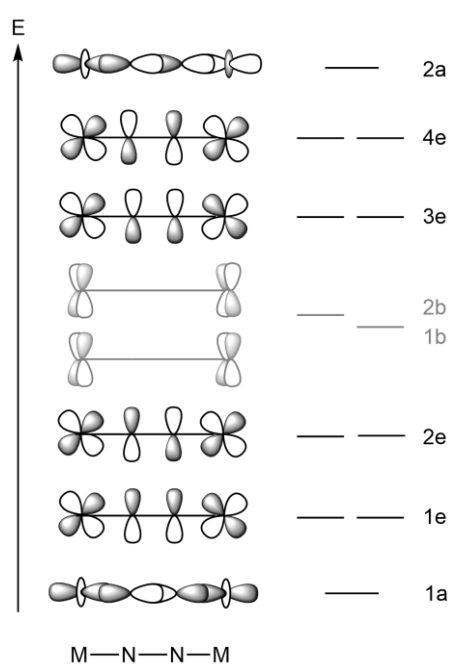
Figure 6: MO scheme for end-on coordinated dinuclear N_2 complexes.

of the metal's d-orbitals with the proper p-orbitals of dinitrogen (Figure 6). The z-axis is determined along the σ-bond (1a), giving rise to four sets of π-orbitals, whose energy is increasing with the number of nodal planes (1e – 4e). For each linear combination, there exist two degenerate molecular orbitals, one for the Md_{xz}-Np_x-Np_x-Md_{xz} and one for the Md_{yz}-Np_y-Np_y-Md_{yz} orbitals (90° rotated). Additionally, in fourfold geometry, there are two δ-orbitals, formed from the Md_{xy}-orbitals, which are essentially non-bonding (1b and 2b). In a threefold geometry, these orbitals are not available due to interactions with the ancillary ligands. The strength of M-N and N-N is determined by the occupancy of all of these molecular orbitals. Filling in 6-electrons from N_2 leads to full occupation of the 1a σ- and the 1e π-level, which are all bonding. Further electrons occupy the 2e level, which weakens the N-N bond. Occupation of the 1b and 2b levels, if available, does not contribute significantly to N_2 binding. The 12 electrons from $[(NH_3)_5Ru$-N_2-$Ru(NH_3)_5]^{4+}$ however fill the orbitals until the 3e level, which is N-N-bonding again, producing in total three N-N-bonding orbitals (5 bonding vs. 2 antibonding MOs). This reflects the minor difference in N_2 activation compared to the mononuclear complex $[(NH_3)_5RuN_2]^{2+}$. With electron poorer metals (3e level vacant) N_2 bond activation increases, as it is in $[(PMe_2Ph)_4ClRe$-N_2-$MoCl_4(OMe)]$, which only has 7 d-electrons. Going further to the left in the periodic table, activation increases, as even δ-orbitals become empty. The group of *Gambarotta* synthesized the titanium dimer $[\{(Me_3Si)_2NTiCl(TMEDA)\}_2(\mu$-$\eta^1$-$\eta^1$-$N_2)]$, which shows strong N_2 activation, in agreement with a formal 4 electron reduction to a $(N_2)^{4-}$ unit (Figure 7).[56–58] However, factors influencing the activation of N_2 are not only derived from the electron count in this simplified molecular orbital scheme. The complex $[\{(Cp^*Ti(\eta^6$-$C_5H_4CR_2)\}_2(\mu$-η^1-η^1-$N_2)]$ (R = *p*-tolyl) shows a considerable smaller activation, although for titanium(I) according to the MO scheme δ-orbitals should be occupied (Figure 7).[59] DFT calculations on these complexes reveal a significant influence of the ligand sphere.[57] Electrons of titanium are involved in π-backbonding to the fulvene ligands, preventing them from interactions with the π*-orbitals of N_2. Although titanium(II) is less electron rich, the ligand sphere allows more electrons to be available for N_2 reduction. Accordingly, the activation of N_2 can also be correlated to the donor/acceptor properties of the ligand environment.

d(NN) = 1.29 Å
ν(NN) = 1284 cm^{-1}

d(NN) = 1.16 Å
ν(NN) = 1749 cm^{-1} (R = *p*-Tol)
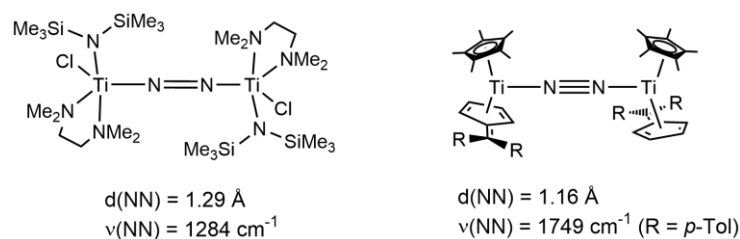
Figure 7: Ti(II) (left) complex exhibiting strong N_2 activation and Ti(I) complexes with significantly smaller activation.

Another example for the ligand influence on the orbital disposition in dinuclear complexes is very well illustrated in the recent work of *Chirik*.[60] His group was able to isolate five terpyridine molybdenum dinitrogen complexes [{(^{Ph}Tpy)(PPh$_2$Me)$_2$Mo}$_2$(μ-η^1-η^1-N_2)][BAr$^F_4$]$_n$, which only vary by oxidation state (n = 0, 1, 2, 3, 4) (Scheme 5).[60] The dicationic complex [{(^{Ph}Tpy)(PPh$_2$Me)$_2$Mo}$_2$(μ-η^1-η^1-N_2)][BAr$^F_4$]$_2$ displays parameters in agreement with a [N_2]$^{2-}$ bridge. DFT calculations describe the HOMO as one of the 3e levels. Because of π-interactions of only one of the MOs in one level with the terpyridine ligand, the 3e orbitals are not degenerate any more, resulting in a diamagnetic complex. Additionally, the LUMO is calculated to be mainly ligand centered and NN antibonding in character. Intriguingly, isolation of the oxidized and the doubly oxidized form of the complex, as well as the reduced and the doubly reduced form has been achieved. Oxidation leads to a weakening of the N-N bond as the electron is removed from the N-N bonding 3e orbital. Further oxidation leads to a slightly weaker N-N bond and formation of a compound with electronic triplet ground state. Reduction of the starting complex by one electron leads to a paramagnetic S = ½ compound, where the electron is located mainly on the terpyridine ligand. Even the second electron of further reduction can be stored in the terpyridine ligand, forming neutral, diamagnetic [{(^{Ph}Tpy)(PPh$_2$Me)$_2$Mo}$_2$(μ-η^1-η^1-N_2)]. So the ligand does not only influence N_2 activation, it can also be redox active and store additional reducing equivalents, enabling such a system as promising platform for N_2 reduction.
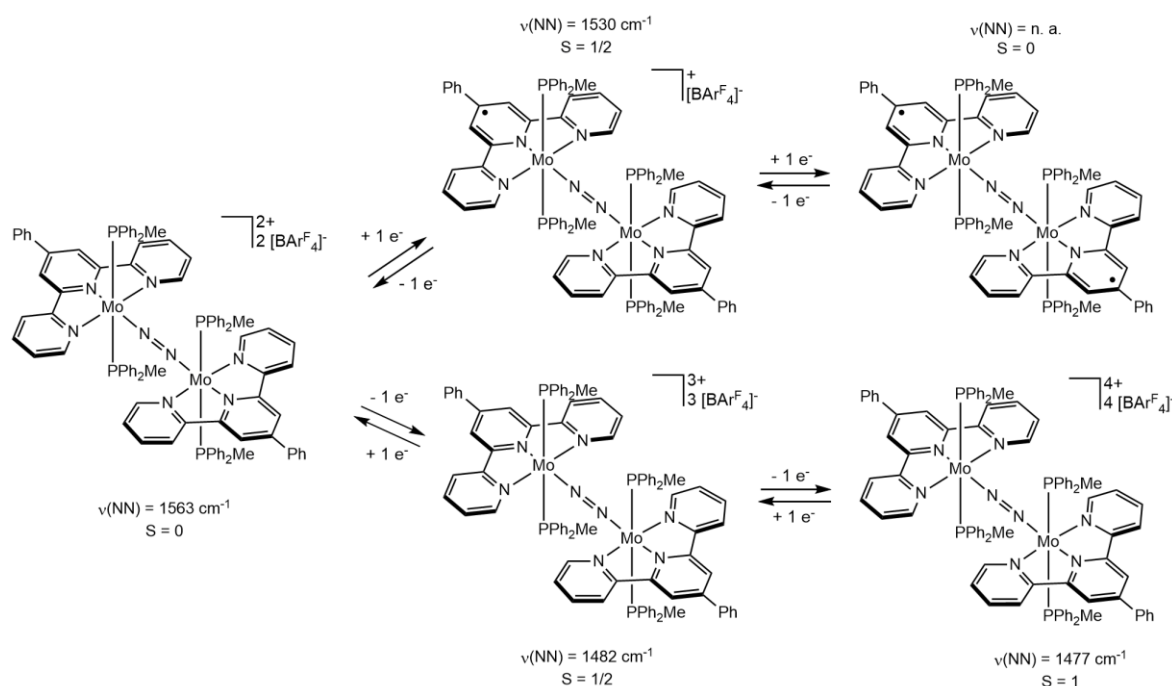
Scheme 5: Transformations of [{(^{Ph}Tpy)(PPh$_2$Me)$_2$Mo}$_2$(μ-η^1-η^1-N$_2$)][BAr$^F_4$]$_n$ (n = 0-4) by one electron redox reactions.

The influence of the metal in dimeric N_2-bridged complexes has been examined by the group of *Sita*, who could isolate and characterize a complete series of isostructural cyclopentadienyl/amidinate complexes (Cp*amM)$_2$(μ-N$_2$) (am = [N(iPr)C(Me)N(iPr)], M = Ti, Zr, Hf, V, Ta, Nb, Mo, W) (Figure 8).[61–63] While steric and electronic environment can be held constant, N_2 activation can be monitored as a function of group and row position of the metal and its formal oxidation state and valence electron count. Whereas for Zr and Hf side-on bridged N_2 complexes could be observed, all other metals showed end-on dinitrogen coordination. NN-bond lengths of all isolated complexes are summarized in Table 1.

*Table 1: N-N bond distances in (Cp*AmM)$_2$(μ-N$_2$) complexes.*

Metal	Coordination mode	d(NN) [Å]	reference
Ti	(μ-η^1-η^1-N$_2$)	1.270(2)	[62]
Zr*	(μ-η^2-η^2-N$_2$)	1.518(2)	[64]
Hf	(μ-η^2-η^2-N$_2$)	1.611(4)	[64]
V	(μ-η^1-η^1-N$_2$)	1.225(2)	[63]
Ta	(μ-η^1-η^1-N$_2$)	1.313(4)	[61]
Nb**	(μ-η^1-η^1-N$_2$)	1.300(3)	[63]
Mo	(μ-η^1-η^1-N$_2$)	1.267(2)	[62]
W	(μ-η^1-η^1-N$_2$)	1.277(8)	[62]

M = Ti, V, Nb, Ta, Mo, W

*Figure 8: Sita´s isostructural (Cp*amM)$_2$(μ-N$_2$) complexes.*

* Exchange of methyl group in aminidate against NMe$_2$.
** Exchange of methyl group in amidinate against phenyl.

The diamagnetic Ti analogue is according to the authors best described as two spin coupled Ti(III,d^1) centers, connected by a $[N_2]^{2-}$ bridge. As Ti possesses a very high fourth ionization potential, further reduction of N_2 is difficult to achieve.[65] Strongest N_2 activation however is observed for the Zr and Hf analogues, where oxidation to formal +IV is less hindered. Ta and Nb dimers show smaller activation, as the reduction potential is lower for these metals. The niobium complex turned out to be kinetically more unstable though and the (μ-η^1-η^1-N_2)-bridged complex could only be obtained by employing the more bulky phenyl substituent within the amidinate ligand. Least activation is observed for the thermally remarkably robust vanadium complex, comprising two antiferromagnetically coupled V(II, d^3) centers. Formal oxidation state assignment is supported by the fact that N_2 is easily displaced by strong π-acceptor ligands, yielding neutral CpamV^{II}(CNR)$_2$. The diamagnetic group 6 analogues are again in agreement with decreasing reduction potential and show a slightly reduced activation of the bridged N_2, compared to Nb and Ta. In contrast to the latter complexes however, group 6 compounds exhibit easy displacement of the N_2 ligand by strong π-acceptors such as CO or isonitriles, giving rise to a M(II, d^4) formulation.

These results imply that a simple consideration of the electron count in the MO scheme in Figure 6, is only half of the truth. The relative energies of the orbitals, their spin population and the ligand environment are influencing the MOs and are therefore rendering the picture of N_2 complexes clearly more complicated.

4.3   Side-on bridging N_2

The side-on coordination mode is not as usual as the end-on one in dinuclear N_2 complexes.[50,66,67] The earliest mention of a such a complex was in 1970, when isotopically labeled Ru complexes [(NH$_3$)$_5$Ru(^{14}N^{15}N)]Br$_2$ and [(NH$_3$)$_5$Ru(^{15}N^{14}N)]Br$_2$ were shown to interconvert over time.[68] The rates of isomerization turned out to be faster than simple dissociation and recoordination of N_2, suggesting an intramolecular rearrangement through side-on coordination. The first structurally characterized side-on N_2 complex was reported in 1973 for a polynuclear nickel-lithium compound.[69,70] For f-block metals side-on coordination is more common, since the group of *Evans* characterized the first one in 1988.[71] The (Cp*$_2$Sm)$_2$(μ-η^2-η^2-N_2) complex contains basically no activated N_2, displayed by its short N-N bond length of d(NN) = 1.088(12) Å and the fact, that N_2 is easily lost upon exposure to vacuum. In contrast, also very strong N_2 activation can be observed in side-on

bridging N_2 as illustrated for the complex $([PNP]ZrCl)_2(\mu-\eta^2-\eta^2-N_2)$ ([PNP] = iPr$_2$PCH$_2$SiMe$_2)_2$N), which displays an N-N bond length of d(NN) = 1.548(7) Å in a planar Zr-N_2-Zr array.[72] Today, there exist a number of side-on bound dinitrogen complexes, mostly with early transition metals and f-block elements. However, the end-on coordination mode is certainly the most common.[66] The question that arises now is what makes the difference between these two binding motifs.

To describe the electronic structure in N_2 side-on bridging complexes, considering the molecular orbital scheme as depicted for the end-on bridging mode (Figure 6), is recommended. However, bonding in side-on N_2 complexes is more sophisticated, since N_2 can be lifted out of the M-M plane or the metals can be twisted against each other due to ligand constraints. In a very simplistic picture, there exist a π (and π^*) symmetric MO, having M-N bonding (and antibonding) and N-N antibonding character (Figure 9). These are generated out of d_{yz} orbitals of the metals with one π^* orbital of dinitrogen. Similarly, there are two basically non-bonding MO combinations out of metal orbitals d_{xz}. But instead of a second π-bond created in the end-on coordination mode, only a δ-bond (and δ^*-bond) with M-N bonding (and M-N antibonding) and N-N antibonding character between the d_{xy} and the second π^* orbital of N_2 can be formed, resulting in a somehow weaker stabilization. Furthermore, the N-N σ-bond is non-bonding (σ_N), as well as the N-N bonding π-orbital formed of p_x orbitals of N_2. In principle, the p_z orbitals for the N-N bonding combination can form a bonding interaction with the respective metal orbitals, but calculations consider these π-donor interactions to be quite small, hence they are neglected in the MO scheme.[73] Compared to end-on bridged N_2 complexes, involving two M-N π-bonds, in the side-on bridging mode, there is only one π- and one δ-bond. As the latter should have less orbital overlap, it should be less stabilized. Hence, the end-on bridging mode usually is energetically preferred over the side-on mode.[67]

Figure 9: MO scheme for side-on coordinated dinuclear N_2 complexes.

So what is the reason the side-on mode is formed at all? The most obvious hypothesis therefore would be that there is just no appropriate d-orbital at the metal available for a second back-donation to dinitrogen. *Fryzuk* investigated this subject and performed calculations on the zirconium complex {ZrCl[N(SiH$_2$CH$_2$PH$_2$)]}$_2$(μ-η^2-η^2-N$_2$).[67] The analysis revealed strong interactions of the amide in the ligand backbone with d-orbitals of the metal, leaving only two d-orbitals for bonding to the dinitrogen ligand. Actually, the amide donates its electrons into the exact orbital necessary for the second π-bonding to dinitrogen, enabling only the side-on coordination mode. Since there were also interactions with the chloride computed, its influence on the coordination mode was investigated chemically by exchange against a Cp ligand and resulted in isolation of the end-on bridging complex [(PNP)ZrCp]$_2$(μ-η^1-η^1-N$_2$) (Scheme 6).[67] This can be rationalized by a modification of the available d-orbitals. A π-orbital of the Cp ligand now overlaps with the d-orbital, which would have been used for δ-bonding in the side-on N$_2$ complex. Since side-on bonding is inhibited, end-on bonding is engaged and the free electron pair of the amide is "pushed back". This assumption is supported by the unusually long Zr-N$_{amide}$ distances of 2.306(3) Å and 2.303(3) Å for the Zr moieties in the end-on complex, which are only slightly shorter than in neutral amine-type Zr(IV) adducts.[74,75]
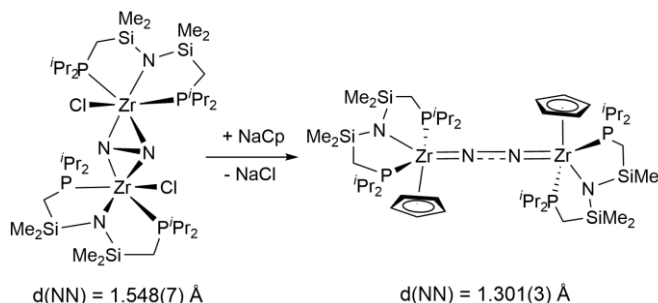
Scheme 6: Transformation of side-on to end-on dinuclear complexes by ligand exchange.

Of course, steric effects also play a role, as the two metal moieties are certainly closer in the side-on mode compared to the end-on one. That already subtle variation in the steric congestion can change the N$_2$ coordination mode has been shown by the group of *Chirik*. The complex [Cp*Zr(η^1-N$_2$)]$_2$(μ-η^1-η^1-N$_2$) was reported in 1974 by the *Bercaw* group.[76] In 2004, *Chirik* could demonstrate the formation of a side-on bridged N$_2$ complex [(η^5-C$_5$Me$_4$H)Zr]$_2$(μ-η^2-η^2-N$_2$), only by alteration of the pentamethyl Cp to tetramethyl Cp ligands (Figure 10).[77] Adding only one methyl group per zirconocene yields again the end-on bridged N$_2$ complex [Cp*(C$_5$Me$_4$H)Zr(η^1-N$_2$)]$_2$(μ-η^1-η^1-N$_2$).[78] Thus, only the steric bulk of one methyl group can make the difference in the N$_2$ coordination mode.[79,80]
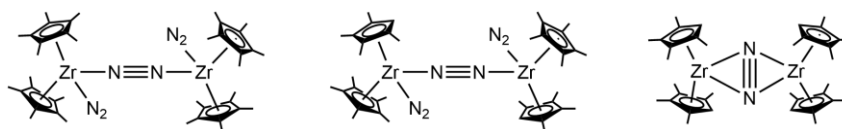
Figure 10: Steric effect on end-on vs side-on N$_2$ binding.

DFT calculations predict the relative intensity of side-on N$_2$ bridged isomers to increase down group 4 in the periodic table.[65] Experimentally, this effect has been

observed for the before mentioned isostructural metal complexes from the group of *Sita* (Table 1). In group 4 complexes of this kind the titanium analogue adopts end-on, whereas the zirconium and hafnium analogues display side-on coordination.[62] As steric interactions can be critical, the covalent radii for the metals were compared. Here, Zr and Hf possess about the same dimension (1.75 Å), Ti on the other hand is significantly smaller (1.60 Å). It is assumed, that only the larger atoms are able to accommodate the more sterically crowded side-on coordination and the smaller analogues, including the later metals like V (1.53 Å), Nb (1.64 Å) or Mo (1.54 Å), can only adopt the end-on bonding motif with this ligand set.

There also exists an intermediate coordination mode for N_2, the side-on end-on coordination. The complex $[(NPN)Ta]_2(\mu\text{-}H_4)$ (NPN = $(Ph)P(CH_2SiMe_2NPh)_2$) was set under an atmosphere of N_2 to generate the complex $[(NPN)Ta]_2(\mu\text{-}H)_2(\mu\text{-}\eta^1\text{-}\eta^2\text{-}N_2)$, exhibiting a side-on coordination of N_2 to one tantalum center and an end-on coordination to the other (Figure 11).[81] As the usual coordination mode for tantalum N_2 complexes is end-on, the authors believe, that the bridging hydride in the complex forces the two metal centers in such a close proximity that an end-on binding motif becomes impossible.[82] The energetic advantage of maintaining the bridging hydrides is believed to prevail over the energy difference to dinuclear end-on coordination.

d(NN) = 1.319(6) Å
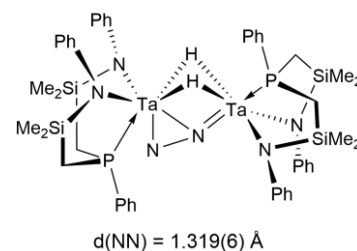
Figure 11: Side-on end-on N_2 bridged tantalum complex.

5   From N$_2$-complexes to N$_2$-splitting

5.1   Dinuclear end-on bridging N$_2$-complexes

<u>The Cummins system</u>

The year 1995 was a milestone in dinitrogen chemistry. For the first time, the complete scission of the N-N triple bond of N$_2$ could be observed proceeding over an N$_2$ bridged dimer into a well-defined terminal nitride. As the group of *Cummins*, tried to recrystallize the sterically demanding triamido molybdenum(III) complex Mo[N(tBu)(Ar)]$_3$ (Ar = 3,5-C$_6$H$_3$Me$_2$) at -35°C under an atmosphere of N$_2$, they observed the formation of a new paramagnetic species.[83] Upon warming to room temperature, the paramagnetism was lost and the formation of a terminal molybdenum(VI) nitride was observed in high yield (76% isolated, Scheme 7). This reaction was not only the first of this kind, it still represents the most intensively studied example of well-defined N$_2$ splitting. Therefore, in the following, factors influencing N$_2$ splitting will be described on the basis of this reaction.
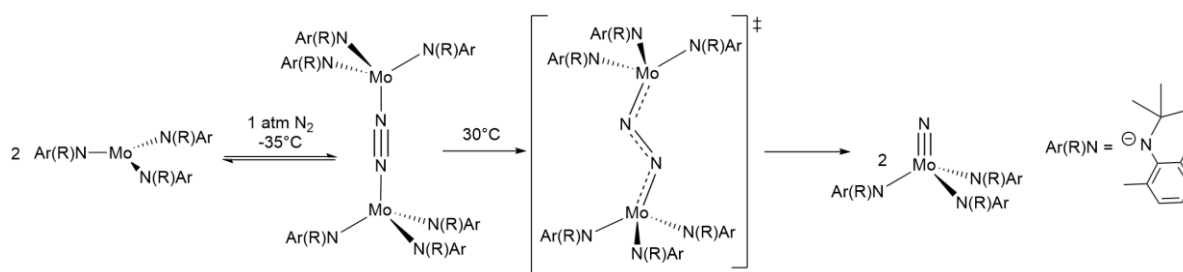
Scheme 7: Cleavage of N$_2$ in terminal nitrides mediated by a triamido molybdenum(III) complex.

After the discovery of the thermally driven N$_2$ cleavage reaction, following work revealed, that the starting compound lies in equilibrium with an end-on bridged, paramagnetic N$_2$ complex {Mo[N(tBu)(Ar)]$_3$}$_2$(μ-η^1-η^1-N$_2$). At room temperature however this equilibrium is shifted far towards the monomeric species.[84] Only minor amounts of nitride could be detected after 12 h in benzene solution and neither the formation of a dimeric species nor a monomeric η^1 terminal N$_2$ complex is observed at room temperature. Regardless, detailed spectroscopic investigations revealed a rather linear MNNM moiety for the dimeric species, which could also be verified by a crystal structure some years later.[85] Depending on the crystallization mode, NN

distances of 1.212(2) or 1.217(2) Å [85] could be found together with a Raman shift of υ(NN) = 1630 cm^{-1} [84], fitting to moderate to strong activation of the coordinated N_2 unit and description as $[N_2]^{2-}$ and formal Mo(IV).[53] Interestingly, also the mono and doubly oxidized forms of the dimer have been isolated, displaying significantly stronger N_2 activation (Figure 12). Nevertheless, only the neutral species is cleaving the N-N bond. This result indicates that N_2 activation itself is not the only factor governing dinitrogen splitting and strong activation does not necessarily lead to N-N cleavage.

d(NN) = 1.212(2) / 1.217(2) Å
ν(NN) = 1630 cm^{-1}
{MNNM}$^{10\pi}$

d(NN) = 1.239(4) Å
ν(NN) = 1503 cm^{-1}
{MNNM}$^{9\pi}$

d(NN) = 1.265(5) Å
ν(NN) = 1349 cm^{-1}
{MNNM}$^{8\pi}$
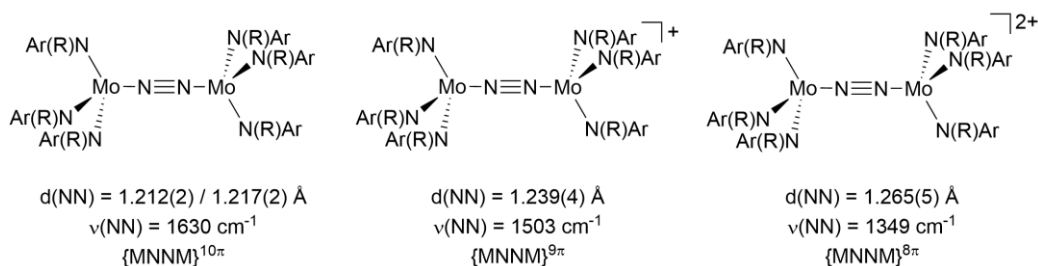
Figure 12: Bond distances, stretching frequencies and number of electron in the MNNM π-system for {Mo[N(tBu)(Ar)]$_3$}$_2$(μ-η^1-η^1-N$_2$)$^{n+}$ (n =0-2).

Electronic structure

The electronic structure of the neutral dimeric complex can again be described by a molecular orbital analysis as in chapter 4.2. In threefold symmetry however, no 1b and 2b δ-bonding MOs are available, because these orbitals are involved in bonding to the ancillary ligands. A $(1e_u)^4(1e_g)^4(2e_u)^2(2e_g)^0$ electronic configuration by description with Mulliken labels and therefore 10π electrons in the MNNM unit, described as {MNNM}$^{10\pi}$, results (Figure 13) and is supported by DFT calculations.[84,85] Furthermore, the total spin of S = 1 is in agreement with SQUID measurements.[85] The HOMO is described by M-N antibonding and N-N bonding character. Oxidizing the compound removes electrons out of this orbital, resulting in a weakened N-N and strengthened M-N bond in accordance with the experimental data ({MNNM}$^{n\pi}$, n = 8, 9).
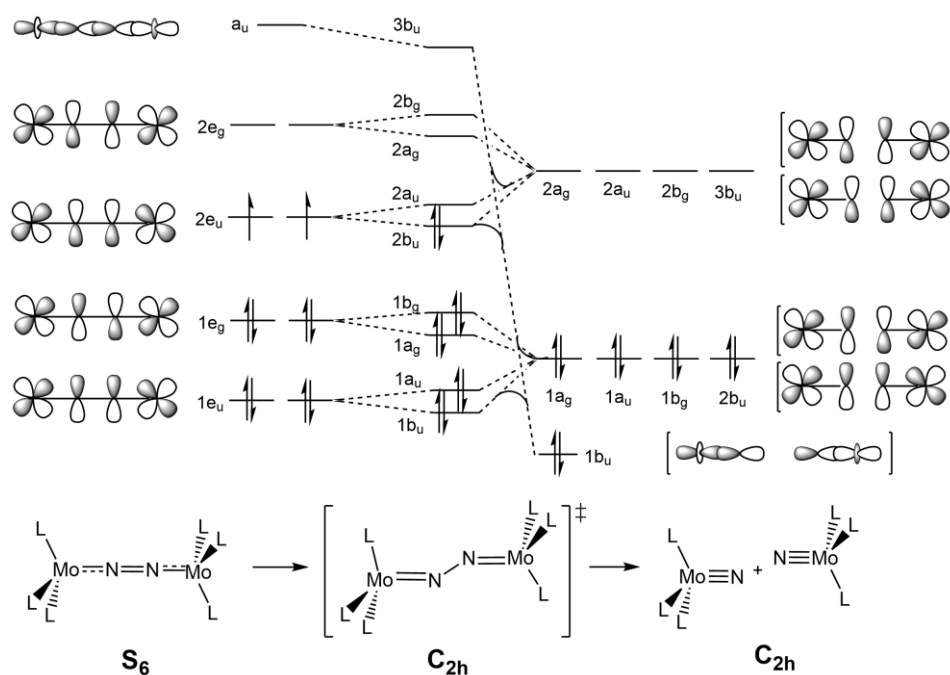
Figure 13: MO scheme for N_2 cleavage in terminal nitrides out of a Mo(III) dinuclear dimer.

Generation of stable closed shell nitrides requires spin flip from the triplet to the singlet state during the splitting process. The mechanism is believed to proceed via a zigzag transition state (TS), incorporating a further reduced N-N single bond, as it has been calculated by *Morokuma* for the hypothetic complex $[Mo(NH_2)_3]_2(\mu-\eta^1-\eta^1-N_2)$.[86] In this transition state, symmetry is reduced leading to degeneracy of the MO e-levels and enabling spin pairing. N-N cleavage out of the linear dimer leads to an excited state and was computed to be energetically unfavorable.

In addition, the dimer accommodates 10 π- and 6 σ-electrons within the MNNM unit. Two nitrido complexes $N\equiv Mo(L)_3$ however require in total 8 π- and 8 σ-electrons. Two electrons must therefore be transferred from π-orbitals in σ-orbitals upon N-N cleavage. In the zigzag TS the doubly occupied $2b_u$ π-orbitals have the appropriate symmetry to be correlated with the energetically higher lying, unoccupied σ-antibonding orbital to form the occupied σ-bonds $1b_u$ in the nitrido complexes. Otherwise, spitting from the linear dimer by simple linear dissociation is symmetry forbidden.[84] Importantly, also the σ-bonding orbital a_u is lowered in energy ($3b_u$) when reaching the TS, thereby favoring mixing of the σ- and π-symmetric orbitals as their energy difference is decreased. The orbital scheme also indicates that a $\{MNNM\}^{10\pi}$ system, is essential in this splitting process. Less electrons cause stronger N_2 activation, but splitting is inhibited because no stable nitrido complexes can be formed. This is supported by the isolated oxidized forms of *Cummins`* dimer, containing $\{MNNM\}^{9\pi}$ and $\{MNNM\}^{8\pi}$ systems and which do not show N-N cleavage. More electrons however would destabilize the dimer by M-N bond degradation associated with an increase of N-N bond strength. The splitting from the dinitrogen

bridged dimer has been computed to be exothermic by about 20 kcal/mol. Driving force is the formation of strong Mo(VI)≡N triple bonds.

Ligand influence

Besides the electronic configuration, also the steric demand of the ligand system plays an important role. On the one hand, ligands must be small enough to allow for dimer formation. For example, Mo[N(R)Ar]$_3$ with large substituents R like adamantyl have been shown to be stable towards dinitrogen, presumably because the steric bulk prevents assembling of two such complexes around one molecule of N$_2$.[87] On the other hand, too small ligands induce different reactions. For example, the dimerization of Mo(NR$_2$)$_3$ (NR$_2$ = NMe$_2$, NMeEt, NEt$_2$) to Mo$_2$(NR$_2$)$_6$ (under N$_2$ atmosphere) is a well-known reaction (Scheme 8) [88] and DFT calculations confirm that the main function of the bulky amido ligand is to offer a free coordination site for N$_2$ binding and prevent dimerization at the same time.[89]
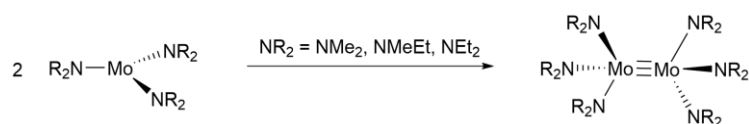
Scheme 8: Dimerization of Mo(NR$_2$)$_3$ with small R-groups.

Besides, also the exchange of the amido ligands against alkoxides ends in the dimerization of the complex without reaction with N$_2$.[90,91] By mixing the respective alkoxy nitrido complexes N≡Mo(OtBu)$_3$ with Mo(N(R)Ar)$_3$, the nitride unit is transferred to the latter, yielding N≡Mo(N(R)Ar)$_3$ and Mo$_2$(OtBu)$_6$ (Scheme 9).[91] This result suggests facile nitrogen atom transfer and stimulated further investigations.[90–92] Adding N≡Mo(OtBu)$_3$ to Mo(N(R)Ar)$_3$ under N$_2$ atmosphere accelerates N$_2$ splitting significantly, yielding both nitrides. Using N≡Mo(NMe$_2$)$_3$ instead of the alkoxynitride resulted in the isolation of the nitrogen bridged compound (Me$_2$N)$_3$Mo(μ-N)Mo[N(R)Ar$_F$]$_3$ (Ar$_F$ = 4-C$_6$H$_4$F) as putative intermediate in the N-atom transfer reaction.[90]
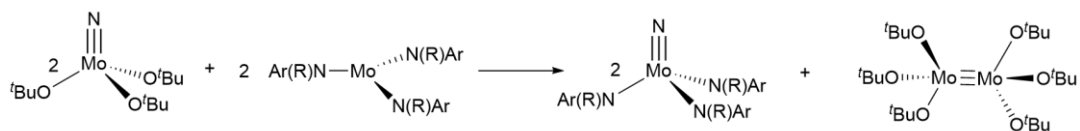
Scheme 9: Nitride transfer by use of sterically less demanding alkoxy-ligands.

Exchanging the R-substitutents of the amide in Mo(NR$_2$)$_3$ against *iso*-propyl groups results in C-H activation and cyclometalation to Mo(H)(η^2-Me$_2$C=NAr)(N(*i*Pr)Ar)$_2$.[93] Unexpectedly, also this compound splits N$_2$, without observable intermediate, into the paramagnetic single nitrogen bridged species {[Ar(*i*Pr)N]$_3$Mo}$_2$(µ-N). In this reaction, the hydride is observed to migrate back to carbon to form three equivalent *iso*-propyl groups again. Molecular orbital considerations predict a {MNM}$^{7\pi}$ unit with a spin ground state doublet, which is supported by magnetic measurements. The mechanism for formation of the single nitrogen bridged species is thought to proceed via initial N$_2$ splitting, generating the nitride species N≡Mo(N(*i*Pr)Ar)$_3$ which then couples with excess Mo(N(*i*Pr)Ar)$_3$ to the nitrogen bridged dimer (Scheme 10). To
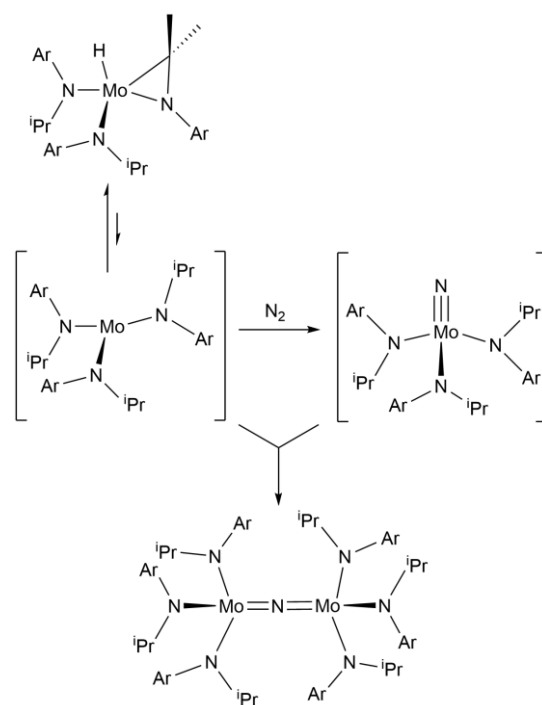
Scheme 10: N$_2$ cleavage into bridging nitride with cyclometalated Mo(H)(η^2-Me$_2$C=NAr)(N(iPr)Ar)$_2$.

test this assumption, the nitride complex N≡Mo(N(*i*Pr)Ar)$_3$ was prepared independently out of N-atom transfer from N≡Cr(O*t*Bu)$_3$ to cyclometalated Mo(H)(η^2-Me$_2$C=NAr)(N(*i*Pr)Ar)$_2$ and subsequently reacted with additional cyclometalated complex to show fast coupling to {[Ar(*i*Pr)N]$_3$Mo}$_2$(µ-N).[93] This stands in contrast to the more bulky N≡Mo(N(*t*Bu)Ar)$_3$, isolable as monomer. Here, such a dimerization is obviously hampered by steric demands. Following calculations confirmed that splitting from {Mo[N(tBu)(Ar)]$_3$}$_2$(µ-η^1-η^1-N$_2$) to the respective terminal nitride is kinetically as well as thermodynamically favored over dimerization to a single nitrogen bridged compound, whereas for smaller ligands (N(*i*Pr)Ar or NMe$_2$) the formation of {[R$_2$N]$_3$Mo}$_2$(µ-N) is both favored kinetically and thermodynamically.[94]

A comparison of *Cummins'* end-on dinitrogen bridged dimer with a structurally related complex of the group of *Schrock* [Mo{R′NCH$_2$CH$_2$}$_3$N]$_2$(μ-η^1-η^1-N$_2$) (R′ = *t*BuMe$_2$Si) reveals that the story of dinitrogen splitting is not only governed by the number of electrons and the steric demand of the ligand.[84,95,96] Both complexes contain the same electron count, formal oxidation and spin state and display similar structural parameters. *Schrock'*s dimer also
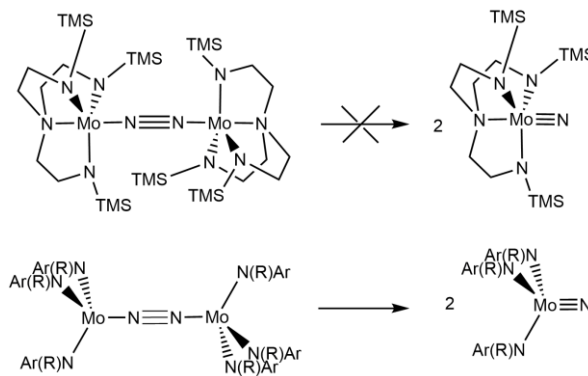
Scheme 11: Comparison of Schrock's triamidoamine Mo(III) and Cummins' triamido Mo(III) N$_2$ dimers towards N$_2$ cleavage.

contains three amido ligands, but a coordination number of 5 with an amine in trans-position to N$_2$. Besides, electropositive silicon substituents at the amide should have an influence on the donor capabilities. The intriguing difference between these two compounds is that *Cummins'* complex splits N$_2$ thermally into nitrides and *Schrock'*s complex does not (Scheme 11). Calculations on a simplified model complex predict the splitting to be endothermic for the latter complex and exothermic for the former.[86] This result is attributed to the trans-ligand in *Schrock'*s dimer, which as σ-donor transfers electron density to the metal and therefore weakens the M-N$_2$ bond. In the MO scheme (Figure 13), this influence can be depicted by lifting the σ-bonding orbital a$_u$ in energy. Hence, mixing between this orbital and the π-symmetric orbital 2b$_u$ in the TS is hampered, because the energy difference is too large. This effect renders the whole splitting mechanism thermodynamically and kinetically unfavorable.

Another reason might be the steric strain imposed by the triamidoamine ligand. Calculations of the group of *Stranger* indicate that rotation of one of the amido ligands at each metal center from the trigonal symmetry in such a way that the NC$_2$ plane stands orthogonal to the MNNM unit leads to stronger π-backdonation from the metal to N$_2$ and enhanced N$_2$ activation, as the electron density at the metal is increased (Scheme 13). This effect is accompanied by a stabilization of the singlet state over the triplet state for the dimer, because the degeneracy of the HOMO is lifted and already results in a bent structure.[97,98] This stands in contrast to the experimentally observed structure and magnetization of the isolated dimer, but the computed results resemble the presumed zigzag transition state.[85] Ligand rotation during the splitting process might be involved. Furthermore, considering N-N cleavage with the less bulky complex Mo(N(*i*Pr)Ar)$_3$, dinitrogen splitting is faster and an intermediate could not be observed. Splitting might be accelerated from expected [Mo(N(*i*Pr)Ar)$_3$]$_2$(μ-η^1-η^1-N$_2$), as ligand rotation of *iso*-propyl groups is easier than in the respective *tert*-butyl analogues.[85,98]
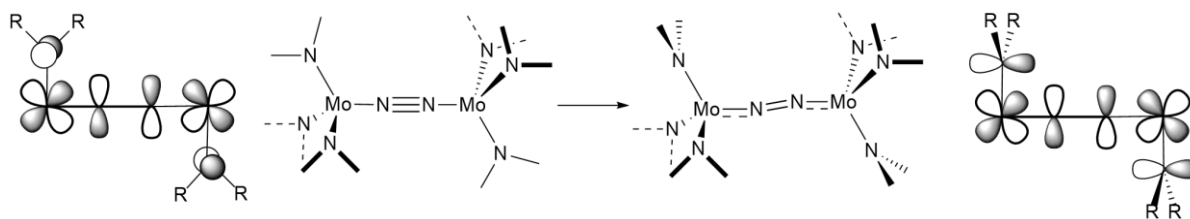
Scheme 12: Scheme 13: Rotation of one NR$_2$ group at each Mo center.

DFT calculations revealed, that π-donors in the ancillary ligands not only lead to stronger N$_2$ activation, but also to a more exothermic splitting reaction.[86,97] Consequently, N$_2$ splitting with complexes exhibiting no or weak π-donor ligands should be more difficult. In 2001, *Floriani* and coworkers synthesized the molybdenum dimer $[(Mes)_3Mo]_2(\mu$-η^1-η^1-$N_2)$ (Mes = 2,4,6-Me$_3$C$_6$H$_2$).[99] This complex displays similarities with the above described system of *Cummins*. Molybdenum is again 4 coordinate, paramagnetic and in the same formal oxidation state, but the mesityl-ligands are no π-donors anymore and the steric bulk is smaller. Importantly, this dimer is thermally stable (refluxing benzene) and does not cleave N$_2$ over time. However, dinitrogen can be split in this system by photolysis, which will be discussed in chapter 6.4.
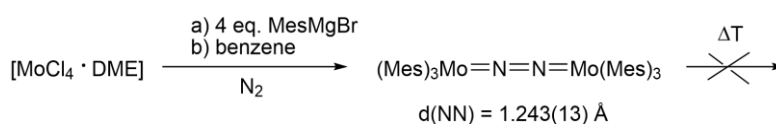
Scheme 14: Synthesis of thermally stable N$_2$-bridged Mo dimer by Floriani.[99]

Photolysis of N$_2$-bridged dimer

Bulk irradiation of the N$_2$ bridged dimer $\{[Ar(tBu)N]_3Mo\}_2(\mu$-$N_2)$ with visible light (λ ≥ 480 nm) at -78°C to exclude thermal decomposition, produced an about 1:1 mixture of N≡Mo[N(tBu)Ar]$_3$ and Mo[N(tBu)Ar]$_3$, presumably under loss of 0.5 equivalents of N$_2$ due to stoichiometry (Scheme 15). As loss of N$_2$ from the dimeric complex has not been observed before, it is most likely due to an electronic excited state. Formation of the nitrido complex resembles thermal N$_2$ cleavage. Frequency resolved pump-probe spectroscopy was performed in the group of *Blank* to get more detailed information about the photochemical mechanism.[100] It turned out photoexcitation at 2.3 eV creates a very short lived excited triplet state, which relaxes through internal conversion in 300 fs to the ground state with subsequent vibrational cooling in subpicoseconds in competition with Mo-N$_2$ bond dissociation. Coupling to structural distortions facilitates the rapid internal conversion and assists the transition to the singlet state, giving propensity to N-N cleavage.
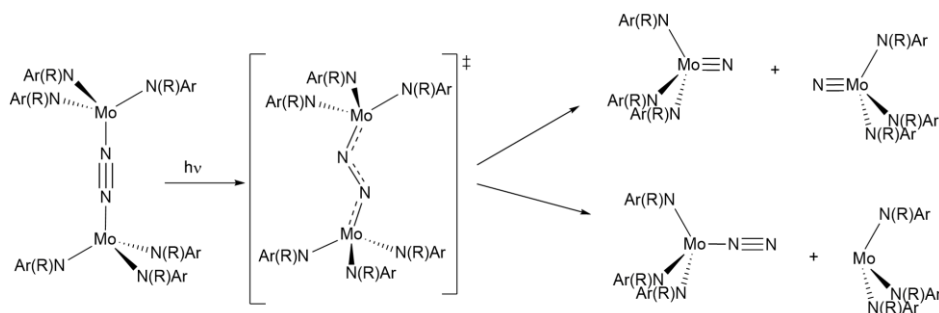
Scheme 15: Competition of N-N and M-N bond cleavage upon photolysis of {Mo[N(tBu)(Ar)]$_3$}$_2$(μ-η^1-η^1-N_2).

These structural distortions have also been found in theoretical examinations on photochemical activation of stable, linear μ-N_2 complexes (M = Fe, Ru) in the group of *Reiher*. The authors suggest population of antibonding π^* orbitals of N_2 upon photochemical excitation resulting in a bent diazenido like structure in the first excited state.[101] This resembles the zigzag transition state, proposed for *Cummins* splitting mechanism and is in agreement with the observation of terminal nitrides as products of N_2 splitting. Qualitatively, the formation of Mo[N(*t*Bu)Ar]$_3$ together with N_2 can be explained by excitation of electrons in 2e$_u$ orbitals (Figure 13). Therefore, the M-N bond is weakened with simultaneous strengthening of the N-N bond, which leads to release of N_2.

Intermediate Trapping

N_2 Splitting from Mo[N(*t*Bu)Ar]$_3$ to the terminal nitride turned out to be redox-catalyzed. In the presence of Na/Hg, the reaction is significantly accelerated.[87] By controlling the reaction parameters, the reduced compound Na[(N_2)Mo(N(*t*Bu)Ar)$_3$], formally a Mo(II) species, could be isolated, containing linearly bound and slightly activated N_2. Since the starting material Mo[N(*t*Bu)Ar]$_3$ is not reduced by Na/Hg, dinitrogen coordination is considered to be the very first step in the cleavage mechanism. The monoanionic compound then presumably reacts with remaining Mo[N(*t*Bu)Ar]$_3$ to an anionic N_2 bridged dimer, which reduces again neutral (N_2)Mo(N(*t*Bu)Ar)$_3$ under generation of the neutral dimer, which is known to split the N-N bond. Oxidation of the trapped anionic complex [(N_2)Mo(N(*t*Bu)Ar)$_3$]$^-$ does not produce the neutral compound, but deliberates N_2 instantaneously to yield the starting material Mo[N(*t*Bu)Ar]$_3$. In contrast, the related isoelectronic complex [(Me$_3$SiNCH$_2$CH$_2$)$_3$N]Mo(N_2) with triamidoamine ligand could be prepared by oxidation of {[(Me$_3$SiNCH$_2$CH$_2$)$_3$N]Mo(N_2)}$_2$-Mg(THF)$_2$ in the group of *Schrock*.[102,103] The monomeric complex was structurally characterized and turned out to be moderately stable. Apparently, the apical amine donor in *Schrock's* complex combined with the more reducing silyl-amides in the ancillary ligand increase the electron density at the metal in such an extent that N_2 end-on binding becomes more

24

stable. The anionic complex [(N$_2$)Mo(N(tBu)Ar)$_3$]$^-$ can be functionalized with electrophiles such as methyl triflate (MeOTf), methyl tosylate (MeOTs) or Me$_3$SiCl to form N$_\beta$-E (E = Me, SiMe$_3$) bonds. With MeOTf even a second methylation to cationic [(N(tBu)Ar)$_3$Mo-NNMe$_2$]OTf is possible (Scheme 16).

d(NN) = 1.171(14) Å
ν(NN) = 1761 cm^{-1}
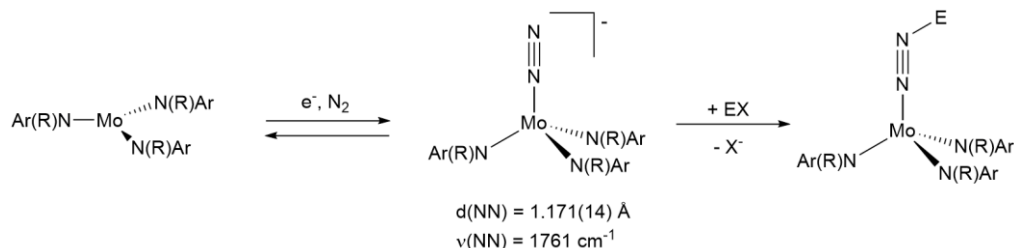
Scheme 16: Formation of mononuclear end-on [(N₂)Mo(N(tBu)Ar)₃]⁻ and subsequent functionalization (EX = MeOTf, MeOTs, Me₃SiCl).

Reactivity of the terminal nitrido complex [Ar(tBu)N]$_3$Mo≡N

The terminal nitride [Ar(tBu)N]$_3$Mo≡N turned out to possess weak nucleophilic character. With a variety of Lewis acids formation of adducts has been observed to give compounds of formula [Ar(tBu)N]$_3$MoN-EX$_3$ (X = F, E = B; X = Cl, E = B, Al, Ga, In; X = Br, E = Al; X = I, E = Al) and [Ar(tBu)N]$_3$MoN-ECl$_2$ (E = Ge, Sn) by simple combination of the nitride with the Lewis acid in a 1:1 ratio.[104] These adducts show only little change in Mo-N bond length. Besides, they were observed to decompose back to the starting materials within 0.5 – 3 h in THF solution at 25°C. With strong electrophiles such as MeOTf, Me$_3$SiOTf or PhC(O)OTf, formation of cationic imido complexes have been observed (Scheme 17). Such imido complexes are well documented in the literature.[105] The Mo-N-C or Mo-N-Si units are linear in the crystal structures and Mo-N bond lengths are slightly elongated compared to the parent nitride ([Ar(tBu)N]$_3$Mo≡N: d(MoN) = 1.651(4) Å[85]; [Ar(tBu)N]$_3$Mo≡N-SiMe$_3^+$: d(MoN) = 1.795(6) Å).[104] Methylimido complex [Ar(tBu)N]$_3$Mo≡N-Me$^+$ can be deprotonated to give a ketimide, displaying a nearly linear M-N-C unit. The N-C bond length is in agreement with the presence of a double bond (d(NC) = 1.300(7) Å), whereas the Mo-N bond distance (d(MoN) = 1.777(4) Å) lies in between a single and a double bond. This ketimide reacts with excess MeI to give the ethylimido complex [Ar(tBu)N]$_3$Mo≡N-Et$^+$, displaying the nucleophilic character of the ketimide carbon. Interestingly, the ethylimido complex could not be obtained by addition of an appropriate Et$^+$ source like EtOTf, EtI or [Et$_3$O]BF$_4$ to the nitride. The authors state, the increased steric bulk of the electrophile presumably slows down the rate of the nucleophilic substitution reaction.[104]
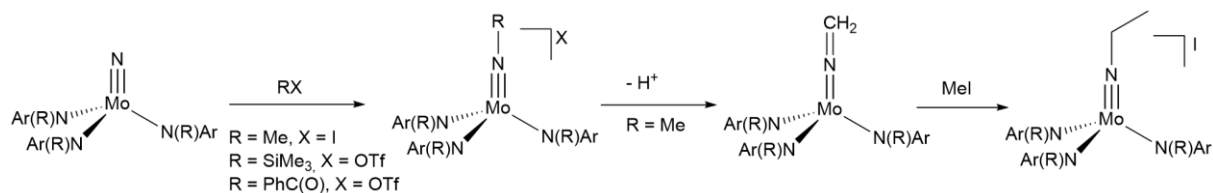
Scheme 17: Functionalization of N$_2$ derived terminal nitrido complex [Ar(^{t}Bu)N]$_3$Mo≡N with electrophiles.

Of particular interest towards the incorporation of N$_2$ derived nitrogen into organic molecules is the splitting of the Mo≡N triple bond. This strong bond is needed to provide a driving force for the splitting of the N≡N triple bond, but for N$_2$ fixation in valuable chemicals, the Mo≡N bond needs to be cleaved again. This proved to be possible, when the nitrido complex was reacted with trifluoroacetic anhydride. Within several minutes in dimethylformamide solution, the formation of an almost quantitative amount of CF$_3$C(O)NH$_2$ has been observed.[106] Following analysis revealed the complex is degraded upon reaction and the observed "additional" protons stem from isobutene elimination of the *tert*-butyl groups of the amide ligands. Attempts to produce isocyanates from the reaction of CO with the terminal nitrido complex failed, although DFT computations predicted a thermodynamically favorable reaction.[107] To rationalize the difference between the molybdenum system and similar vanadium nitrides reacting with CO to isocyanates[108,109], further DFT calculations were carried out. Based on these studies, a metal-carbonyl intermediate was proposed for the vanadium model complex, which isomerized to give the isocyanate complex, thereby avoiding a large reaction barrier.[107]

An elegant route for nitrogen functionalization and N-atom transfer was published in 2006, wherein dinitrogen was transformed into organonitriles and the metal complex could be recovered in high yield to form a synthetic cycle (Scheme 18).[110] Starting from Mo[N(tBu)Ar]$_3$, N$_2$ is split into nitrido complexes N≡Mo[N(tBu)Ar]$_3$, which can be functionalized with acyl chlorides RC(O)Cl (R = Ph, ^{t}Bu, Me) under assistance of silyl triflates. Acyl chlorides do not react with the nitride alone, the latter needs to be activated by silylation to allow for acylation. Reduction with magnesium anthracene in the presence of Me$_3$SiCl produces a trimethylsiloxyl-substituted ketimide, which can be reacted with Lewis acids like SnCl$_2$ or ZnCl$_2$ to remove the oxygen moiety and release the respective organonitrile under generation of the chlorinated complex [Ar(^{t}Bu)N]$_3$MoCl. Further reduction by Mg affords the starting material Mo[N(tBu)Ar]$_3$. In this
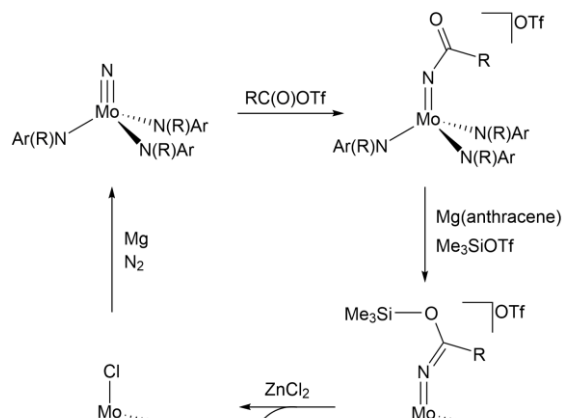
Scheme 18: Synthetic cycle for N$_2$ cleavage and conversion in nitriles by a molbydenum triamido complex.

cycle, nitrile release in up to 38% over all steps proved to be possible. Each molybdenum center is oxidized by 3 electrons upon N_2 cleavage and re-reduction is a purely metal centered process. Driving force in this synthetic scheme is formation of the very strong CN triple bond (D^0(HC≡N) = 937 kJ mol^{-1}).[111]

In a similar approach for generation of cyanides, the nitrido complex was reacted with a mixture of MeOCH$_2$Cl and ^{i}Pr$_3$SiOTf.[112] The resulting methoxymethyl-imido complex can easily be deprotonated to give [Ar(^{t}Bu)N]$_3$MoN=CH-OMe. As described above, nitrile extrusion under oxygen removal can be carried out using SnCl$_2$ with concomitant generation of [Ar(^{t}Bu)N]$_3$MoCl. However, HCN elimination proved to be difficult, as free ligand and nitride complex have been observed and no HCN could be collected via vacuum transfer. If the reaction is carried out in the presence of base (Me$_3$SiNMe$_2$, 10 eq), the major product turned out to be the molybdenum(IV) cyanido complex [Ar(^{t}Bu)N]$_3$Mo-CN (Scheme 19). In the reaction, no external reducing agent like Mg was employed for molybdenum reduction. Instead, electrons for the formal reduction from Mo(VI) to Mo(IV) originate from the carbon, which was deprotonated during the reaction, formally delivering 2 electrons to the molybdenum center. In this way, in the overall process N≡N is transformed to Mo≡N, which is then transformed to C≡N being again the driving force for the reaction without the use of strong reducing agents.
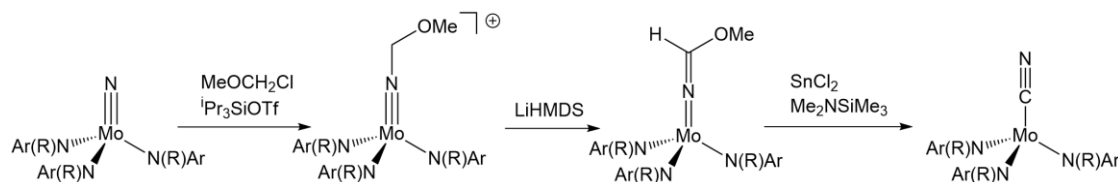
Scheme 19: Functionalization of N₂ derived nitride into cyanide ligand.

5.2   Dinuclear side-on bridging N₂-complexes

Defined N$_2$-splitting into nitrides mediated by side-on bound dinitrogen has not been examined in such detail so far. The first unequivocally established cleavage in two bridging nitrides was promoted by a vanadium complex and demonstrated in 1999 by the group of *Cloke*. Reduction of a diamidoamine vanadium(III) complex {V(N[N´]$_2$)Cl}$_2$ (N[N´] = (Me$_3$Si)N[CH$_2$CH$_2$N(SiMe$_3$)]$_2$) with one equivalent of KC$_8$ under N$_2$ atmosphere led to the isolation of neutral bis(μ-nitrido) complex

[V(N[N´]$_2$)]$_2$(μ-N)$_2$ (Scheme 20).[113] That both nitrides originate from the same N_2 molecule was confirmed by labelling experiments employing a $^{14}N_2/^{15}N_2$ mixture. The V_2N_2 core is planar with d(NN) = 2.50(2) Å, indicating that the N≡N triple bond has been completely cleaved by concomitant oxidation of the metals to V(V, d^0) in agreement with the diamagnetic character. Further one electron reduction (or direct 2 electron reduction from the V(III) chloro complex) is possible to form anionic V(V, d^0)/V(IV, d^1) in agreement with magnetic measurements. Thorough experiments were carried out for understanding the electronic and vibrational structure of the reaction products.[114]

The proposed diamidoamine V(II) intermediate displays similarities with the triamido Mo(III) system of *Cummins*. The electronic configuration is the same and the ligand environment is comparable. However, side-on coordination is assumed based on the labelling experiments. DFT calculations confirm side-on bonding of N_2 to V(II) with subsequent coordination of another V(II) to form a side-on bridged dimer, which then cleaves the N-N bond.[115] Side-on coordination was pointed out to be preferred over end-on coordination due to the orbital disposition imposed by the diamidoamine ligand. In this way, a trans-ligand is avoided, which would raise the σ-orbitals in energy. In addition, only in a side-on coordination mode, transition of electrons in σ-antibonding orbitals can be achieved, which was stated to be a prerequisite for N_2 cleavage. Importantly, again a {MNNM}$^{10\pi}$ electronic configuration seems to be necessary for complete N_2 reduction.

Reactivity of the nitrido complexes has not been reported to the best of our knowledge.
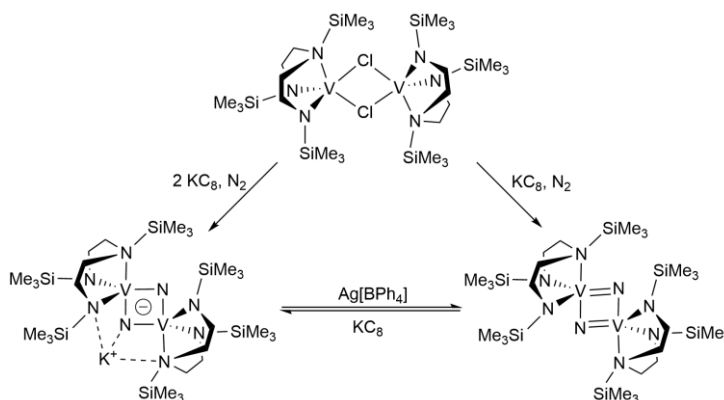
Scheme 20: N_2 Splitting into bis(μ-nitrido) complex [V(N[N´]$_2$)]$_2$(μ-N)$_2$.

28

6 Initial N$_2$-splitting along the periodic table

6.1 Actinides

N$_2$ cleavage with f-block elements is rare, despite a variety of N$_2$ complexes, displaying all sorts of activation. In 2002, the group of *Gambarotta* showed N-N bond splitting by reduction of the uranium(III) complex K[(Et$_8$-calix[4]tetrapyrrole)U(DME)] under N$_2$ atmosphere.[116] The product was identified as mixed-valent U^V/U^{IV} compound K[{K(calix[4]tetrapyrrole)U}$_2$(μ-NK)$_2$] in 61% isolated yield. Each bridging nitride also interacts with one potassium center. Reactivity of this new compound has not been reported so far.
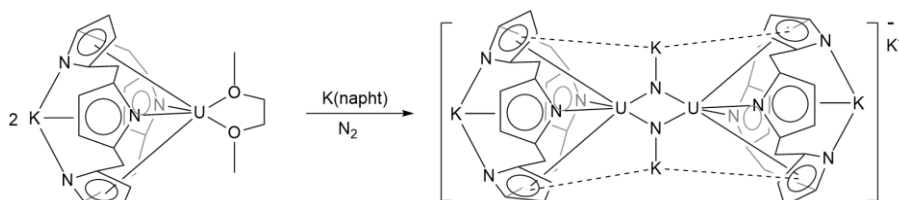
Scheme 21: N$_2$-splitting promoted by uranium.

N$_2$ cleavage with concomitant double hydrogen atom abstract to an amine moiety has been reported for a thorium compound.[117] Reduction of thorium(V) compound K{[O$_2$]$_2$ThCl} ([H$_2$O$_2$] = (2-hydroxy-3-*tert*-butyl-5-methyl-C$_6$H$_2$)$_2$CH$_2$) with K(naphtalenide) in DME under N$_2$ atmosphere results in isolation of K{[O$_2$]$_2$Th(NH$_2$)(DME)} in up to 47% yield. Labelling experiments with ^{15}N$_2$ unequivocally confirm gaseous N$_2$ as origin of the amide, the source of the hydrogen atoms however as well as the mechanism of formation remain unclear.
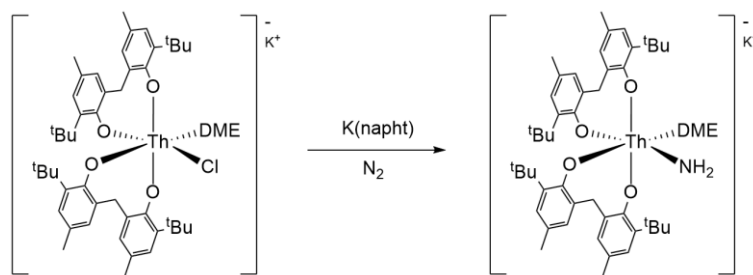
Scheme 22: N$_2$ cleavage into an amide group mediated by a thorium compound.

6.2 Group 4

Titanium: N$_2$ cleavage mediated by group 4 metals is hard to achieve, because very low valent species are needed to provide enough electrons for N$_2$ reduction. The group of *Gambarotta* demonstrated N$_2$ splitting by reduction of a well-defined titanium(III) complex LTiCl (L = 2,5-{(C$_4$H$_3$N)CPh$_2$}$_2$C$_4$H$_2$N(Me)) with 1.5 equivalents of Na/Hg.[118] The nitride-imide bridged complex [Na(dme)$_3$][(LTi)$_2$(μ-NH)(μ-N)] was isolated in 25% yield from the reaction mixture. By the use of more reducing equivalents another product [Na(dme)$_3$]$_4$[{LNa}$_2$][(LTi)$_2$-(μ-N)$_2$] with two separate dianionic moieties was obtained. The presence of [{LNa}$_2$]$^{2-}$ indicates some kind of degradation during the reaction. Treatment of the nitrido complexes with HCl resulted in ammonia formation. Whereas the complexes proved to be unreactive towards methylation, silylation using Me$_3$SiCl was possible yielding mononuclear LTiNSiMe$_3$. Dinitrogen splitting turned out to be very sensitive towards the choice of solvent, as only in DME splitting products could be observed. Identical reactions in THF only led to intractable mixtures. The mechanism for splitting is proposed to proceed via two electron reduction to a Ti(I) species with side-on coordinated N$_2$, which is again reduced with subsequent hydrogen atom abstraction from the solvent or ligands to form the nitrido-imido complex [(LTi)$_2$(μ-NH)(μ-N)]$^-$. Excess reducing equivalents is likely to reduce the N$_2$ complex further to the bis(μ-nitrido) [(LTi)$_2$-(μ-N)$_2$]$^{2-}$.

Another approach to achieve N$_2$ splitting with group 4 metals has been investigated by the group of *Hou*. Instead of using only 2 metal centers which need to deliver 3 electrons each, they used 3. Notably, reducing equivalents were not introduced by strong alkali metals, but by the use of H$_2$ (Scheme 23).[119,120] Reaction of the titanium(IV) alkyl complex Cp′Ti(CH$_2$SiMe$_3$)$_3$ (Cp′= C$_5$Me$_4$SiMe$_3$) with hydrogen (4 atm) affords a mixture of the trinuclear polyhydrides (Cp′Ti)$_3$(μ$_3$-H)(μ$_2$-H)$_6$ and (Cp′Ti)$_4$(μ-H)$_8$ (not depicted in Scheme 23) in 69% and 10% yield respectively. The latter is also the main product in similar reactions of the higher group 4 analogues Zr and Hf and stable towards N$_2$.[121] The former however reacts with N$_2$ (1 atm) under partial H$_2$ elimination
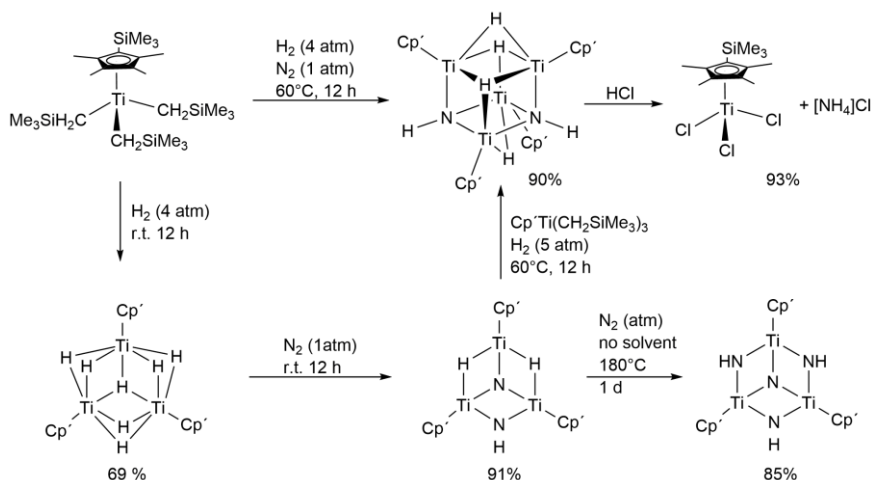
Scheme 23: Ammonia synthesis out of N$_2$ and H$_2$ mediated by a polynuclear titanium hydride.

30

to (Cp´Ti)$_3$(μ_2-NH)(μ_3-N)(μ_2-H)$_2$, where the N-N bond has been split under retention of the formal oxidation states of titanium (formally two Ti(III, d^1) and one Ti(IV, d^0)). The reaction can be monitored by low temperature NMR experiments, revealing formation of a dinitrogen side-on end-on bridged complex. At -10°C, N$_2$ splitting takes place almost quantitatively to a bis(μ-nitrido) complex. At 20°C the latter isomerizes to the observed nitrido-imido-dihydrido complex (bottom center, Scheme 23). Further N$_2$ incorporation has been observed upon heating (180°C) to produce (Cp´Ti)$_3$(μ_3-N)(μ_2-NH)$_3$. The latter as well as the nitrido-imido-dihydrido complex are stable towards hydrogenation. However, in the presence of Cp´Ti(CH$_2$SiMe$_3$)$_3$ a reaction with H$_2$ is observed, resulting in quantitative formation of the bis(imido) complex (Cp´Ti)$_3$(μ_3-NH)$_2$(μ_2-H)$_4$. Furthermore, direct reaction of Cp´Ti(CH$_2$SiMe$_3$)$_3$ under H$_2$ (4 atm) and N$_2$ (1 atm) at 60°C also leads to generation of the bis(imido) complex in 90% yield. Addition of anhydrous HCl affords NH$_4$Cl together with Cp´TiCl$_3$ almost quantitatively.

In very recent work, the group of *Hou* demonstrated further N$_2$ incorporation of (Cp´Ti)$_3$(μ_3-NH)$_2$(μ_2-H)$_4$.[122] Heating the neat complex to 180°C under N$_2$ atmosphere (1 atm) affords the diimide/dinitride complex [(Cp´Ti)$_4$(μ_3-NH)$_2$(μ_3-N)$_2$] in about 95% yield (Scheme 24). Intriguingly, this complex reacts with a variety of acid chlorides to the respective nitriles in good yields (60-85%, 60°C, 12 h). Nitrogen transfer from N$_2$ into organic substrates is therefore accomplished in two simple steps. A μ-oxo Ti(II) complex [(Cp´TiCl$_2$)$_2$(μ-O)] is characterized as reaction product besides unidentified paramagnetic Ti(III) species. Addition of ethereal HCl to the crude mixture after reaction with acid chlorides yields the trichloride [Cp´TiCl$_3$] (83%), which is the starting material for the synthesis of Cp´Ti(CH$_2$SiMe$_3$)$_3$. In this way, a synthetic cycle is closed, in which N$_2$ is converted into organic nitriles via reaction with H$_2$ and acid chlorides with the possibility of catalyst recycling. Importantly, the system is independent of further reagents like strong reducing agents or bases. It is noteworthy, that the tetranitride analogue [(Cp´Ti)$_4$$_2$($\mu_3$-N)$_4$], obtained by dehydrogenation of the diimide/dinitride complex, does not react with acid chlorides under the same reaction conditions.
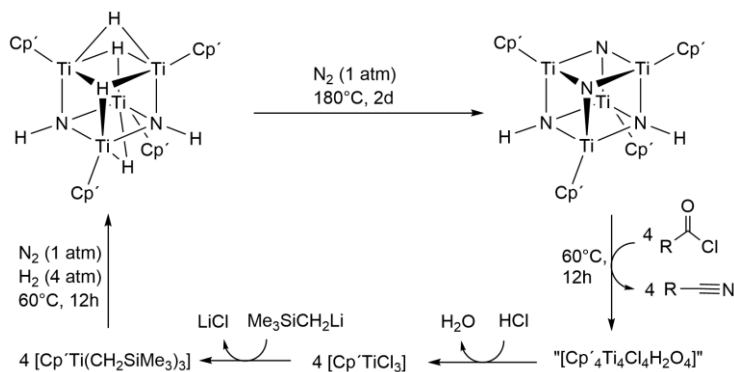
Scheme 24: Synthetic cycle for the transformation of N$_2$ and acid chlorides into nitriles promoted by Ti complexes.

Zirconium and Hafnium: The higher homologues of group 4 have not been observed to initially split N$_2$, although N$_2$ activation can be very strong in these complexes. Nevertheless, N$_2$ cleavage has been achieved by functionalization of N$_2$ complexes, e.g. by hydrogenation. *Chirik* and coworkers could demonstrate generation of side-on bridging N$_2$ complex [(η^5-C$_5$Me$_4$H)$_2$Zr]$_2$(μ-η^2:η^2-N$_2$).[78] Unlike the end-on analogue with a slightly different ligand set (see chapter 4.3), which reacts with H$_2$ under elimination of N$_2$, the side-on complex is hydrogenated to form [(η^5-C$_5$Me$_4$H)$_2$ZrH]$_2$(μ-η^2:η^2-N$_2$H$_2$) (Scheme 25).[77]. H$_2$ is subsequently split over the M-N bond under nitrogen reduction to generate the diazenido unit. The dihedral angle between the Zr moieties (θ = 64°) turned to be crucial as calculations predict no reaction with H$_2$ at a dihedral angle of 0°. Only in the twisted confirmation, the HOMO is a π-symmetric orbital with NN antibonding character and a metal centered LUMO, which is well suited to accommodate a hydride ligand.[78] Heating the hydrogenated complex to more than 45°C results in H$_2$ loss and N-N bond cleavage to form [(η^5-C$_5$Me$_4$H)$_2$Zr]$_2$(μ-NH$_2$)(μ-N), which can be treated with HCl to afford two equivalents of NH$_4$Cl. Furthermore, ammonia can be generated in 10-15% yield by heating the diazenido complex to 85°C under H$_2$ atmosphere
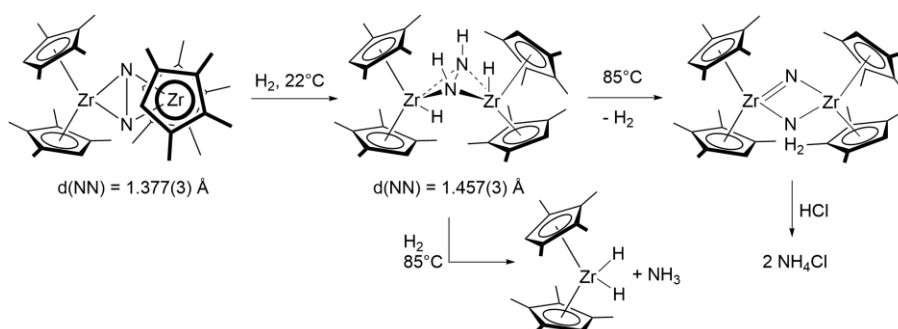
Scheme 25: Ammonia formation out of N$_2$ and H$_2$ mediated by a zirconocene complex.

The similar hafnocene N$_2$ complex ((Me$_2$Si(η^5-C$_5$Me$_4$)(η^5-C$_5$H$_3$-3-^{t}Bu)Zr)$_2$(μ-η^2:η^2-N$_2$) has been observed to react with CO to different products depending on the CO concentration (Scheme 26).[123] Stoichiometric CO addition results in N-N bond cleavage, N-C bond formation and activation of one C-H bond of the ancillary ligand. NH$_4$Cl and HNCO can be liberated from the complex by addition of HCl. If 1 atm of CO is admitted to the dinitrogen complex, N-N bond cleavage is accompanied by C-N and C-C bond formation to a bridging oxamidide ligand (N$_2$C$_2$O$_2$)$^{4-}$. Protonolysis with excess HCl yields the respective mononuclear dichloride complex along with free oxamide H$_2$NC(O)-C(O)NH$_2$ in more than 90% yield.
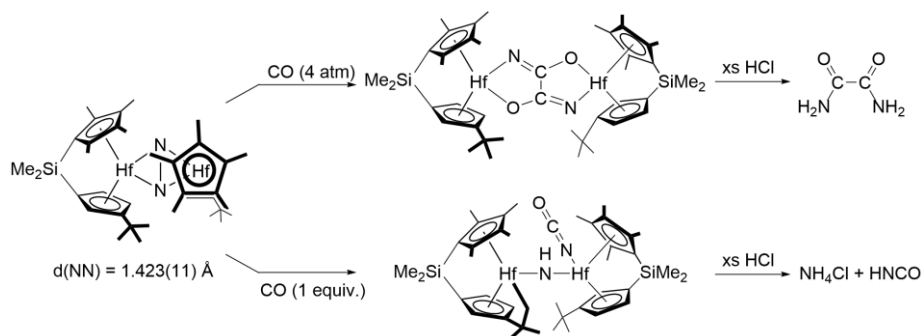
Scheme 26: Generation of N$_2$ and CO derived oxamide or ammonia mediated by a hafnocene complex.

6.3 Group 5

Vanadium: The first example of vanadium mediated cleavage of N$_2$ was reported in 1995 by the group of *Gambarotta*. The mononuclear V(II) complex [(Me$_3$Si)$_2$N]V[CH$_2$(SiMe$_2$)N(SiMe$_3$)](PMe$_3$) was pressurized with 60 atm of H$_2$.[124] Unexpectedly, a new compound was isolated in 45% yield which turned out to be a mixed-valent species with both a dinuclear vanadium cation and anion. The cation proved to be the trihydrogen bridged complex {[(Me$_3$P)$_3$V]$_2$(μ-H)$_3$}$^+$ with the anion containing two bridging nitrides [{[(Me$_3$Si)$_2$N]$_2$V}$_2$(μ-N)$_2$]$^-$ (Scheme 27, top). The origin of the nitrides was proposed to be N$_2$, as no corresponding ligand decomposition products could be detected, but was not unambiguously confirmed. One year later, *Gambarotta* and coworker demonstrated the formation of a single-nitride bridged divanadium complex presumably derived from N$_2$.[125] In the reaction of TMEDA (tetramethylethylenediamine) with Li$_4$[(oepg)VCl$_2$] (oepg = octaethylporphyrinogen) a side-product formed, which was identified as [Li(tmeda)$_2$]{[(oepg)VLi$_2$]$_2$(μ-N)} (Scheme 27, bottom) and isolated in up to 25% yield from the reaction mixture. The nitride is coordinated square planar to four lithiums and sandwiched between two V(oepg) moieties. A magnetic moment of μ$_{eff}$ = 2.85 μ$_B$ was determined, which is significantly lower than expected for two V(III, d^2) centers, accounting for magnetic coupling between these two metals over the nitride bridge. The source of the nitride seemed to be N$_2$, but could not be proven definitely by labelling experiments.
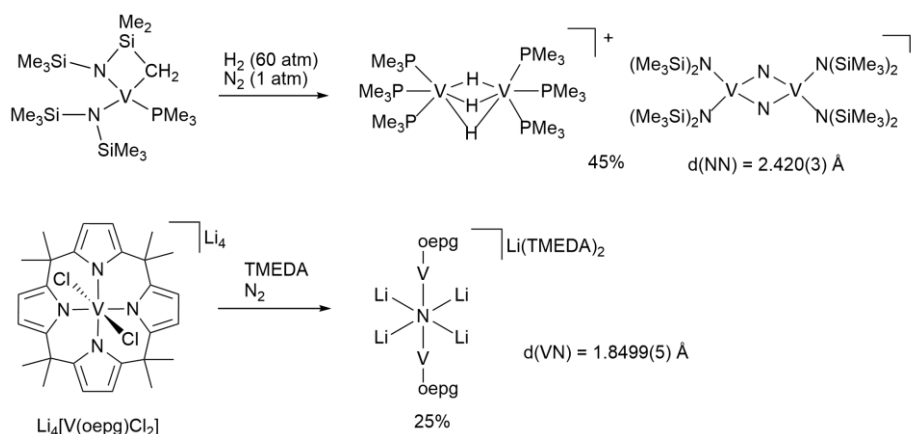
Scheme 27: N$_2$ splitting reactions promoted by vanadium complexes.

Gambarotta looked further into N$_2$ activation with low valent vanadium complexes and reported formation of a stable end-on N$_2$ bridged V(II)/V(II) complex.[126] Tripyrrolide starting compound [(MeTP)V(THF)] (MeTP = 2,5-{2-[(C$_6$H$_5$)$_2$C]pyrrole]$_2$(N-Me-pyrrole)) exhibits two σ-interactions with the outer pyrrole rings and one π-interaction with the methylated pyrrole ring in the middle of the ligand (Scheme 28). The fourth coordination site is occupied by Lewis basic solvents. If the latter is extracted with a strong Lewis acid, N$_2$ coordinates forming the dinuclear complex [(MeTP)V]$_2$(μ-η^1-η^1-N$_2$). By reduction with KC$_{8.8}$ (1 equivalent per V) N$_2$ cleavage is observed producing the nitride bridged species [(MeTP)V]$_2$(μ-N) in 52% isolated yield. Magnetic measurements are in accordance with V(III, d^2)/V(IV, d^1) oxidation states. Upon addition of aqueous HCl, 43% of ammonia could be collected. In contrast to *Cloke*'s vanadium system (see chapter 5.2), splitting is not achieved from V(II) but from a more reduced species. Another difference is that N$_2$ is coordinated end-on, whereas in *Cloke*'s case DFT predict a side-on coordination.[115] The side-on mode might be hampered for steric reasons, allowing only for end-on coordination. Therefore, a more electron rich system might be needed to achieve splitting, as orbitals in the right symmetry to allow transition in σ-orbitals must be occupied. However, the mechanism is still unclear, since the splitting reaction from the dimer to the single-nitride bridged compound is unbalanced and the nature of possible side-products is unknown.
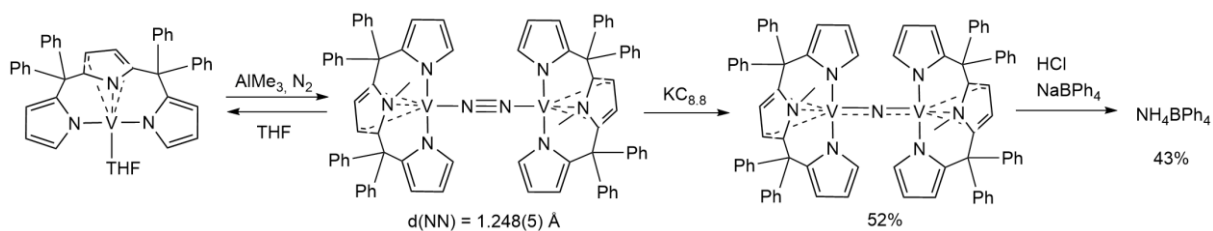
Scheme 28: N$_2$ Cleavage into bridging nitride by reduction of a V(II) N$_2$ bridged complex and subsequent ammonia formation.

Reduction of vanadium(III) complex [(ONO)V(THF)] (ONO = 2,6-(3-^{t}Bu-5-Me-2-OC$_6$H$_2$CH$_2$)-4-^{t}Bu-(p-tolyl)NC$_6$H$_4$) with KH (2 equiv.) under N$_2$ atmosphere resulted in the isolation of paramagnetic [{K(DME)}$_2${(ONO)V(μ-N)}]$_2$ in 61% yield with concomitant formation of H$_2$ (Scheme 29).[127] The N-N distance was found as 2.550(3) Å, indicative for complete N-N bond scission. The complex is stabilized by four potassium ions and magnetic measurements are in accordance with a V(IV, d^1) oxidation state for both vanadiums in the planar V$_2$N$_2$ core. Oxidation with benzoquinone generated the terminal vanadium(V) nitride [{K(DME)}{(ONO)-VN}]$_2$. Regeneration of the bridging nitrides by reduction with KH was not successful, suggesting that V(V) nitride is no intermediate in the N$_2$ splitting process. The authors propose V(I) being responsible for N$_2$ splitting. However, this would imply a {MNNM}$^{12\pi}$ electronic configuration in contrast to what has been stated in chapter 5.1, which rather points towards V(II). Furthermore, apparently the introduced alkali metals are mandatory to stabilize the structure. Generation of H$_2$ during N$_2$ splitting might be a consequence of these additional electrons and protons introduced by KH, which have to be released in order to obtain the right electronic configuration {MNNM}$^{10\pi}$.

Nitrogen atom transfer to CO or isonitriles was accomplished, generating isocyanate and carbodiimide complexes. C-N bond formation is accompanied by reduction of V(V) back to V(III). The isocyanate ligand can be replaced by addition of alkynes. In toluene solution, potassium isocyanate precipitates under quantitative formation of [(ONO)V(η^2-MeCCMe)]. Regeneration of the starting material [(ONO)V(THF)] is possible by simply dissolving the complex in THF and removing the volatiles under vacuum. Therefore, a synthetic cycle comprising N$_2$ splitting into nitrides, nitrogen atom transfer to CO, release of isocyanate and regeneration of the starting material is accomplished.
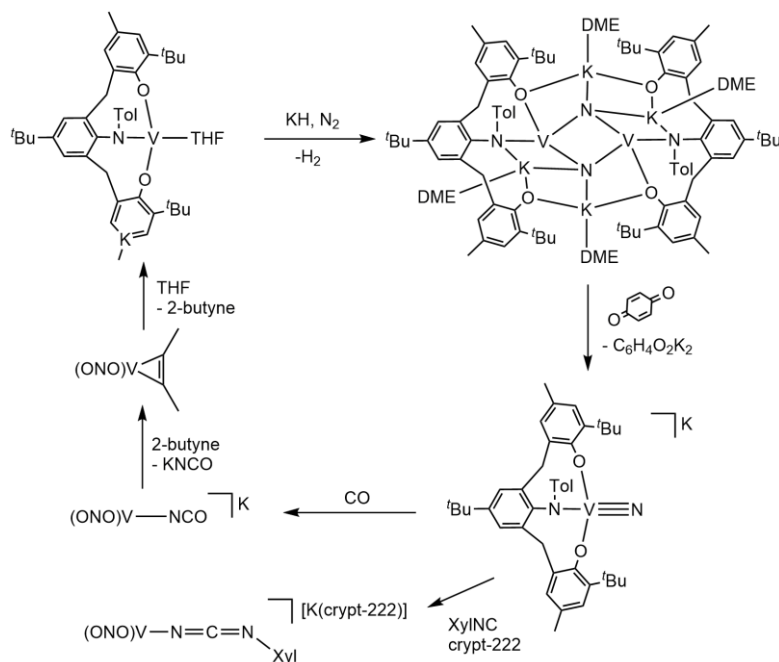
Scheme 29: Synthetic cycle for N$_2$ to isocyanate conversion promoted by vanadium complexes.

The group of *Mindiola* examined N$_2$ activation with vanadium(II) in analogy to *Cummins'* molybdenum(III) complex. [128] The complex (nacnac)V(ODiiP) (nacnac = [(2,6-^{i}Pr$_2$C$_6$H$_3$)NC(CH$_3$)]$_2$CH; ODiiP = 2,6-di-*iso*-propylphenoxide) exhibits trigonal planar geometry around vanadium and SQUID data is consistent with a V(II, d^3) high spin configuration. With N$_2$ the end-on bridged, diamagnetic compound [(nacnac)(ODiiP)V]$_2$(μ-η^1-η^1-N$_2$) is formed, displaying significant N$_2$ activation and two antiferromagnetically coupled V(III) centers. However, the complex turned out to be indefinitely stable at room temperature. Thermally and photochemically only liberation of N$_2$ was observed under regeneration of the starting material (Scheme 30). Reduction also failed to cleave the N$_2$ bond. To gain more insights into why the vanadium dimer does not split N$_2$, despite having the right geometry and electron configuration, DFT calculations have been carried out. The results show that N$_2$ cleavage from the dimer into terminal nitrides is thermodynamically and kinetically prohibited, due to weaker d-π* interactions in both the dimer and the nitride and a large enery barrier for structure distortions in the rigid ligand framework. To achieve a zigzag like structure and allow for transition between π and σ subspaces, structural changes are necessary, which are precluded by the chelating nacnac ligand.
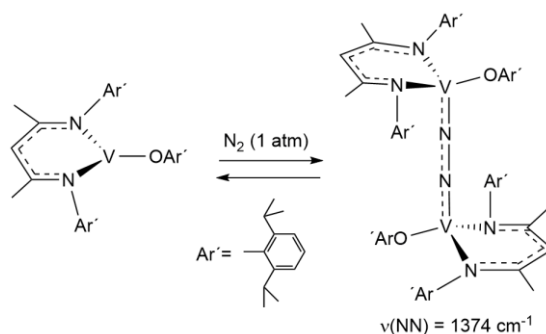
Scheme 30: Reversible formation of dinuclear N$_2$ bridged [(nacnac)(ODiiP)V]$_2$(μ-η^1-η^1-N$_2$).

Niobium: First N$_2$ cleavage using niobium was reported for calix[4]arene systems. The dimer M$_2$\{[(*p*-*t*Bu-calix[4]-(O)$_4$)Nb]$_2$(μ-η^1-η^1-N$_2$)\} was prepared from [\{p-*t*Bu-calix-[4]-(O)$_4$\}$_2$Nb$_2$(μ-M)$_2$] (M = Li, Na, K) containing a Nb(III)=Nb(III) double bond by simple addition of N$_2$.[129,130] The bridging dinitrogen is considerably activated (d(NN) = 1.390(17) Å, υ(NN) = 1372 cm^{-1} for M = Na). Two electron reduction of the dimer using Na in THF results in N$_2$ cleavage and formation of bis(μ-nitrido) species [\{p-*t*Bu-calix[4]-(O)$_4$\}$_2$Nb$_2$(μ-N)$_2$(μ-Na)$_2$Na$_2$], which turned out to be in solution in equilibrium with the terminal Nb(V) nitride Na$_2$[\{p-*t*Bu-calix[4]-(O)$_4$\}NbN]. The role of the solvent was revealed to be crucial as in DME (dimethoxyeethane) another main-product was found, where the NN bond was retained and a Nb-Nb bond formed. In this [\{p-*t*Bu-calix[4]-(O)$_4$\}$_2$Nb$_2$(μ-η^2-η^2-N$_2$)(μ-Na)$_3$-Na] complex, dinitrogen is side-on coordinated, stabilized by additional interactions with the sodium metals and preorganized to form the bridging nitrides. Heating of the latter consistently led to the bis(μ-nitrido) compound again. Formation of the side-on coordinated compound was attributed to a metal centered reduction and stabilization of this biradical by metal-metal bond formation. Thermally induced electron transfer from the metals to nitrogen, then cleaves the NN bond. If the reaction of the Nb=Nb starting material with N$_2$ is carried out in toluene instead of DME or THF, no N$_2$ bridged complex could be isolated but the formation of trinuclear nitride bridged [\{p-*t*Bu-calix[4]-(O)$_4$\}$_3$Nb$_3$(μ-N)$_2$Na$_3$] is assumed, which breaks up upon addition of TMEDA into the bis(μ-nitrido) compound [\{p-*t*Bu-calix[4]-(O)$_4$\}$_2$Nb$_2$(μ-N)$_2$\{μ-Na$_2$-(TMEDA)$_2$\}Na$_2$] and the single nitride bridged species [\{p-*t*Bu-calix[4]-(O)$_4$\}$_2$Nb$_2$(μ-N)][Na(TMEDA)$_2$].The different reaction mechanisms and products are attributed to different reaction rates in each solvent, which allows for fine tuning of the desired products.[130]

Heterobimetallic N$_2$ cleavage was demonstrated by the group of *Cummins* in 2000, comprising molybdenum and niobium triamido complexes. Nucleophilic reactivity at the β-nitrogen of [(N$_2$)Mo(N[R]Ar)$_3$]$^-$ has been demonstrated (see chapter 5.1).[87] Accordingly, reaction of NbCl(N[*i*Pr]Ar)$_3$ with [Na(THF)$_x$][(N$_2$)Mo(N[R]Ar)$_3$] afforded neutral, paramagnetic N$_2$ bridged complex (Ar[*t*Bu]N)$_3$Mo(μ-N$_2$)Nb(N[*i*Pr]Ar)$_3$ (Scheme 31).[131] One electron reduction yielded the known molybdenum(VI) nitride (Ar[*t*Bu]N)$_3$MoN and the isoelectronic terminal nitride [K(cryptand-222)][(N)Nb(N[*i*Pr]Ar)$_3$]. Oxidation of the latter produced a niobazene cyclic trimer \{(μ-N)Nb(N[*i*Pr]Ar)$_2$\}$_3$ in up to 41% yield. Interestingly, the trimer exhibits 2 different Nb-N bond length, one short (average d(NbN) = 1.791(7) Å) and one long (average d(NbN) = 2.004(6) Å), which are attributed to π-interactions with the amide lone pairs of the ancillary ligands. Importantly, *Cummins* and coworkers developed a synthetic cycle for N$_2$ to nitrile conversion, similar to the homometallic molybdenum system, published shortly after.[110,132] Addition of [(N$_2$)Mo(N[R]Ar)$_3$]$^-$ to the niobium(IV) compound Nb(OTf)(N[Np]Ar)$_3$ (Np = neopentyl) affords the heterodinuclear complex (Ar[Np]N)$_3$Nb(μ-N$_2$)Mo(N[*t*Bu]Ar)$_3$, which splits N$_2$ upon 1 electron reduction to the respective terminal nitrides. In a methathetical N for OCl

exchange, addition of acyl chlorides RC(O)Cl generates nitriles RCN, NaCl and the niobium(V)-oxo complex Nb(O)(N[Np]Ar)$_3$. By addition of trifluoromethanesulfonic anhydride (Tf$_2$O), the oxo-group is converted into triflate (OTf), generating Nb(OTf)$_2$(N[Np]Ar)$_3$. The latter can be reduced with CoCp$_2$ to the starting compound Nb(OTf)(N[Np]Ar)$_3$.[132] By ligand modification an acylimido complex could be trapped, which converts into the oxo-complex upon heating. Therefore acylimido complexes are implicated as intermediates in nitrile generation. A variety of nitriles can be synthesized in high yield, providing the opportunity of selective, atom-efficient ^{15}N-labelling employing ^{15}N$_2$.
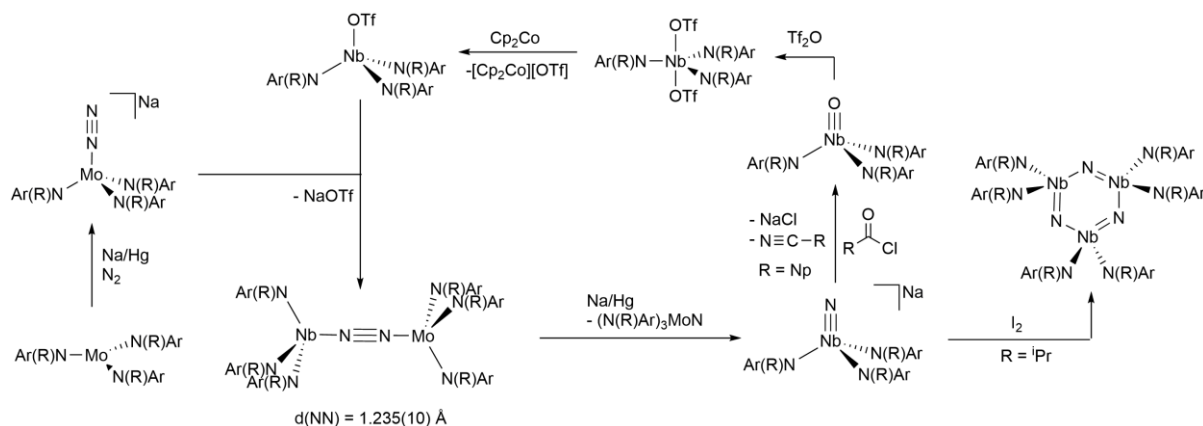
Scheme 31: Synthetic cycle for N$_2$ to organonitrile conversion mediated by a heterobimetallic Nb/Mo system.

The niobium(III) compound [P$_2$N$_2$]NbCl (P$_2$N$_2$ = PhP(CH$_2$SiMe$_2$NSiMe$_2$CH$_2$)$_2$PPh) can be reduced under N$_2$ atmosphere to afford paramagnetic dinuclear {[P$_2$N$_2$]Nb}$_2$(μ-η^1-η^1-N$_2$) (Scheme 32).[133] Magnetic measurements reveal the existence of two antiferromagnetically coupled Nb(IV, d^1) centers and therefore a [N$_2$]$^{4-}$ bridge. Consistently, protonation of the dimer with HNMe$_3$Cl yields hydrazine in 62% yield. Heating of the dimer at 110°C for 12 h results in formation of a new paramagnetic compound, which was identified as single nitride bridged dinuclear complex. The second nitrogen of the N$_2$ unit was observed to insert into the ligand backbone giving [PN$_3$]Nb-(μ-N)-Nb[P$_2$N$_2$] ([PN$_3$] = PhPMe(CHSiMe$_2$NSiMe$_2$CH$_2$P(Ph)-CH$_2$SiMe$_2$NSiMe$_2$N)). Magnetic examinations as well as crystallographic data support disproportionation of the two Nb centers into a Nb(III, d^2)/Nb(V, d^0) couple with S = 1.
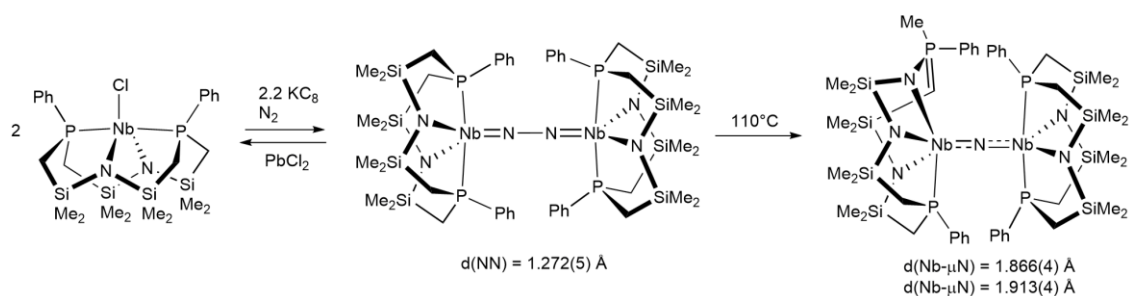
Scheme 32: N$_2$ cleavage into a bridging nitride under insertion of one nitrogen in the M-P bond.

The mechanism of the splitting reaction is proposed to proceed via initial nitride formation. Phosphine attack at the nitride allows for P-N bond formation. Subsequent insertion of the nitride into the C-Si bond results in N-Si bond formation and transfer of the methylene group to the phosphorous. The resulting phosphamethylene is then protonated from an adjacent CH$_2$ group. However, the {MNNM}$^{8\pi, 2\delta}$ unit is not in agreement with the electronic configuration for NN splitting stated in chapter 5. The complex may be destabilized by the two strong π-donors in the ligand backbone, opening the possibility of induced NN splitting by phosphine attack at one nitrogen. Following DFT studies compared *Fryzuk'*s Nb system with *Cummins'* Mo system.[134] In contrast to the latter, N$_2$ cleavage was calculated to be largely endothermic from the Nb-N$_2$-Nb dimer to terminal nitrides, whereas formation of the single bridging nitride was found exothermic. The ligand constraints in the [P$_2$N$_2$] were observed to have a dramatic effect on the overall reaction enthalpy, but especially on the N$_2$ cleavage step. Allowing the ligands to relax, revealed rotation of the amides about 90°C in a way that they lie in plane with the Nb-N bond. In this way the product nitride was found significantly lower in energy. Additionally, the exchange of the PR$_3$ groups by NR$_3$ groups were found to similarly increase the exothermicity of the reaction, as the resulting nitride would be considerably more stabilized with more electronegative and stronger bonding amine ligands.

In 2002, the group of *Kawaguchi* demonstrated N$_2$ cleavage by reduction of a Nb(V) dimer.[135] The complex [Nb(^{t}Bu-L)Cl$_2$]$_2$ with tridentate aryloxide ligands was reduced with 6 equivalent LiHBEt$_3$ and formation of the bis(μ-nitrido) complex [{Nb(^{t}Bu-L)(μ-N)Li(thf)}$_2$] was observed in 41% yield. As reduction under argon afforded a bridging hydride complex, dinitrogen splitting was considered to proceed via such an intermediate under H$_2$ elimination. This assumption was supported when in 2007 a (μ-H)$_4$ complex was isolated.[136] HNEt$_3$([O$_3$]NbCl$_3$) (H$_3$[O$_3$] = tris(3,5-di-tert-butyl-2-hydroxyphenyl)methane) can be reduced with 4 equivalents of LiHBEt$_3$ to generate K$_2${([O$_3$]Nb)$_2$(μ-H)$_4$} under reduction of Nb(V, d^0) to Nb(IV, d^1). The small Nb-Nb distance in the crystal structure indicates a metal-metal bond, accounting for the observed diamagnetism of this species. Interestingly, although rather high valent, the complex reacts with N$_2$ under H$_2$ elimination and N-N bond cleavage to the bis(μ-nitrido) complex K$_2${([O$_3$]Nb)$_2$(μ-N)$_2$} (Scheme 33). Four of the six electrons needed

for N$_2$ splitting have been stored in the hydride ligands and two in the metal-metal bond, allowing for splitting without further reagents. Addition of 2,6-lutidinium chloride results in formation of ammonia in 61% yield under formation of the chloride complex ([O$_3$]NbCl$_3$)$^-$.[137] The latter can be recycled to hydrido complex K$_2${([O$_3$]Nb)$_2$(μ-H)$_4$} with KHBEt$_3$, thus generating a synthetic cycle for conversion of N$_2$ into NH$_3$.
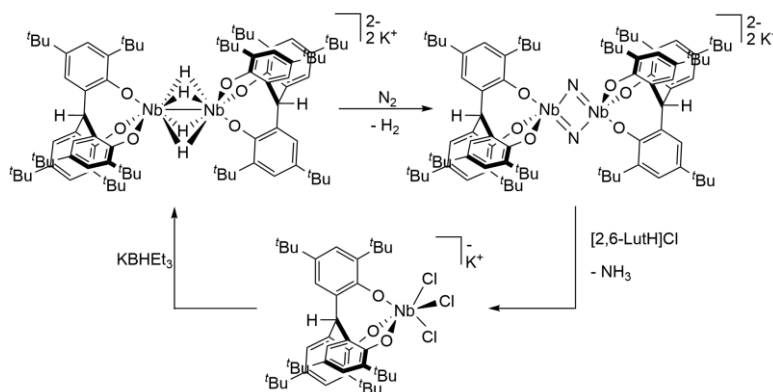
Scheme 33: Synthetic cycle for N$_2$ derived ammonia formation mediated by a Nb triaryloxide complex.

C-N bond formation was demonstrated by addition of methyl iodide (MeI) (Scheme 34). Whereas one bridging nitride is readily methylated, methylation of the second needs prolonged heating yielding neutral ([O$_3$]Nb)$_2$(μ-NMe)$_2$ after 5d at 60°C.[136] Cleavage into monomers is accomplished by addition of a Lewis base: Addition of pyridine (py) generates the mononuclear imido complex [O$_3$]Nb(NMe)(py)$_2$.[137] Whereas the bridging nitride species does not react with CO$_2$, presumably because of low nucleophilicity and large steric bulk, a reaction of the mononuclear imido complex and CO$_2$ is observed generating a mixture of ureate complex [O$_3$]Nb[(NMe)$_2$CO](py) and dinuclear bis(μ-oxo) {[O$_3$]Nb}$_2$(μ-O)$_2$ in a 2:1 ratio. The reaction is proposed to proceed via initial [2+2] addition of CO$_2$ with subsequent extrusion of isocyanate MeNCO and formation of an oxo complex, which then dimerizes. Isocyanate is reacting with another imido complex to form the observed ureate complex. However, no intermediates or free MeNCO could be detected. Liberation of the carbodiimide out of the product has not been shown yet.
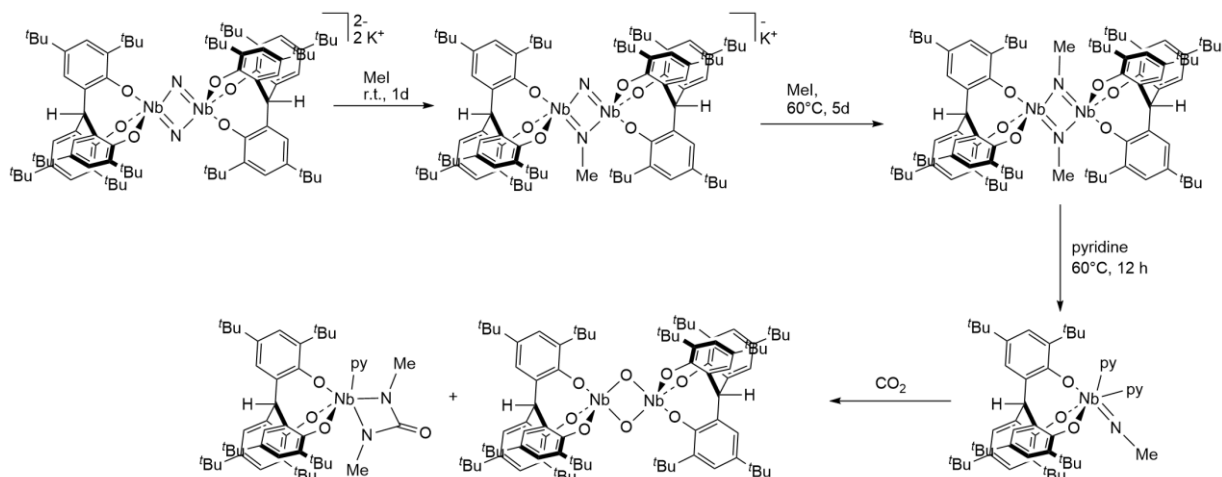
Scheme 34: Functionalization of N_2 derived bis(µ-nitrido) Nb complex with MeI.

The group of Mindiola recently demonstrated N_2 splitting starting from Nb(IV) and Nb(V) aryloxide complexes under reducing conditions.[138] 4 electron reduction of dinuclear complex $[(ArO)_2Nb(\mu-Cl)Cl_2]_2$ (ArO = 2,6-bis(diphenylmethyl)-4-*tert*-butylphenoxide) yields the Nb(III) compound $K_3[(ArO)_4Nb_2(\mu-Cl)_3Cl_2]$, which is stable towards dinitrogen (Scheme 35). Two electron reduction yields Nb(IV) complex $[trans-(ArO)_2NbCl_2(THF)_2]$. Four electron reduction of the latter or direct six electron reduction of the dinuclear starting material readily affords the bis(µ-nitrido) complex $[(ArO)_2Nb]_2(\mu-N)_2$ at room temperature. Further reduction is possible yielding anionic $K[(ArO)_2Nb]_2(\mu-N)_2$, which can in turn again be oxidized to the neutral form. Addition of anhydrous HCl (ex.) to both nitrido complexes led to formation of NH_4Cl. However, a synthetic cycle was not possible, as also the aryloxide ligands are protonated and dissociate. Since the chloride bridged Nb(III) complex does not react with N_2, the authors conclude that bridging chlorides or metal-metal bonds prevent reactions with N_2.
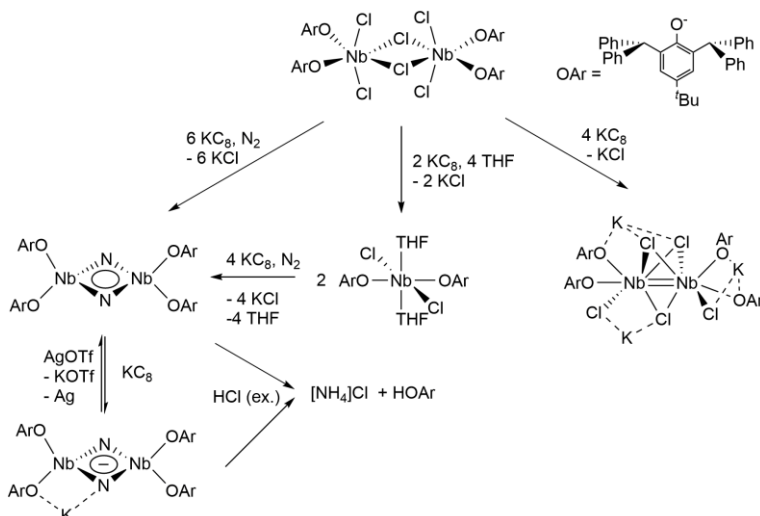
Scheme 35: Reduction of a Nb(V) dimer with different reducing equivalents.

Tantalum: Storage of reducing equivalents for N$_2$ in the form of hydrides has been well examined with tantalum complexes. *Fryzuk* and coworkers demonstrated that dinuclear Ta(IV) hydride complex {[NPN]Ta}$_2$(μ-H)$_4$ ([NPN] = PhP(CH$_2$SiMe$_2$NPh)$_2$) reacts with N$_2$ to partially release H$_2$ and to produce dinitrogen compound {[NPN]Ta}(μ-H)$_2$(μ-η^2-η^1-N$_2$) with N$_2$ being bound side-on end-on.[81] Subsequent treatment with boranes[139], silanes[140–142], aluminum or zirconium hydrides[143,144] or with 1,2-cumulenes[145] led to cleavage of the dinitrogen bond.

A surface organometallic approach for N$_2$ functionalization is examined in the group of *Quadrelli*. Ta(III) and Ta(V) hydrides are grafted on a silica surface and exhibit thermal robustness without dimerization or sintering, preserving the molecular site isolation and environment of homogenous complexes. These silica supported complexes [($\equiv$SiO)$_2$TaH$_x$] (x = 1, 3) not only activate ammonia or hydrazine, but also N$_2$.[146–148] The reaction with N$_2$ produces imido-amido-tantalum(V) [($\equiv$SiO)$_2$Ta(=NH)(NH$_2$)] at 250°C under atmospheric pressure of H$_2$.[146] DFT calculations reveal that tantalum always stays in its high oxidation state and dinitrogen is reduced by hydride transfers or reduction with H$_2$, which is the source of protons and electrons.[149]

The group of *Sita* examined all group 5 metals in the Cp*am ligand framework towards reactions with N$_2$.[63] They discovered, that reduction of the vanadium(III) precursor Cp*amVCl under N$_2$ leads to thermally robust dinuclear [Cp*amV](μ-η^1-η^1-N$_2$). Similar to *Mindiola*'s experiments (see above) N$_2$ cleavage did not seem to be possible and only replacement of N$_2$ with isonitriles was observed. End-on N$_2$ bridged complexes with niobium[63] and tantalum[61] were also synthesized and these display significantly stronger N$_2$ activation (see Table 1). The stability of the dimers strongly depends on the substituents of the amidinate ligand with bigger substituents like phenyl, producing the most stable complexes. Small ligand substituents like methyl and/or temperatures above 0°C afford the respective bis(μ-nitrido) complexes, thus thermal cleavage of the N-N bond (Scheme 36). The niobium N$_2$ complexes turned out to be the least stable, cleaving directly into the dinuclear nitride species with methyl substituted amidinate. Kinetic measurements suggest that the energy barrier for N$_2$ cleavage with niobium is significantly smaller as for the tantalum analogue and sterically demanding substituents stabilize the N$_2$ complex kinetically. The mechanism is likely to proceed via side-on coordinated N$_2$ as it has been proposed for *Floriani*'s[130] and *Fryzuk*'s[133] niobium complexes and by theoretical investigations.[94,150] As intermediate mononuclear nitrides could not be ruled out, additional experiments were performed by isotopic labelling.[63] Kinetic isotope effects as well as crossover experiments support side-on configuration. In addition, treatment of the tantalum end-on bridged N$_2$ complex with N$_2$O generated side-on bound N$_2$ and a bridging oxo [Cp*amTa]$_2$(μ-η^2-η^2-N$_2$)(μ-O), confirming that this coordination mode is possible with Ta(V). Functionalization of the tantalum nitride could be achieved in terms of N-Si bond formation with silanes.[61] No reaction of the

nitride with H$_2$ could be observed and DFT calculations show a large energy barrier as well as high endothermicity for this hydrogenation.[150]
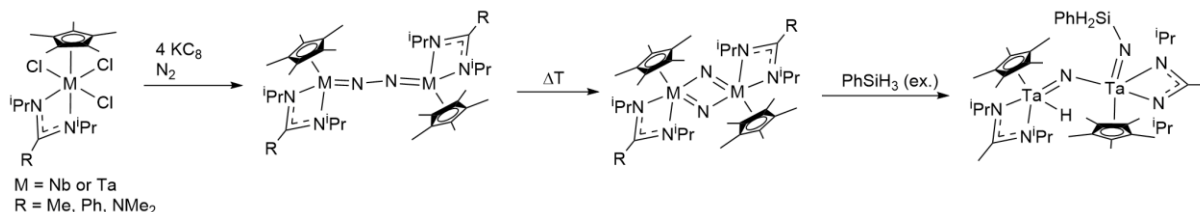
Scheme 36: Reduction of Nb or Ta complexes to produce end-on bridging N$_2$ dinuclear dimers which thermally cleave the N-N bond and functionalization of the resulting nitrides with silanes.

6.4 Group 6

Thermal N$_2$ cleavage promoted by molybdenum

Molybdenum complexes are very well studied in N$_2$ activation chemistry, not only because Mo has been found in the cofactor of the nitrogenase, but also because of the aforementioned first defined N$_2$ splitting of *Cummins*. In 2012, the group of *Schrock* achieved full N$_2$ cleavage in terminal nitrides by employing a Mo(III) complex with POCOP pincer ligand (POCOP = 2,6-[OP(^{t}Bu)$_2$]$_2$C$_6$H$_3$).[151] Reduction of (POCOP)MoI$_2$ with Na/Hg and 15-crown-5 under N$_2$ atmosphere produces [Na(15-crown-5)][(POCOP)Mo(N)(I)] (Scheme 37). The Mo≡N bond length is comparable with *Cummins* Mo(VI) nitrido complex (d(MoN) = 1.659(2) Å and d(MoN) = 1.651(4) Å respectively). *Schrock*'s nitride however is in accordance with a Mo(IV) low spin formulation. The splitting mechanism has not been examined in detail, but it has been proposed to proceed via a (μ-η^1:η^1-N$_2$) bridged dimer analogous to *Cummins* system, which then splits into a Mo(V) nitride which is subsequently reduced to the observed anionic Mo(IV) nitride. Alternatively, presumably formed Mo(II)-N$_2$-Mo(II) dimer is first reduced by two electrons and cleaves thereupon. The last assumption would be supported by molecular orbital considerations in analogy to *Cummins* system. In both cases the starting compounds are isoelectronic Mo(III) complexes, but in *Schrock*'s system, the complex is in a fourfold geometry. In a MO scheme of the dimer, this results in two additional δ-orbitals. To reach the same {MNNM}^{10π} electron configuration as in *Cummins* dimer, there is need for 4 additional electrons (2 per molybdenum) consistent with experimental data. Another driving force for the N-N bond cleavage would then be the electronic repulsion between the two negatively charged molybdenum units.

Protonation of the nitrido complex with [Et$_3$NH][BAr$^F_4$] leads to formation of a neutral species, in which the proton bridges between the Mo and one P atom. Since

the nitride could not be protonated, catalytic ammonia formation seemed unpromising. So it was not surprising, that under *Nishibayahshi*´s conditions [36] only 0.34 equivalents and under *Schrock*´s catalysis conditions [31] 0.30 equivalents of ammonia were detected.
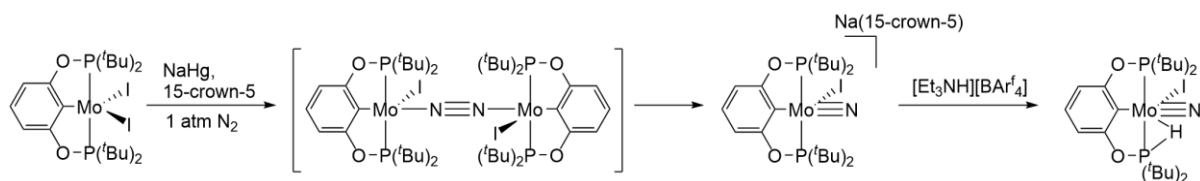
Scheme 37: N$_2$ Cleavage and subsequent protonation of the formed terminal nitride with Schrock´s {(POCOP)Mo} system.

Recently, the group of *Mézailles* reported N$_2$ splitting by 2 electron reduction of a Mo(III) complex with PPP pincer ligand (P^{Ph}P$_2$^{Cy})MoCl$_3$ in the presence of NaI under N$_2$ atmosphere.[152] An analogous mechanism to *Schrock*´s system has been proposed and the terminal nitride [(P^{Ph}P$_2$^{Cy})Mo(N)(I)] was observed in 80% spectroscopic and 60% isolated yield (Scheme 38). An intermediate Mo(I) dimer is in agreement with a {MNNM}$^{10\pi4\delta}$ electronic configuration as it may be involved in *Schrock*´s example. The respective η^1-η^1-N$_2$-bridged Mo(0) ({MNNM}$^{12\pi4\delta}$) compound with additional end-on coordinated N$_2$ [(P^{Ph}P$_2$^{Cy})Mo(N$_2$)$_2$(μ-N$_2$)Mo(N$_2$)$_2$(P^{Ph}P$_2$^{Cy})] was reported earlier and did not result in N$_2$ splitting into nitrides.[153]
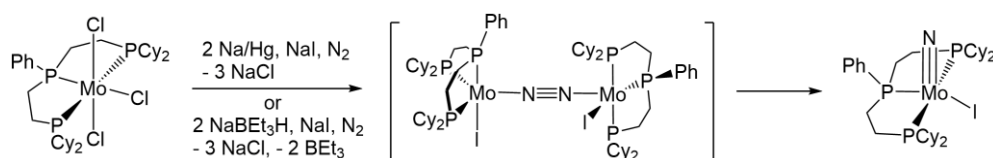
Scheme 38: 2 electron reduction of (PPP)MoCl$_3$ yielding the terminal nitride (PPP)Mo(N)(I).

The terminal nitride could be functionalized by addition of silanes under N-Si bond formation. Importantly, the use of bis(silanes) enables a second intramolecular Si-H insertion and generates free bis(silyl)amine and a molybdenum(II) hydride (Scheme 39). The latter could not be characterized yet, however reduction to Mo(II) could be verified by addition of PMe$_3$ and resulted in the isolation of [(P^{Ph}P$_2$^{Cy})Mo(H)(I)(PMe$_3$)]. Regeneration of the Mo(I) species to close a synthetic or even catalytic cycle could not be accomplished so far, but represents an intriguing approach. Removal of one H-atom would generate the Mo(I) species required for N$_2$ splitting without the need of strong reducing agents.
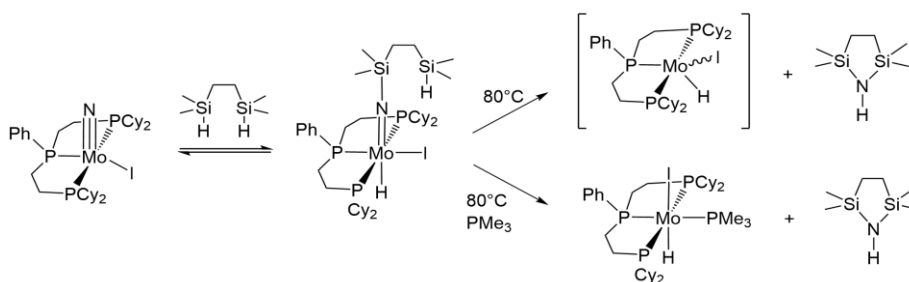
Scheme 39: Functionalization of a N$_2$ derived terminal nitride with bis(silanes).

N$_2$ cleavage by photolysis promoted by molybdenum and tungsten

First photoinduced N$_2$ splitting was demonstrated by the group of *Floriani* in 2001. Exposure of thermally stable [(Mes)$_3$Mo]$_2$(μ-η^1-η^1-N$_2$) to UV light (λ = 365.0 nm) produces the single nitrogen bridged compound [(Mes)$_3$Mo]$_2$(μ-N). *Floriani* proposes a mechanism that consists of initial light induced N$_2$ splitting into monomeric nitrides, which then act as a Lewis base and react with excess starting material to form a transient tetranuclear [Mo-N-Mo-N-N-Mo-N-Mo] species. This compound loses N$_2$ and forms the observed bridging nitride (Scheme 40). In agreement with a {MNM}$^{7\pi}$ system leading to a doublet spin state, the isolated compound is paramagnetic with μ_{eff} = 1.68 μ_B. The linear M-N-M core (179.1(3)°) displays M-N bond distances (d(MoN) = 1.952(5) and 1.936(5) Å) which are significantly longer than in similar [L$_3$Mo]$_2$(μ-N) compounds.[90,92,93] An alternative mechanism is proposed by *Cummins*, who could demonstrate N-N and M-N cleavage being in competition. Coupling of intermediate terminal nitride with (Mes)$_3$Mo would also generate the observed nitrogen bridged species.[85]
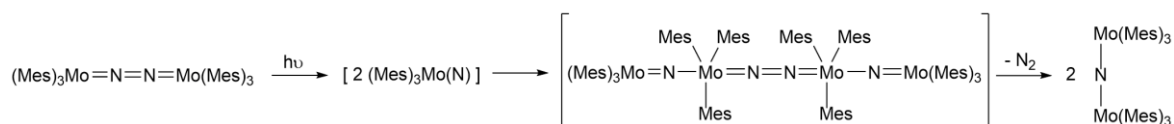
Scheme 40: N$_2$ cleavage by photolysis of N$_2$ bridged dimer [(Mes)$_3$Mo]$_2$(μ-η^1-η^1-N$_2$) as proposed by Floriani.

In 2014, the groups of *Nishibayashi* and *Yoshizawa* published an end-on N$_2$ bridged dimer supported by a ferrocenyldiphosphine ligand, which cleaves N$_2$ under visible light irradiation at room temperature into the corresponding terminal nitrides. Moreover, the nitrides can be oxidized to reform the N-N bond and to produce an N$_2$ bridged dimer again.[154,155] The dinuclear monocationic complex [{Mo(depf)(Cp*)}$_2$(μ-η^1-η^1-N$_2$)][BAr^F$_4$] (depf = 1,1'-bis(diethylphosphino)ferrocene) can either be oxidized to the dicationic compound or reduced to the neutral dimer (Scheme 41). As in the case of *Cummins* isolated N$_2$ bridged dimers (Figure 12), the

neutral complex exhibits the lowest N_2 activation and longest Mo-N bond distances (d(MoN) = 1.955(4) Å). With increasing positive charge, N_2 activation becomes larger (d(NN) = 1.226(4) Å for the cation, not depicted in Scheme 41). However, only the neutral complex contains a {MNNM}$^{10\pi}$ system stated necessary for splitting. Consistently, only the neutral complex cleaves the N-N bond, not thermally though, but upon photochemical excitation (580 nm > λ > 400 nm) to form the corresponding Mo(IV) terminal nitrides. Simulated UV/Vis spectra and electron density difference maps point out loss of electron density for a transition around 500 nm, which could therefore be responsible for the cleavage of the bridging N_2. Oxidation of the nitride leads to dimerization to the dicationic N_2-bridged complex [{Mo(depf)(Cp*)}$_2$(μ-η^1-η^1-N_2)][BAr$^F_4$]$_2$ (**A**). Coupling of nitrides is usually observed for late transition metals. For rhodium and iridium nitrides a nitridyl radical M=N· is proposed as key reactive intermediate with spin density being almost equally distributed over the M-N unit.[156,157] In contrast, nearly no spin density on the nitrogen could be found by DFT calculations for the molybdenum system. If oxidation is carried out in the presence of cyclohexadiene though, a mixture of the dicationic dimer and the cationic Mo(IV) imide results (**B**), demonstrating hydrogen atom abstraction still being possible. In the presence of a proton source, the same products are observed with concomitant generation of H_2. Besides, 0.37 equivalents of ammonia could be detected by reaction with excess CoCp$_2^*$ and [LutH][BAr$^F_4$] under argon.
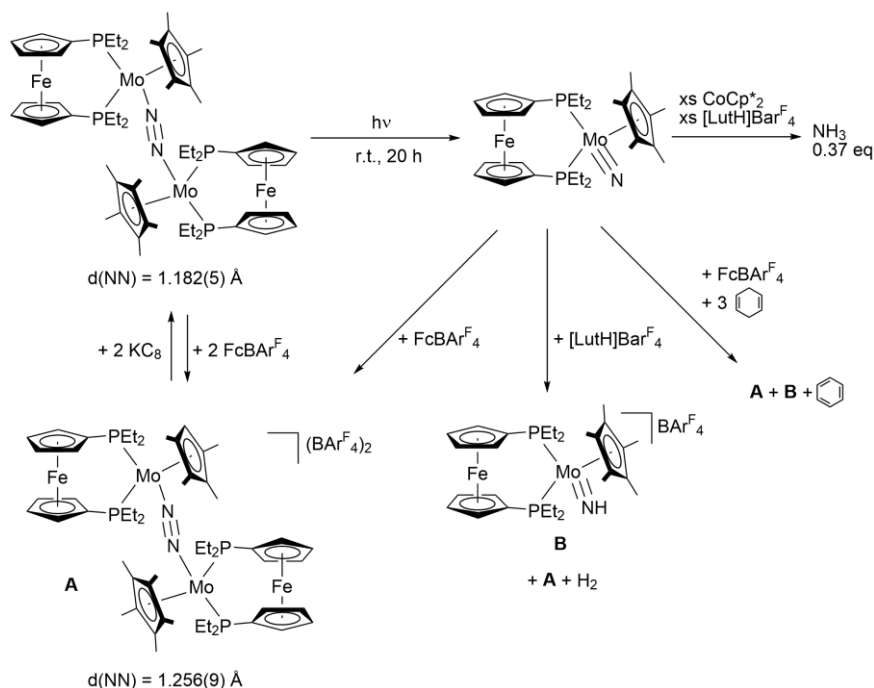
Scheme 41: N_2 cleavage and functionalization mediated by a {Mo(depf)(Cp*)} complex.

Sita and coworkers demonstrated formation of end-on coordinated N$_2$ bridged dinuclear molybdenum and tungsten complexes bearing Cp* and amidinate ligands.[62] These complexes exhibit a {MNNM}$^{8\pi, 4\delta}$ unit and proved to be thermally stable. Exposure to irradiation however, results in splitting of the N-N bond.[158] In the case of molybdenum two products were identified, a bis(μ-nitrido) complex [Cp*amMo]$_2$(μ-N)$_2$ with formal Mo(V, d^1), Mo(V, d^1) centers and a single nitrogen bridged species [Cp*amMo]$_2$(μ-N) with formal Mo(III, d^3), Mo(IV, d^2) centers (Scheme 42).
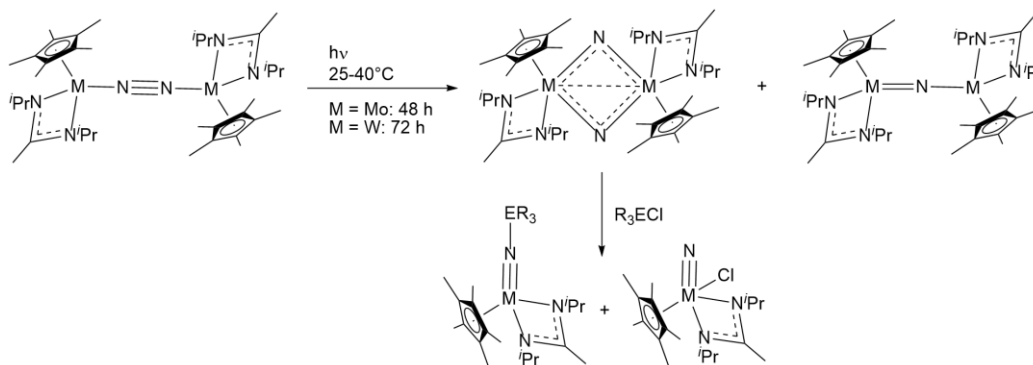
Scheme 42: N$_2$ cleavage in μ-nitrido and complexes and bis(μ-nitrido) complexes and functionalization of the latter with electrophiles.

These findings are consistent with the reported observation of both N$_2$ cleavage and N$_2$ extrusion upon photolysis of N$_2$-bridged dinuclear complexes as described earlier (see chapter 5.1).[85,99] For the corresponding tungsten analogues, only the bis(μ-nitrido) complex were found. These react with R$_3$ECl (R$_3$E = Me$_3$Si, Ph$_3$Si, Me$_3$Ge, Me$_3$C) to produce a 1:1 mixture of the mononuclear nitride-chloride complex Cp*amM(N)(Cl) and the functionalized imido complexes Cp*amM(N-ER$_3$). The mechanism is thought to proceed via chloride-atom abstraction and capture of the so formed ECl$_3$ radical to give two mononuclear species. Interestingly, combination of the photochemical N$_2$ cleavage with the functionalization in a one pot reaction yielded solely the imido complex and the dichloride Cp*amMCl$_2$ in a 2:1 ratio. Since reaction of the imido complexes with CO to liberate isocyanates under formation of a bis-CO complex had been shown before, N$_2$ derived nitrogen group transfer is possible with isocyanate yields up to 64%.[158,159] The bis-carbonyl complexes is converted to the respective dichlorides by reaction with CO$_2$ and Me$_3$SiCl. The dichloride complexes can be reduced under N$_2$ atmosphere with sodium to yield the N$_2$-bridged dinuclear compounds again.[62] In this way, a synthetic cycle can be closed for transformation of N$_2$ into isocyanates. To simplify this multistep cycle, *Sita* and coworkers worked out a more efficient path (Scheme 43). Reaction of the imido complexes with CO$_2$ (1.4 - 4.8 bar) and excess Me$_3$SiCl produces directly the dichloride together with free isocyanate. Here, simultaneous nitrogen group and oxygen atom transfer takes place. The whole N$_2$ fixation reaction in one pot yielded up to 82% of recovered starting

material after one cycle, providing a highly efficient platform and an excellent starting point for catalytic N_2 functionalization.
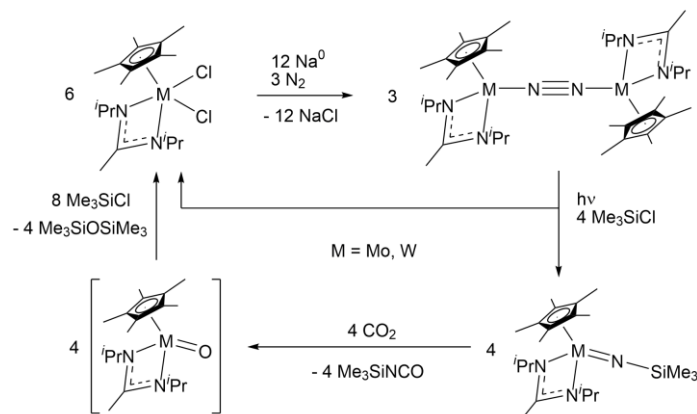
Scheme 43: Synthetic cycle for N₂ to isocyanate conversion by Sita.

Chromium: An evalution of the group of *Schrock* in 2006 pointed out, that N_2 activation with chromium is more difficult compared to molybdenum especially attributed to the low lying high spin states and the weak reduction potential of Cr(III) compounds.[160] In addition, DFT calculation in the group of *Stranger* predict N_2-splitting with Cr(III) in a triamido ligand system to be unlikely due to thermodynamic reasons.[97] In 2007 however, the first example of N_2 cleavage mediated by a well-defined chromium complex was reported by the groups of *Budzelaar* and *Gambarotta*.[161] Reduction of N_2 bridged dichromium complexes with diiminepyridine ligands {[{2,6-[2,6-(^{i}Pr)$_2$PhN=C(CH$_3$)]$_2$(C$_5$H$_3$N)}Cr(THF)]$_2$(μ-η^1-η^1-N$_2$) with 2 equivalents of NaH lead to a species with a bridging NNH unit. The N-N bond was elongated but still intact and the hydrogen stemmed from one of the methyl groups in the diimine ligand transferred in a formal hydrogen atom abstraction from carbon to the N_2 unit. Treatment with an additional equivalent of NaH, splits the N-N bond and forms an anionic chromium imide. Ammonia could be collected in 87% yield after addition of aqueous HCl and further workup. Another example of ammonia formation mediated by chromium N_2 complexes was reported by the group of *Mock* upon addition of several equivalents of acid to a formal chromium(0) bis(η^1-N$_2$) complex.[162] However, ammonia was only a side-product with the main product being hydrazine.

6.5   Group 7

For transition metals of group 7, no initial N_2 cleavage has been observed until the start of this PhD thesis in 2013, although nitrides are well-known.[105] For manganese,

dinitrogen coordination and even its functionalization into azomethane has been reported, however the N-N bond has not been cleaved.[163]

6.6 Group 8

Iron: Iron is together with molybdenum the most studied metal for dinitrogen activation, as both are present in the active site of the nitrogenase and iron surfaces are used as catalysts in the *Haber Bosch* process. Accordingly, there have been published many dinitrogen complexes of iron and formation of ammonia with such complexes is not unknown, however these complexes and/or their mechanisms are often rather ill-defined and yields are low.[46,164–167] Iron nitrides are also known and exhibit interesting reactivity. Ammonia formation by hydrogen atom transfer has been reported and even electrophilic character of iron nitrides by reactions with CO or isonitriles has been shown, pointing towards an intriguing path towards nitrogen functionalization into organic compounds.[168,169] Nevertheless, iron dinitrogen complexes have not been reported to cleave into defined nitrides until 2011. *Holland* and coworkers reported a multinuclear iron potassium complex with N₂-derived bridging nitride units.[170] The authors started their investigations using bulky, low coordinate iron(II) chloro complexes as starting materials, which are depending on their steric demand either mono- or dinuclear. Two electron reduction of the mononuclear β-diketiminate complex LFeCl (L = HC[C(^{t}Bu)N(2,6-^{i}Pr$_2$C$_6$H$_3$)]$_2$) yields dinuclear N₂ bridged K₂[LFeNNFeL], where dinitrogen is end-on bridging two iron centers and side-on to two potassium ions.[171] N₂ is relatively strongly activated for a formally iron(0) compound (d(NN) = 1.23 Å, υ(NN) = 1589 cm^{-1}).[164,166] Decreasing the steric bulk by using a methyl substituted diketiminate ligand led to the isolation of a compound containing 2 potassium, 4 iron, 2 chloride atoms together with two bridging nitrides (Scheme 44).[170] The N-N distance of 2.799(2) Å accounts for complete scission of the bond. The rather complicated structure involves one nitride bridging three iron centers and the other nitride bridging two irons and to potassiums. Each potassium interacts with two chlorides, which are connected to the fourth iron. NMR studies suggest that the structure is also held in solution. Mössbauer spectra reveal the existence of two high-spin Fe(II) and two high-spin Fe(III) centers, which is in agreement with a 6 electron reduction of N₂ by four formal Fe(I) formed by reduction of the Fe(II) precursor. The participation of four iron centers for N₂ reduction avoids the formation of high oxidation states and five Fe-N bonds provide a driving force for the reaction. Theoretical investigations indicate that initial formation of a FeNNFe core is followed by coordination of a third Fe(I) complex in a side-on mode, which is only possible if the steric demand of the ligands allows such a conformation. After rearrangement to a side-on / side-on / end-on conformation, the fourth iron coordinates and enables N-N cleavage. These investigations also point out

the importance of an alkali metal for stabilization of the resulting nitride.[172] Following research revealed that apparently the right number and size of the alkali metals influences the N-N splitting reaction. Too many alkali metals introduced by over-reduction or too big alkali metals like caesium have been found to inhibit N-N cleavage, presumably because they cannot hold the right geometry of the Fe$_3$(N$_2$) unit necessary for splitting.[173] Addition of 100 equivalents of anhydrous HCl gave ammonia in 82 ± 4 % yield, demonstrating the nucleophilic reactivity of the nitrides. Unfortunately, the complex degrades under these conditions what imposes difficulties to a catalytic application.[167,170] The bis(μ-N) complex is reported to degrade slowly in benzene solution at room temperature with the main decomposition product being a LFe(benzene) complex.[174] Therefore, coupling of the nitrides back to N$_2$ was assumed. Addition of strong π-acceptor ligands like isonitriles or CO supports this assumption as they stabilize the resulting Fe(I) species LFe(L´)$_3$ (L´ = CO, CNAr) under release of N$_2$. These results demonstrate that the system can both cleave and form the N-N bond without thermodynamic sinks which are often a problem in nitride chemistry.
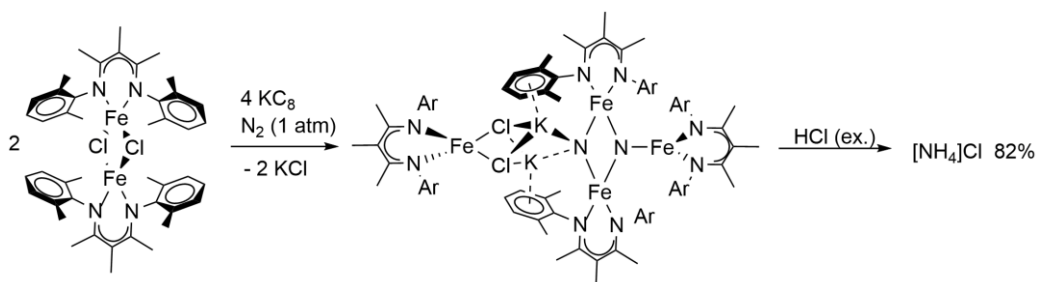
Scheme 44: N$_2$ cleavage and ammonia formation mediated by a dinuclear iron compound.

Murray and coworkers used the multimetal cooperative approach to design a triiron(II) complex, which is reported to cleave dinitrogen after reduction with KC$_8$ under N$_2$ atmosphere.[175] The three iron centers in the main product were found to bridge through three NH$_x$ functions. Mössbauer spectra show the presence of mixed-valent triiron (II/II/III) centers in the resulting complexes. Since there are three nitrogen atoms per cluster, intra- and inter-complex cooperativity is assumed for the N$_2$ splitting process. The origin of the hydrogens in the bridging NH$_x$ moieties could not be determined so far. Reaction in silylated glassware, deuterium labelling experiments and addition of compounds with weak C-H bonds (9,10-dihydroanthracene) did not give any satisfactory results. Upon addition of HCl about 30% of ammonia could be detected, indicating that only one of three nitrogen units can be liberated in this way.

Ruthenium: Despite many ruthenium N_2 complexes, cleavage of the N≡N bond has not been observed so far. Ruthenium nitrides on the other hand are well-known and even reported to react with H_2 to form ammonia.[176] Nevertheless, ruthenium dinitrogen complexes show only minor N_2 activation and N-N bond splitting in defined complexes has only been reported for the reaction of ruthenium hydride complexes with hydrazine.[177,178] DFT calculations however, suggest ruthenium pincer complexes to be the most promising of the group 8 metals concerning NH_3 formation from N_2 and H_2.[179]

Osmium: Osmium dinitrogen complexes have not been shown to cleave N_2 in the electronic ground state so far. *Vogler* and coworkers demonstrated however N_2 cleavage from the mixed valent Os(II)/Os(III) complex $\{[(NH_3)_5Os](\mu\text{-}\eta^1\text{-}\eta^1\text{-}N_2)\}^{5+}$ by irradiation in aqueous solution.[180] Formation of the osmium(VI) nitride $[Os^{VI}(NH_3)_4N]^{3+}$ was stated by comparison of UV/Vis and excitation spectra. Another product was identified as $[Os^{III}(NH_3)_4(H_2O)]^{3+}$. Disproportionation of the unstable osmium(V) nitride $[Os^V(NH_3)_4N]^{2+}$ as intermediate after N_2 cleavage is assumed. Consistently, in the presence of oxygen as oxidant the yield in Os(VI) nitride product was enhanced. Striking is the presumed protonation of intermediate $[Os^{IV}(NH_3)_4N]^+$ to release ammonia and form the observed aqua-complex. The presence of Os^{II} turned out to be crucial as by irradiation of the Os(III)/Os(III) dinitrogen bridged complex in a qualitative experiment only vigorous evolution of N_2 was observed. The higher energy of metal to ligand charge transfer (MLCT) for Os^{III} compounds was attributed to this observation. Irradiation of the mixed-valent species in the presence of OCl_2 yielded a new species, which was identified as $[Os(NH_3)_5NO]^{3+}$ and represents unusual oxidative N_2 cleavage.[181]

7   Scope of this work

Several examples for transition metal (TM) mediated inital N_2 splitting were described in the previous chapter. However, defined systems for full 6 electron reduction of N_2 into nitrides still remain scarce. The formation of strong M-N bonds in order to overcome the large N_2 dissociation energy is a prerequisite, accordingly examples are reported commonly for early transition metals until group 6.. As the bond dissociation energies (BDEs) for diatomic $[M{\equiv}N]^+$ decrease along the TM series (M = Ti–Cu), N_2 cleavage into nitrides is favored with these systems.[182] However, the main disadvantage of these formed terminal nitrides is their stability and inertness towards N-centered functionalizations due to the aforementioned strong $M{\equiv}N$ bonds. Even if such functionalizations are achieved, the availability of empty d-orbitals caused by high oxidation states strengthens the resulting $M\text{-}NR_x$ bond and liberation of the functionalized nitrogen containing moiety is subject to significant kinetic and thermodynamic barriers.[14]

By going to the right in the periodic table, more electron rich complexes are generated and population of M-N π^* orbitals disfavors multiple bonded nitrogen. Low valent late transition metal terminal nitrides are challenging to synthesize and only few examples for such complexes are reported, employing iron,[183–187] ruthenium,[176,188] osmium,[189] rhodium[157,190] and iridium,[156,191] albeit not from N_2.[14]

Aim of this thesis is combining strong $M{\equiv}N$ BDE and thus enabling N_2 cleavage with mid to late transition metal nitride reactivity observed for electron rich complexes. Rhenium as group 7 element accounts for the metal of choice. N_2 splitting into nitrides, their functionalization and finally the liberation of nitrogen-containing compounds on the same metal platform represents the central goal.

As described in chapter 5, prerequisite for N_2 cleavage is an $\{MNNM\}^{10\pi}$ entity, which affords a low valent rhenium species as stable precursor for N_2 activation. Furthermore, the complex must allow for N_2 coordination, i.e. by offering a vacant coordination site. Flexible platforms for stabilizing various oxidation states have been successfully demonstrated by the *Schneider* group with the PNP pincer ligand of two phosphine and one amide donor bridged by an ethylene backbone prone to further amide donor fine tuning by ligand oxidation. By variations of the ligand such as reduction of steric bulk on phosphorous or decreasing the amides π-donor strength upon backbone oxidation, the splitting process can be examined in more detail to get more insights about the requirements and steric and electronic influences.

With the nitride in hand, functionalization experiments and reactivity studies will be executed. Rhenium nitrides usually react nucleophilic,[105] however electrophilic reactivity cannot be excluded. The aim of all functionalization reactions is to extrude the nitrogen containing moiety in order to convert N_2 into chemically more valuable compounds. Standard experiments comprise protolysis or hydrogenation reactions to liberate ammonia. As described in chapter 1, about one-fifth of all NH_3 produced in the *Haber-Bosch* process is used for organic molecules.[11,12] In this regard, N_2 is reduced to NH_3 in a tremendously energy extensive process, which then needs to be reacted in a second step with organic compounds, like alkenes. Therefore, using N_2 directly as NH_3 surrogate under ambient conditions is an appealing goal. Especially organic nitriles represent an attractive synthetic target, as the conversion of N_2 to RCN conserves the high energy triple bond. Therefore, the high energy demand for the cleavage of the strong $N{\equiv}N$ bond (941 kJmol^{-1}) can be offset by the formation of strong $C{\equiv}N$ bonds ($D^0(HC{\equiv}N) = 937$ kJmol^{-1}) in a "triple bond metathesis", rendering this reaction thermodynamically feasible.[111]. Besides, generation of amines by hydrogenation of an alkylimido complex represents an interesting target reaction.

Therefore, C-N bond formation will be focused. The formed imido complexes must be characterized and transformed into amines by hydrogenation or to nitriles. Possible strategies for the latter reaction type have been demonstrated by *Cummins* and *Tuczek*.[110,112,132,192] Envisaged is not only the extrusion of the formed nitrile, but also the recovery of the starting material to close a synthetic cycle. Such a cycle comprising N_2 splitting, functionalization and liberation of N-containing molecules represents the final goal of all efforts.

II   Results and discussion

1 Re(III) starting platform

1.1 (PNP^{tBu})ReCl$_2$

Parts of this chapter were published in the *Journal of the American Chemical Society* under the title: *"Dinitrogen Splitting and Functionalization in the Coordination Sphere of Rhenium"* in 2014.[193]

Precursor for the (PNP)Re(III) platform is the Re(V) complex Re(O)(Cl)$_3$(PPh$_3$)$_2$ (**1**), which can easily be prepared from commercially available Re$_2$O$_7$ or KReO$_4$.[194] Reduction of these oxo-complexes with excess PPh$_3$ in the presence of acetonitrile leads to the Re(III) precursor Re(Cl)$_3$(PPh$_3$)$_2$(NCMe) (**2**).[195] As ligand, the PNP pincer bridged by ethylene groups with *tert*-butyl substituents on the phosphorous atoms was chosen. As the aim was to synthesize an electron rich, coordinatively undersaturated species, the electronic donor properties of this ligand as well as the steric shielding of the substituents was thought to be beneficial. Accordingly, addition of pincer ligand ^{H}PNP^{tBu} to the Re(III) precursor **2** in THF solution together with a base (NEt$_3$) affords highly air sensitive, violet (PNP)ReCl$_2$ (**3**) after 2 h at reflux in high yield. Without a base, no selective reaction could be observed. In the following "PNP" without further indication always describes the monoanionic pincer ligand with *tert*-butyl substituents on the phosphorous atoms.
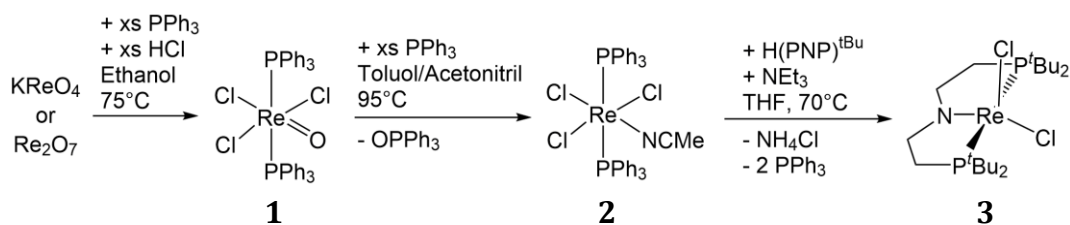
Scheme 45: Synthesis of Re(III) platform (PNP)ReCl$_2$.

On the NMR timescale, **3** exhibits C_{2v} symmetry, whereas in the crystal structure a distortion from both trigonal bipyramidale and square pyramidal geometry is observed (τ = 0.37). The complex is diamagnetic in the ground state ($\delta(^{31}P)$ = -51.5 ppm) attributed to the strong π-donor amide in the ligand backbone as indicated by the sum of bond angles around the nitrogen atom (360°) and the short Re–N distance (1.923(7) Å).[1]

*Figure 14: Molecular structure of **3** in the crystal. ORTEP plot with anisotropic displacement parameters drawn at the 50% probability level. The C–H hydrogen atoms are omitted for clarity. Selected bond lengths [Å] and angles [°]: Re1–Cl1 2.331(2), Re1–Cl2 2.364(2), Re1–N1 1.923(7), Re1–P1 2.402(2), Re1–P2 2.407(3); N1–Re1–Cl1 109.7(3), N1–Re1–Cl2 140.8(3), Cl1–Re1–Cl2 109.49(9), P1–Re1–P2 163.04(9).*

3 is thermodynamically stable (up to 110°C), but degrades quickly in the presence of moisture, oxygen or upon longer exposure (> 1 day) to chlorinated solvents (DCM). With acetonitrile as coordinating solvent, equilibrium formation was observed. Small amounts are tolerated (about 1-2 equivalents), whereas addition of 10 equivalents to a benzene solution of **3** yields a green precipitate, which reforms the violet starting material after separation and dissolution in THF. In a CD_2Cl_2/d_3-Acetonitrile mixture, the formation of a diamagnetic species ($\delta(^{31}P)$ = -18 ppm) displaying broadened signals in the ^{1}H-NMR, could be observed, that has not been fully characterized so far. However single crystals were obtained out of a benzene/acetonitrile/pentane solution, which confirm coordination of acetonitrile to **3** (Figure 15).[1] The Re-N_{MeCN} bond distance is elongated compared to the Re-N_{PNP} bond length (2.074(2) and 1.901(2) Å respectively) and in agreement with an ordinary single bond. The Re-N_{PNP} bond distance is even slightly shorter than in **3** (Δd = 0.02 Å). The amide is still planar (sum of angles:359°), but the acetonitrile ligand is a little bent (Re-N-C: 170.9 (2)°), indicating some "push-pull" relation by π-donation from the PNP-amide in metal orbitals, which backdonate into C-N antibonding orbitals of the nitrile ligand. The C≡N

---

[1] X-Ray diffraction was performed by Dr. Christian Würtele.

bond distance of the latter (1.137(3) Å) is however slightly shorter than for free acetonitrile (1.157 Å).[196]
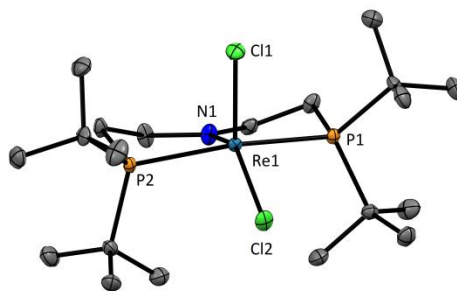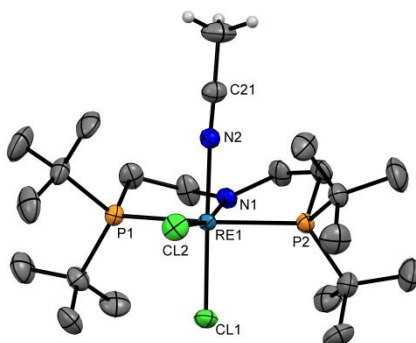

*Figure 15: Molecular structure of to **3** coordinated by acetonitrile. ORTEP plot with anisotropic displacement parameters drawn at the 50% probability level. The C–H hydrogen atoms are omitted for clarity, except for the acetonitrile ligand. Selected bond lengths [Å] and angles [°]:Re1–Cl1 2.3681(6), Re1–Cl2 2.5058(6), Re1–N1 1.901(2), Re1–N2 2.074(2), Re1–P1 2.4415(7), Re1–P2 2.4184(7), N2-C21 1.137(3); N1–Re1–Cl1 105.23(7), Cl1–Re1–Cl2 89.57(2), Cl2–Re1–N2 83.90(6) N2-Re1-N1 81.48(9), P1–Re1–P2 165.48(2), Re1-N2-C21 170.9(2).*

1.2 (^{H}PNP^{iPr})ReCl$_3$

The sterically less demanding *iso*-propyl derivate of the PNP ligand is well examined in our group[197–200] and prepared in a straightforward synthesis. To test, if the steric bulk is indeed a prerequisite for the synthesis of **3**, its application in the rhenium system was tested.

Heating a mixture of the free ligand ^{H}PNP^{iPr} and the precursor complex **2** in THF to 70°C for 1 h leads to a clear green solution of the Re^{III} compound [(^{H}PNP^{iPr})ReCl$_3$] (**4**, Scheme 46).
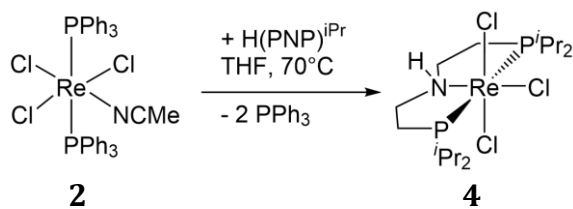
Scheme 46: Synthesis of PNP^{iPr}-derivative **4**.

In agreement with an octrahedrally coordinated complex with a d^4 electron count, the product shows paramagnetically shifted signals in the ^{1}H-NMR spectrum (Figure 16) and no ^{31}P-NMR signal. Interestingly, the observed signals are very sharp and even show some multiplet-like structure. One signal of the backbone protons is probably superimposed by the benzene signal and the amine proton is shifted far downfield (δ_H = 138.5 ppm). Some diamagnetic impurities could not be removed and the complex has not beeen fully characterized yet.
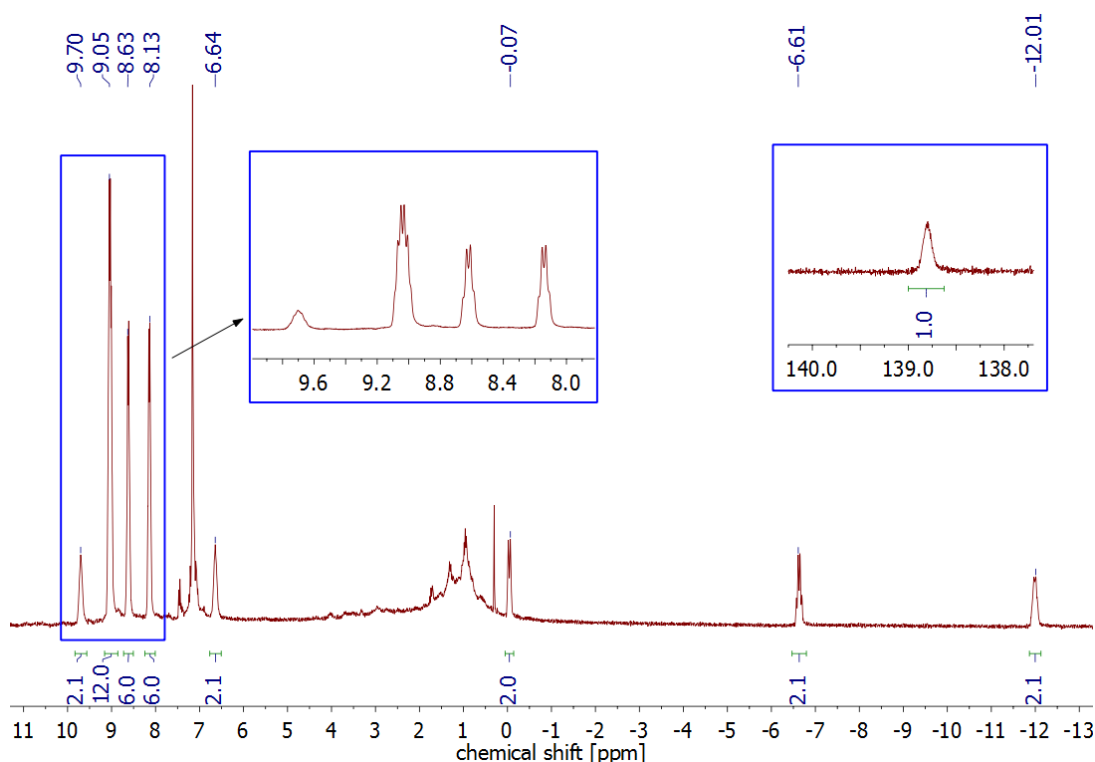
Figure 16: ^{1}H-NMR spectrum of **4** in C_6D_6.

In analogy to the synthesis of **3**, NEt$_3$ was added to the reaction mixture to deprotonate **4** in situ to a five coordinate dichloro species. However, no reaction was observed and also direct addition of NEt$_3$ to **4** does not lead to deprotonation.

Stronger bases were then tested. Deprotonation with 1 equiv. KBTSA or KO^{t}Bu gives two diamagnetic signals (δ_P = -1 and -18 ppm) in an about 2:3 ratio in the ^{31}P-NMR spectrum. However, these products have not been identified so far. Deprotonation employing 1,3,5-Triazabicyclo[4.4.0]dec-5-ene (TBD) as base results in selective formation of another product (δ_P = -6 ppm), which still contains signals corresponding to TBD in the ^{1}H-NMR spectra after workup. Single crystals of this complex could be obtained and X-ray analysis revealed coordination of hexahydropyrimidinopyrimidine (hpp) to the rhenium complex (Figure 17).[2] TBD can be deprotonated to hpp, a bisdentate ligand, forming the complex [(PNP^{iPr})Re(hpp)Cl] (**5**) upon elimination of two equivalents of HCl, although illustrating coordination and deprotonation of the PNP^{iPr} ligand (Scheme 47).
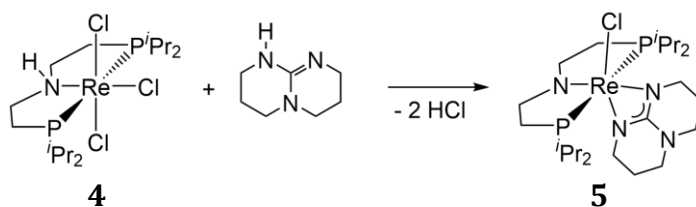
*Scheme 47: Reaction of **4** with TBD generating **5**.*

A disorder has been found in the unit cell of the crystal structure with a population of 0.878(2) on the main domain. The two substructures are quite similar and exhibit usual bond lengths. The Re-N$_{PNP}$ bond distance is comparable with **3** (1.9193(17) Å) and the amide is also planar (sum of angles at N = 359.6° and 360.0°) in both substructures of **5**. However, the C-N$_{PNP}$-C angle of the main structure (115.7(4)°) is about 3-5° larger than usually observed, whereas the same angle for the minor complex is particularly small (98.5(6)°). Different refinement did not change this result significantly. Striking difference in both substructures is the opposite orientation of the two ^{i}Pr-groups of the ligand backbone on the site of the chlorine atom. It seems like this orientation is compressing the backbone, leading to a smaller angle at the amide.

---

[2] X-Ray analysis was performed by Dr. Christian Würtele.
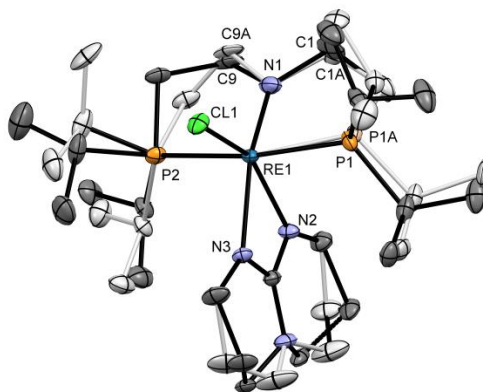
*Figure 17: Molecular structure of **5**. ORTEP plot with anisotropic displacement parameters drawn at the 50% probability level. The C–H hydrogen atoms are omitted for clarity. Disorder depicted in grey. Selected bond lengths [Å] and angles [°]: Re1-N1 1.9193(17), Re1-N2 2.1499(15), Re1-N3 2.2143(15), Re1-Cl1 2.3860(15); N1-Re1-Cl1 111.63(5), N1-Re-N2 99.91(7), N2-Re1-N3 59.53(6), P1-Re-1-P2 169.22(8), P1A-Re1-P2 160.60(11), C9-N1-C1 115.7(4), C9A-N1-C1A 98.5(6).*

1.3 (P=N=P)ReCl$_2$ and (P=NP)ReCl$_2$

The utilized PNP ligand provides the intriguing opportunity for functionalization of the alkylamido to enamido (P=NP) or dienamido (P=N=P) units (P=N=P = N(CHCHP^{t}Bu$_2$)$_2$). By oxidation of the backbone, the ligand´s rigidity as well as the π-donor properties of the amide can be fine-tuned.[201] H-atom abstraction using the 2,4,6-tri-*tert*-butylphenoxy radical (PhO·) proved to be the method of choice.[202] Addition of benzoquinone or its derivatives in analogy to the iridium case only leads to complex degradation.[203] Addition of 6 equiv. of PhO· to the dichloro complex **3** results in full conversion to the divinyl compound [(P=N=P)ReCl$_2$] (**6**). Its ^{31}P-NMR signal is slightly broadened (full width at half maximum (FWHM) = 0.12 ppm) and shifted far into the negative region (δ$_P$ = -276 ppm). Besides, also its ^{1}H-NMR (notably δ$_H$(tBu) = 2.6 ppm, δ$_H$(PCH$_2$) = 0.9 ppm, Figure 18) and ^{13}C-NMR signals are rather unusual for these kinds of coordination compounds. This behavior indicates mixing in of paramagnetic excited states and therefore contribution of temperature independent paramagnetism (TIP).[204] Identification of the corresponding signals in the NMR spectra has been accomplished by means of H,H-COSY and H,C-HSQC NMR spectroscopy. A paramagnetic side-product in varying amounts (5-20%) is observed (δ$_H$ = 15.2 ppm) in the reaction, which is tentatively assigned to [(P=N=P)ReCl$_3$] (**7**, Scheme 48). Control experiments suggest this assignement, as **7** can be prepared

independently from trichloro complex **23** (see chapter 4.3) by H-atom abstraction with PhO· (Figure 19) and can be converted cleanly into **6** by reduction with CoCp$_2$ (Scheme 49). The origin of the additional chloride could not be determined, as no other degradation products were observed by NMR spectroscopy and no chlorinated solvents or other additives were used.
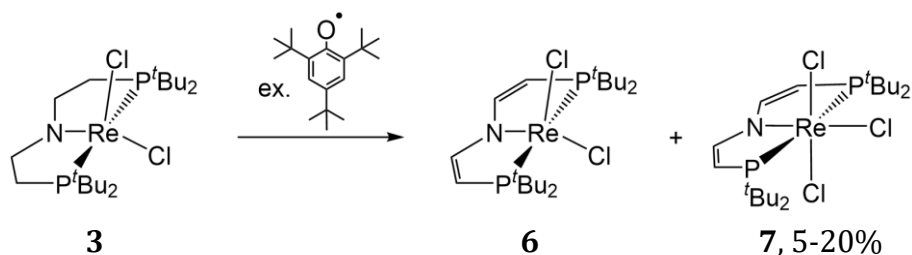
*Scheme 48: Reaction of **3** with excess PhO· to **6**, contaminated with **7**.*
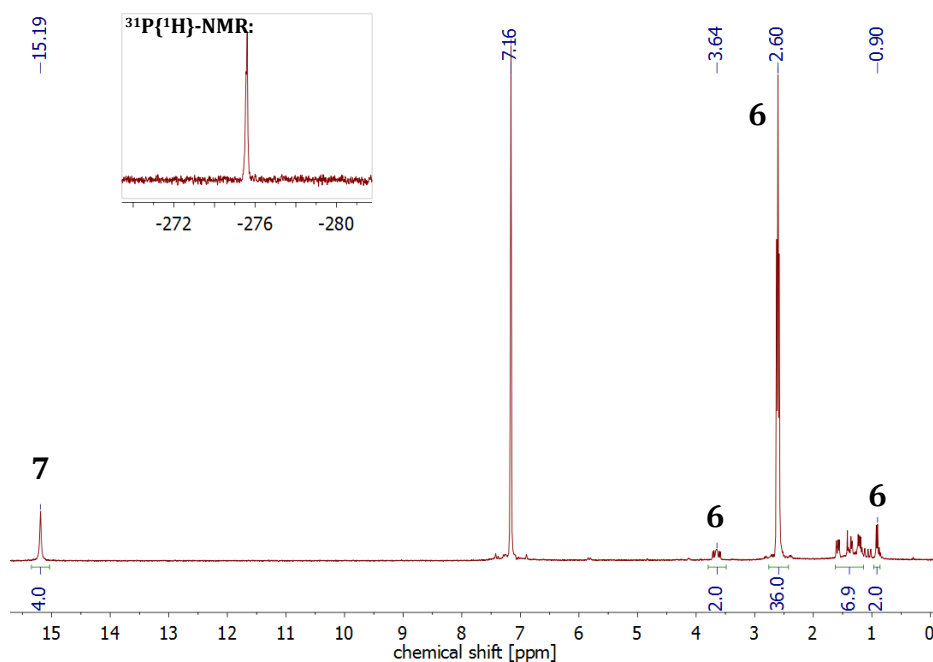
*Figure 18: ^{1}H-NMR spectrum of **6** and small amounts of **7** in C$_6$D$_6$ after removal of 2,4,6-tri-tert-butylphenol by washing with pentane; Expansion: ^{31}P{^{1}H}-NMR spectrum.*
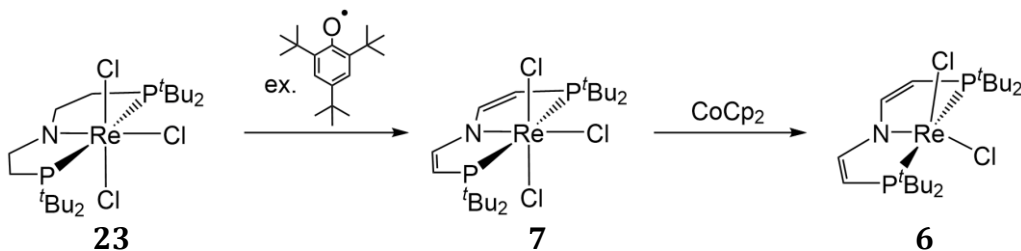
*Scheme 49: Control experiments for the identification of **7**.*
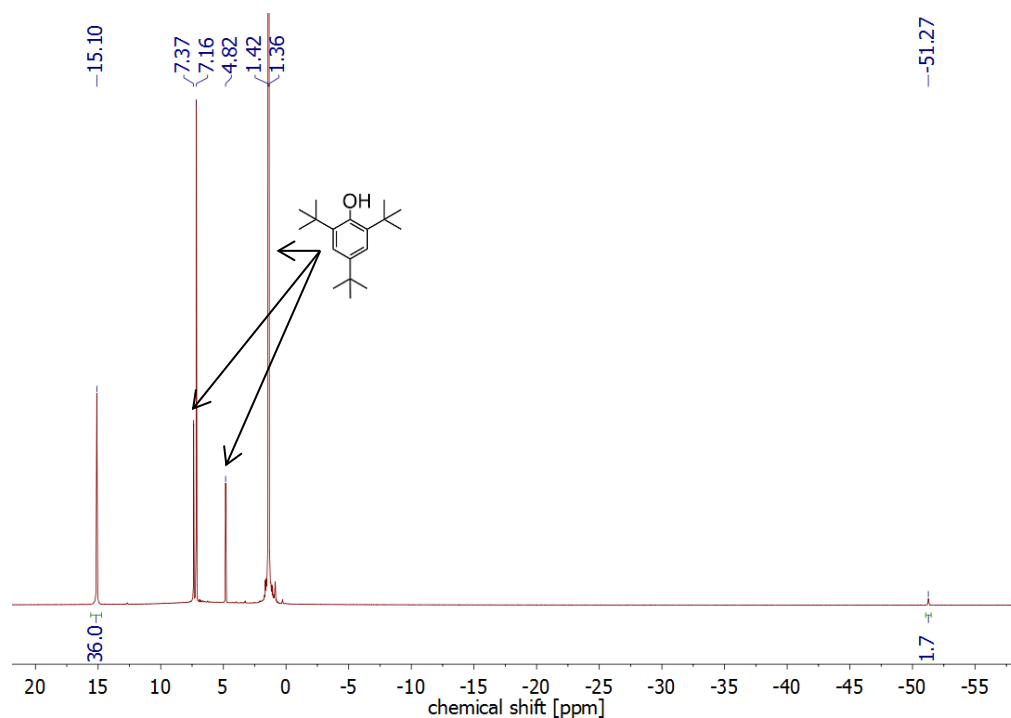
*Figure 19: ¹H-NMR spectrum of the reaction mixture of **23** and PhO· in C₆D₆.*

If only 2-2.5 equiv. of PhO· are used, a C_1 symmetric species is observed in the NMR spectra, which corresponds to the enamido complex **8** with a chemical shift (³¹P-NMR) in between the alkylamide **3** and the dienamide **6** (Figure 20). The constitution of **8** is supported by LIFDI mass measurements, but **8** could not be isolated as it is always contaminated either with **3** or **6** or both and they all show similar solubility properties. Further addition of PhO· generates **6** (Scheme 50).
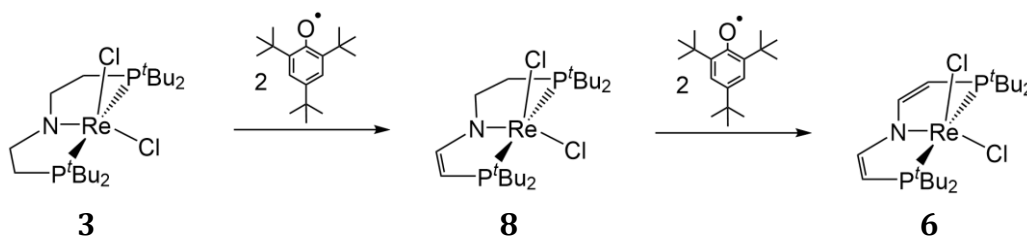
*Scheme 50: Reaction of **3** with PhO· to enamido **8** and dienamido **6**.*

63
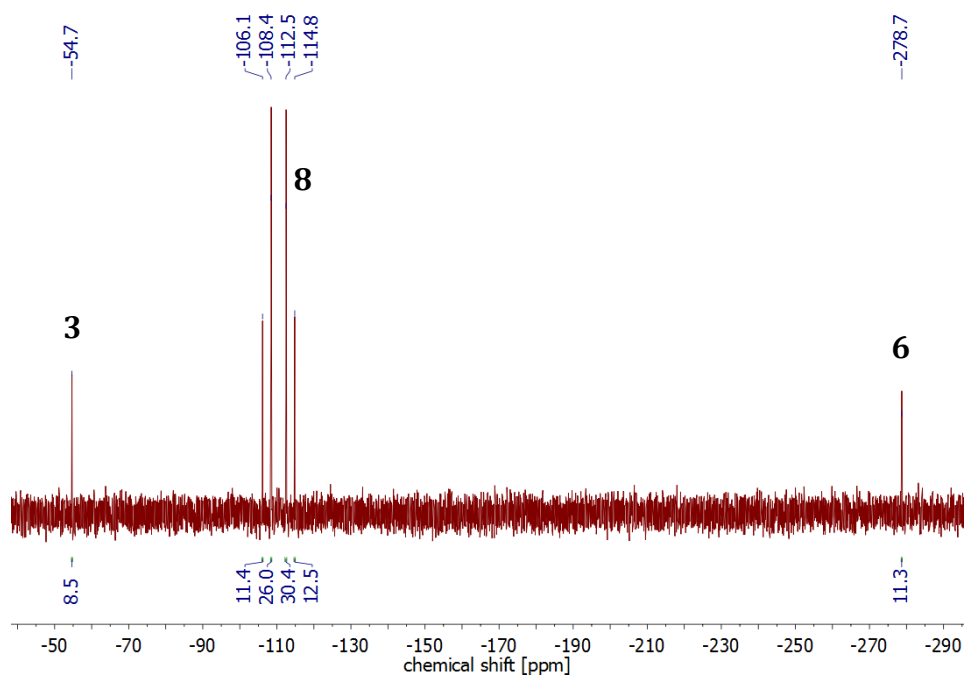
Figure 20: $^{31}P\{^1H\}$-NMR spectrum of **3** with 2.5 equiv. of PhO· to form **8** in C_6D_6.

In the following, this thesis focuses on the *tert*-butyl substituted ligand with the fully saturated ligand backbone (PNP).

2 Dinitrogen splitting

This chapter has been published partly in the *Journal of the American Chemical Society* under the title: *"Dinitrogen Splitting and Functionalization in the Coordination Sphere of Rhenium"* in 2014.[193]

2.1 Nitride synthesis

3 is rapidly reduced by 1 equiv. Na/Hg in THF. Under N_2 atmosphere, (PNP)Re(N)Cl (**9**) is obtained in 90% spectroscopic yield upon comparison (^{31}P, ^{1}H, ^{13}C NMR) with an original sample, prepared by reaction of the dichloro complex **3** with an azide source ([PPN]N_3). The use of $^{15}N_2$ afforded the ^{15}N-nitride isotopologue ($\delta(^{15}N) = 371$ ppm, Figure 21), confirming N_2 as source for nitride formation. Accordingly, reduction of **3** with Na/Hg under argon only gives an intractable mixture of compounds by NMR, which were not further characterized, and no indication for the formation of the nitride. Nitride formation could also be observed after addition of the nitride transfer reagent Li[DBABH] to **3** (Scheme 51). Moreover, reduction of **3** with Co(Cp*)$_2$ under N_2 also gives the nitride with slightly lower yields up to 75%. A hydride complex is found as main side product ($\delta_P = 31.2$ ppm; $\delta_H = -9.28$ ppm), which did not incorporate deuterium upon use of d$_8$-THF, possibly pointing toward traces of water or CoCp$_2$* itself as origin for the reduced yield. However, to the best of our knowledge, this is the first report of well-defined N_2 splitting into nitrides, which allows the use of organometallic reducing agents as also utilized in protocols for catalytic ammonia generation.[31,39,44]
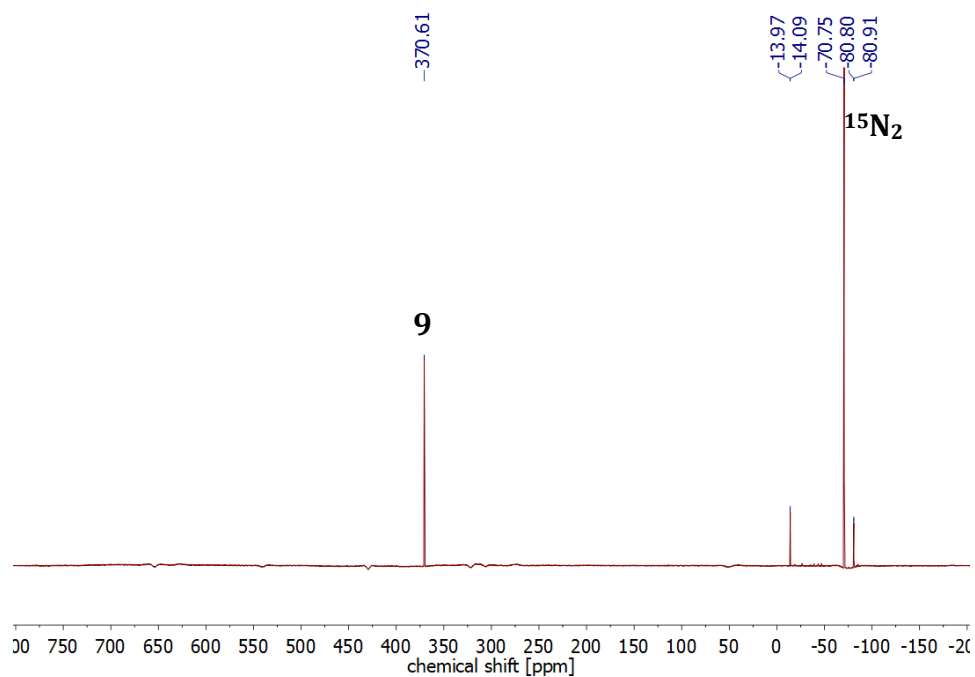
Figure 21: ^{15}N-NMR spectrum of $\mathbf{9}$ in d_8-THF obtained from $^{15}N_2$[205] besides an impurity (-14.0 ppm (d, J = 6.1 Hz) and -80.9 ppm (d, J = 6.1 Hz)).
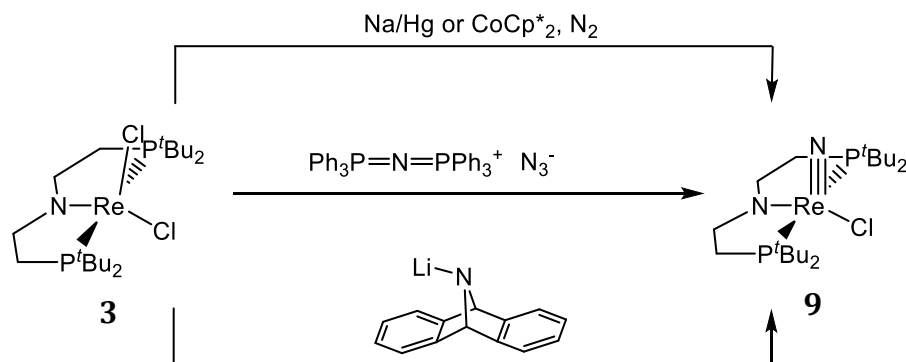
Scheme 51: Different synthetic routes to the nitride complex $\mathbf{9}$.

The ^1H and ^{13}C-NMR spectra of $\mathbf{9}$ indicate C_s symmetry as expected for a square-pyramidal nitride complex. All efforts to grow single-crystals suitable for X-ray diffraction were unsuccessful. Computational modeling confirmed the square-pyramidal geometry with the nitride in apical position and a typical Re≡N bond length (1.65 Å).[105] The lack of a low-lying, vacant d-orbital results in the absence of Re−N_{PNP} π−bonding with the pincer ligand, as expressed in a long bond distance (2.03 Å), pyramidal nitrogen coordination and high amide basicity (see below).

66

The nitride complex **9** was characterized by cyclic voltammetry (CV) in CH_2Cl_2. A reversible redox wave was found at − 0.13 V vs $FeCp_2/FeCp_2^+$ assignable to the Re^V/Re^{VI} redox couple. At more positive potential, an irreversible second oxidation is observed. Comparison with the CV of protonated $[(^HPNP)Re(N)Cl]^+$ (synthesis and characterization see below) suggests the latter as decomposition product. Importantly, no reduction of the nitride was observed within the electrochemical window of the solvent.
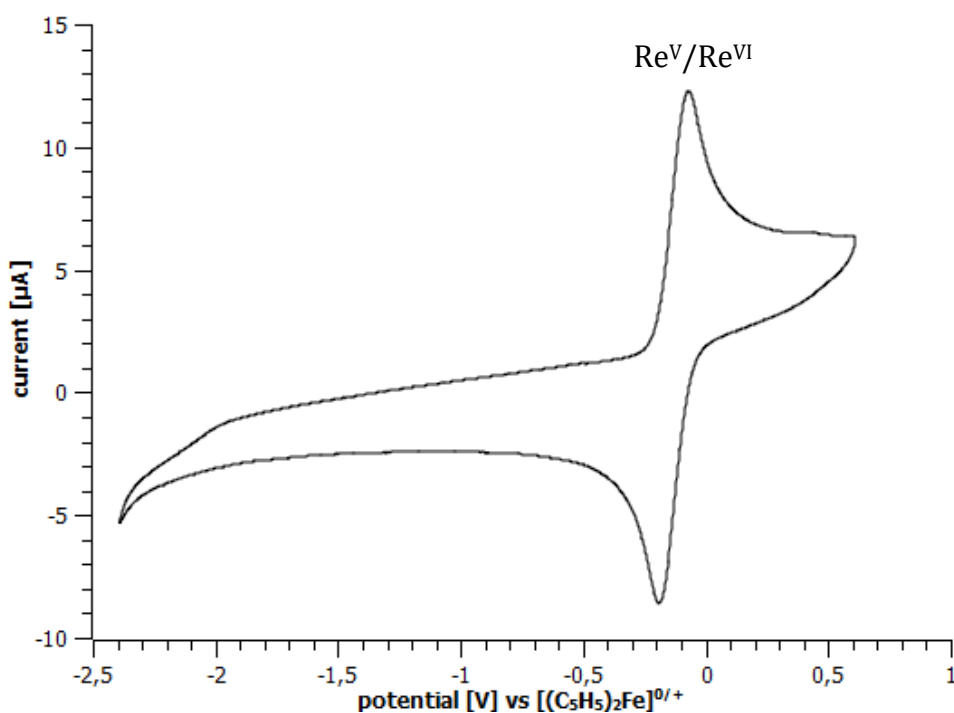
Figure 22: CV of (PNP)Re(N)Cl in CH_2Cl_2 (1 mM, 0.1 M $[N^nBu_4][PF_6]$, RT, glassy carbon working electrode, scan rate 400 mV/s).
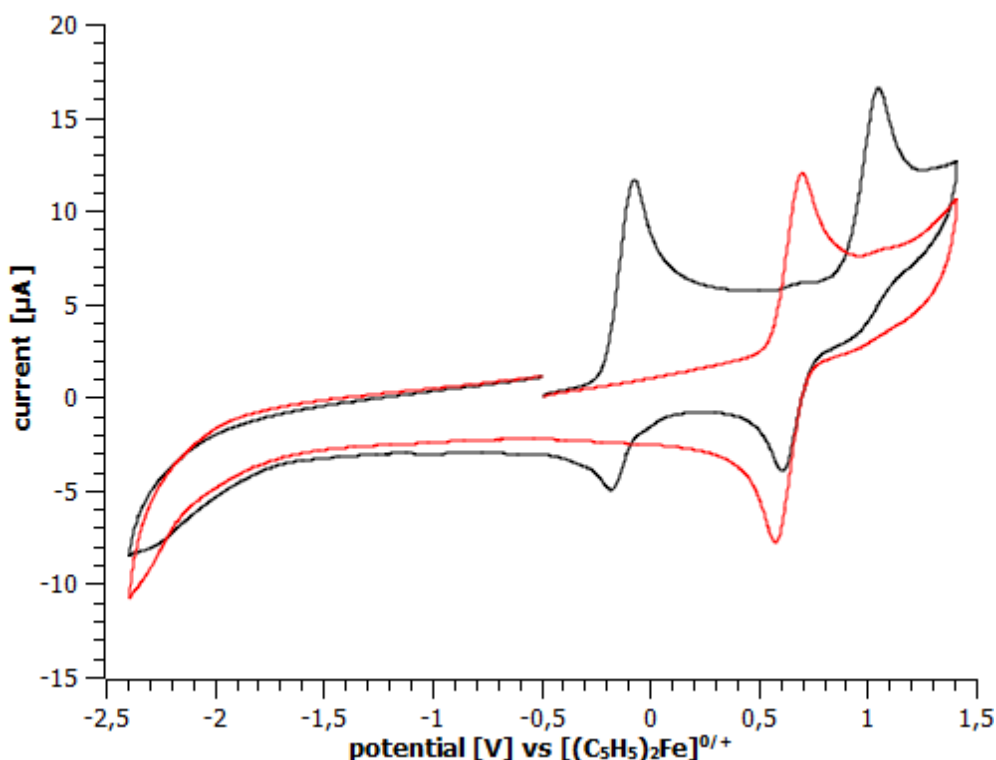
Figure 23: CVs of (PNP)Re(N)Cl (black) and [(HPNP)Re(N)Cl]+ (red) in CH2Cl2 (1 mM, 0.1 M [NnBu4][PF6], RT, glassy carbon working electrode, scan rate 400 mV/s).

2.2 The Mechanism of N$_2$ Splitting

N$_2$ splitting with *Cummins'* Mo triamido system proceeds from a linear N$_2$-bridged dimer via a zigzag {Mo=N−N=Mo} transition state to the final nitrides.[84,86,97,134,206] An analogous mechanism was proposed for reverse N−N coupling with [IrN(P=N=P)].[156] Given the steric bulk of the Re(PNP) platform, a dimeric intermediate like [(PNP)ClRe(N$_2$)ReCl(PNP)] (**10**), which is formed upon reduction of **3**, represents a reasonable intermediate. While at the current stage no experimental mechanistic data are available, this pathway was evaluated computationally. For the dimer, both the triplet and an open-shell singlet states were found to be very close in energy. Both exhibit approximate square-pyramidal metal coordination and an almost linear {Re−N=N−Re} moiety (D$_{NN}$: 1.20 Å). A transition state towards N$_2$ cleavage could only be located on the singlet surface with a zigzag {Re=N−N=Re} conformation (D$_{NN}$: 1.64 Å). A moderate barrier has been found with $\Delta G^{\ddagger} = 84.4$ kJmol^{-1} and conformational

refinement could lower this barrier to $\Delta G^{\ddagger} = 71.4$ kJmol^{-1} later on (D3-PBE/def2-TZVP//def2-SV(P), Figure 24).[3] N$_2$ cleavage was computed to be exergonic by 98.3 kJmol^{-1}, suggesting this route to be a feasible mechanism for dinitrogen splitting.[4]
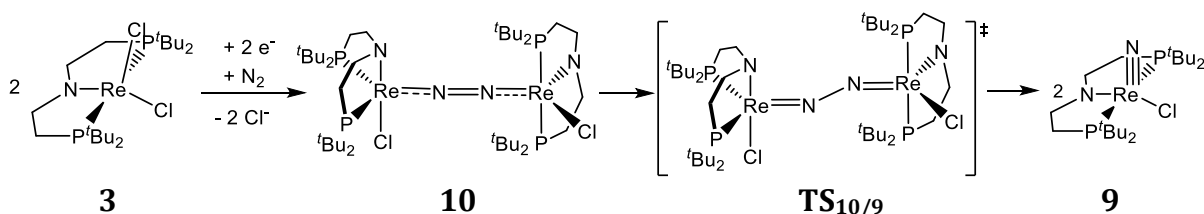
Scheme 52: Proposed mechanism of N$_2$-splitting by reduction of 3.
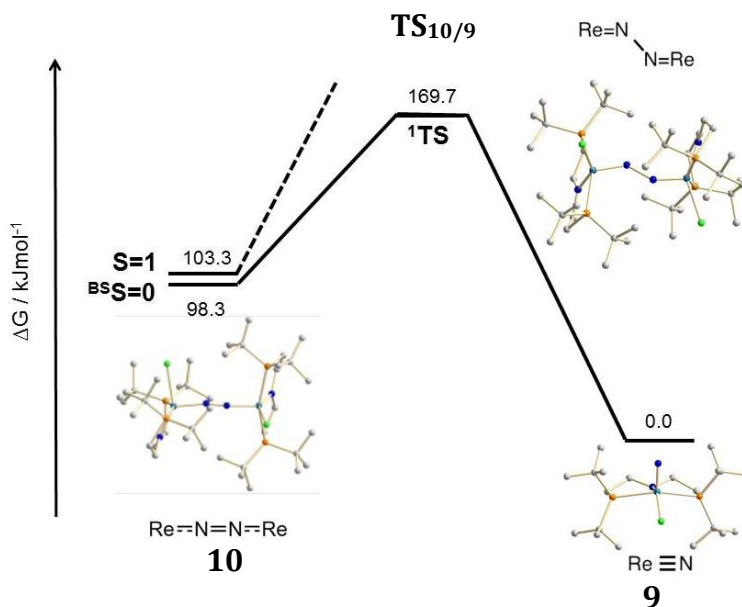
Figure 24: Computed Free Energies for N$_2$ Splitting Starting from dimer 10 (D3-PBE/def2-TZVP//def2-SV(P)).

---

[3] The PBE functional showed good performance in previous studies on PNP pincer nitride chemistry.[176] A higher barrier ($\Delta G^{\ddagger} = 117.8$ kJmol^{-1}) was found for a single-point calculation of the transition state with hybrid functional PBE0 (D3-PBE0/def2-TZVP//D3-PBE/def2-SV(P)), which is considered as an upper limit.

[4] DFT Calculations were performed by Dr. Markus Finger.
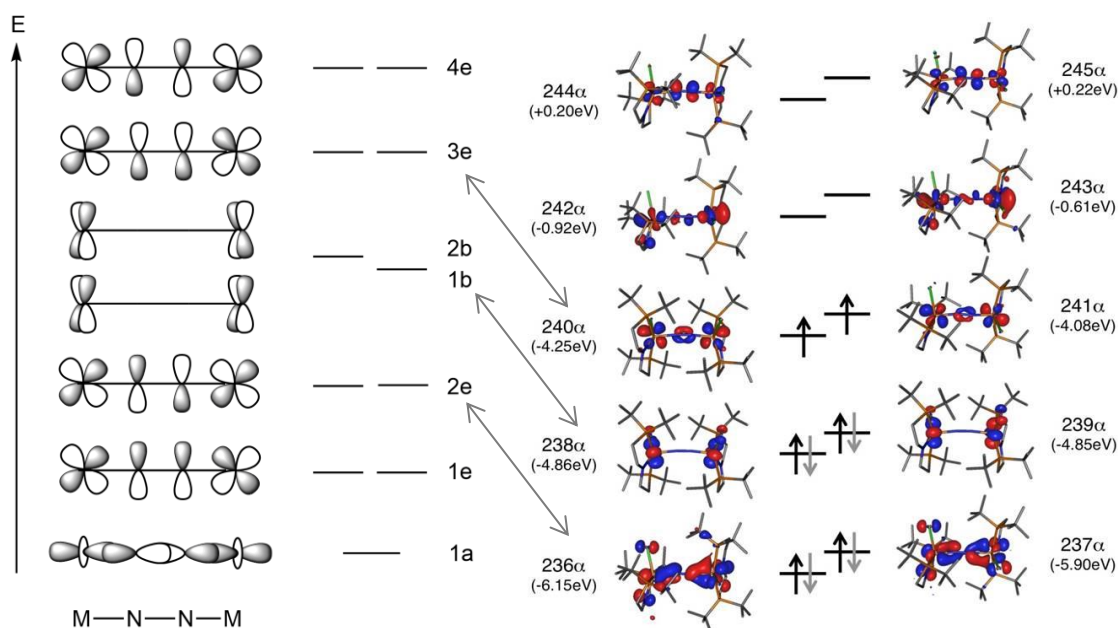
Figure 25: Qualitative MO-scheme (left) and calculated MO´s (right) for dimer **10.**

The calculated MO´s (Figure 25) fit well to the qualitative molecular orbital scheme, which has been introduced in Chapter I.5.1 (Figure 5). Because of fourfold symmetry, a set of basically non-bonding δ-orbitals (1b and 2b) is occupied. However, there are still a total of 10 electrons in the π-system of a tentative Re(II) dimer and therefore enough electrons for full N_2 reduction and generation of stable closed shell nitrides (Figure 26). The HOMO has been found to be the MN antibonding and NN bonding orbital, similar to *Cummins* system, mentioned in the introduction.
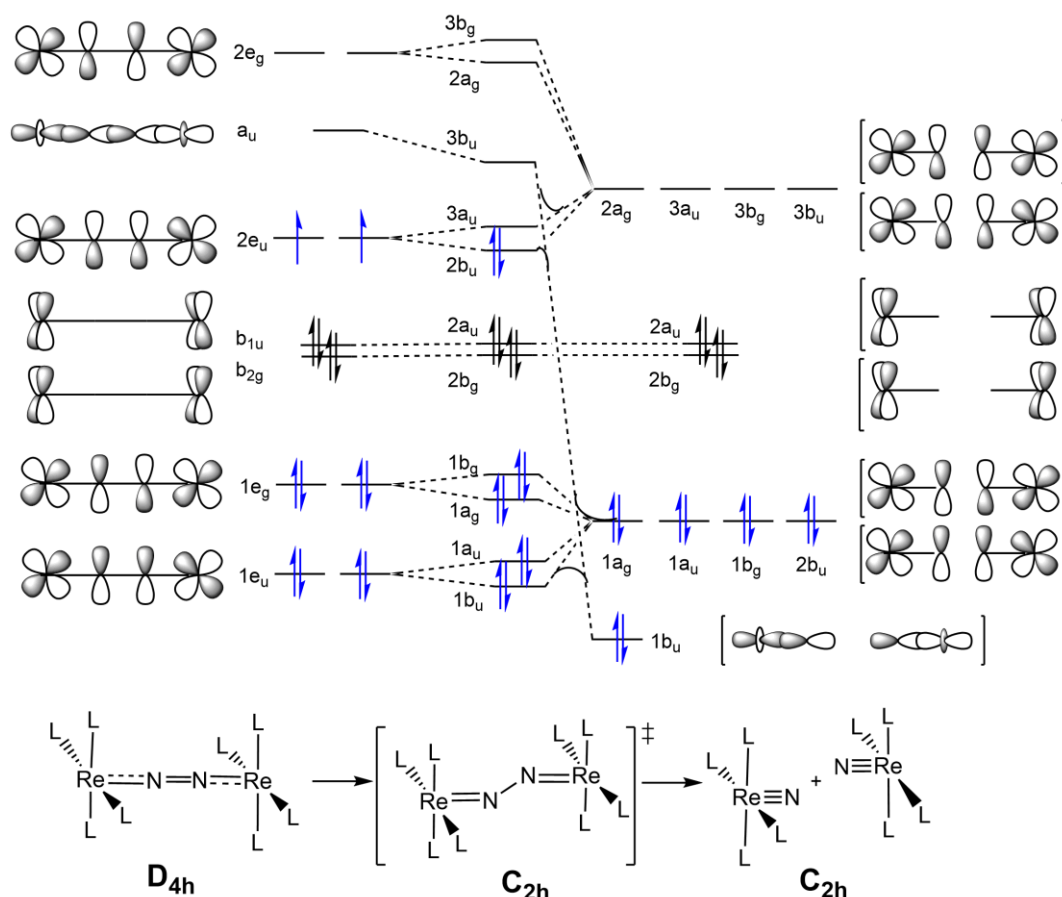
*Figure 26: MO scheme for N_2 splitting from dimer **10** into **9**; blue: electrons in the {MNNM} π-system.*

Because of the bulky ^{t}Bu-substituents on the PNP ligands, these are supposed to exhibit a staggered conformation in the dimeric complex (Scheme 52). A more symmetric arrangement with all phosphorous atoms in one plane cannot be adopted due to steric reasons. The π-donor amide is therefore interacting with both d_{xz} and d_{yz} orbitals (both orbitals of one MO set) in an equal manner, keeping the $2e_u$ level degenerate and therefore a triplet state dimer. In the zigzag transition state, symmetry is lowered, which allows for mixing of the σ-N-N-antibonding orbital $3b_u$ with the $2b_u$ π-orbitals. Transition of electrons is therefore possible and stable closed shell nitrides are created.

The fast splitting reaction without an observable N_2-complex may partly be attributed to the influence of the π-donor in the ligand backbone. As stated by the group of *Cummins*, ligand rotation to allow for π-backbonding from one amide into the MO with π* character of N_2 is believed to occur, lowering the barrier for splitting (Scheme 12). The PNP ligand already imposes such a geometry. Additionally, both orbitals of the $2e_u$ set are raised in energy due to the π-donor influence favoring "relaxation" in a zigzag confirmation. Additionally, steric repulsion between the bulky ^{t}Bu-groups is believed to support the N-N splitting reaction.

2.3   Possible implications of ligand variations

2.3.1   A decreased steric bulk

The steric bulk of the substituents at the phosphorous atoms is proposed to play an important role in the N_2 splitting mechanism. Because of the sterically demanding *t*Bu-groups, DFT calculations predict a twisted confirmation for the tentative N_2-bridged intermediate dimer 10, leading to an energetically rather high lying open shell singlet state. Splitting is then achieved via a triplet transition state to the nitride **9** on the singlet surface (Figure 27, black). If the steric demand was decreased for example by utilization of methyl-substituents, rotation of the {(PNP)ReCl} fragments would be possible. In an inversion symmetric arrangement of the dimer, the amide in the ligand backbone N_{PNP} interacts with only one of the $2e_u$ orbitals, resulting in an energetic splitting of these orbitals and therefore formation of a closed shell singlet state dimer. Computations predict a strong stabilization of this dimeric species in the singlet state, with the triplet state being about 71 kJmol^{-1} higher in energy. In fact, this stabilization would even lead to a nearly isothermal splitting reaction with a quite high transition state ($\Delta G^{\ddagger}$ = 126.0 kJmol^{-1}, D3-PBE/def2-TZVP//def2-SV(P), Figure 27, blue).[5]
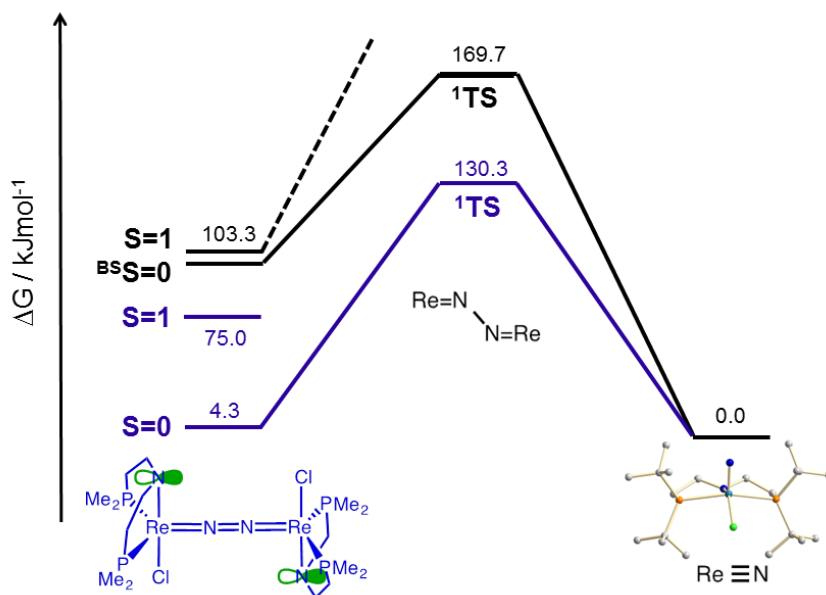
*Figure 27: Computed Free Energies for N$_2$ Splitting Starting from dimer **10**; black: PNP^{tBu}, blue: PNP^{Me} (D3-PBE/def2-TZVP//def2-SV(P)).*

---

[5] DFT calculations carried out by Dr. Markus Finger.

Hence, there is the possibility to isolate such an N_2-bridged intermediate and to study its reactivity. Furthermore, confirmation of these computational results by experimental evidence provides an opportunity towards tuning of the N_2 splitting reaction energies and might even lead to catalytic N_2 activation.

However, in this thesis the focus lies on the first described system with the *tert*-butyl ligand system. Further work will examine the role of different substituents on the phosphorous atoms.

2.3.2 Oxidation of the ligand backbone

The π-donor strength of the amide in the ligand backbone is believed to have a significant influence on the N_2 splitting mechanism (vide supra) and lowering its strength should have an impact at least on the speed of the reaction. In this way an intermediate might be observed or even captured. Furthermore, the amide in the nitrido complex **9** displays strong basicity due to the lack of available d-orbitals for π-backbonding and protonation to $[(^HPNP)Re(N)(Cl)]^+$ (**12**) is the pronounced reactivity (see next chapter). Delocalizing the amide´s electron density over the ligand backbone offers a path towards more reactivity at the nitrido unit or at the metal center. By lowering the π-donor strength of the amide, d-orbital splitting at the metal is decreased, orbitals sink in energy and should therefore become available e.g. for H_2 coordination.

Preliminary reactivity tests towards N_2 splitting did not give definite results. **6** was converted to the nitrido compound **11** by addition of $[PPN]N_3$ to determine its spectroscopic signature (δ_P = 71 ppm in C_6D_6). Afterwards, N_2 splitting was tested by reduction of **6** with 1 equiv. Na/Hg under N_2 atmosphere. Some small signals in the region around 60 ppm in the ^{31}P-NMR spectrum were detected right after the reaction, which have vanished the day after and could perhaps correspond to some N_2 bridged intermediate (Figure 28). Only the very small signal in a similar region to **11** of the ^{31}P-NMR spectrum is left and indicates that a nitride might have formed (δ_P = 67 ppm in d_8-THF). However, isobutene formation and the lack of any bigger, distinct signals in the NMR spectra propose over-reduction by the strong reducing agent.
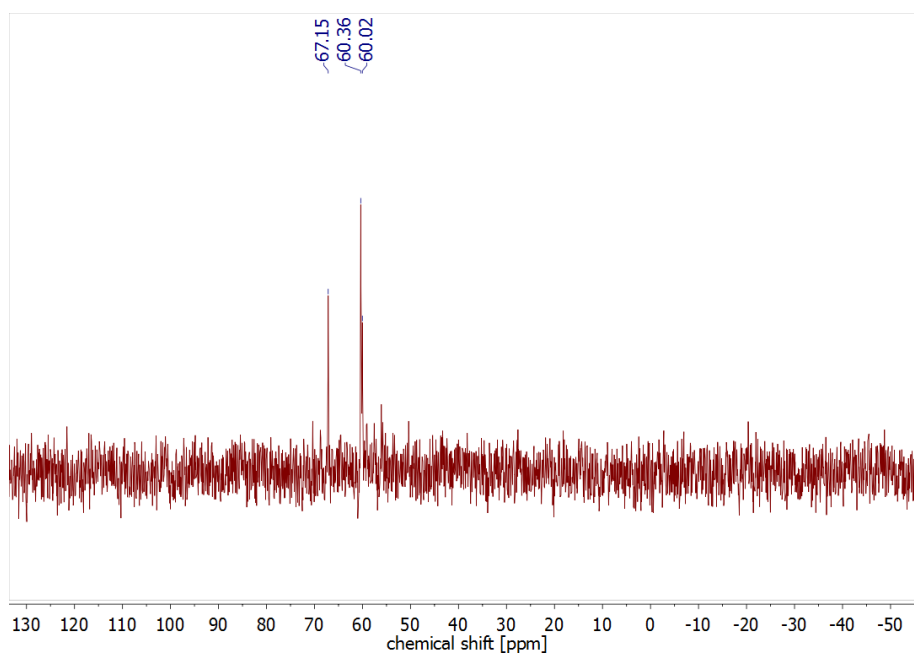
*Figure 28: $^{31}P\{^1H\}$-NMR spectrum of the reaction mixture of **6** with 1 equiv. Na/Hg under N_2 atmosphere about 10 min after the reaction in d_8-THF.*

The same reduction carried out under an atmosphere of argon does not show any ^{31}P-NMR signals and besides isobutene no characteristic signals in the ^1H-NMR spectrum.

A cyclovoltamogram of **6** has not been measured yet and no weaker reducing agents, like $CoCp_2^*$ have been tested. As reduction of **6** is different under N_2 and argon atmosphere, a reaction with N_2 is likely to occur. However, more experiments are necessary to evaluate the outcome and the intermediates in this reaction.

3 Nitride functionalization

Parts of this chapter have been published in the *Journal of the American Chemical Society* under the title: *"Dinitrogen Splitting and Functionalization in the Coordination Sphere of Rhenium"* in 2014[193] and in the Journal *Angewandte Chemie int. Ed.* under the title "*Conversion of Dinitrogen into Acetonitrile under Ambient Conditions*".[207]

3.1 Ammonia formation?

Our group recently reported hydrogenolysis of terminal nitride $[Ru^{IV}(N)(PNP)]$ with H_2 to ammonia at mild conditions.[176] In contrast, **9** does not react with H_2 even under more forcing conditions (3 bar H_2 , 80°C, 18 h) or in the presence of base (KOtBu). Presumably, the strong nitride trans influence prevents H_2 heterolysis at the vacant site, due to the lack of available d-orbitals for coordination. These are involved in π-bonding to the nitride and therefore energetically augmented. Coordination at this site therefore seems to be hampered.

Protonation of the nitride with several acids (HCl, HOTf) results in exclusive protonation of the amido group giving $[(^HPNP)Re(N)Cl]X$ (X = Cl, OTf) (**12**) even with up to 12 equiv HCl. DFT computations confirmed that amide over nitride protonation is thermodynamically favored by $\Delta G^0 = 31.9$ kJmol^{-1}. The identical NMR data of **12-Cl** and **12-OTf** (except N−H) and the molecular structures from single-crystal X-ray diffraction indicate that the anions are not coordinated to the metal in solution and in the solid state.[6] This observation reflects the strong nitrido trans influence and stabilizing N−H ⋯X hydrogen bonding. The Re ion in **12-Cl** is square-pyramidally coordinated with only minor distortion (τ = 0.04) and a typical Re≡N triple bonding distance (1.642(4) Å).[105]

---

[6] X-Ray diffraction was performed by Dr. Christian Würtele.
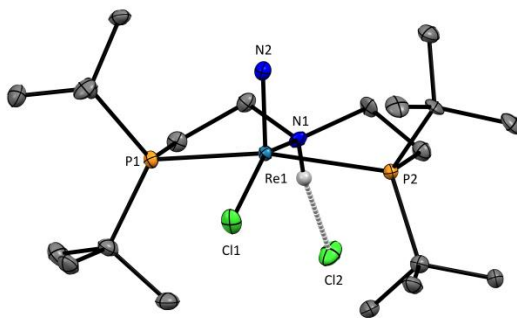
*Figure 29: Molecular structure of **12-Cl** in the crystal. ORTEP plot with anisotropic displacement parameters drawn at the 50% probability level. The C–H hydrogen atoms are omitted for clarity. Selected bond lengths [Å] and angles [°]: Re1–Cl1 2.4001(12), Re1–N1 2.132(4), Re1–N2 1.642(4), Re1–P1 2.4578(13), Re1–P2 2.4420(12); N1–Re1 – Cl1 153.93(12), N1–Re1–N2 99.59(19), Cl1–Re1–N2 106.48(15), P1–Re1–P2 157.35(5).*

In analogy to the parent nitride, the CV of **12-OTf** features a reversible oxidation wave, yet at more positive potential (+0.64 V, Figure 23) owing to the positive charge. Importantly, as for the neutral nitride, no reduction was observed. Chemical reduction with KC_8 only generated **9** and H_2. Hence, the electrochemical results and reactivity indicate that the formation of ammonia seems not accessible on this route.

Although the cyclic voltammogram of nitride complex **9** did not show a reduction wave until a potential of -2.4 V vs. Fc/Fc^+ in DCM (Figure 22), chemical reduction with a very strong reducing agent (KC_8) proved to be possible. Addition of 2 equiv. of KC_8 and 2 equiv. of 18-crown-6 resulted in nearly complete disappearance of the spectroscopic signature of **9**. In benzene, the NMR spectra showed formation of a C_1 symmetric species in 80% yield (δ_P = 113.7 ppm (d, $^2J_{PP}$ = 103 Hz) and 30.1 ppm (d, $^2J_{PP}$ = 103 Hz)), exhibiting only three signals for ^tBu-groups of the ligand backbone (δ_H = 1.82, 1.64 and 1.22 ppm) with ^1H-^{31}P coupling constants of 11.0 - 12.5 Hz (Figure 30). The fate of the fourth ^tBu-group is indicated by isobutene formation (δ_H = 4.8 ppm (hept, J = 1.2 Hz) and 1.59 ppm (t, J = 1.2 Hz)). Upon reduction, it seems that one of the ^tBu-groups of the PNP ligand is eliminated, which is the reason for the low symmetry of the complex. The exact structure of this complex has not been identified though. About 10% of a side-product was formed (δ_P = 107.3 ppm) and this amount increased to about 30%, when the reaction was carried out in THF instead of benzene (Figure 31) and which is a rather acceptable amount for further conversions. The complex exhibits signals in agreement with a C_s symmetric compound in the NMR spectra. In contrast to the asymmetric species described above, it features pentane solubility. However, this complex could not be isolated due to formation of different unidentified side-products. Reduction without ligand degradation would offer an interesting route towards functionalization of the nitride, but further experiments

(for example low temperatures) are suggested to identify the nature of these reaction products.
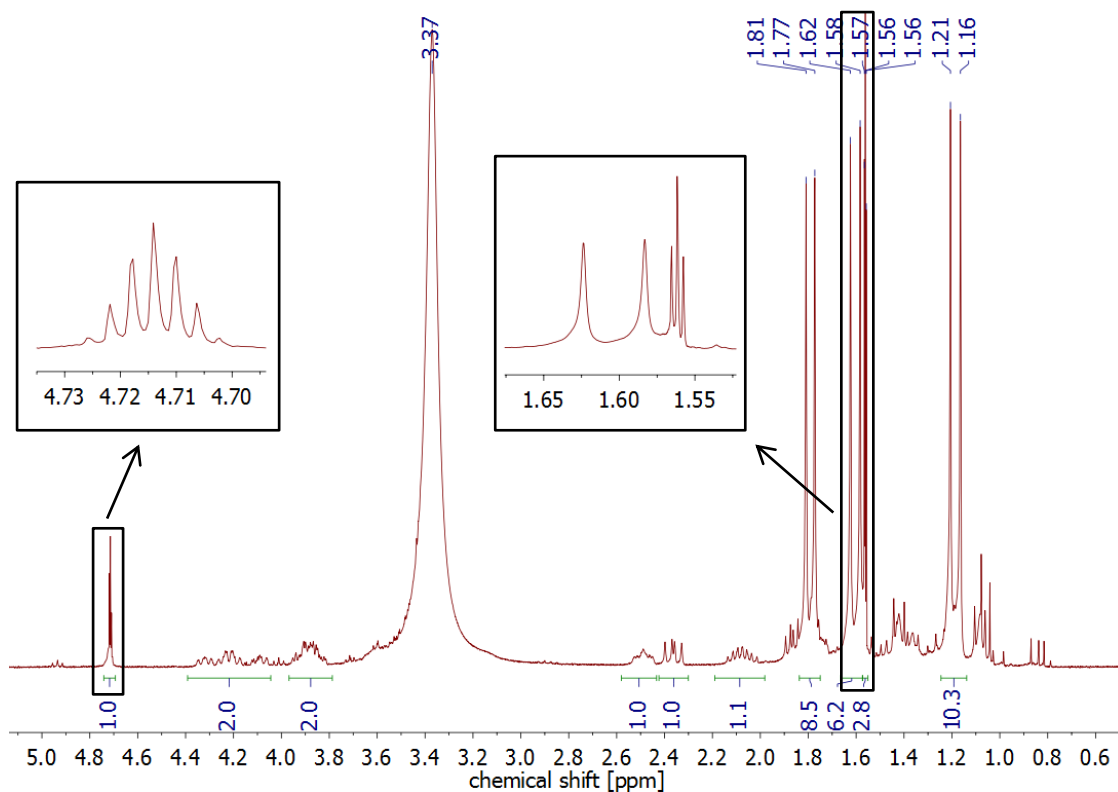
*Figure 30: ¹H-NMR spectrum of the reduction of **9** with 2 equiv. KC₈ and 18-crown-6 in C₆D₆; Expansion: signals corresponding to isobutene formation.*
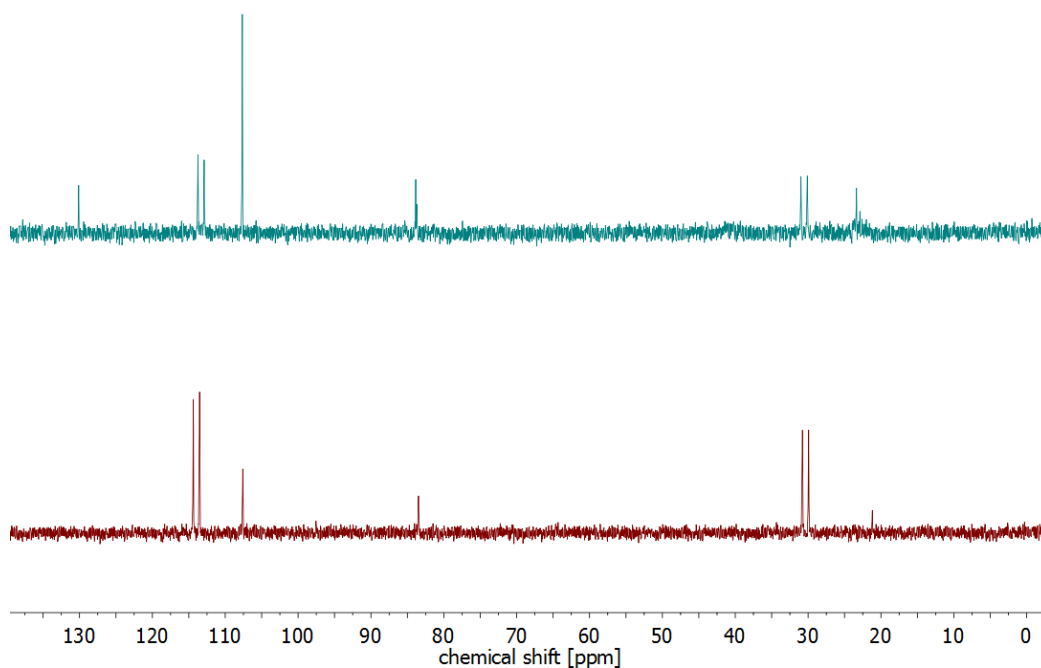
*Figure 31: ³¹P{¹H}-NMR spectra of the reduction of **9** with 2 equiv KC₈ and 18-crown-6; Top: in d₈-THF; Bottom: in C₆D₆.*

77

3.2 Reaction with nucleophiles

To test for reactivity towards nucleophiles, metal organyls were added to **9.** Addition of methyl lithium (MeLi) to the nitride **9** allows for quantitative exchange of the chloride substituent by a methyl group. In this way, the complex $[(PNP)Re(N)(CH_3)]$ (**13**) could be isolated and fully characterized.
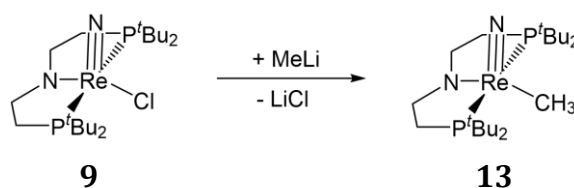
*Scheme 53: Synthesis of **13** from **9** and MeLi.*

^{1}H and ^{31}P-NMR spectra of **13** are similar to **9**. A new signal corresponding to the methyl group appears at 2.32 ppm (t, $^3J_{HP}$ = 4.1 Hz) in the ^{1}H-NMR spectrum with the appropriate signal at -17.6 ppm in the ^{13}C-NMR spectrum, indicating metal coordination (Figure 32).
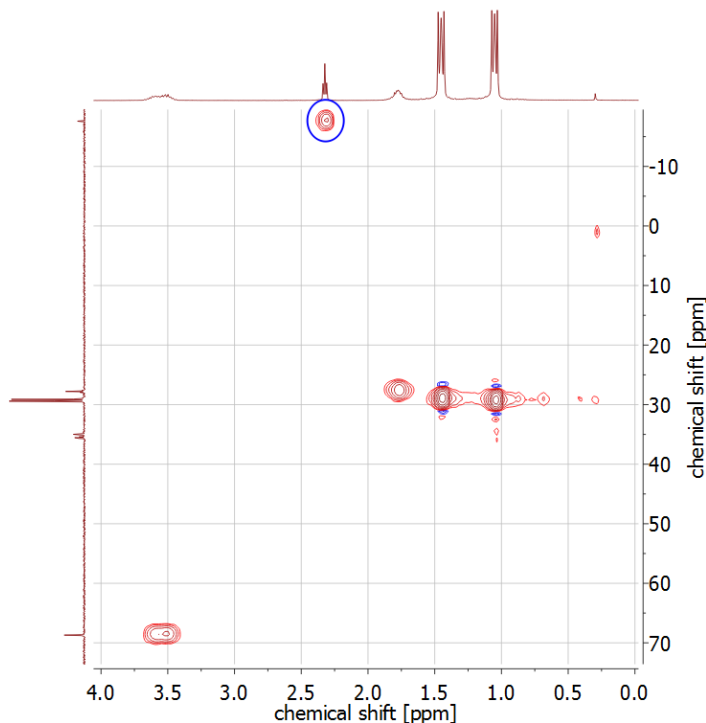
*Figure 32: ^1H-^{13}C HSQC NMR spectrum of **13**.*

78

The solid state structure of the complex describes a square pyramid with the nitride in the apical position and only minor distortions (τ = 0.10, Figure 33).[7] The Re≡N bond length (1.656(5) Å) is in a typical range for terminal rhenium(V) nitrides.[105] The Re-N$_{PNP}$ bond length (2.054(4) Å) is elongated compared to most other {(PNP)Re} complexes and the nitrogen is pyramidally coordinated, as also predicted for **9** by DFT. In fact, the Re-N$_{PNP}$ bond distance is only slightly shorter than in the protonated complex **12** (Δd =- 0.08 Å), indicating only minor π-bonding between the amide and the metal center as it has been supposed for **9**. The ease of protonation of parent **9** is in agreement with this observation. Further reaction with a second equivalent of the metal organyl was not observed. Furthermore, **9** is stable in the presence of Grignard reagents (MeMgCl, ^{i}PrMgCl, PhMgBr) or hydride sources (LiHBEt$_3$).
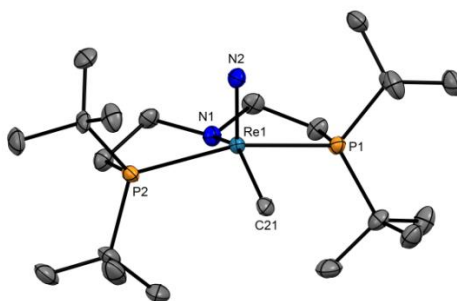
*Figure 33: Molecular structure of complex **13** derived by single-crystal X-ray diffraction. ORTEP plots with anisotropic displacement parameters set at 50% probability. Hydrogen atoms are omitted for clarity. Selected bond lengths [Å] and angles [°]: Re1-N2 1.656(5), Re1-N1 2.054(4), Re1-C21 2.208(5), N2-Re1-N1 110.6(2), N1-Re1-C21 147.73(18), P1-Re1-P2 153.80(5).*

---

[7] X-Ray diffraction was performed by Dr. Christian Würtele.

3.3   Reaction with isonitriles

Introduction of a trans-substituent to the nitride at the rhenium center should increase nitride centered reactivity upon weakening of the Re≡N bond strength. As coordination at this vacant site is proved to be hampered due to the strong trans-influence, strong ligands like isonitriles were investigated. To follow this approach, *tert*-butyl-isonitrile (CN^{t}Bu) was added to a solution of **9**. A slow reaction yielding two diamagnetic, C$_s$ symmetric main products in a 1:1 ratio is observed in ^{1}H and ^{31}P NMR spectra (δ_P = 94 and 61 ppm), which is complete after 2 d at 70°C. Besides, characteristic signals for the formation of isobutene are observed in the ^{1}H-NMR spectrum. Since the elimination of a *tert*-butyl group as isobutene should be accompanied by H$^+$ release, the reaction was next carried out in the presence of DBU as base. The reaction is not accelerated, but turned out to be selective to one of the products observed before (δ_P = 94 ppm), besides isobutene. After workup, the pentane insoluble material exhibits signals in the ^{1}H-NMR spectrum similar to the nitride **9** with no observable signals for a *tert*-butyl group of the isonitrile (Figure 34). Hence, elimination of its ^{t}Bu-group as isobutene under HCl abstraction is assumed, generating the cyanide complex **14** (Scheme 54a). This type of dealkylation is known and has already been observed for ^{t}Bu-isocyanide complexes.[208,209]
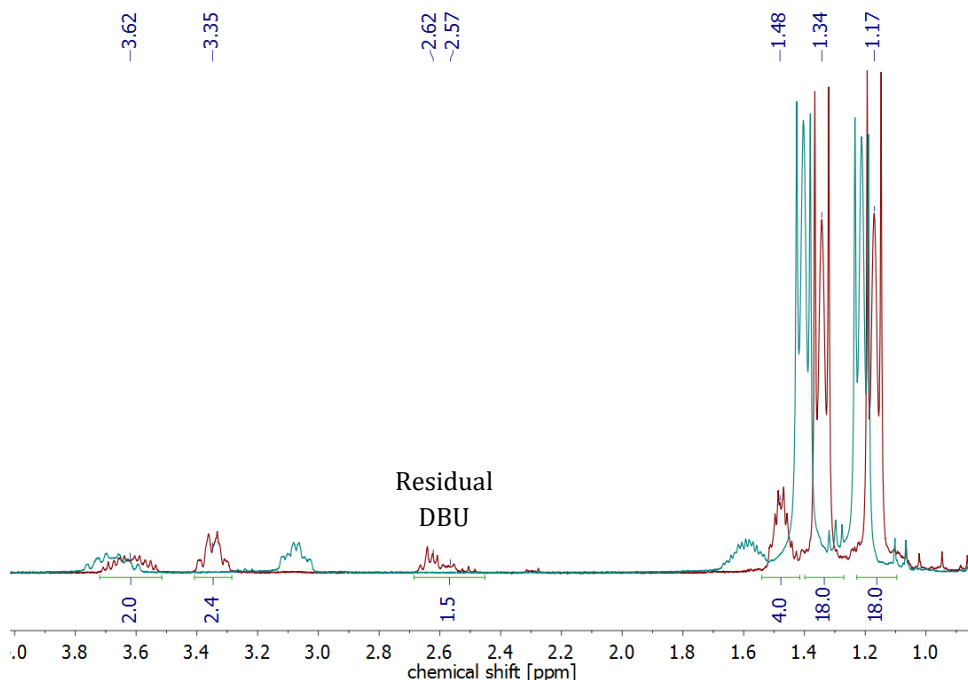
*Figure 34: Comparison of ^{1}H-NMR spectra of **14** (red) and **9** (green) in C$_6$D$_6$.*
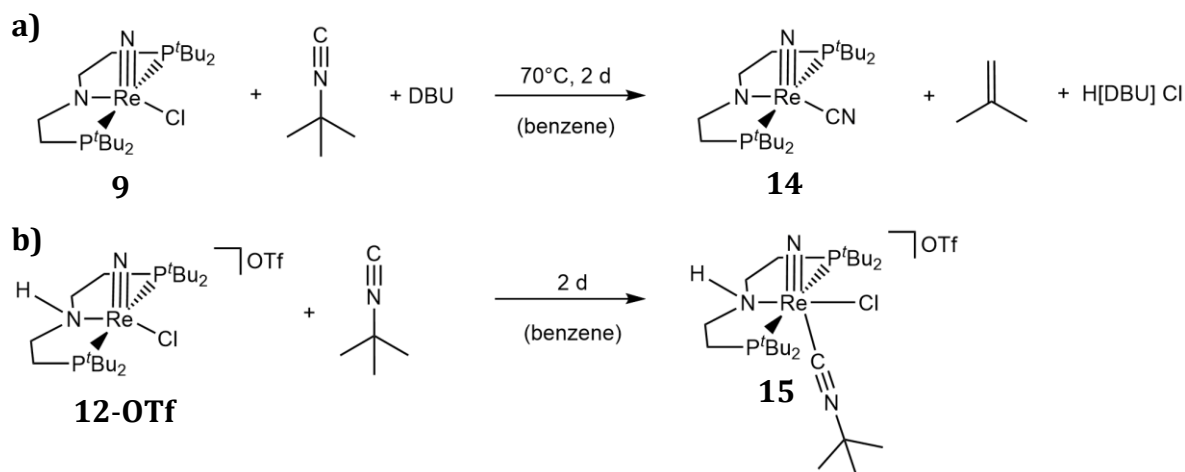
Scheme 54: Assumed reaction of the nitride **9** with isonitrile and DBU as base to **14** (a) and of the protonated nitride **12-OTf** with isonitrile to **15** (b).

Addition of isonitrile to the protonated nitride **12-OTf** generates selectively the other product **15** (δ_P = 61 ppm) with one singlet for the *tert*-butyl group of the isonitrile ligand in the ^{1}H-NMR spectrum in agreement with the above described observations (Scheme 57b). Complete characterization of the reaction products has not been carried out yet.

In this way, the chlorido ligand of **9** could easily be exchanged by a cyanido ligand in **14**. Furthermore, a reaction between **9** and isonitriles is demonstrated, illustrating that additional coordination to the nitrido complex is at least possible. However, these results point out that a ligand *trans* to the nitride is preferably avoided, unless the amide in the ligand backbone is protonated to an amine. The choice of another isonitrile, where its substituent is not as prone to elimination, might be able to activate the nitride moiety by coordination, at least as intermediate in further functionalizations.

3.4   Reaction with electrophiles

Typically early and mid TM nitrides react nucleophilic.[105] In order to functionalize the nitride unit, **9** was converted with different electrophiles. The use of organohalides (MeI), acid chlorides (acetyl chloride), anhydrides (acetic anhydride, trifluoroacetic anhydride), aldehydes, silicon compounds (Me$_3$SiCl, Me$_3$SiBr, Me$_3$SiOTf), phosphines (PPh$_3$, PMe$_3$), CO$_2$ and CO did not result in any reaction with the nitride.

With an organic electrophile, such as an alkyl triflate, **9** reacts selectively at the nitrido ligand. Imido complex [Re(≡NMe)Cl(PNP)]OTf (**16a**) is selectively formed with MeOTf (Scheme 55).[193] Methylation of the nitrido, rather than the amido group of the PNP backbone is indicated by the absence of ^{1}H-NOESY crosspeaks with the pincer backbone protons (Figure 35) and confirmed by single crystal X-ray diffraction. The square-pyramidally coordinated Re ion (τ = 0.16) in the imido complex exhibits a typical bond length (1.700(2) Å)[105] to the slightly bent (168.31(17)°) methylimido ligand. The amido nitrogen features planar coordination, indicating N$_{PNP}$ → Re π-donation, unlike in parent **9**. Importantly, DFT computations confirm that nitride over amide methylation is, in fact, favored by ΔG^0 = 33.2 kJmol^{-1}, contrasting with the thermodynamic preference of protonation. *Caulton* and co-workers reported the same selectivity for electrophilic amide vs nitride attack in case of [RuN{N(SiMe$_2$CH$_2$P^{t}Bu$_2$)$_2$}], which was attributed to steric effects.[210]
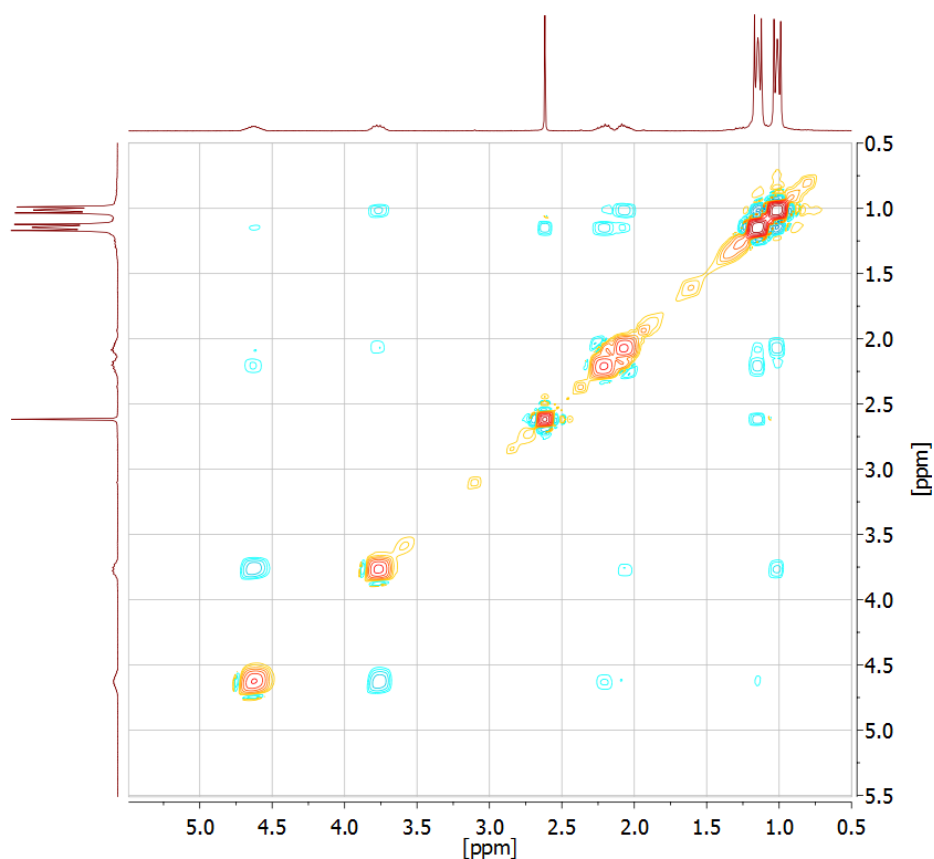
Figure 35: ^{1}H,^{1}H NOESY NMR spectrum of **16a.**
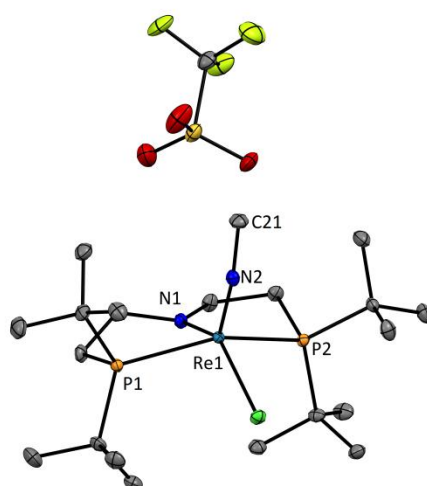
Figure 36: Molecular structure of **16a** *in the crystal. ORTEP plot with anisotropic displacement parameters drawn at the 50% probability level. The C–H hydrogen atoms are omitted for clarity. Selected bond lengths [Å] and angles [°]:Re1–Cl1 2.4030(5), Re1–N1 1.9486(18), Re1–N2 1.700(2), Re1–P1 2.4776(6), Re1–P2 2.4450(6); N1–Re1–Cl1 141.23(6), N1–Re1–N2 115.58(9), Cl1–Re1–N2 103.14(7), P1–Re1–P2 150.99(2), Re1–N2–C21 168.31(17).*

In analogy, the ethylimido complex **16b** is obtained upon reaction of nitride **9** with ethyl triflate (EtOTf) in essentially quantitative isolated yield (a = methyl-, b = ethyl-substituted, Scheme 55). Usually, the only observed side-product is protonated nitride **12**, which can be removed by washing with diethylether or crystallization out of toluene/ether. The NMR spectroscopic features of **16b** are close to **16a**, suggesting square-pyramidal geometry with the imide in the apical position as confirmed by X-ray diffraction for **16a** (Figure 36).[207]
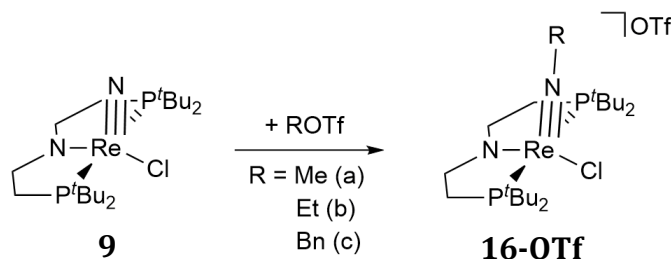
*Scheme 55: Synthesis of imides **16-OTf** by addition of alkyl triflates to **9**.*

Generation of the imides **16a/b-BF₄** can also be achieved using Meerwein salts [Me₃O][BF₄] or [Et₃O][BF₄].

To expand the reactivity scope to organotriflates containing π-systems, benzyl triflate was synthesized according to published procedures out of the respective organo-halide (benzylbromide) and AgOTf and used *in situ*.[211] Interestingly, the alkylation is only possible if a non-nucleophilic base (2,6-di-*tert*-butyl-2-methyl-pyridin) was added to the organotriflate mixture prior to the addition to **9**. Otherwise, the latter is almost quantitatively converted to the protonated species **12**, presumably due to the instability of the formed organotriflate. [(PNP)Re(NBn)(Cl)]OTf (**16c-OTf**, c = benzyl-substituted) is isolated in up to 60% yield and characterized by NMR spectroscopy and LIFDI mass spectrometry. The color of the complex and the chemical shift of its ^{31}P-NMR signal (δ_P = 90 ppm) is in the same region as for **16a** and **16b**. A singlet is observed for the benzylic NCH₂Ph group at 4.60 ppm in the ^{1}H-NMR spectrum (Figure 37), which shows coupling to the phenyl-groups in the aromatic region of the H,H-COSY-NMR spectrum (Figure 38). C-N bond coupling is indicated by NOESY cross peaks of the aromatic signals with the ^{t}Bu groups of the PNP ligand as well as to the benzylic protons (Figure 39). The signals for the PNP-backbone have a similar chemical shift compared to the other imido complexes **16a/b**.
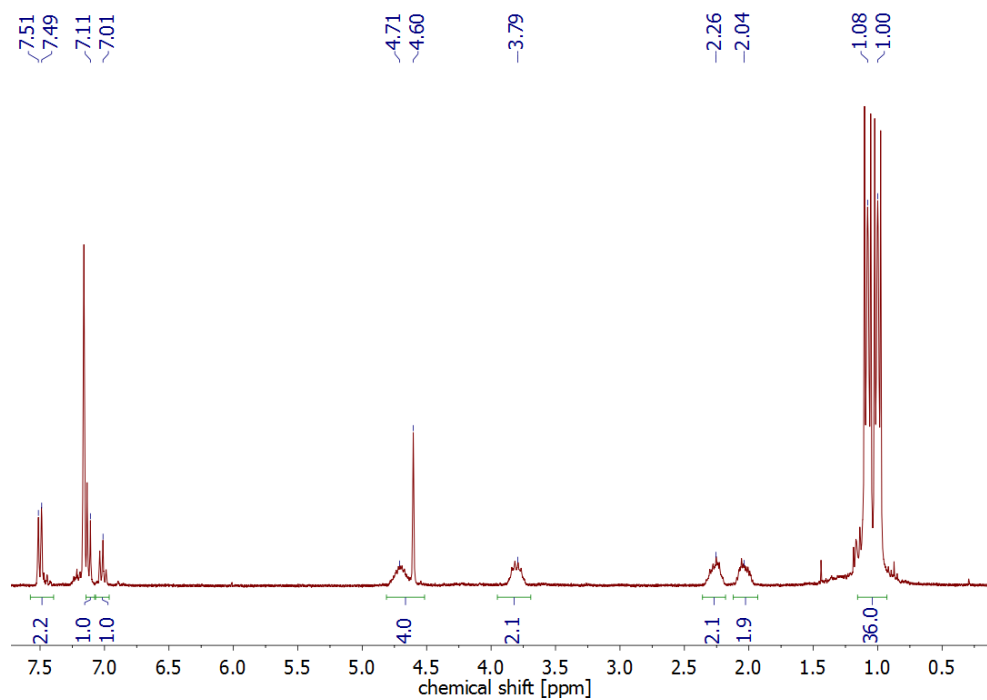
Figure 37: ^1H-NMR spectrum of isolated **16c-OTf** in C_6D_6.
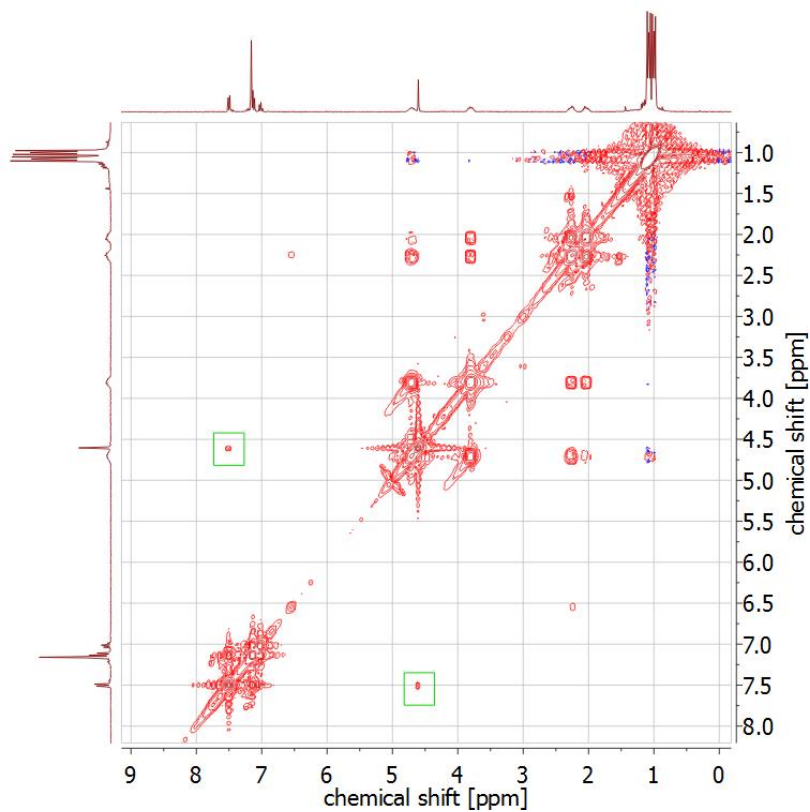
Figure 38: $^1H,^1H$-COSY NMR spectrum of **16c-OTf** in C_6D_6.
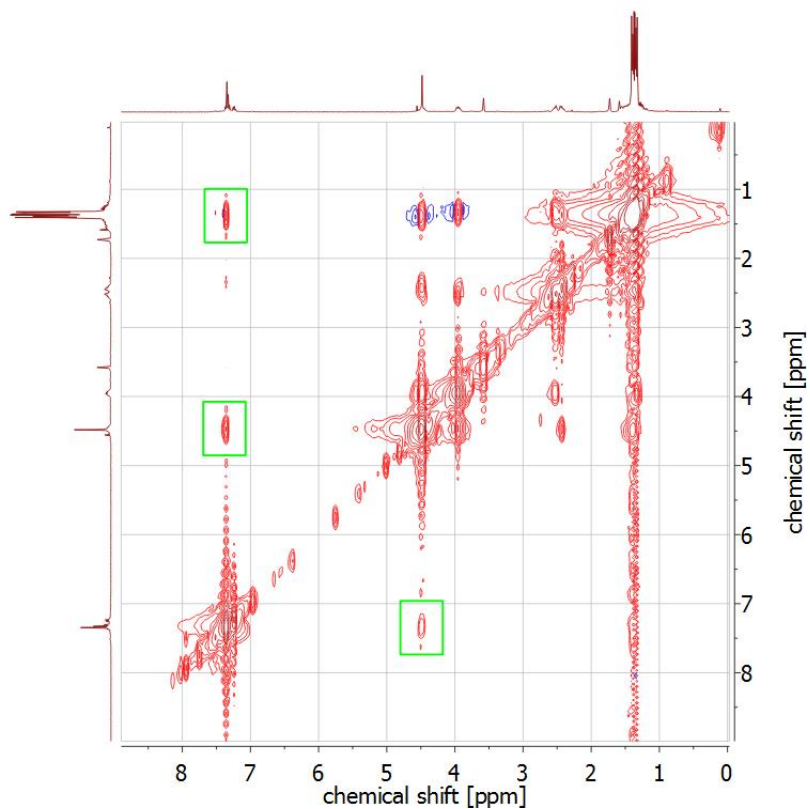
*Figure 39: $^1H,^1H$-NOESY spectrum of **16c-OTf** in d_8-THF.*

Hence, N_2 splitting and functionalization of the resulting nitride in terms of C-N bond formation has been accomplished. The next step represents the cleavage of the Re-N bond and the release of nitrogen containing organic molecules.

3.5   Reaction with trifluoromethanesulfonic anhydride

The yield of the benzylation is acceptable (60% isolated), however far lower than the yield for methyl- and ethylation (almost quantitative). In an attempt to avoid the formation of **12** as main side-product, another procedure to prepare organotriflates was utilized. This procedure uses the respective alcohol, a non-nucleophilic base and trifluoromethanesulfonic anhydride (Tf$_2$O).[212,213] Following this approach, the tentative organotriflate mixture was directly added to **9** without further workup. Intriguingly, **16c-OTf** was only observed in minor amounts in the resulting mixture with the main product being a new diamagnetic, C$_s$ symmetric species (δ_P = 102 ppm). A new signal was observed in the ^{19}F-NMR spectrum besides the triflate anion, indicating a reaction between **9** and Tf$_2$O. If the latter is purely added to **9**, the color of the solution immediately changes from yellow to green and selective formation of the new species is observed. Only signals for the ^{t}Bu substituents and the ligand backbone are observed in the ^{1}H-NMR spectrum. Product identification was accomplished by single crystal X-ray analysis[8] (Scheme 56) and LIFDI mass spectrometry, which allow an assignment as [(PNP)Re(NTf)Cl]OTf (**17-OTf**). Unfortunately, due to strong disorder, the crystallographic resolution does not allow for description of bond lengths and angles. This product could be isolated in high yield (87%) from the reaction mixture.
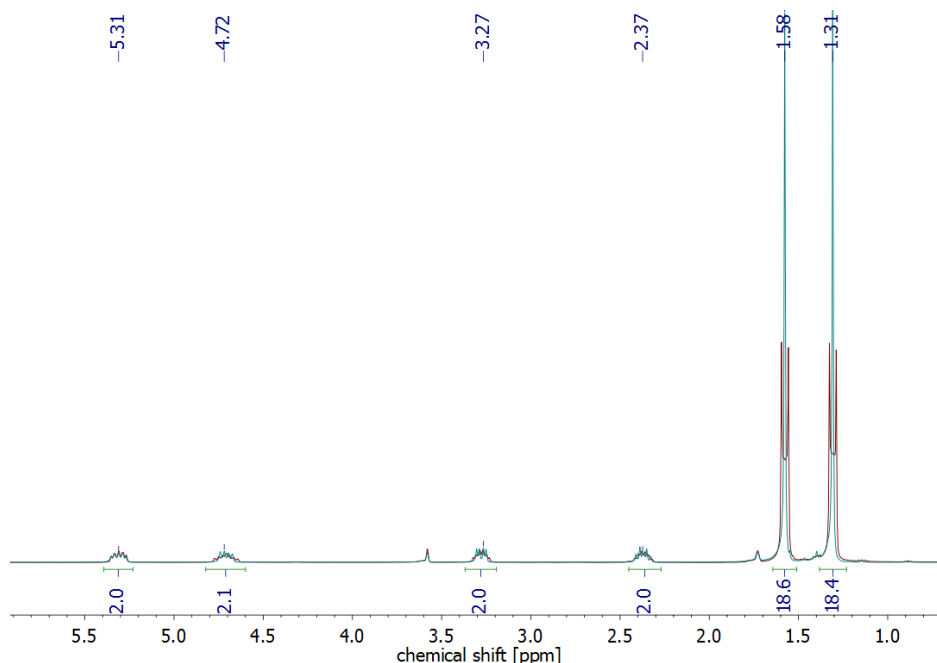
Figure 40: ^{1}H-NMR and ^{1}H{^{31}P}-NMR spectrum with selective phosphorous decoupling at 102 ppm of **17-OTf** *in d$_8$-THF.*

---

[8] Determination of the molecular structure was performed by Christian Volkmann.
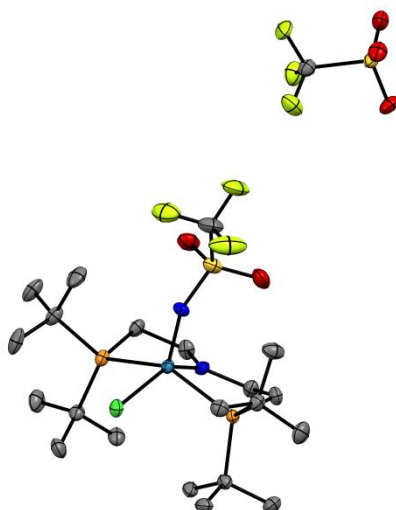
*Figure 41: Molecular structure of complex **17-OTf** derived by single-crystal X-ray diffraction. ORTEP plots with anisotropic displacement parameters set at 50% probability. Hydrogen atoms are omitted for clarity.*

Heating a solution of **17-OTf** in benzene (50°C, 3 days) or toluene (100°C, 18 h) results in selective formation of the protonated nitride **12-OTf**. The fate of the triflyl-group is indicated by ^{19}F-NMR spectroscopy, which shows for benzene one (δ_F = -62.4 ppm) and for toluene three (δ_F = -61.5 (39%), -62.1 (26%) and -62.3 ppm (35%)) new signals (Figure 42), which correspond to trifluoromethyl benzene (-64.0 ppm)[214] and *ortho-*, *meta-* and *para*-trifluoromethyl toluene (-62.5 (para), -63.3 (meta) and -63.6 (ortho) ppm), respectively.[215] Further analysis of this reaction e.g. by GC-MS has not been carried out yet.
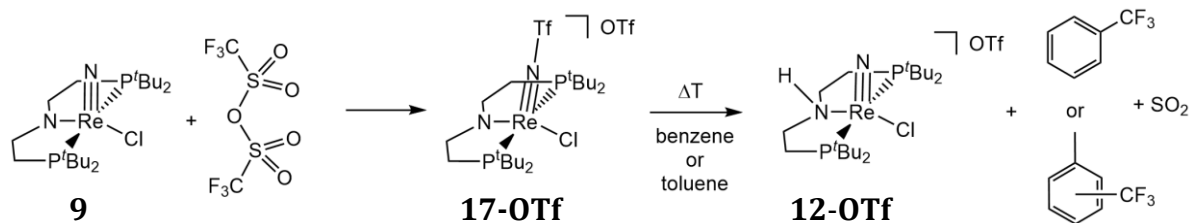
*Scheme 56: Reaction of **9** with Tf$_2$O to produce **17-OTf** and its presumed degradation in aromatic solvents.*
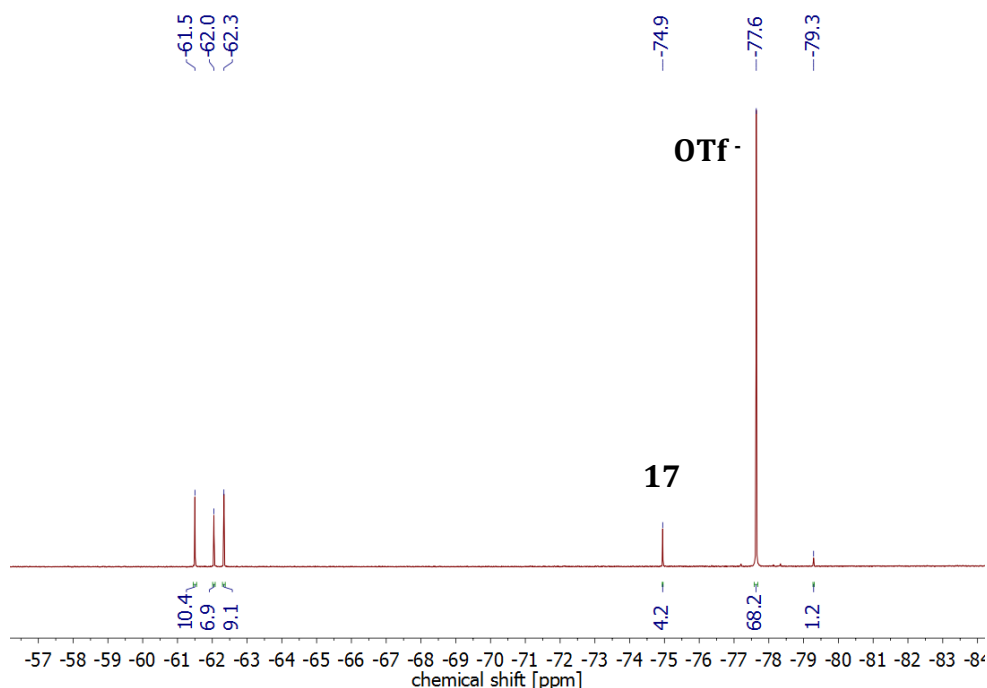
*Figure 42: $^{19}F\{^1H\}$-NMR spectrum of **17-OTf** after heating to 100°C for 18 h in d_8-toluene.*

Addition of a base to deprotonate **12**-**OTf** back to **9** might enable a catalytic application of this reaction. However, this base must be stable under the reaction conditions and strong enough to deprotonate **12**-**OTf**. Catalytic trifluoromethylation of arenes and heteroarenes is a highly studied field especially in organic and pharmaceutical chemistry.[216,217] Common cross-coupling reactions usually require stoichiometric reactants, harsh conditions and/or preactivated substrates and are in general catalyzed by late TM (Cu, Ag, Pd, Ni). Various CF_3 sources, which exhibit nucleophilic (e.g. Me_3SiCF_3),[218] electrophilic (e.g. Umemoto´s reagent)[219] or radical reactivity (e.g. Langlois´ reagent, $NaSO_2CF_3$) are known.[220,221] Prefunctionalized (hetero)arenes, aryl halides and boronic acids are usually used with nucleophilic or electrophilic CF_3 reagents. Trifluoromethylation of non-activated arenes can be achieved by CF_3 radicals as shown for the first time by *MacMillan* in 2011, using photoredoxcatalysis with ruthenium complexes and CF_3SO_2Cl as CF_3 source.[222] Remarkable progress has been made recently by the groups of *Li* and *Mi*, which used TM free photocatalysis for trifluoromethylation of arenes, employing $NaSO_2CF_3$.[223] In this context, the observed CF_3-group transfer reactivity of **17-OTf** is a novel contribution. Catalysis with mid/early TM is uncommon, only a base and Tf_2O are needed and the use of Tf_2O as CF_3 source has not been shown to the best of my knowledge. However, in first instance, it hast to be clarified, if the observed trifluoromethylation is actually a thermally induced process or photoinduced and if the mechanism involves electrophilic $^+CF_3$ or $\cdot CF_3$ radicals.

Further preliminary reactivity tests of **17·OTf**, did not give any satisfactory results. With H_2 or alkenes, no reaction is observed. Hydrid sources (LiHBEt$_3$), Grignard reagents (MeMgCl) and phosphines (PMe$_3$) cause degradation in various signals in the ^{1}H- and ^{31}P-NMR spectra. However, the easy functionalization with Tf$_2$O might offer a route to a more activated {ReN}-moiety and therefore allow different functionalizations of the nitrogen unit.

4   Conversion of Dinitrogen to Organonitriles

Parts of this chapter have been published in 2016 in the Journal *Angewandte Chemie int. Ed.* under the title: "*Conversion of Dinitrogen into Acetonitrile under Ambient Conditions*".[207]

4.1   Strategy for N_2 into organonitrile transformation

According to thermochemical arguments, nitriles are attractive targets as the formation of strong C≡N bonds (D^0(HC≡N) = 937 kJmol^{-1}) facilitates offsetting the large N_2 bond energy (941 kJmol^{-1}).[111] Cummins and co-workers reported elegant synthetic cycles for the six-electron transformation of N_2 to nitriles mediated by Mo and Nb complexes.[110,132] The routes start with initial dinitrogen splitting,[83] followed by nitride acylation with silyltriflate and acylchloride. Subsequent stepwise three-electron reduction requires further silyltriflate and Lewis acid (SnCl$_2$ or ZnCl$_2$) for oxygen removal with nitrile release in up to 38% yield over all five steps.[110] In this synthetic scheme re-reduction of the (formal) catalyst is a purely metal-centered process (Scheme 57, a).
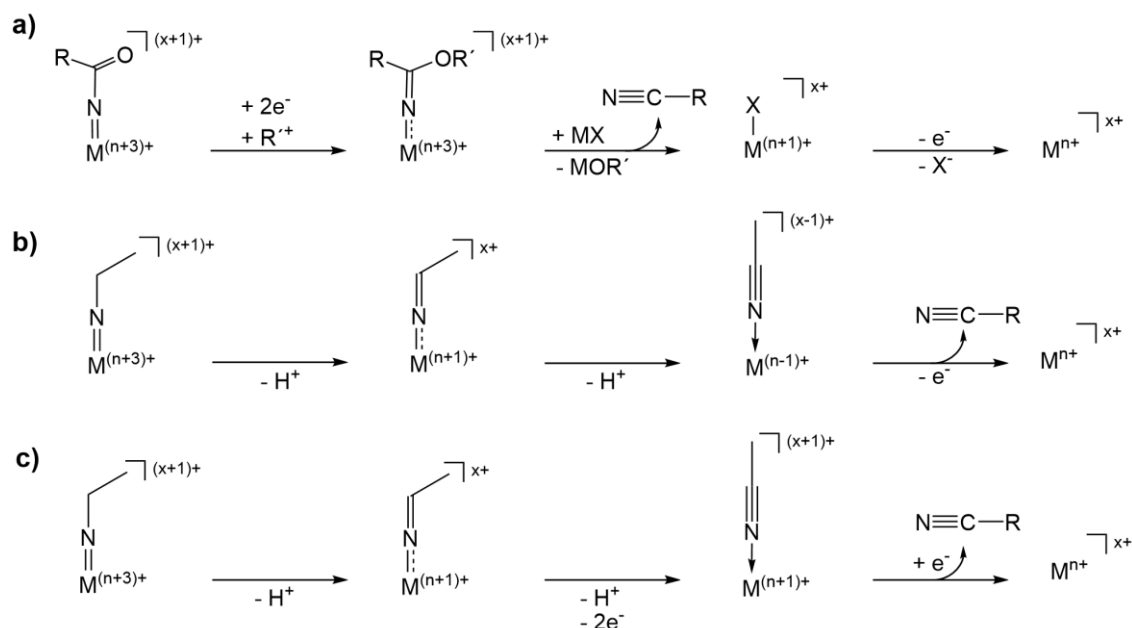
Scheme 57: Schematic pathways of nitrile synthesis after N_2–splitting and functionalization: Through nitride acylation established by Cummins et al. (a)[110] or through nitride alkylation (b and c) evaluated herein.

This work was the inspiration to evaluate new ways of N_2 into nitrile conversion, which rely on intramolecular electron transfer: The interconversion of imido and nitrile ligands via 1-azavinylidenes (or ketimides) by simple double de/protonation was previously reported (Scheme 57, b), but not applied to N_2 fixation.[192,224] Importantly, both deprotonation steps are associated with formal metal/ligand two-electron redox steps offering new strategies for metal reduction within a (pseudo)-catalytic N_2 functionalization cycle (Scheme 57, b and c). Following these strategies, in this chapter several routes for the conversion of N_2 into acetonitrile via rhenium-mediated N_2 splitting, nitride alkylation, and ligand oxidation are reported leading up to a synthetic cycle in three steps in over 50% yield per cycle.

4.2   Acetonitrile release by double deprotonation

In the previous chapter, dinitrogen splitting upon reduction of rhenium(III) pincer complex **3** with Na/Hg or CoCp*$_2$ and alkylation of the resulting rhenium(V) nitride **9** to the imido complexes **16a-c-OTf** was reported. This chapter is focusing on the conversions of **16b-OTf**.

16b-OTf is deprotonated quantitatively with KN(SiMe$_3$)$_2$ (KBTSA) giving the respective red-brown 1-azavinylidene rhenium(III) complexes [(PNP)Re(N=CHCH$_3$)Cl] (**18b**; Scheme 58). The synthesis of **18b** can also be carried out as a one-pot reaction directly from **9** by successive alkylation and deprotonation in benzene with almost quantitative spectroscopic and over 80% isolated yield.
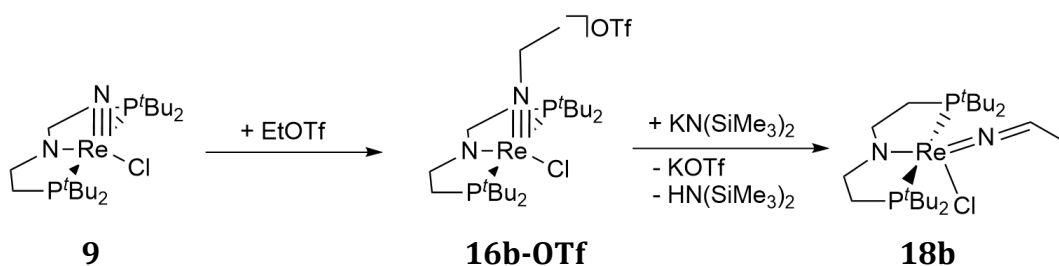
Scheme 58: *Alkylation of* **9** *and deprotonation of the resulting imide* **16** *to yield the azavinyildene species* **18**.

Spectroscopic characterization of complex **18b** indicates the presence of two isomers in about 60:40 ratio with diagnostic ^{1}H, ^{13}C, and ^{15}N NMR signals for the azavinylidene ligands, respectively (Figure 44). This observation is in line with the

formation of two stereoisomers as a result of hindered 1-azavinylidene rotation about the Re=N and N=C double bonds owing to strong Re→N back bonding. The N=C double bond stretching vibration of the ketimide can be assigned to a weak band in the vibrational spectrum at 1594 cm^{-1}, which shifts by 22 cm^{-1} upon ^{15}N-labelling.
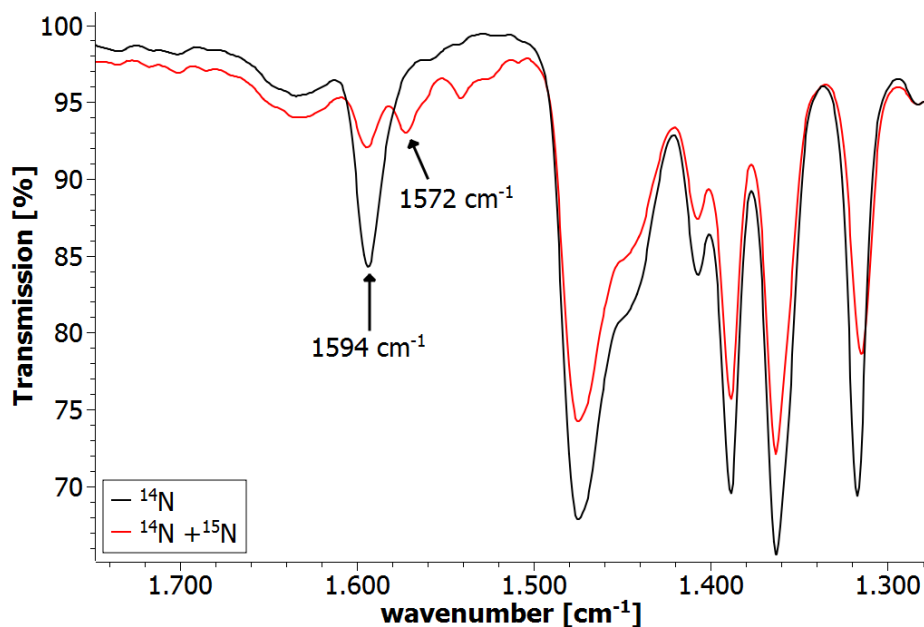
*Figure 43: IR spectrum of **18b** (black) and 50% ^{15}N labelled **18b-^{15}N** (red) with bands assigned for υ(C=N).*
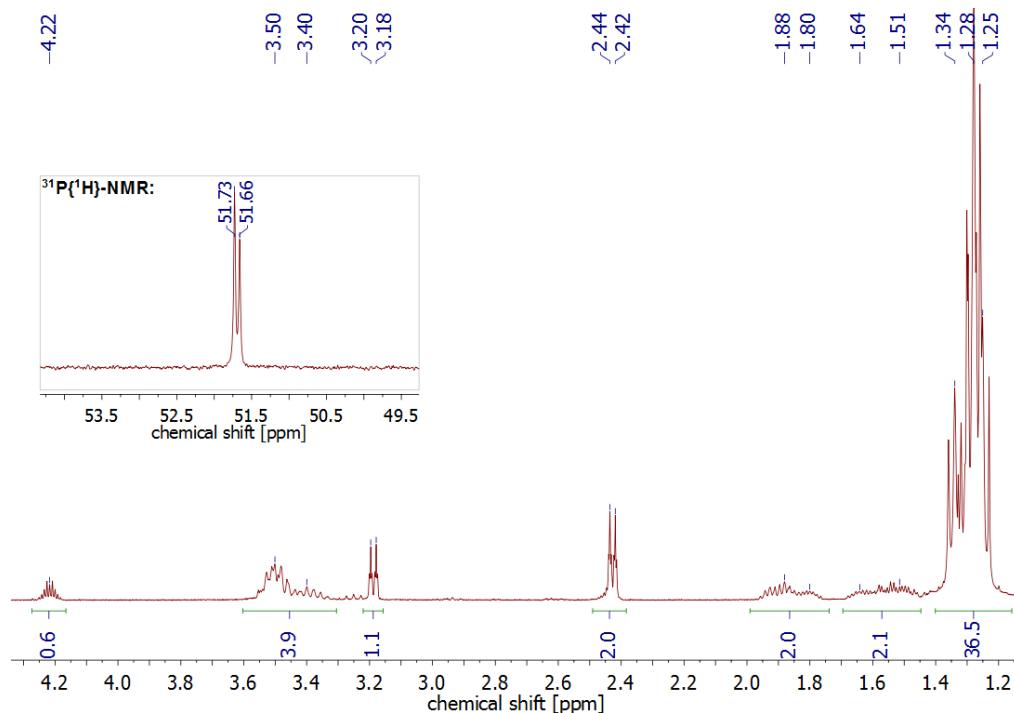
*Figure 44: ^{1}H and ^{31}P{^{1}H}-NMR spectra of the two isomers of **18b** in C_6D_6.*

93

The structural assignment of **18b** is confirmed by single-crystal X-ray diffraction (Figure 45).[9] The coordination geometry around the rhenium ion is close to that in the methylimide **16a** and all N-Re-N and N-Re-Cl bond angles of the two structures are the same within 5°. However, the almost linear Re-N-C moiety of **18b** exhibits considerably longer Re-N (Δd =+ 0.12 Å) and shorter C-N (Δd = -0.17 Å) bonds than **16a**, in line with the changes in Re-N and C-N bond orders and with the only other structurally characterized rhenium 1-azavinylidene complex reported.[225]

*Figure 45: Molecular structures of complex **18b** derived by single-crystal X-ray diffraction. ORTEP plots with anisotropic displacement parameters set at 50% probability. Hydrogen atoms except for the azavinylidene ligand are omitted for clarity. Selected bond lengths [Å] and angles [°]: Re1–N1 1.948(5), Re1–N2 1.822(4), Re1–Cl1 2.3962(14), N2–C20 1.273(7), C20–C21 1.489(10); N1-Re1-N2 120.5(2), N1-Re1-Cl1 135.07(15), N2-Re1-Cl1 104.39(16), P1-Re1-P2 162.01(5), Re1-N2-C20 174.3(5), N2-C20-C21 125.7(7).*

The ketimido complex **18b** can be further deprotonated if the resulting rhenium(I) ion is stabilized by strong π-acceptor ligands. For example, the reaction of **18b** with KBTSA and *tert*-butylisonitrile (CN*t*Bu, 2 eq) gives the bis-isonitrile complex [(PNP)Re(CN*t*Bu)$_2$] (**19**) immediately in almost quantitative yield with concomitant release of acetonitrile (Scheme 59, Figure 46). If no external base is added, the amide in the ligand backbone is protonated and the octahedrally coordinated tris-isonitrile complex [(HPNP)Re(CN*t*Bu)$_3$]Cl (**20**) is generated in about 90% spectroscopic yield over the course of 10 days (Scheme 59). Two intermediates (δ_P = 58 and 62 ppm) are observed during the reaction, but escaped further characterization (Figure 47). Heating of the reaction mixture (60°C) leads to degradation in several compounds. Besides the characteristic C$_s$ symmetric signals in the ^{1}H-NMR spectrum of **20** (N-H: δ_H = 7.8 ppm in C$_6$D$_6$, three singlets for CN*t*Bu), the structural assignment could be verified by X-ray analysis (Figure 48).[9] The crystallographic resolution however, does not allow for description of bond lengths and angles due to strong disorder.

---

[9] X-ray diffraction was performed by Christian Würtele.
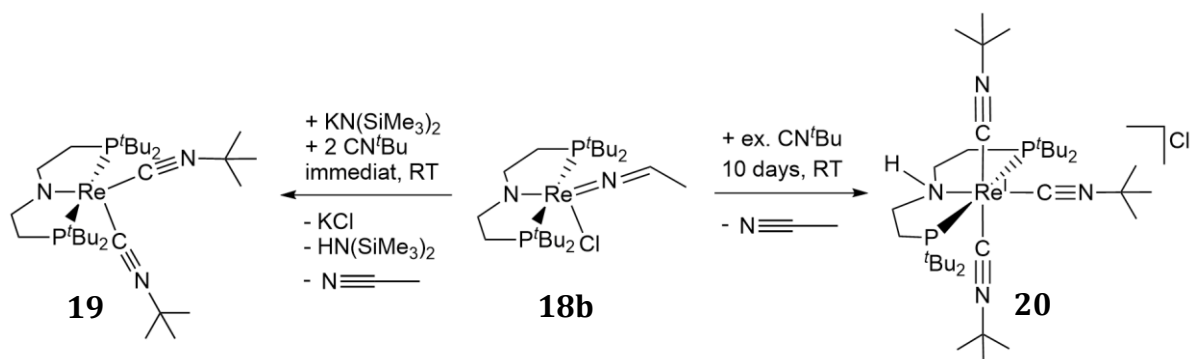
Scheme 59: Reactions of ethylazavinylidene 18b with CNtBu under different conditions.
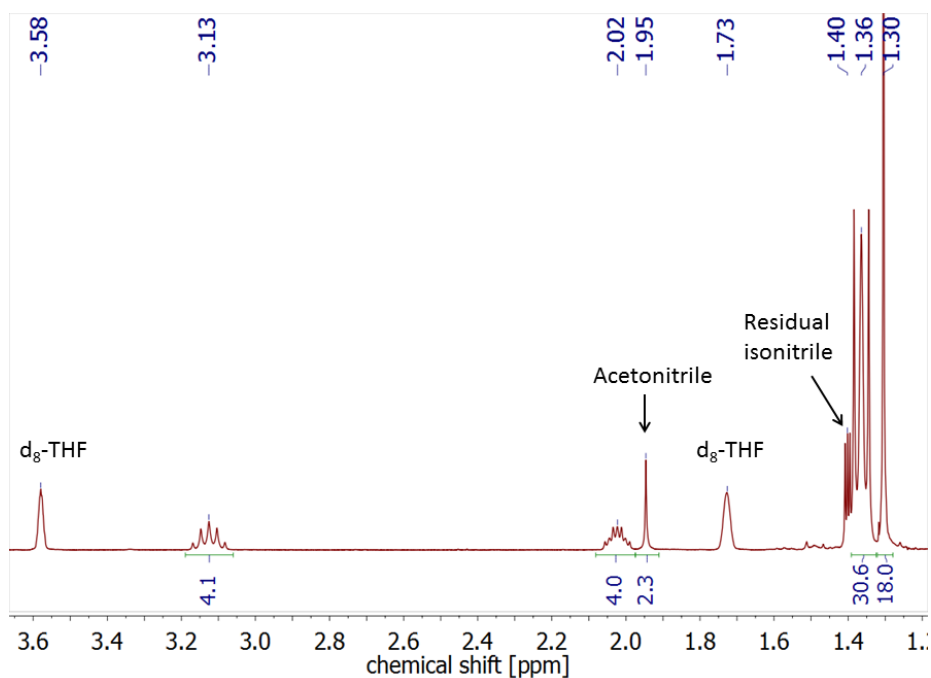
Figure 46: Deprotonation of 18b with KN(SiMe₃)₂ in d₈-THF in the presence of CNtBu (2.2 eq).
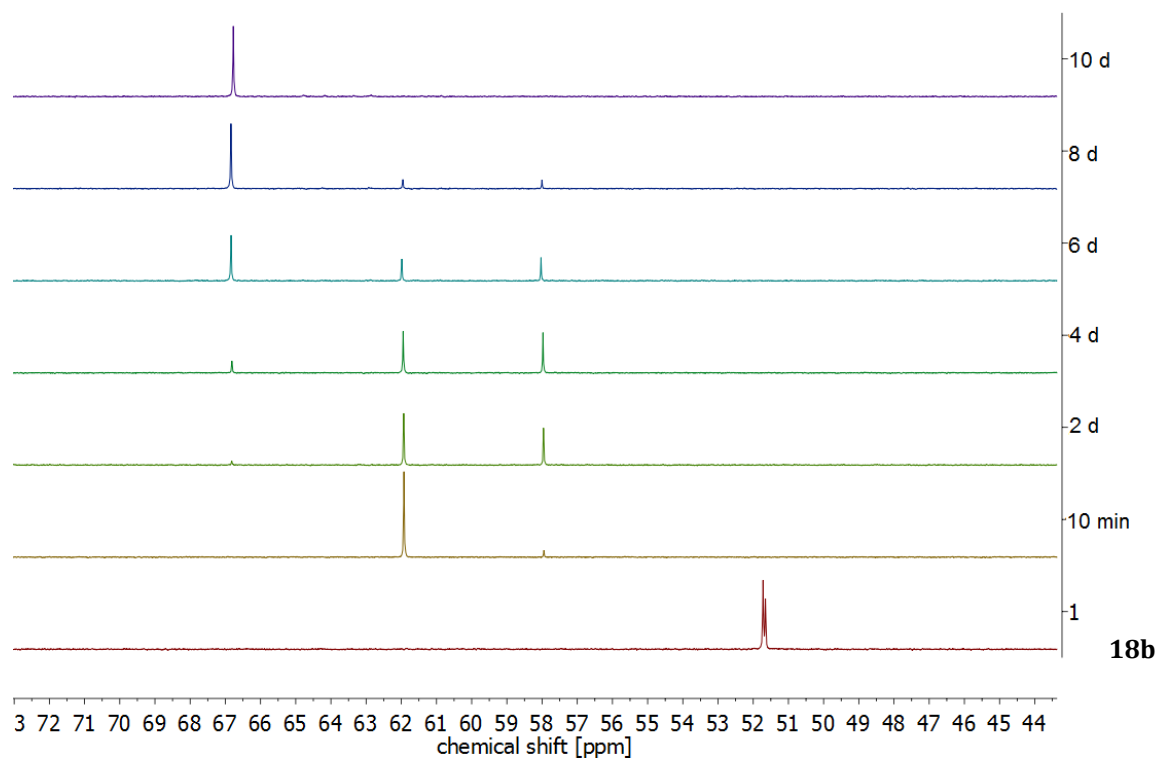
*Figure 47: Time dependent ³¹P{¹H} NMR spectra of the addition of excess CNᵗBu to **18b** in C₆D₆.*

While **19** has C$_{2v}$ symmetry in solution on the NMR time-scale, in the crystal (Figure 48) this compound features one strongly bent isonitrile ligand (C26-N3-C27: 134.2(4)°) while the other isonitrile remains almost linear (C21-N2-C22: 168.7(5)°).[10] Such a strong bending is rare and indicates an unusually high degree of Re→C π-back bonding as a consequence of the electron-rich nature of the {(PNP)Re^I} fragment.[226] Accordingly, the C26-N3 bond (1.222(5) Å) of the bent isonitrile is considerably longer than in the linear isonitrile moiety (C21-N2: 1.181(6) Å).

---

[10] X-ray diffraction was performed by Christian Würtele.
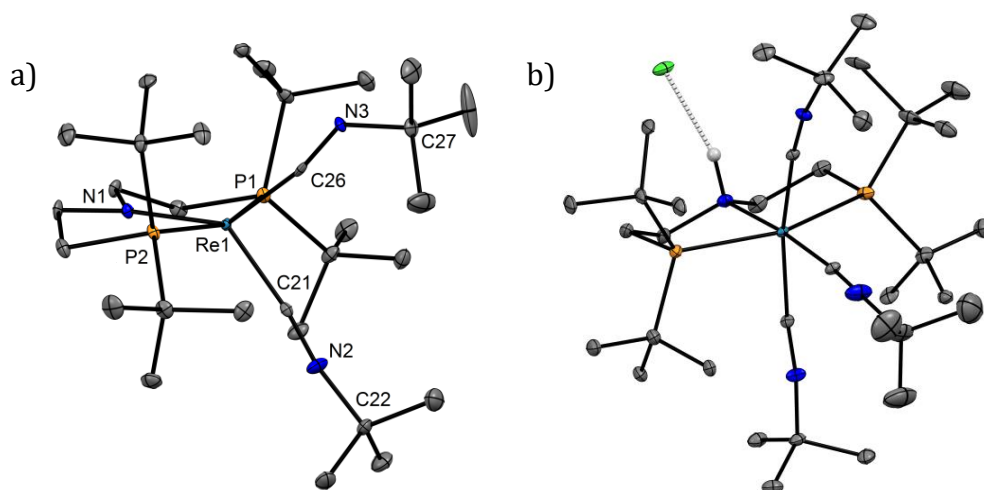
*Figure 48: Molecular structures of complexes **19** (a) and **20** (b) derived by single-crystal X-ray diffraction. ORTEP plots with anisotropic displacement parameters set at 50% (a) and 30% (b) probability. Hydrogen atoms are omitted for clarity. Selected bond lengths [Å] and angles [°] for **19**:Re1–N1 2.028(3), Re1–C21 1.937(4), Re1–C26 1.906(4), C21–N2 1.181(6), C26–N3 1.222(5); N1-Re1-C21 131.76(15), N1-Re1-C26 140.30(15), Re1-C21-N2 171.9(4), Re1-C26-N3 168.9(3), C21-N2-C22 168.7(5), C26-N3-C27 134.2(4).*

The electronic asymmetry is also resolved in the IR spectrum, which features bands in two regions at around 1960 cm^{-1} and 1760 cm^{-1}, respectively assignable to the linear and bent isonitriles (Figure 49). The low-energy stretching mode reflects the strongly reduced character of the bent isonitrile. Both bands are split into two, respectively, which can be rationalized with conformational isomers, as was previously reported for complexes with mixed linear/bent isonitriles.[226]
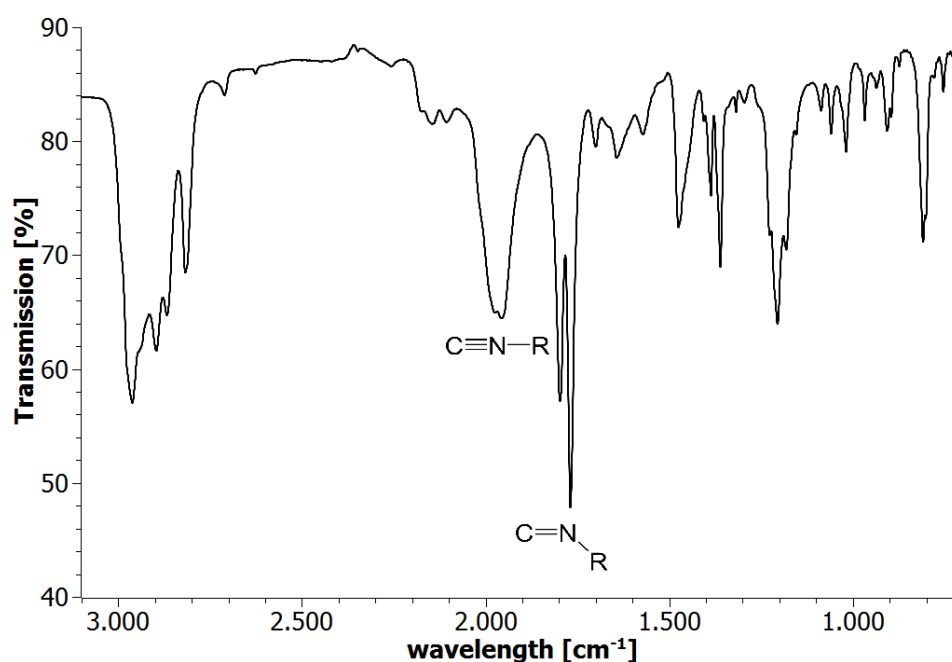
*Figure 49: IR spectrum of **19** (KBr pellet).*

For completion, the reactivity of imido complex **16b-OTf** towards isonitriles was examined. As expected, in the presence of 2 equiv. of base, the bis(isonitrile) complex **19** is formed selectively, since the first equivalent of base deprotonates the imide to **18b**, which can be further deprotonated to **19** under release of acetonitrile (Scheme 59). However, CN^{t}Bu also immediately reacts with the imido complex **16b-OTf** without a base. In a stoichiometric reaction, the selective formation of a new compound is monitored (δ_P = 33.6 ppm). Curiously, a signal shifted rather to the high field region of the ^{1}H-NMR spectrum is observed (d_H = -0.0 ppm), which couples only to a doublet at a chemical shift of 3.9 ppm, as stated by COSY-NMR spectroscopy (Figure 50). These signals are assigned to a newly formed azavinylidene group. A broad signal in the low field region (d_H = 6.0 ppm) coupling to backbone protons, indicates protonation of the backbone nitrogen. It is assumed, that coordination of the isonitrile favors proton migration from the ethyl substituent to the amide N_{PNP}, generating [(^{H}PNP)Re(NCHCH$_3$)(CN^{t}Bu)(Cl)]OTf (**21**, Scheme 60). Although the complex is cationic, the comparatively high electron density is expressed by strong shielding and a considerable high field shift of the N=CH-R proton.
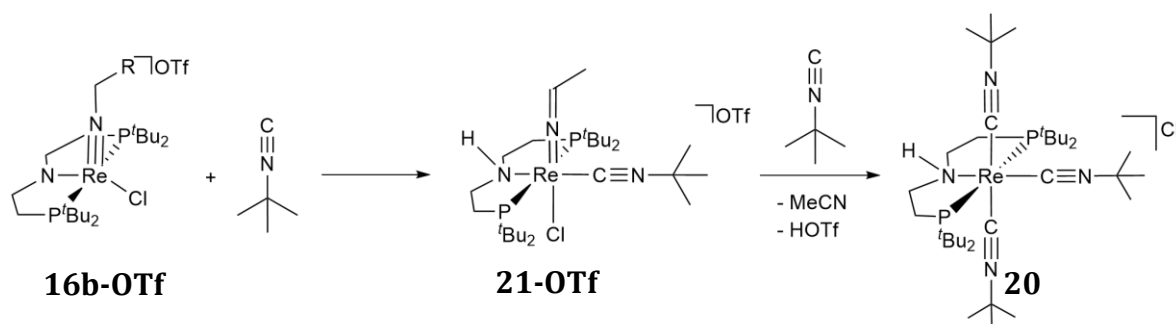
*Scheme 60: Formation of **21** and **20** upon addition of isoniriles to **16b**.*

Structural confirmation could be obtained by X-ray diffraction (Figure 51). The bond lengths of the azavinylidene ligand are similar to **18**, however the Re-N-C unit is slightly more bent (166.6° compared to 172.6° (**18a**) and 174.3° (**18b**)). The isonitrile ligand is bound linearly (179.6°) and the Re-C bond length is a little elongated compared to the bis(isonitrile) complex **19** (Δd = +0.1 Å).

If further equivalents of isonitrile are added to **21**, degradation to **20** occurs with spectroscopic yields of 65% and formation of various side-products.
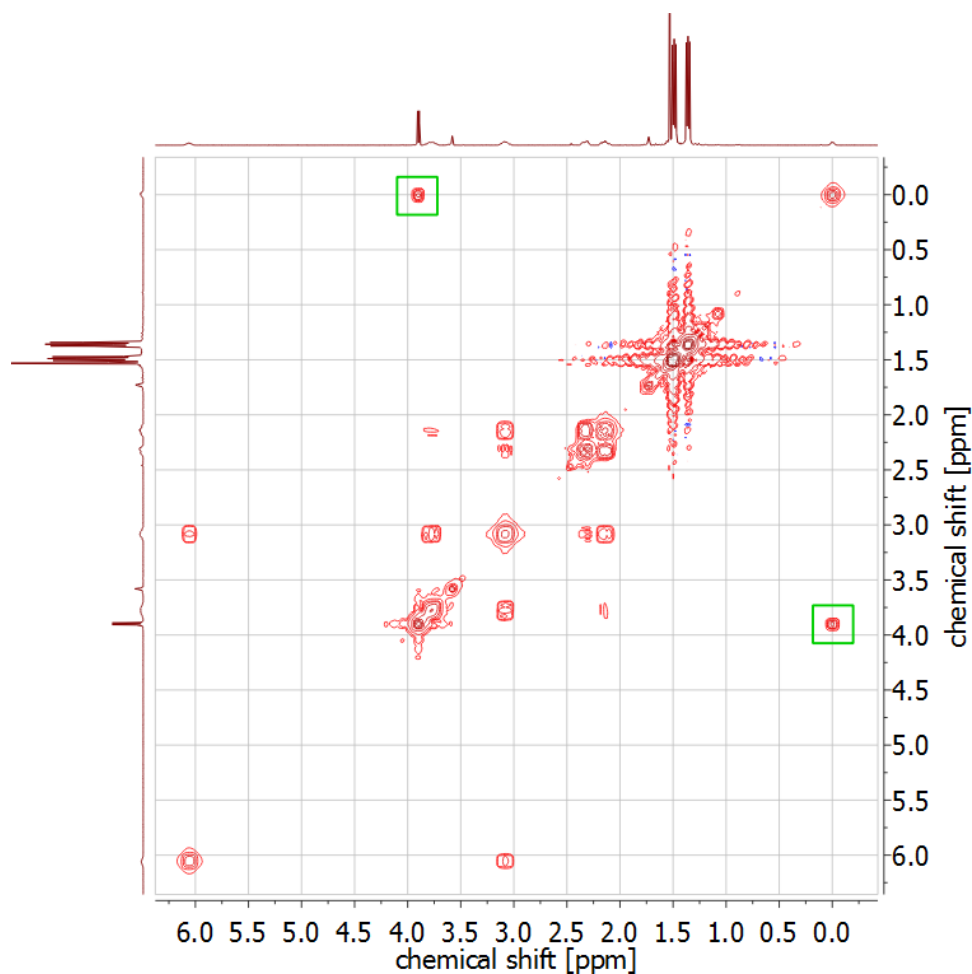
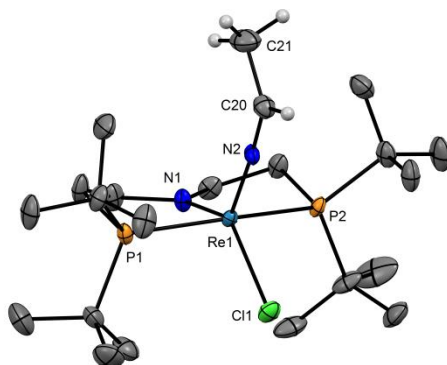*Figure 50: ¹H,¹H-COSY-NMR spectrum of **21** in d₈-THF.*

*Figure 51: Molecular structure of complex **21** derived by single-crystal X-ray diffraction. ORTEP plots with anisotropic displacement parameters set at 50% probability. Hydrogen atoms are omitted for clarity except for the azavinylidene ligand and the N-H proton. Selected bond lengths [Å] and angles [°]: Re1–N1 2.2020(11), Re-N2 1.8177(12), Re1-C23 2.0137(14), N2-C21 1.2785(18), C23-N3 1.1587(18); N1-Re1-N2 114.71(5)°, N2-Re1-C23 84.59(5)°, C23-Re1-Cl1 77.85°, N1-Re1-Cl 82.84°, P1-Re1-P2 159.520(12)°, Re1-C23-N3 179.56(14), Re1-N2-C21 166.60(12).*

4.3 Acetonitrile release by oxidative functionalization

Intramolecular four-electron charge transfer from the ethylimido ligand to the metal by double deprotonation (Scheme 57b) is in fact feasible, if the electron-rich {(PNP)Re^{I}} fragment is trapped by π-accepting ligands, such as isonitriles. However, regeneration of parent **3** on this route was unsuccessful, so far. Therefore, conversion of **18b** by oxidative functionalization of the azavinylidene ligand was examined. Cyclic voltammetry (CV) reveals reversible oxidation of **18b** at low potential (E$_0$ = -0.58 V) and irreversible oxidation beyond +0.55 V (Figure 52).
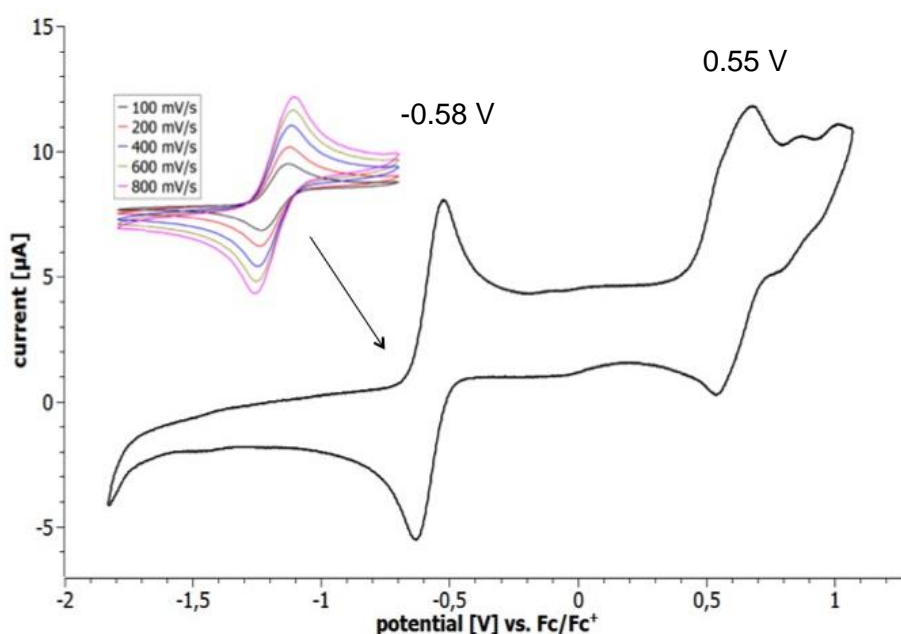
*Figure 52: Cyclic voltamogram of complex **18b** (2 mM, DCM, 100 mV/s).*

Accordingly, chemical oxidation with one equivalent of AgPF$_6$ in CH$_2$Cl$_2$ results in the formation of a red, paramagnetic product (Figure 53). While this compound could not be isolated due to slow degradation, in situ hydrogen-atom transfer (HAT) with 2,4,6-tri-*tert*-butylphenoxy radical (after preceding oxidation of **18b** with AgOTf) gives the vinylimido complex [(PNP)Re(N-CH=CH$_2$)Cl][OTf] (**22-OTf**) in spectroscopic yields beyond 80% (Scheme 61). The vinyl substituent in **22** is unequivocally identified by its ^{1}H-NMR signature (Figure 54), while the signals for the pincer ligand exhibit only small differences from those of the imido and ketimido complexes **16** and **18**. Notably, without preceding oxidation of **18b** (with AgPF$_6$ or AgOTf) no reaction is observed with 2,4,6-tri-*tert*-butylphenoxy radical.

100
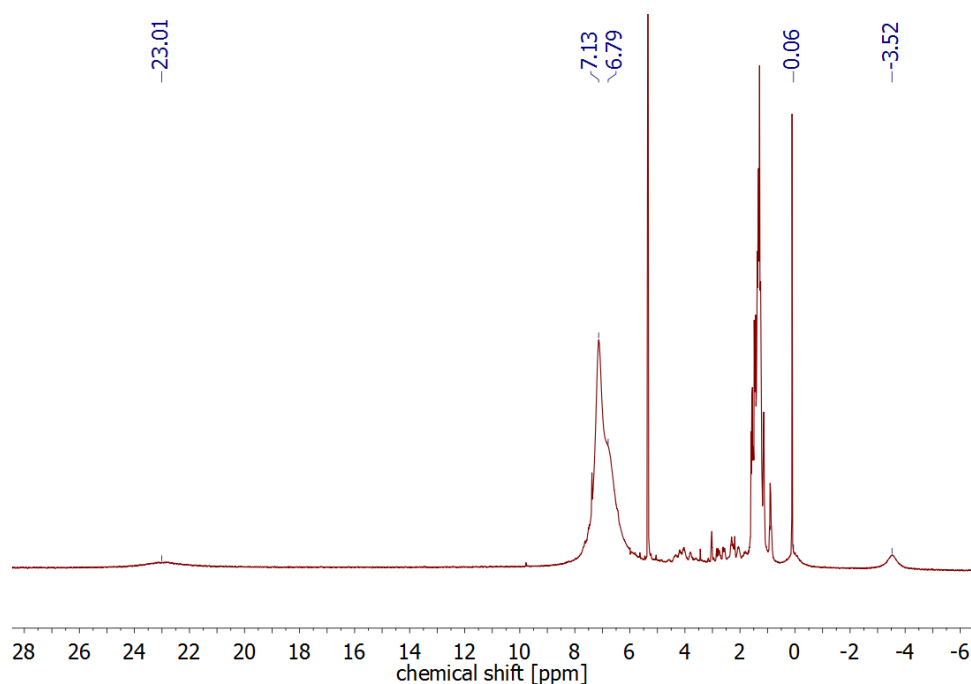
*Figure 53: ^{1}H-NMR spectrum of the 1e$^-$ oxidation of **18b** with Ag$^+$ in CD$_2$Cl$_2$.*
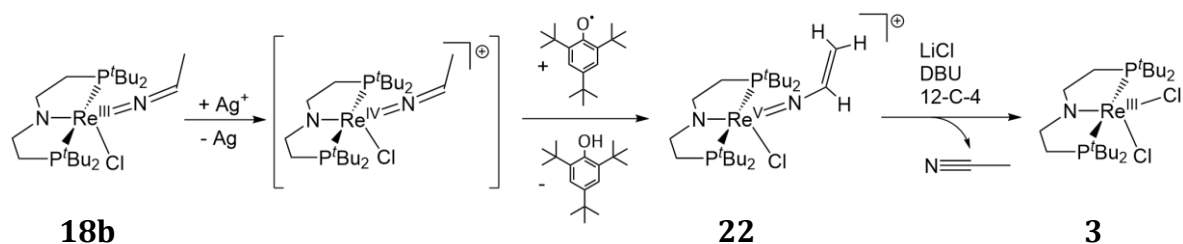
*Scheme 61: Synthesis of acetonitrile upon oxidation of N$_2$–derived ketimide **18b**.*

Hence, formal hydride abstraction from **18b** by stepwise one-electron oxidation and subsequent HAT favors the formation of an unusual rhenium(V) vinyl imide over the rhenium(III) acetonitrile tautomer (Scheme 62). This observation again emphasizes the distinct tendency of the electron-rich {(PNP)ReCl} core for M→N back bonding. However, the nitrile isomer [(PNP)Re(NCMe)Cl]$^+$ was computed to exhibit a triplet ground state that lies only around ΔG^0 = +16 kJmol^{-1} higher in energy than **22**. This result suggests that acetonitrile elimination might be accessible on the rhenium(III) stage by trapping of the {(PNP)ReCl}$^+$ fragment. Accordingly, the reaction of **22** with LiCl, crown ether (12-C-4) and substoichiometric amounts of 1,8-diazabicyclo[5.4.0]undec-7-ene (DBU) results in formation of parent **3** and acetonitrile, closing a full synthetic cycle. Without DBU no reaction is observed and

101

the non-nucleophilic base presumably facilitates proton transfer for vinyl-group tautomerization.
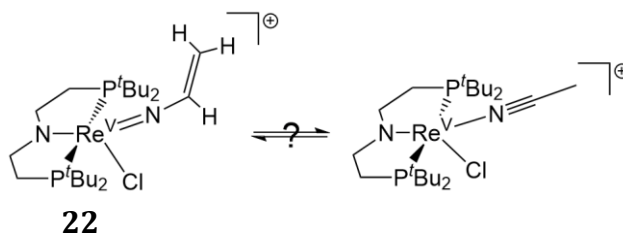
*Scheme 62: Proposed equilibrium between **22** and its acetonitrile tautomer.*
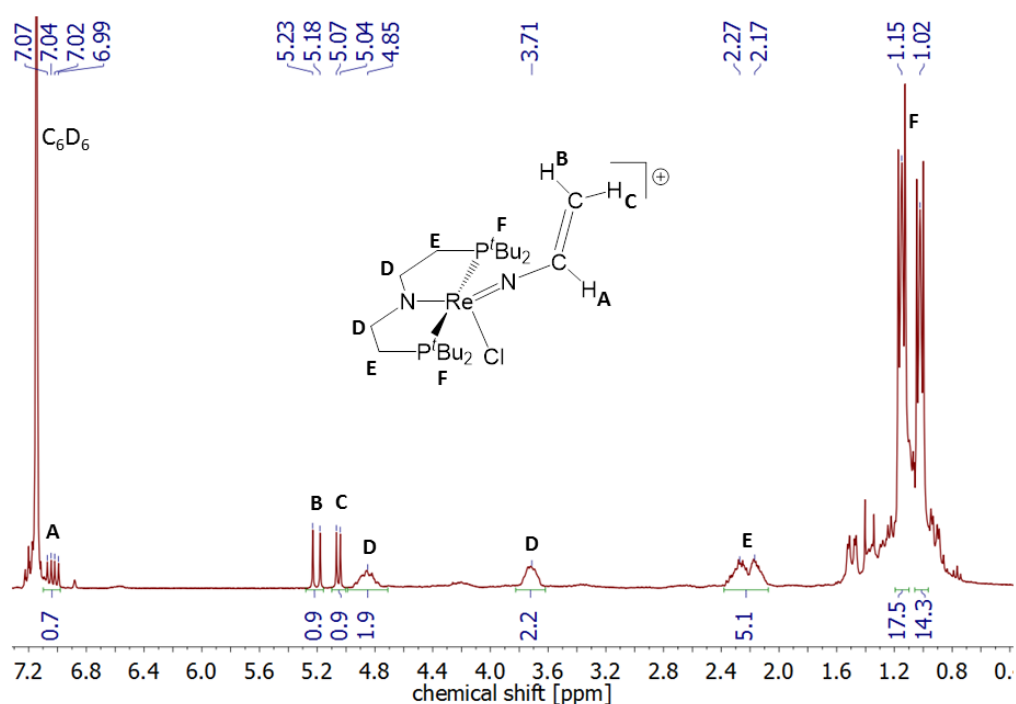
*Figure 54: ^{1}H-NMR spectrum of the synthesis of **22** from **18b** in C_6D_6.*

Albeit the spectroscopic yield in **3** and MeCN is only around 30% (internal ^{1}H-NMR standard naphthalene, Figure 55) besides several other unidentified products, these results define the requirements for oxidative acetonitrile release from **18b**: A two-electron oxidant and a base for formal hydride removal in combination with a chloride source to stabilize rhenium(III).

To raise the overall yield of the synthetic cycle, several reagents were screened that fulfill the aforementioned requirements. For example, **18b** reacts with a mixture of CuCl$_2$ (2 eq) and DBU (1 eq) to give **3** in around 20% spectroscopic yield (^{31}P-NMR, Figure 56). The main product however turned out to be a C$_1$ symmetric species,

102

indicating an alteration of the ligand backbone. Not only the azavinylidene ligand is prone to oxidation, but also the CH_2 groups of the saturated ethylene bridges (see chapter II.2), which might occur under these reaction conditions. Best results were obtained using N-chlorosuccinimide (NCS) for oxidation. Reaction of **18b** with 2 eq NCS (Scheme 5) gives free acetonitrile in over 90% yield by ^{1}H-NMR (internal standard hexamethylbenzene, Figure 57).
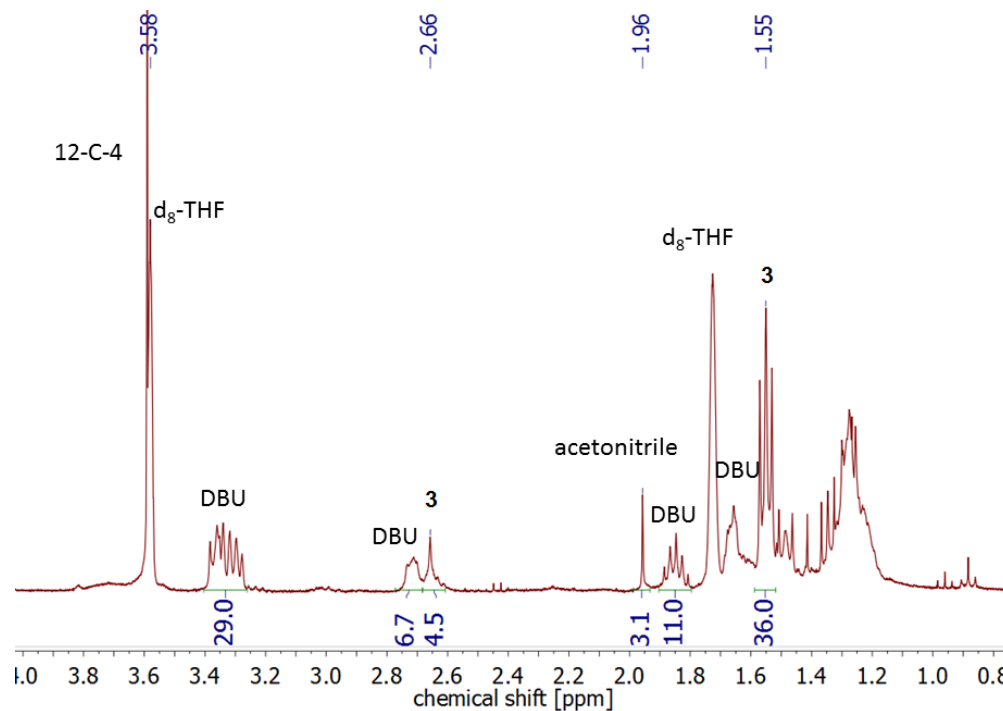
*Figure 55: ^{1}H-NMR spectrum of the release of acetonitrile from **22** with LiCl/12-C-4/DBU in d$_8$-THF.*

103
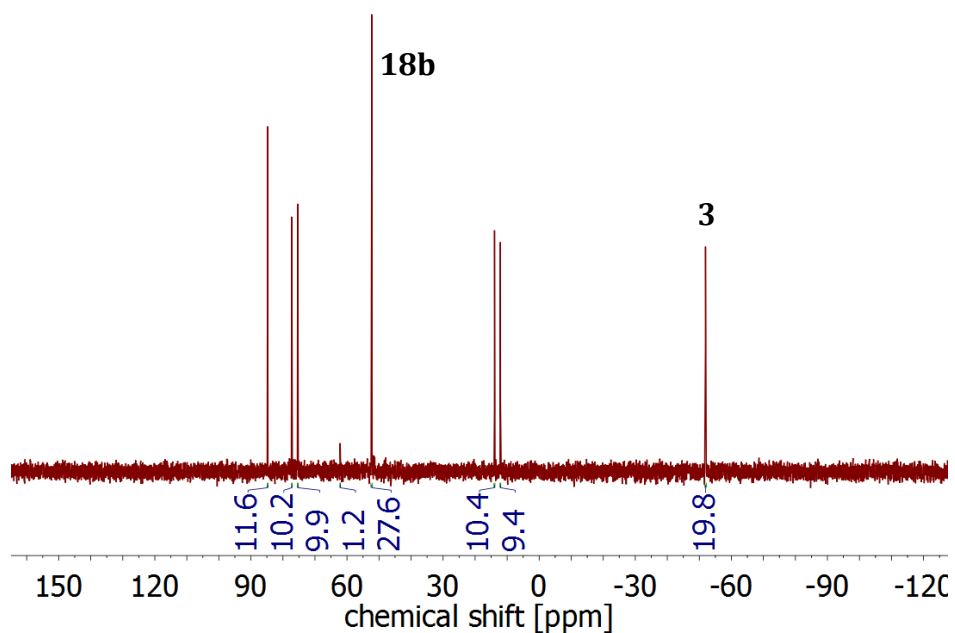
*Figure 56: ³¹P{¹H}-NMR spectrum of the oxidation of **18b** with 2 eq CuCl₂ and 1 eq DBU in THF; Integrals are normalized to 100%.*
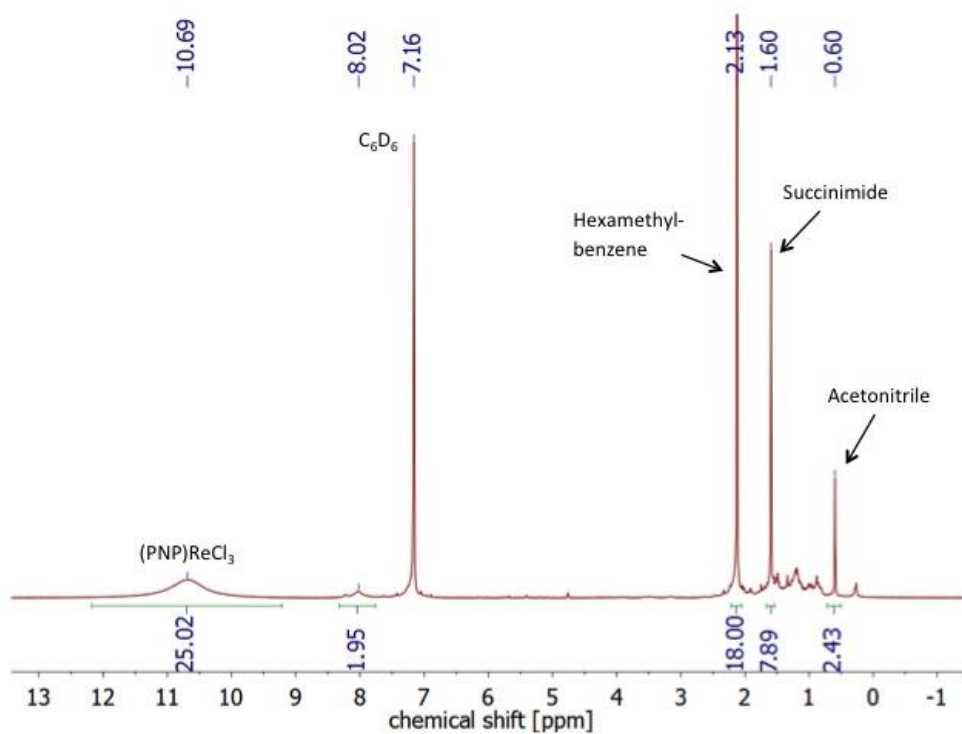
*Figure 57: ¹H-NMR spectrum of the reaction of **18b** with N-chlorosuccinimide (2 eq) in C₆D₆ (hexamethylbenzene as internal standard).*

In addition, rhenium(IV) complex [(PNP)ReCl$_3$] (**23**) is obtained almost quantitatively according to comparison of the ^{1}H-NMR (δ_H(^{t}Bu) = 10.7 ppm) and UV/Vis spectra with an authentic sample (Figure 58). Complex **23** was independently prepared by oxidation of **3** with 1 equivalent NCS and fully characterized. The molecular structure determined by single-crystal X-ray diffraction (Figure 59) reveals octahedrally coordinated rhenium with some distortion mainly arising from the pincer bite angle.[11] The magnetic moment in solution at room temperature from Evans´ method (1.5 μ_B) is in agreement with a d^3 low-spin configuration resulting from the strong pincer π-donation and some orbital contribution to the magnetic moment that leads to reduction of the magnetic moment with respect to the spin-only value. Contrariwise, EPR measurements did not show any signal. The facile synthesis of rhenium(IV) complex **23** from parent rhenium(III) dichloride **3** and NCS (1 eq) indicates that **3** could in fact be an intermediate in the oxidation of **18b** with NCS.
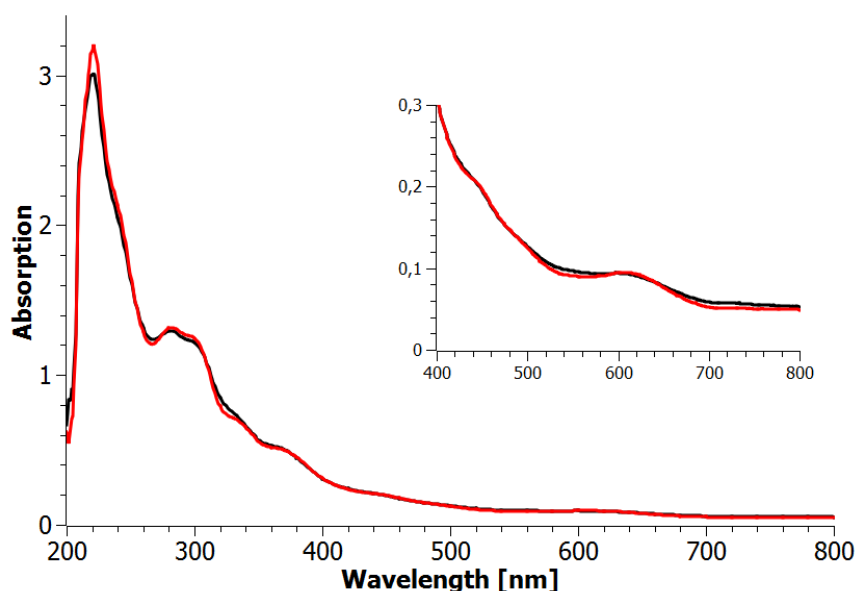
*Figure 58: UV-vis spectra of isolated **23** in THF prepared by oxidation of **3** (red spectrum) and of* ***18b*** *(black spectrum) with N-chlorosuccinimide, respectively.*

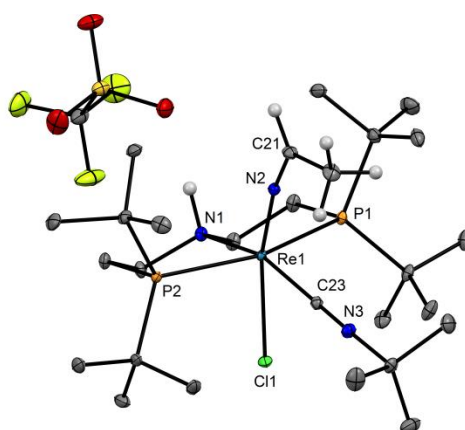[11] X-ray diffraction was performed by Christian Würtele.

*Figure 59: Molecular structures of complex **23** derived by single-crystal X-ray diffraction. ORTEP plots with anisotropic displacement parameters set at 50% probability. Hydrogen atoms are omitted for clarity. Selected bond lengths [Å] and angles [°]:Re1–N1 1.9038(16), Re1–Cl1 2.3893(5), Re1-Cl2 2.4024(5), Re1–Cl3 2.3700(5); N1-Re1-Cl1 91.50(5), N1-Re1-Cl2 178.69(5), N1-Re1-Cl3 91.59(5), P1-Re1-P2 160.046(16), Cl1-Re1-Cl2 88.090(17), Cl1-Re1-Cl3 176.471(16).*

Finally, the synthetic cycle could be closed by reduction of **23** with Na/Hg (2 eq) under dinitrogen (1 bar) at room temperature (Scheme 63). The nitride **9** is obtained in over 70% spectroscopic yield (Figure 60). This full cycle of N_2 conversion into acetonitrile was further confirmed with a ^{15}N-labeled sample producing ^{15}N-labeled acetonitrile (δ_N = -129.9 ppm). The reaction of **23** with only one equivalent of reductant (CoCp*$_2$) under argon quantitatively gives complex **3** as determined by ^{1}H and ^{31}P-NMR spectroscopy, indicating that N_2-splitting starting from **23** might also pass through rhenium(III) complex **3** as an intermediate.
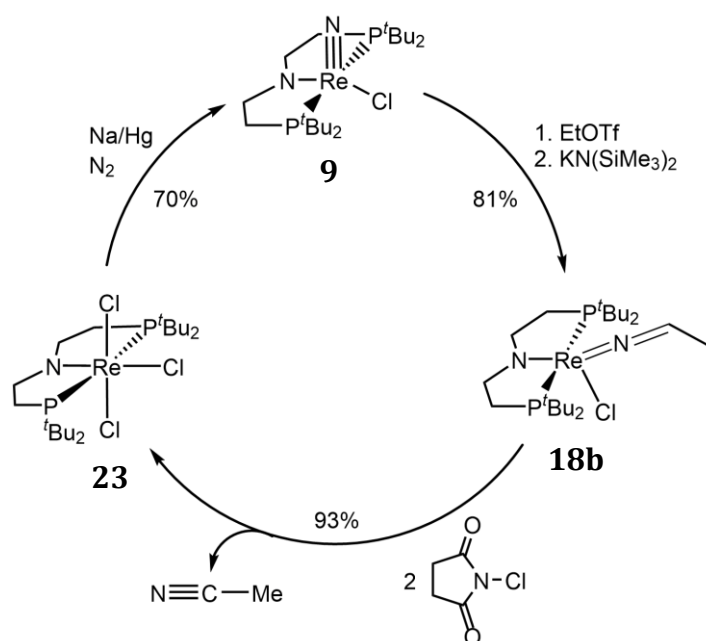
Scheme 63: Most efficient synthetic cycle for acetonitrile synthesis from N_2 with (PNP)Re complexes.

106
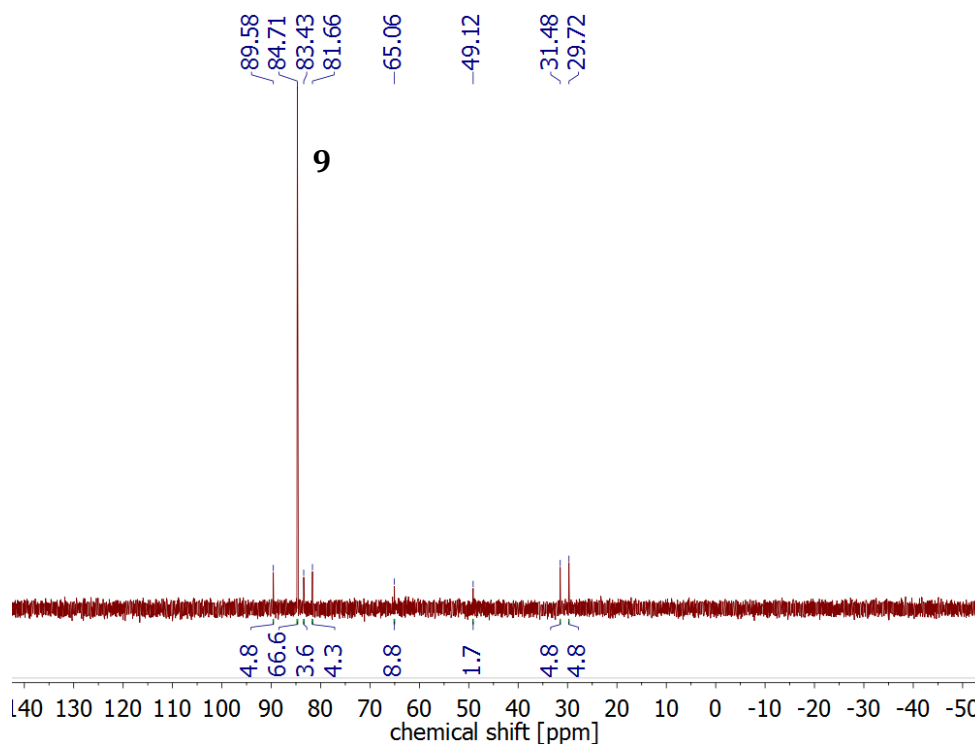
*Figure 60: $^{31}P\{^1H\}$ NMR spectrum of the reduction of **23** with Na/Hg (2 eq) under N_2 (1 bar) at r.t.*

In summary, the best synthetic cycle is composed of three simple reaction steps with 52% overall yield. A catalytic application is due to the need for both, strong electrophiles (EtOTf) and reducing conditions (Na/Hg) difficult. The solvent of choice to carry out the whole synthetic cycle in one pot has been found to be 1,4-dioxane, as it is sufficiently polar for the N_2 reduction step, but inert towards ring opening polymerization in contrast to THF. However, it was not possible so far to run the complete cycle a second time as no N_2 splitting could be achieved anymore in the presence of formed acetonitrile, succinimide, bis(trimethylsilyl)amine and KOTf.

4.4   Formation of benzonitrile

In analogy to the acetonitrile release by conversion of **16b-OTf**, the synthesis of benzonitrile from **16c-OTf** was envisaged to expand the reported synthetic cycle towards nitriles containing π-systems. **16c-OTf** displays the same reactivity as its ethyl analogue and can easily be deprotonated by KO^{t}Bu or KBTSA to the azabenzylidene complex **18c** (Scheme 64). In the NMR spectra, **18c** also displays two sets of signals in the same region as observed for **18b** in agreement with two stereo isomeric structures. The benzylic protons displays small coupling to the phosphorous atoms ($^4J_{HP}$ = 2.0 and 2.2 Hz) as usually observed for ketimido species **18**. Interestingly, some of the signals of the phenyl groups are broadened in the ^{1}H-NMR spectrum (Figure 61) and in contrast to the corresponding imide **16c-OTf** (Figure 38), no cross peaks between the phenyl groups and the benzylidene protons are observed in the H,H-COSY NMR spectrum (Figure 62), which might indicate exchange of these protons. In the H,H-NOESY spectrum, spatial proximity between the phenyl groups and the ligand backbone is still observed by cross peaks (Figure 63).
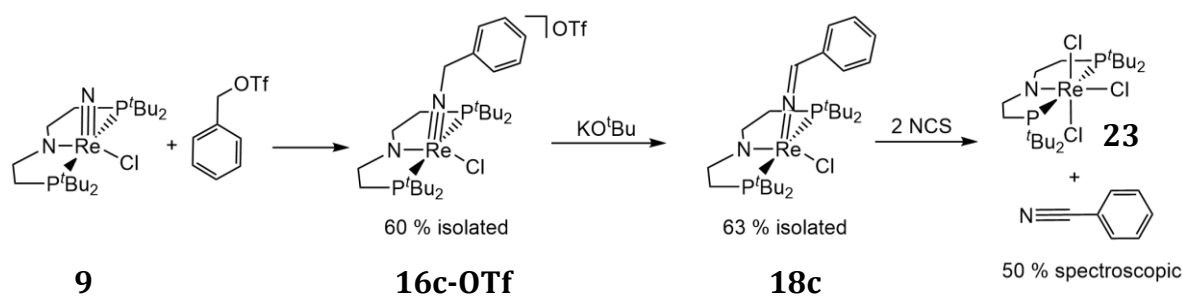
*Scheme 64: Synthesis of 18**c** by benzylation of the nitride **9** with subsequent deprotonation and benzonitrile release upon reaction with NCS.*
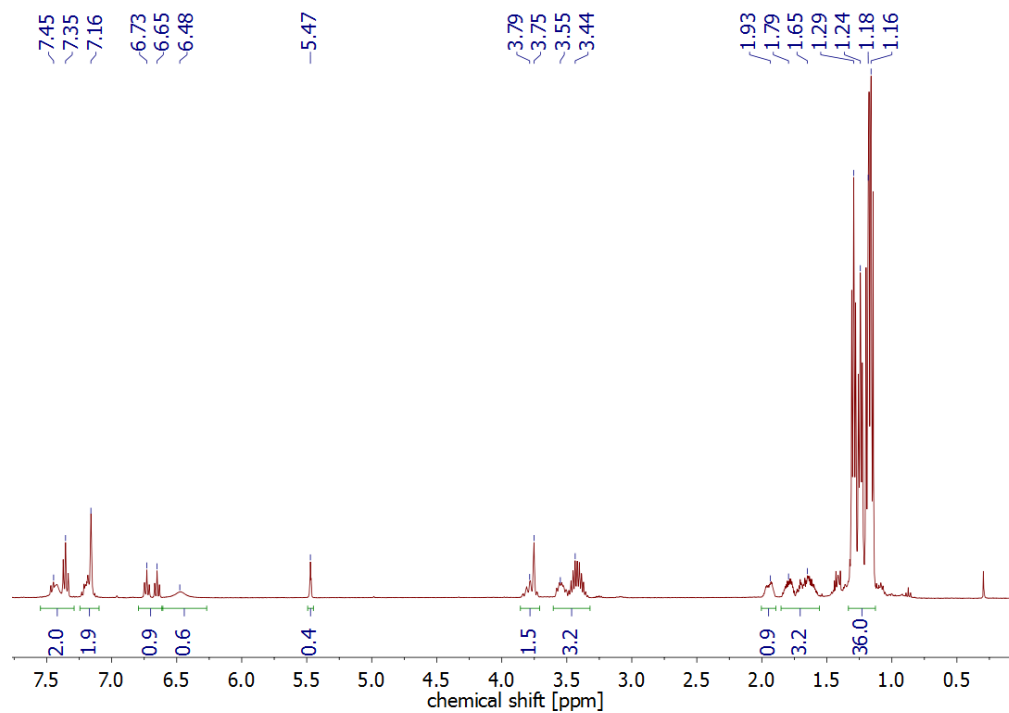
*Figure 61: ¹H-NMR spectrum of **18c** in C₆D₆.*
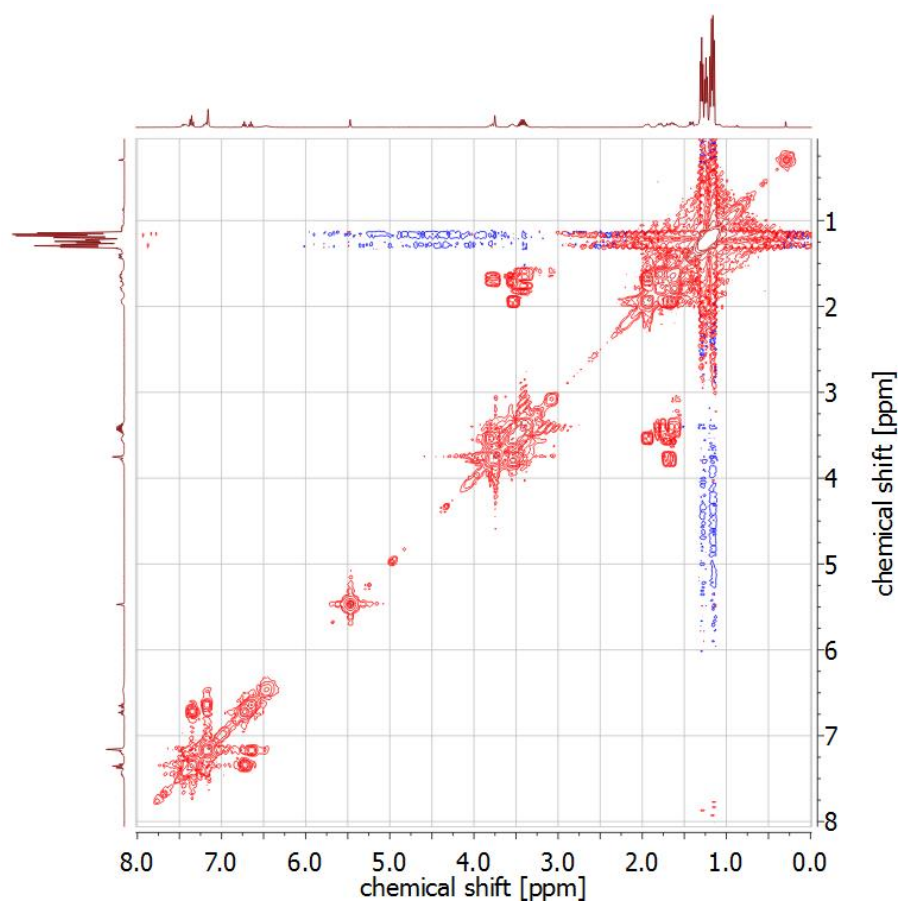
*Figure 62: ¹H,¹H-COSY NMR spectrum of **18c** in C₆D₆.*
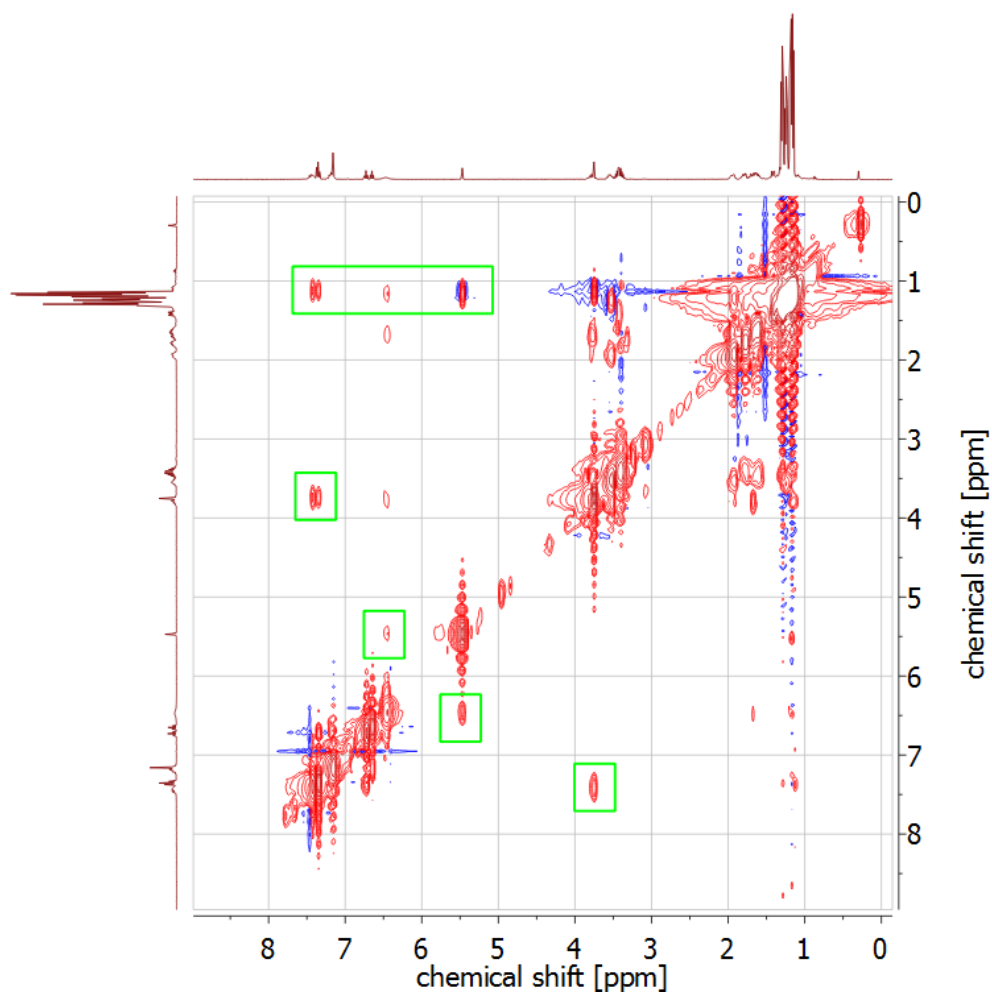
*Figure 63: $^1H,^1H$-NOESY NMR spectrum of **18c** in C_6D_6.*

Single crystals of **18c** were examined by X-ray diffraction.[12] The asymmetric unit cell contained two complex molecules of **18c**, with one being disordered at one site of the PNP ligand backbone (Figure 64). The two structures are very similar and all bond length and angles are the same within 0.01 Å and 3.5° and describe a distorted square pyramide with the benzylidene group in the apical position (τ = 0.4). Comparison with **18b** does not reveal any significant differences.

---

[12] X-ray analysis was performed by Dr. Christian Würtele.

*Figure 64: Molecular structures of complex **18c** derived by single-crystal X-ray diffraction. ORTEP plots with anisotropic displacement parameters set at 50% probability. Hydrogen atoms are omitted for clarity, except for the azabenzylidene groups. Selected bond lengths [Å] and angles [°]: Re1-N1 1.938(2), Re1-N2 1.798(2), Re1-Cl1 2.3964(6), N2-C21 1.289(3), Re2-N3 1.944(2), Re2-N4 1.796(2), Re2-Cl2 2.3952(6), N4-C48 1.287(3); N1-Re1-N2 114.54(10), N1-Re1-Cl1 137.19(8), P1-Re1-P2 161.80(2), Re1-N2-C21 170.2(2), N3-Re2-N4 115.83(9), N3-Re2-Cl2 137.88(6), P3-Re2-P4 161.62(2), Re2-N4-C48 173.7(2).*

In analogy to the release of acetonitrile,[207] the reaction with 2 equiv. NCS generates signals corresponding to benzonitrile in about 50% spectroscopic yield (based on ^{1}H-NMR integration with hexamethylbenzene as internal standard) with concomitant formation of **23** (Scheme 64). A synthetic cycle for benzonitrile generation out of N_2 is therefore possible with an overall yield of about 13%. However, these are preliminary results as full characterization of **16c-OTf** and **18c** as well as ^{15}N-labelling experiments have not been carried out yet. Nevertheless, the N_2 functionalization route is not only limited to alkyltriflates, but can also be used for π-conjugated systems.

In summary, these results describe a new strategy for dinitrogen functionalization to valuable chemicals beyond ammonia, which still represents a rare reaction type. Besides the thermochemical attractiveness of forming C≡N triple bonds after N_2 splitting, this work also offers mechanistic implications regarding the restoration of low-valent rhenium after N_2 splitting. As demonstrated, the alkylimide to nitrile ligand oxidation can be partially coupled with metal re-reduction. Such proton-coupled metal–ligand redox processes are therefore of particular relevance for future efforts to design truly (electro-)catalytic variants of N_2 transformation to organic compounds.

5   Reactivity of the methyl-imido analogue

5.1   Deprotonation and characterization of the methyl-ketimide

In 2011, the group of Cummins demonstrated N_2 conversion to cyanide with the Mo(N^{t}BuAr)$_3$ system. After N_2 splitting, alkylation and deoxygenation in the presence of base, they could observe the formation of a cyanido complex (Scheme 19).[112] HCN could not be detected.

In analogy to acetonitrile release of the ethyl-substituted complex **16b-OTf**,[207] the question arose whether the formation of cyanides or HCN is possible from the methyl-substituted complex **16a-OTf**. Hence, the latter was deprotonated as described in the previous chapter and **18a** could be isolated in high yield (Scheme 65).
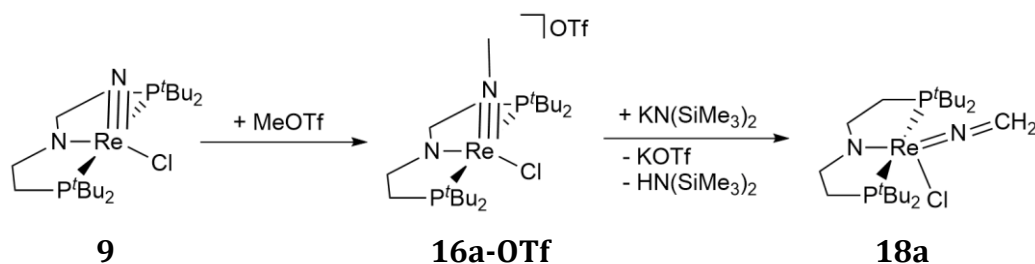
*Scheme 65: Synthesis of methyl-ketimido complex **18a**.*

The spectroscopic signature is similar to **18b** and **18c**, although there is only one isomer. Nevertheless, the two protons of the N=CH$_2$ group display two characteristic multiplets with coupling to each other ($^2J_{HH}$ = 4.8 Hz) and to the phosphorous atoms ($^4J_{HP}$ = 2.4 Hz). Single crystal X-ray analysis[13] revealed also comparable bond lengths to **18b**, only the N2-C21 bond distance of the azavinylidene group is slightly shorter (Δd = 0.03-0.04 Å). The Re-N-C angle is still close to linear (172.6(2)°), but the

---

[13] X-ray analysis was performed by Dr. Christian Würtele.

structure around the rhenium center is more distorted. **18a** is best described as a heavily distorted square pyramide, with the chloride in the apical position (τ = 0.46), whereas **18b** and **18c** display a similar geometry, but with the azavinylidene/azabenzylidene ligand in the apical position (τ = 0.45 and 0.40 respectively).
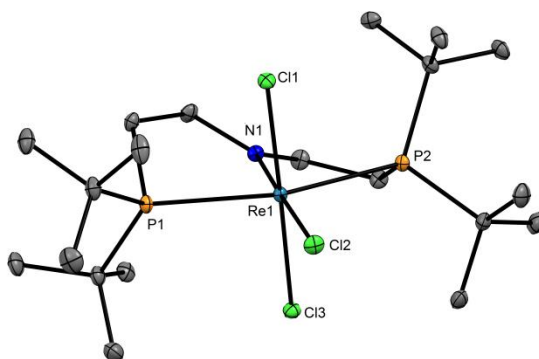

*Figure 65: Molecular structure of complex **18a** derived by single-crystal X-ray diffraction. ORTEP plots with anisotropic displacement parameters set at 50% probability. Hydrogen atoms except for the azavinylidene ligand are omitted for clarity. Selected bond lengths [Å] and angles [°]: Re1–N1 1.9563(15), Re1–N2 1.8365(16), Re1–Cl1 2.3775(5), N2–C21 1.248(3); N1-Re1-N2 134.81(7), N1-Re1-Cl1 117.51(5), N2-Re1-Cl1 107.67(5), P1-Re1-P2 162.140(16), Re1-N2-C21 172.56(16).*

Since the objective is an oxidative functionalization of **18a** as it has been found for **18b**, the product was characterized by cyclovoltammetry. The cyclovoltammogram displays similar to **18b** a reversible and an irreversible oxidation wave, although the potentials are shifted to slightly higher values (Figure 66).
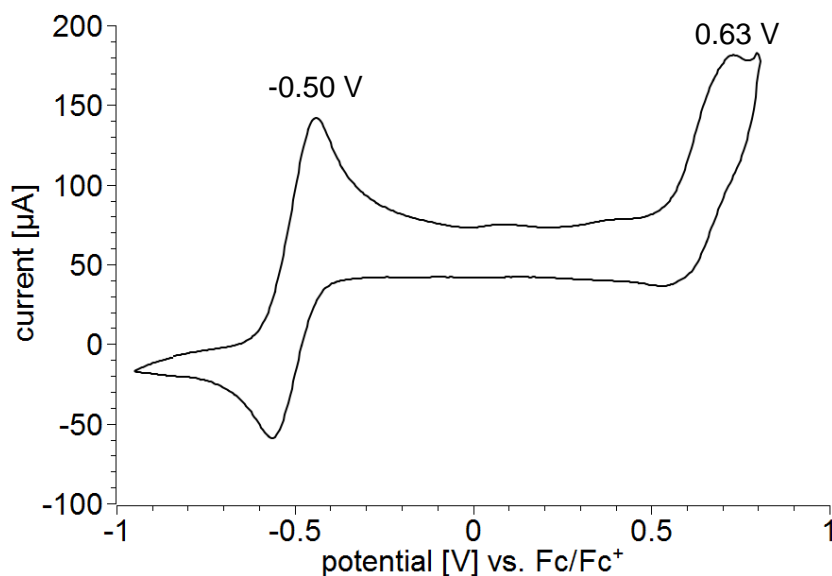
*Figure 66: Cyclovoltammogram of **18a** vs Fc/Fc+ in DCM (200 mV/s, GC-Working electrode, 0.1 M [N^{n}Bu$_4$][PF$_6$]).*

Reversibility for the lower wave was proven by scanning only in the region from -1 to 0 V with different scan rates (Figure 67). The rather quasi-reversible behavior of this wave in the bigger potential window (Figure 66) is therefore attributed to the second, completely irreversible oxidation wave.
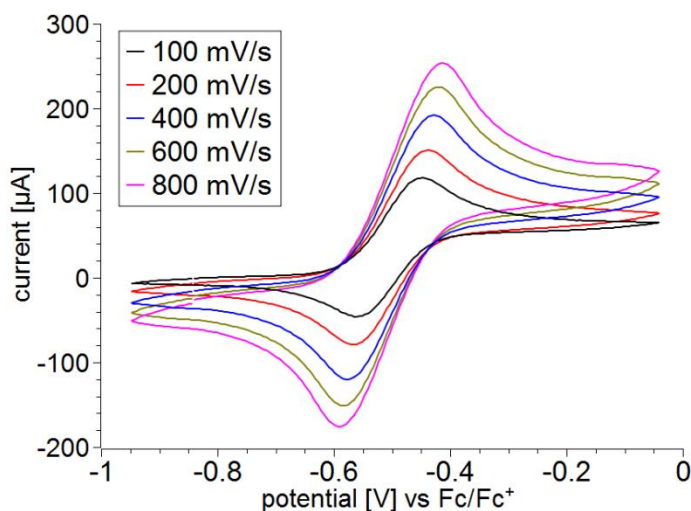
*Figure 67: Cyclovoltammogram of **18a** vs Fc/Fc$^+$ in DCM with different scan rates.*

5.2   Oxidative functionalization of the methyl-ketimide

Chemical oxidation of **18a** with 1 equiv. Ag$^+$ however does not generate a paramagnetic complex similar to **18b**. Instead, a mixture of diamagnetic complexes is formed with the main product exhibiting only a singlet for the N=CH$_2$ group in the ^{1}H-NMR spectrum (Figure 69, note: chloride exchanged by a methyl group: δ_H(ReCH$_3$) = 3.54 ppm, δ_H([ReNCH$_2$)]$_2$) = 2.78 ppm) in contrast to parent **18a**. This behavior would be in agreement with a dimerization of the complex. Exchanging the chloride substituent of **18a** by a methyl group (**25a**, see below) followed by 1 e$^-$ oxidation allowed for crystal growth and X-ray diffraction of the product **24** (Figure 68).[14] The obtained structure confirmed the dimerization of the complex to form a {Re-N-CH$_2$-CH$_2$-N-Re} bridge, but unfortunately, due to disorder problems, the crystallographic

---

[14] Determination of the molecular structure was performed by Dr. Christian Würtele.

resolution does not allow for description of bond lengths or angles. Since the reaction affords some side-products with similar solubility, **24** has not been fully characterized yet. It is assumed, that **18a** forms a radical upon oxidation, with couples with another formed radical at the CH_2-group (Scheme 66).
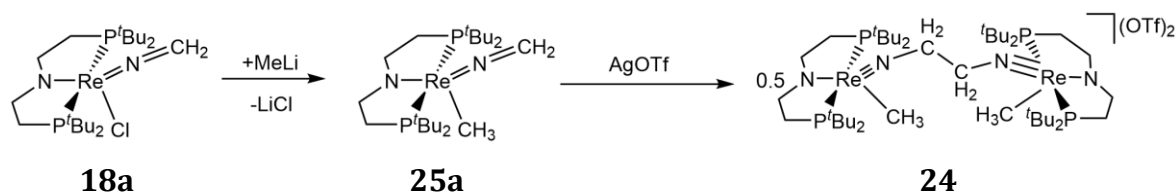
*Scheme 66: Chloride exchange by a methyl group and dimerization of **25a** to **24** upon oxidation.*
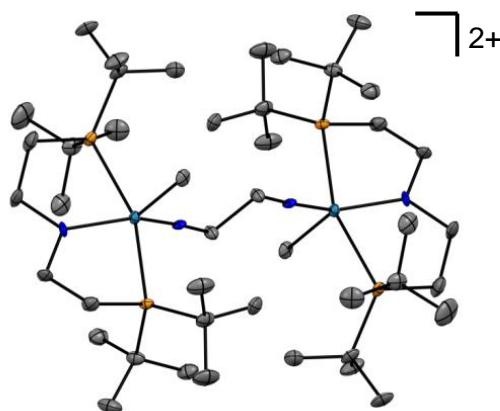
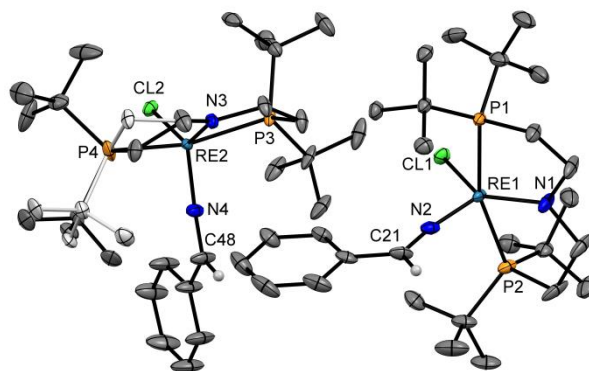*Figure 68: Molecular structure of **24** derived by single-crystal X-ray diffraction. ORTEP plots with anisotropic displacement parameters set at 30% probability. Anions omitted for clarity.*
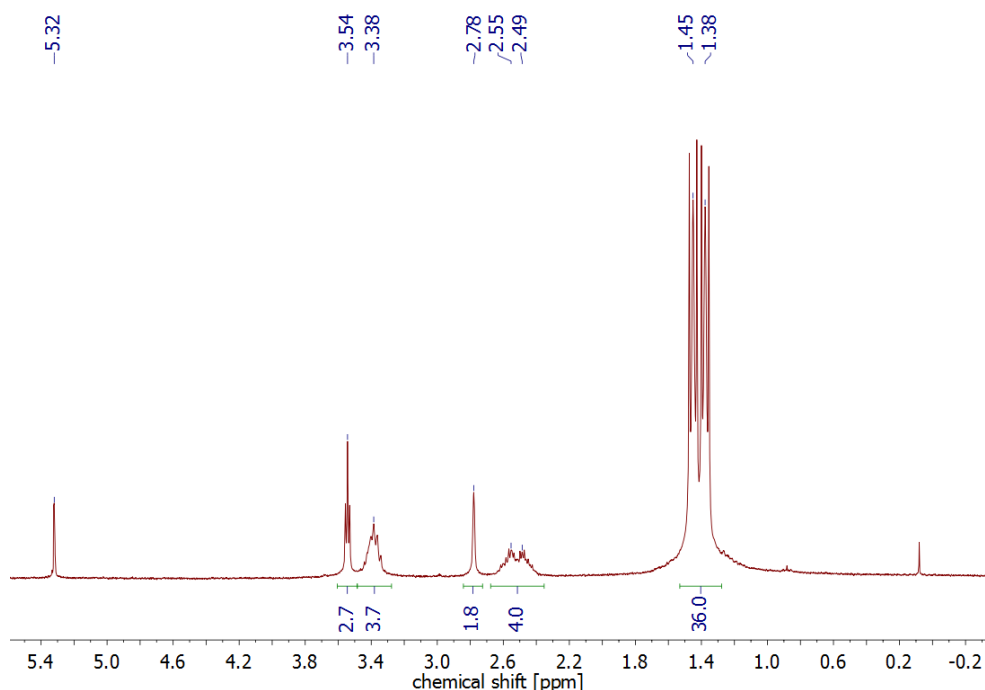
*Figure 69: ^{1}H-NMR spectrum of **24** after crystallization in CD_2Cl_2.*

To verify the radical reactivity of oxidized **18a**, a trapping reaction was performed. The redox potential of the trityl cation ($^+CPh_3$) is high enough to oxidize **18a** (-0.11 vs Fc/Fc$^+$ in acetonitrile).[227] The oxidized form then instantaneously couples with the so generated trityl radical ($\cdot CPh_3$) to form $[(PNP)Re(NCH_2CPh_3)(Cl)][PF_6]$ (**16d-PF$_6$**) (Scheme 67).
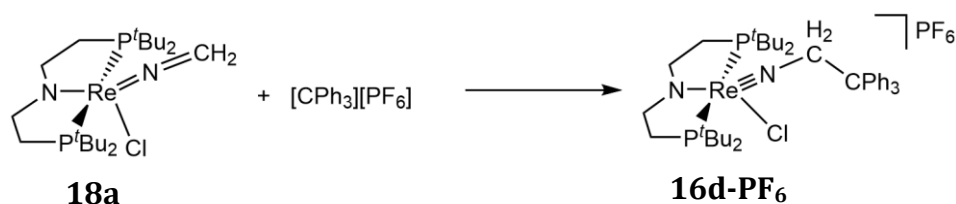
*Scheme 67: C-C Coupling of **18a** with the trityl cation.*

The spectroscopic yield (^{31}P-NMR integration) is about 50%. The main side-product (40%) turned out to be **16a**, tentatively due to residual moisture in the tritylsalt $[CPh_3][PF_6]$. That coupling indeed occured was verified by 2D-NMR spectra. In the ^{1}H-NMR spectrum of the resulting mixture, a singlet at 4.52 ppm is assigned to the NCH_2CPh$_3$ group, since the spectroscopic signature of **16a** is known (NCH_3 at 2.86 ppm). HSQC in combination with DEPT135 spectra confirm this signal to be a CH$_2$ group (Figure 70). In the ^{1}H-NOESY spectrum, distinct coupling between this signal

and the aromatic signals of the phenyl substituents (NCH$_2$CPh_3) as well as one *tert*-butyl group of the PNP ligand can be detected (Figure 71).

No nucleophilic reactivity of the methylene unit towards carbon electrophiles (MeOTf) has been reported, so nucleophilic attack of **18a** at the trityl cation is unlikely.
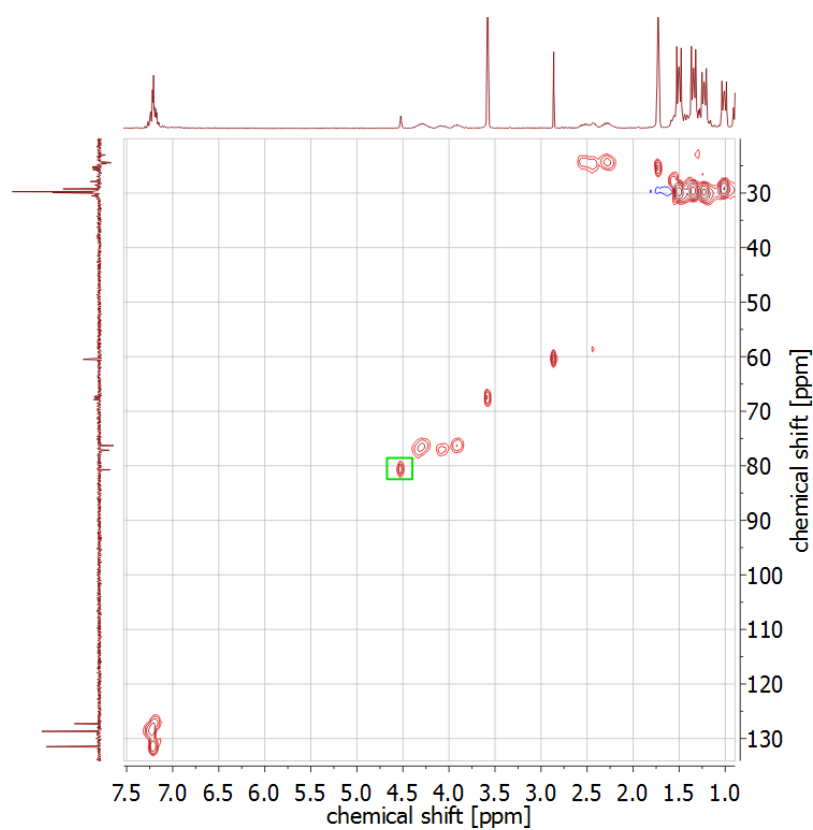
*Figure 70: HSQC spectrum of an about equimolar mixture of **16a** and **16d** in d$_8$-THF; vertical trace is the DEPT 135 spectrum of the same reaction mixture.*
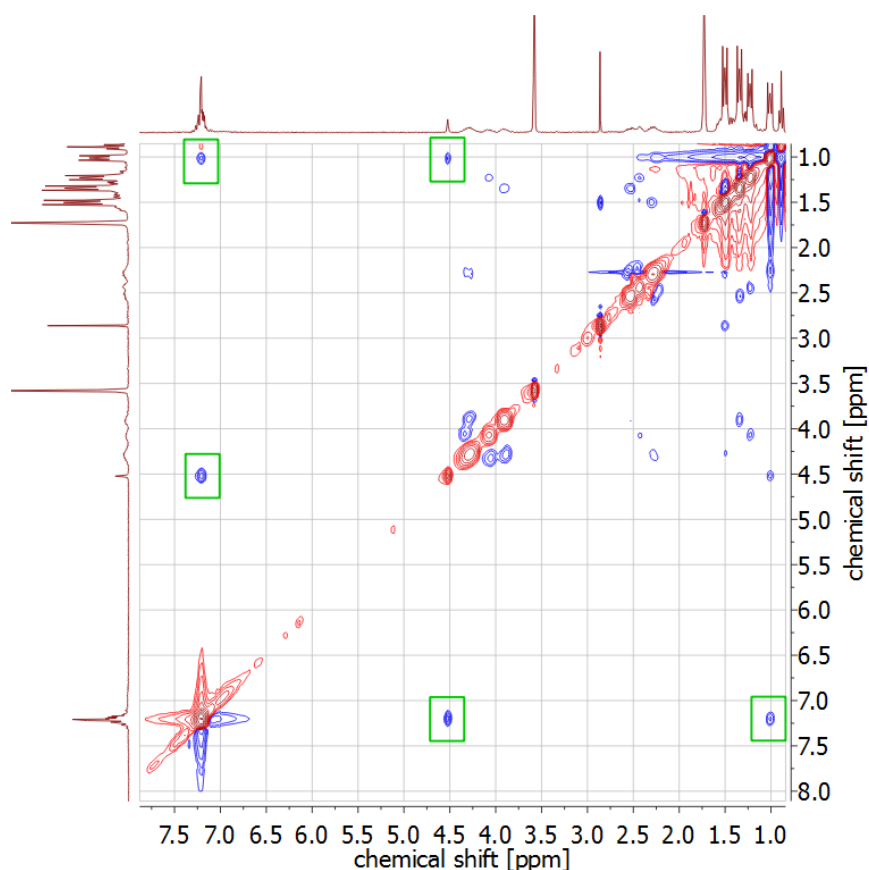
*Figure 71: ^{1}H-NOESY spectrum of a mixture of **16a** and **16d** in d_8-THF.*

Deprotonation of this mixture with KBTSA affords the compounds **18a** and **18d**. The ^{31}P-NMR signal for the latter is in a slightly different region as for all other azavinylidene species (δ_P = 41 and 44 ppm). Interpretation of the ^{1}H-NMR spectrum is hampered due to excessive signal overlap.
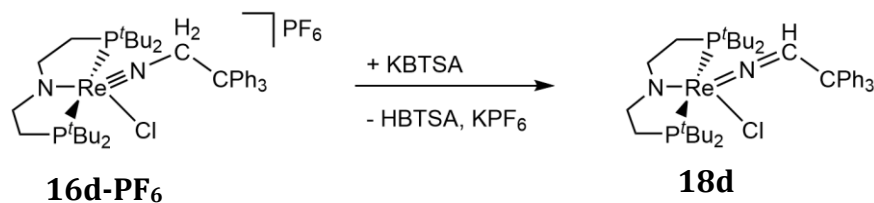
*Scheme 68: Deprotonation of **16d-PF$_6$** to **18d**.*

However, single crystals of **18d** suitable for X-ray diffraction could be obtained. The structure is disordered in one arm of the PNP ligand, but illustrates the C-C coupling reaction upon oxidation (Figure 72). Interestingly, the geometry of this complex resembles more a square pyramid than all other azavinylidene complexes (τ = 0.33), maybe due to steric reasons. All bond lengths are comparable to **18a-c**. Striking

difference is the Re-N-C angle of the azavinylidene unit (164.55(15)°), which deviates significantly from linearity and about 10° from the angles observed for **18a-c**. This might be due to steric reasons, as the bulky phenyl groups are rather close to one of the *t*Bu-groups of the PNP ligand. All other angles are within 5° similar to **18a-c.** Since **18d** has not been isolated, nitrile release has not been tested.
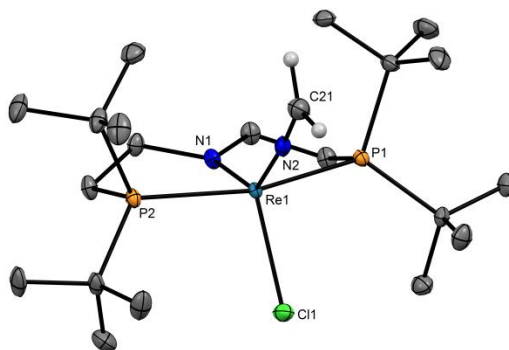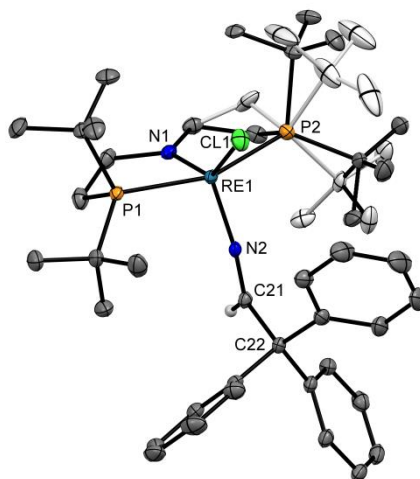

*Figure 72: Molecular structure of complex **18d** derived by single-crystal X-ray diffraction. ORTEP plots with anisotropic displacement parameters set at 50% probability. Hydrogen atoms except for the azavinylidene ligand are omitted for clarity. Selected bond lengths [Å] and angles [°]: Re1–N1 1.9403(17), Re1–N2 1.8237(16), Re1–Cl1 2.4120(5), N2–C21 1.283(2), C21-C22 1.556(3); N1-Re1-N2 113.37(7), N1-Re1-Cl1 138.73(5), N2-Re1-Cl1 107.88(5), P1-Re1-P2 158.747(18), Re1-N2-C21 164.55(15).*

Cyanide generation from **18a** by an oxidative approach similar to **18b** seems to be difficult, since the oxidized form is not stable at all. Addition of 2 equiv. NCS to a solution of **18a** however results in formation of **23**, verified by ^{1}H-NMR spectroscopic investigations as well as a LIFDI mass record of the reaction mixture. Nevertheless, the reaction is rather unselective, as also diamagnetic and paramagnetic side-products are detected in the NMR spectra (^{1}H-NMR: Figure 73). A yield for **23** could not be determined so far. Mass spectrometry does not show any cyanide containing complex. Contrariwise, absorption bands in the range of 2260-2220 cm^{-1} in the IR-spectrum of the dried residue of the reaction (Figure 74) indicate coordinated or substituted C≡N (free CN^{-} = 2076 cm^{-1}).[228,229] Further investigations are necessary to clarify the fate of the {CN} unit.
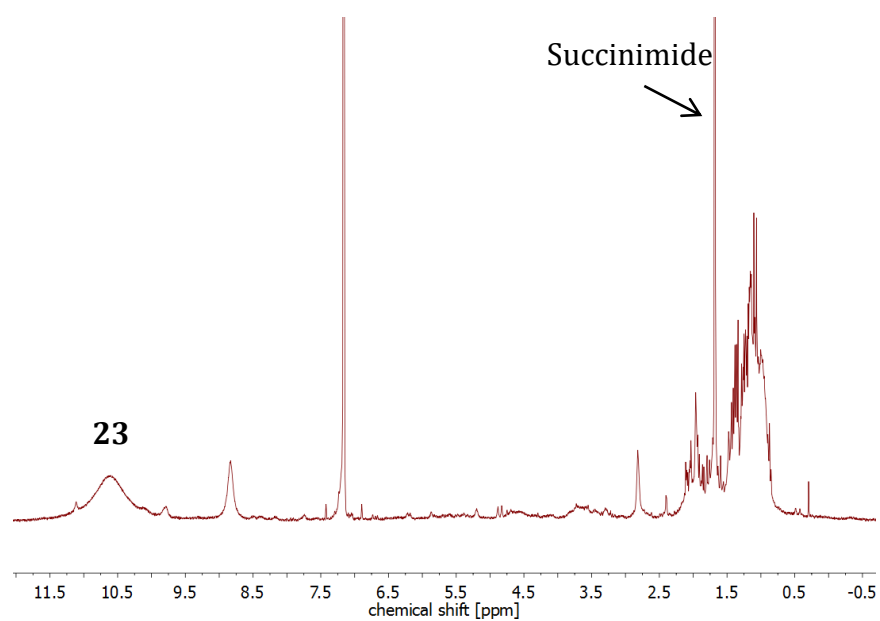
*Figure 73: ^{1}H-NMR spectrum of **18a** with 2 equiv. NCS in C_6D_6.*
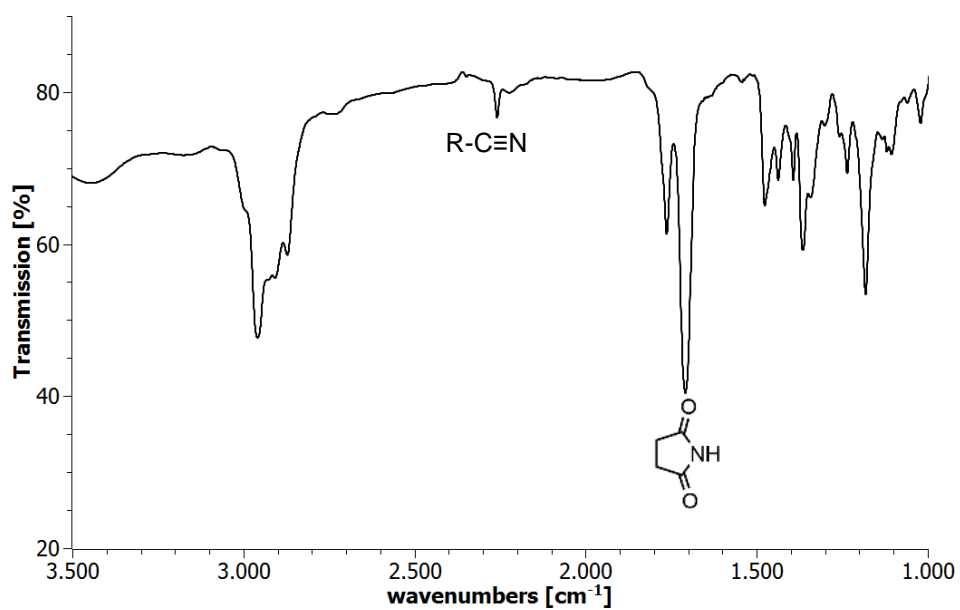
*Figure 74: IR spectrum (KBr) of the dried residue of the reaction of **18a** with 2 equiv. NCS; Selected wavenumbers [cm^{-1}]: υ(R-C≡N): 2259, 2224 (w); υ(C=O) = 1763, 1709 (s).*

6 Further reactivity of the imides and ketimides

6.1 Reaction with metal alkyls

Linear {M-N-R} imido moieties often display electrophilic reactivity.[105] To verify, if generation of amides is possible, the imido complexes **16** were tested towards nucleophiles like lithium organyls or grignard reagents. However, no reactivity at the imido nitrogen has been observed. Instead, 2 equiv. of MeLi or MeMgCl deprotonate the imide and substitute the chloride ligand to generate [(PNP)Re(NCHR)(CH$_3$)] (**25**, Scheme 69). The structural parameters for **25a** are basically the same as for **16a** (Figure 75) and the NMR data is similar. The new Re-CH$_3$ group of **25a** displays a triplet in the ^{1}H-NMR spectrum at 2.2 ppm ($^3J_{HP}$ = 4.2 Hz) and a negative chemical shift in the ^{13}C-NMR (-10 ppm). The same reaction starting from **16b** generates **25b,** identified by a similar spectroscopic signature. No further reactivity is observed if an excess of metal organyl is used.
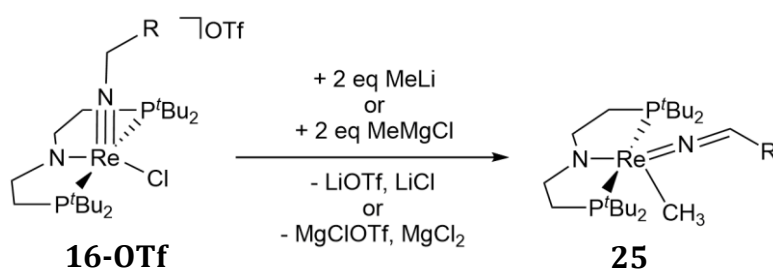
Scheme 69: Reaction of **16** with 2 equiv. of metal organyl to **25**.
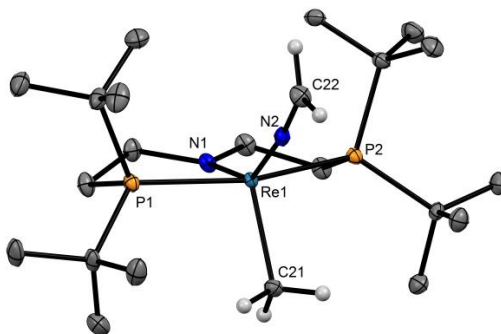
*Figure 75: Molecular structure of complex **25a** derived by single-crystal X-ray diffraction. ORTEP plots with anisotropic displacement parameters set at 50% probability. Hydrogen atoms except for the azavinylidene and methyl ligand are omitted for clarity. Selected bond lengths [Å] and angles [°]:Re1–N1 1.9837(14), Re1–N2 1.8416(15), Re1–C21 2.1416(18), N2–C22 1.271(2); N1-Re1-N2 143.36(6), N1-Re1-C21 112.59(7), N2-Re1-C21 104.04(7), P1-Re1-P2 161.895(16), Re1-N2-C22 169.52(14).*

The use of PhMgBr also leads to deprotonation of the imide with a spectroscopic signature similar to **18a**, but the resulting complex does not incorporate any aromatics, as observed by NMR spectroscopy. Only very small signals are observed in the aromatic region of the ^{1}H-NMR spectrum, pointing towards residual Grignard reagent. Unexpectedly, the spectra are not identical with **18a** (Figure 76). The main difference is described by the chemical shift of the two signals for the NCH$_2$-group, which are shifted by about 0.6 ppm each to higher field. An exchange of the chloride substituent by bromide is most likely, but has not been examined in more detail yet.
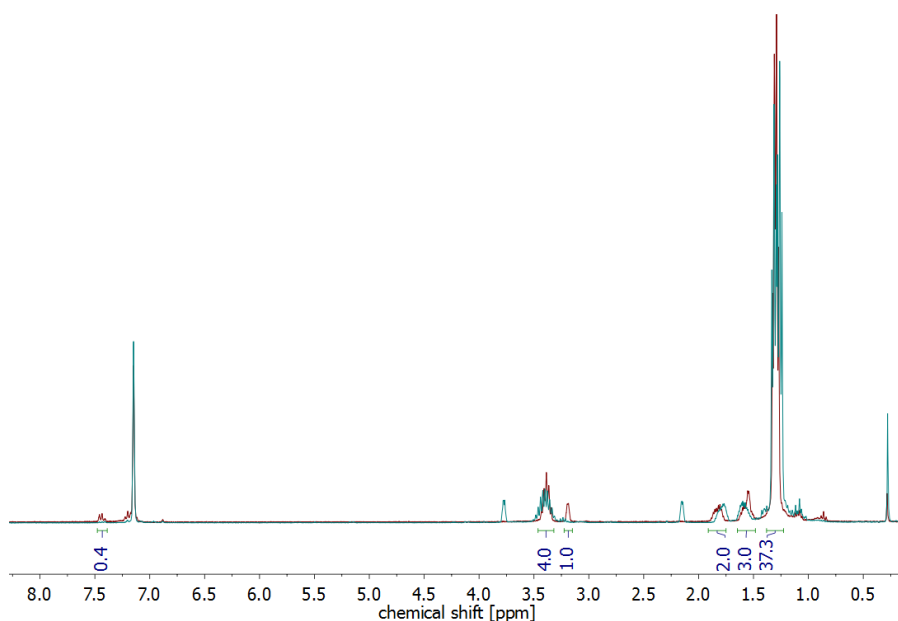
*Figure 76: ^{1}H-NMR spectrum of **18a** (green) and the resulting complex from deprotonation of **16a** with PhMgBr (red, signals integrated) in C$_6$D$_6$.*

6.2 Imide reduction

To further analyze the reactivity of the imido complexes **16**, cyclic voltammetry was carried out using **16a**. The resulting voltammogram exhibits two irreversible reduction waves at a potential of -1.8 and -2.1 V in THF vs Fc/Fc⁺ (Figure 77).
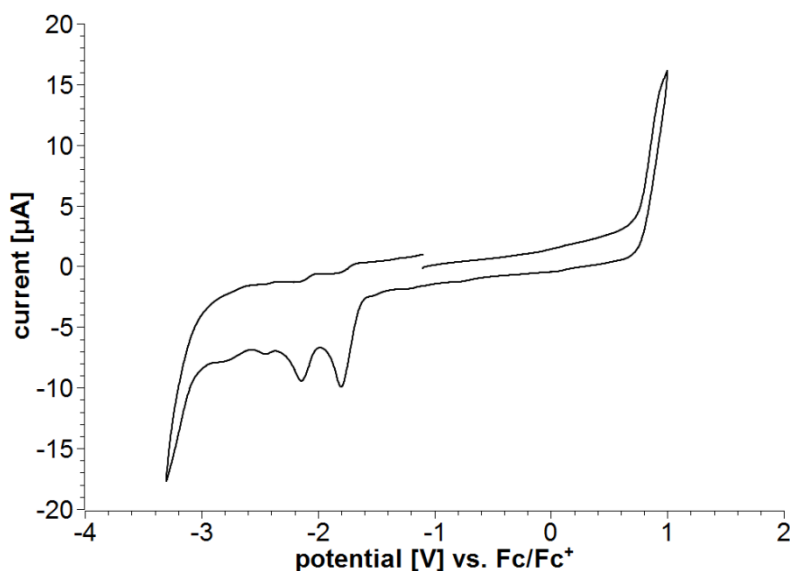
*Figure 77: Cyclovoltammogram of **16a** (1 mM) vs Fc/Fc⁺ in THF (400 mV/s, GC-Working electrode, 0.1 M [NⁿBu₄][PF₆]).*

Chemical 2 electron reduction of **16a** using 2 equiv. KC_8 in THF produces selectively one diamagnetic, C_s symmetric compound in about 90% spectroscopic yield (δ_P = 79 ppm). This compound features the characteristic signals for a N=CH₂ group as well as a hydride signal at a chemical shift of -4.3 ppm (d₈-THF) in the ¹H-NMR spectrum. Hence, not only reduction from Re^V to Re^III took place, but also chloride abstraction and most likely β-hydrogen elimination to produce [(PNP)Re(NCH₂)(H)] (**26a,** Scheme 70). For **16b**, similar results are obtained, albeit the spectroscopic yield in **26b** is lower (60% based on ³¹P-NMR integration).
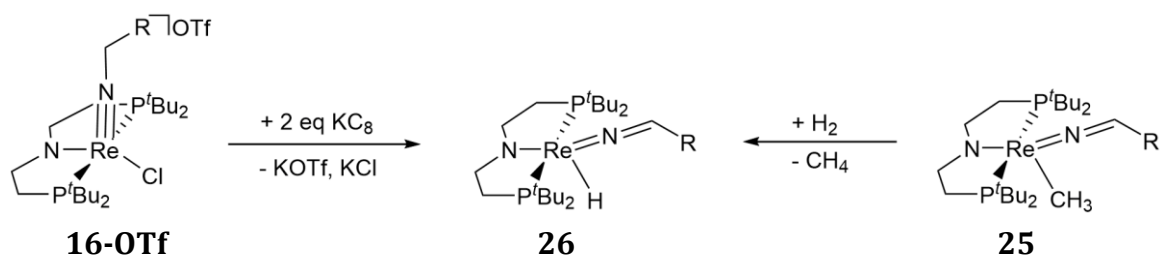
Scheme 70: Reactions to produce **26** by reduction of **16** and by hydrogenation of **25**.

To verify the structural assignment of the products, H_2 was added to **25** and formation of the same compound was achieved (Scheme 70)**,** proving that there is no chloride left in **26**. After heating to 70°C for 18 h (**25a**), complete conversion is observed under release of CH_4 (Figure 78).
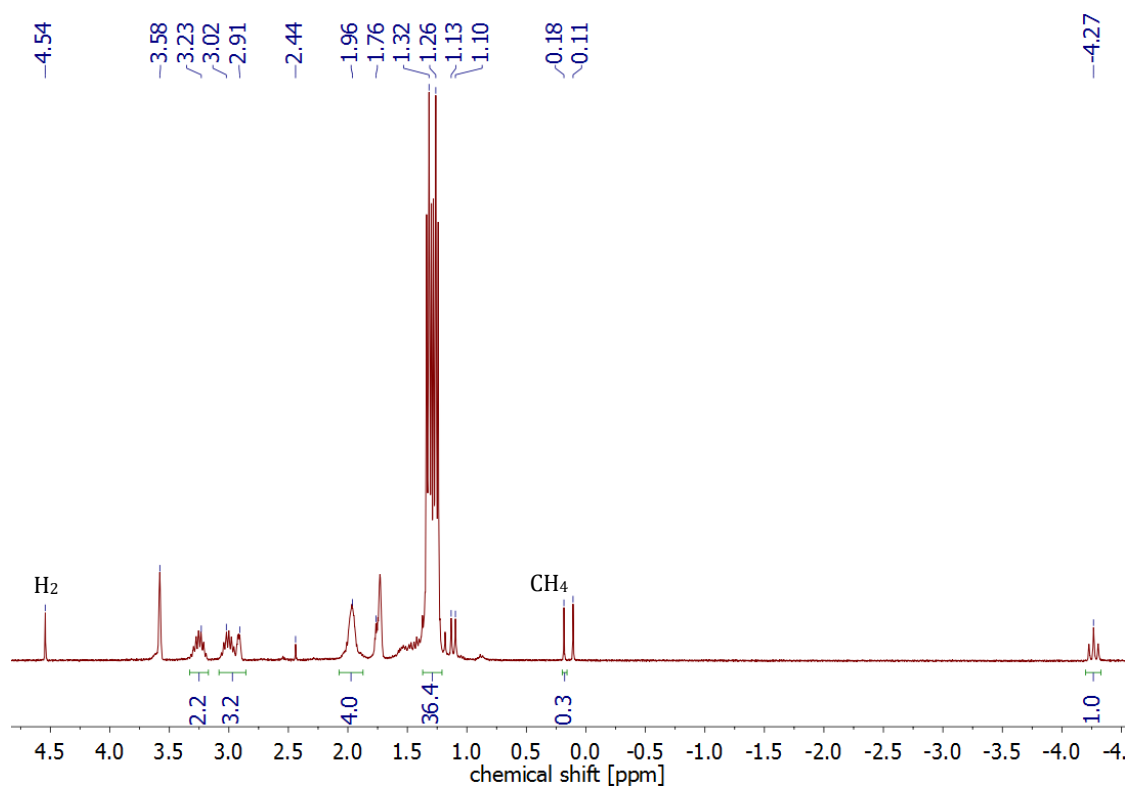
Figure 78: ^{1}H-NMR spectrum of the addition of H_2 to a solution of **25** in d_8-THF after 18 h at 70°C.

6.3 Hydrogenation reactions

Hydrogenation of the imido complexes is an interesting goal, as it offers the possibility of amine generation out of N_2-derived complexes. A reaction of **16a** with H_2 gas is not observed, unless small amounts of MeOTf or HCl are present, indicating catalysis of protons or Lewis acids. A new product is formed thereby in spectroscopic yields of about 85% (δ_P = 66 ppm). No signals in the negative region of the ^{1}H-NMR spectrum are observed, but deprotonation of this product with 2 equiv. KO^{t}Bu yields **26** again. Hydride signals might therefore be suppressed (broadend) by exchange with H_2 gas or are located in the positive region of the spectrum. The product is assumed to be [(^{H}PNP)Re(NCH$_3$)(H)(Cl)]OTf (**27**), although full spectroscopic characterization is lacking (Scheme 71).

Furthermore, hydrogenation of **18** is slow and results in two products in an 1:1 ratio after heating to 80°C for several days. One of them is **26**, as compared with original spectra (e.g. from imide reduction, see above), indicating that HCl is eliminated. The other one is **27**, as compared with hydrogenation of **16**, pointing towards HCl addition (Scheme 71). Hence, **18** disproportionates upon hydrogenation into **26** and **27**. Accordingly, the hydrogenation is selective towards **26** in the presence of a base as the formed HCl is trapped. In the presence of HCl on the other hand, only **27** is observed, supporting the above stated assignments.
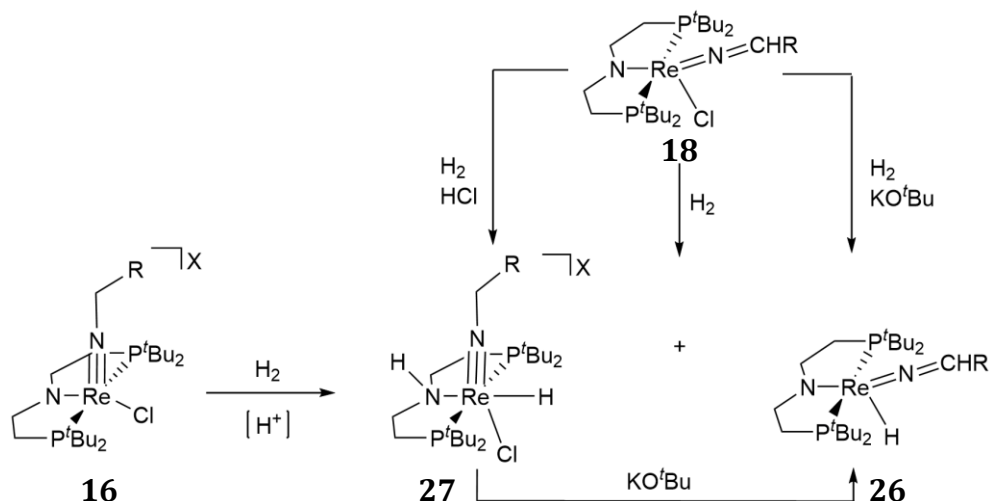
Scheme 71: Hydrogenation reactions of 16 and 18.

Protonation of **26** is accomplished using 1 equiv. of HOTf, HBAr$^F_4$ or NH$_4$PF$_6$ and yields the imido complex **28** (Scheme 72). Expected signals for an alkyl group as well

as one hydride signal (δ_H = -6.2 ppm, CD_2Cl_2) are observed in the ^{1}H-NMR spectrum. The ^{31}P-NMR shift is similar to all other imido complexes (δ_P = 97 ppm). Similar to **16**, hydrogenation of **28** is possible, if some residual acid is present forming a new C_s symmetric compound **29**. However, this reaction is much faster and takes only a few minutes indicated by color change from green to rose, compared to three days at 80°C for **16** to yield blue **27**. Presumably, the presence of the hydride as strong σ-donor enhances the electron density at the metal, which favors H_2 coordination and splitting. Moreover, also for **29**, no hydride signals in the negative region of the ^{1}H-NMR spectrum can be observed anymore, pointing towards exchange with gaseous H_2, self-exchange or a positive chemical shift. Unfortunately, the product could not be isolated, since vacuum application led to partial back-reaction to **28**.
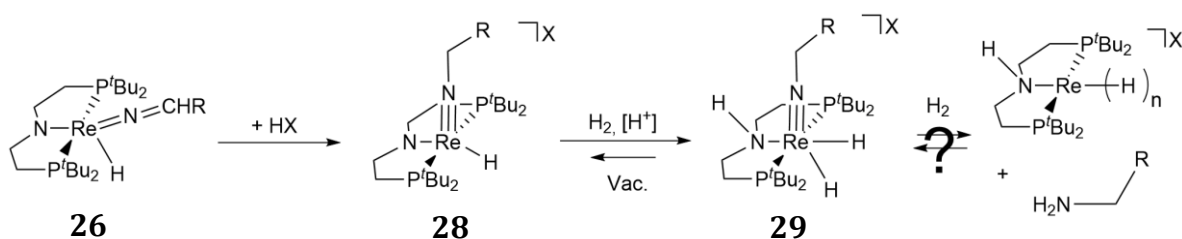
*Scheme 72: Hydrogenation of **28**: Possibility of amine release?*

Equilibrium formation between **29** and a polyhydride under an atmosphere of H_2 represents a viable route to generate amines. To verify this assumption, hydrogenation of **28-BAr$^F_4$** was carried out in the presence of an additional equivalent of HBAr$^F_4$ in order to protonate (and preferably precipitate) potentially formed amine. In this way, a reaction back to **28** by vacuum application would be hampered. As before, **29** formed selectively. However, after evacuation of the reaction mixture, the same product distribution of **29** and **28** was found. Therefore, amine generation out of hydrogenation of the N_2-derived imido complexes has not been accomplished so far.

III Summary

To fulfill the task of rhenium mediated N_2 splitting, a low valent, coordinatively unsaturated rhenium pincer complex was synthesized. The synthesis of Re(III) complex **3** containing *tert*-butyl substituents on the phosphorous atoms is straightforward and achieved in good yields (usually around 80% isolated). The complex is indefinitely stable at room temperature under argon atmosphere and no reaction with N_2 is observed. On the other hand, reduction of this complex under N_2 atmosphere using Na/Hg or $CoCp^*_2$ generates the nitrido complex **9** in high spectroscopic yields. Although no well resolved crystal structure of this complex was obtained, comparison of its spectroscopic signature with an authentic sample prepared from an azide source ([PPN]N_3) as well as ^{15}N-labelling confirmed the existence of a terminal nitride. Spectroscopically, no intermediates could be detected. However, the splitting mechanism is proposed to proceed via a linear μ-η^1-η^1-N_2 dimer analogous to the mechanism observed by *Cummins*.[83,84] DFT calculations predict this mechanism to be a feasible route with a broken symmetry singlet state dimer as reaction intermediate. During N-N splitting a *zigzag* transition state is reached with a moderate barrier, which cleaves into the nitride complexes. The N-N splitting process was calculated to be exergonic by about 98 kJmol^{-1}. A {MNNM]$^{10\pi4\delta}$ system is believed to play an important role for the N-N cleavage to take place and is therefore stated to be a prerequisite. This is in agreement with most other dinuclear systems, which also contain a 10π-electron system and which also reduce N_2 into metal nitrides.

The utilized PNP ligand allows for simple variations in order to probe the influence of steric bulk, rigidity and π-donor strength of the involved amide. As DFT calculations predict a lower steric bulk to impede N-N splitting and may allow for isolation of an N_2 bridged intermediate, the *iso*-propyl-derivative PNP^{iPr} was employed. A five-coordinate amide like **3** seems to be disfavored. Contrariwise, the octrahedrally coordinated amine 4 is formed. However, the latter has not been used for N_2 splitting in this thesis. Oxidation of the ligand backbone to enamide **8** and dienamide **6** can easily be accomplished by H-atom abstraction. The nitride **11** is a stable species, but a preliminary N_2 splitting test from **6** did not unambiguously confirm, that cleavage is possible with these systems.

A reaction of the nitride complex **9** with CO, CO_2 or H_2 gas has not been observed. Protonation of **9** yields the amine, nitride **12-X**, which is protonated at the backbone nitrogen and not at the nitride functionality. However, the nitride was found to react nucleophilic. Functionalization in terms of N-C coupling was achieved by reaction with strong electrophiles like alkyl triflates or alkyl oxonium compounds (Meerwein salts) to generate the respective imido complexes **16-X**. Addition of Tf_2O generates the triflated compound **17-OTf**. Weaker electrophiles like alkyl halides, acid chlorides, silicon compounds or anhydrides do not show a reaction with the nitride.

Usually, coordination *trans* to the nitride is inhibited due to its strong *trans* influence. However, strong σ-donors, like isonitriles do show a reaction. CN^{t}Bu in combination with a base presumably forms the cyanide complex **14**. The *tert*-butyl group of the isonitrile is thus eliminated as isobutene. With strong electrophiles like MeLi, chloride exchange by a methyl group to **13** could be observed. Grignard reagents or hydride sources do not react with **9**. Synthesis and found reactivity of **9** is summarized in Scheme 73.
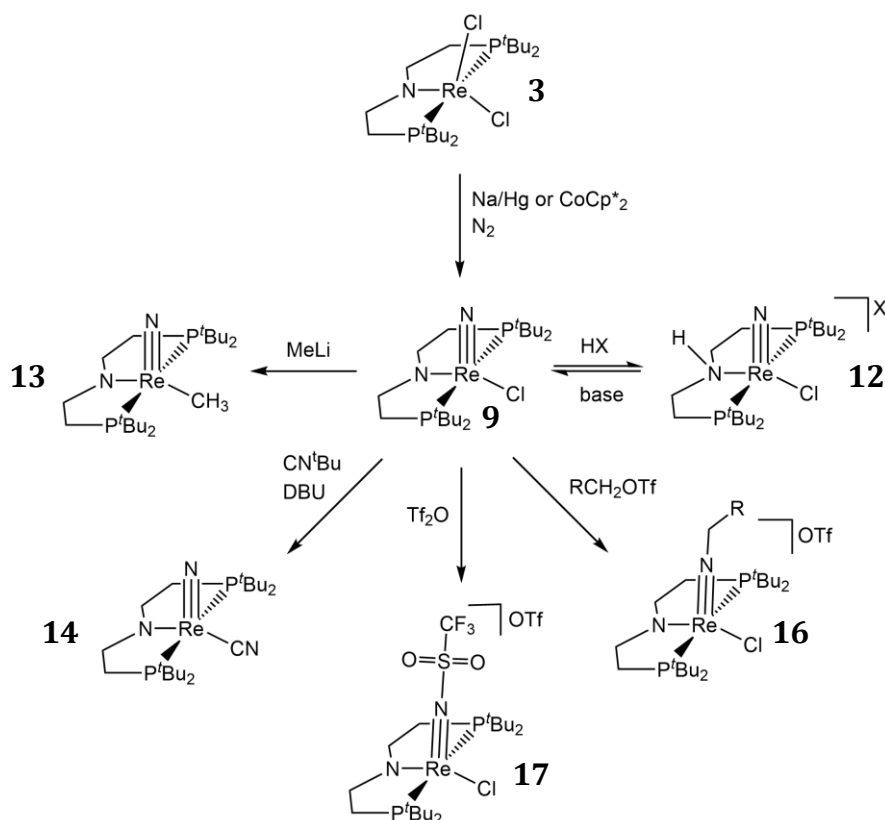
Scheme 73: Synthesis of the nitride complex 9 by N$_2$ splitting from 3 with subsequent functionalizations.

17-OTf displays interesting reactivity upon heating in aromatic solvents. Clean generation of **12-OTf** is observed and CF$_3$-group transfer to the solvent is assumed. By addition of a suitable base, a catalytic application would be an intriguing possibility, although this was not tested during the course of this thesis.

The imido complexes **16** can be deprotonated by KO^{t}Bu or KBTSA to generate the respective azavinylidene species **18**. If the deprotonation is carried out with MeLi or MeMgCl, additionally substitution of the chloride by the methyl group is observed to yield **25**. Addition of H$_2$ to the latter leads to exchange of the methyl group by a hydride substituent in **26**. The complex **26a** can also be synthesized by 2 electron

reduction from **16a-OTf**. Reduction from **16b-OTf** to **26b** is possible, but not as selective. Protonation of the azavinylidene species **18** and **26** to the respective imido complexes **16** and **28** is possible, however excess acid can cause degradation. Protonation of **25** has not been tested. These transformations are summarized in Scheme 74.

Hydrogenation of the imides and the azavinylidenes is possible, but usually protonation at the backbone nitrogen and the generation of a hydride is observed and no reactivity at the N_2-derived nitrogen.
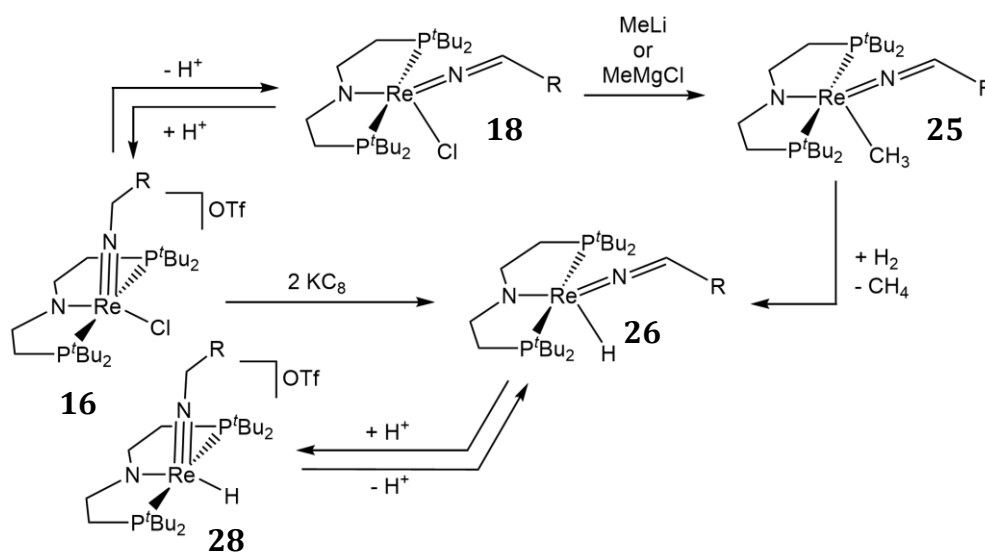
Scheme 74: Transformations of all characterized azavinylidene species.

With the objective of acetonitrile release from **18b**, deprotonation of the latter was tested. However, only in the presence of strong π-acceptors like isonitriles (CN^{t}Bu) a stabilization of the Re(I) species was observed under release of the nitrile. In **19**, the high electron density is expressed by an unusual, but not unprecedented, bending of one isonitrile ligand due to strong π-backbonding. However, the starting material for N_2 splitting, complex **3**, could not be recovered from **19**. In a second step, deprotonation and 2 electron oxidation was combined in order to oxidize the resulting Re(I) directly back to Re(III). Oxidation and simultaneous H-atom abstraction resulted in formation of the vinyl compound **22-OTf** instead of acetonitrile. However, the nitrile could be liberated in low yields by addition of a chloride source under generation of **3**. Addition of a chlorinating agent (NCS) to **18b** resulted in formation of the trichloro complex **23** with concomitant release of acetonitrile. The latter can be reduced by one electron to **3** or by 2 electrons under N_2 atmosphere to yield **9**. In this way a synthetic cycle for the transformation of N_2 in acetonitrile is achieved with an overall yield of 52% (Scheme 75).
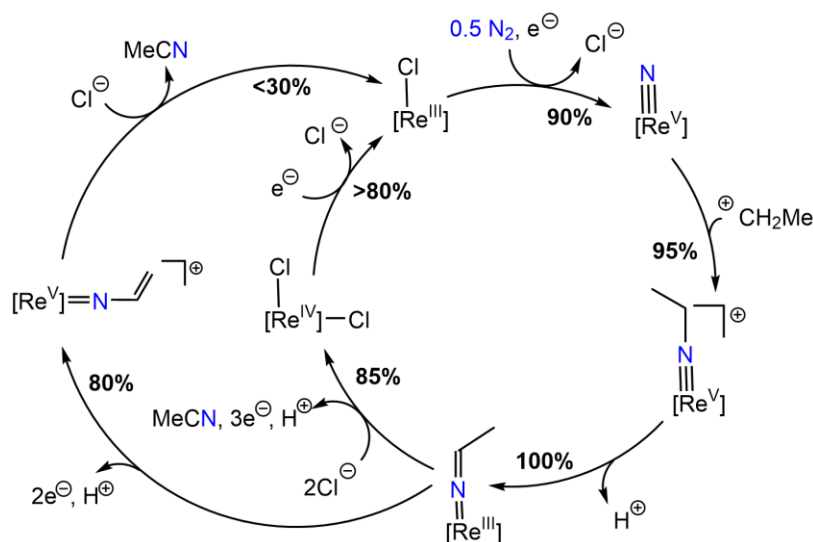
Scheme 75: Synthetic cycles for the conversion of N$_2$ into acetonitrile.

Oxidation of the azavinylidene analogue **18a** resulted in C-C coupling, indicating that the oxidized form is quite unstable. If only an oxidizing agent (Ag$^+$) is added to the reaction, the main product turned out to be the dimer **24**. In situ formation of the trityl radical by oxidation of **18a**, allowed for the detection of the C-C coupling product **16d**. Utilizing this radical reactivity may allow for further functionalizations of the N$_2$-derived moiety.

Chlorination of **18a** by NCS seems to produce **23** as observed for **18b**. However, the reaction is not as clean and the fate of the {CN} moiety is unclear.

In summary, rhenium mediated N$_2$ splitting in terminal nitrides could be achieved. A {MNNM]$^{10\pi}$ electronic configuration is assumed to be necessary to lead to N-N cleavage. Unfortunately, the nitride turned out to be rather stable with efficient Re≡N π-backbonding. NH$_3$ could not be generated in any way. However, functionalization with strong electrophiles leads to C-N bond formation. Further conversion of these imides could be achieved to liberate acetonitrile carrying N$_2$ derived nitrogen. By recovering of the starting material, a synthetic cycle could be closed. The system still has potential for the generation of different nitriles or even cyanide. A truly catalytic process seems unlikely with this system, but an electro-catalytic application might be feasible. Furthermore, the ligand system offers the possibility of fine-tuning of the steric and electronic requirements to not only obtain more insights into the N$_2$ splitting mechanism, but also to achieve more reactivity at the formed nitrido unit.

IV Experimental details

1   Methods

1.1   General Methods

Inert Gas

All reactions with reagents sensitive to air or moisture were performed using standard Schlenk techniques under an atmosphere of argon or N_2 where indicated (both 5.0, *Linde* gas). H_2 gas (5.0) was passed through a steel coil cooled with liq. N_2 to freeze out all moisture. All glassware was pretreated in a KOH/isopropanol bath, neutralized with diluted HCl, washed with deionized water and heated to 120°C. Before utilization, the glassware was heated under applied vacuum and flushed with argon in three cycles. Solvents were added via steel cannulas and rubber septum or trap-to-trap transferred in the reaction vessel. Glass fiber filters (Whatman GF/B) attached to Teflon cannulas with Teflon band were used for standard filtrations. A glass frit (G4) was charged with hot celite (min. 24 h at 120°C) for filtration over celite. Dewar vessels cooled with isopropanol/N_2 *liq.* or dry ice baths were used for low temperature synthesis. All small scale experiments (< 20 µmol) were performed in *J-Young* NMR tubes.

Glove box

Small scale reaction work up and weighing of sensitive materials was carried out in a glove box of *MBraun* under argon atmosphere. The atmosphere was circulated through columns filled with activated carbon, copper catalyst and molecluar sieves (4 Å) to remove traces of oxygen, moisture and solvents.

Solvents

Pentanes, benzene, THF, toluene, DCM and diethylether were passed through columns packed with activated alumina and/or molecular sieves in a solvent purification system of *MBraun*. Methanol, ethanol, ispropanol, acetone and DMSO were dried by stirring over molecular sieves. Triethylamine was distilled from KOH under argon. Acetonitrile was dried over CaH_2 and distilled under argon. Deuterated solvents were dried over Na/K-alloy (C_6D_6 and d_8-THF) or CaH_2 (CD_2Cl_2), distilled by trap-to-trap transfer *in vacuo*, and degassed by three freeze-pump-thaw cycles, respectively. All solvents were stored under argon atmosphere.

1.2 Analytical Methods

Elemental Analysis

Elemental analyses were obtained from the Analytical Laboratories at the Georg-August University (Göttingen, Germany) on an *Elementar Vario* EL 3.

NMR Spectroscopy

NMR spectra were recorded on a *Bruker* Avance III 300, *Bruker* Avance III 400 MHz or a *Bruker* Avance DRX 500 spectrometer and were calibrated to the residual proton resonance of the solvent (C_6D_6: δ_H = 7.16 ppm, δ_C = 128.39; d_8-THF: δ_H = 3.58 ppm, CD_2Cl_2: δ_H = 5.32 ppm). ^{31}P and ^{15}N NMR chemical shifts are reported relative to external phosphoric acid and nitromethane (δ = 0.0 ppm), respectively. Signal multiplicities are abbreviated as: s (singlet), d (dublet), t (triplet), m (multiplet), br (broad).

Mass Spectrometry

Electrospray mass spectrometry was performed with a *Bruker* HCT ultra ESI-MS under N_2 atmosphere. LIFDI mass spectrometry was carried out on a *JEOL* AccuTOF JMS-T100GCV spectrometer. The sample solution was introduced to the spectrometer via a steel cannula from a vial with rubber septum under argon atmosphere.

IR Spectroscopy

IR spectra were recorded on a *Thermo Scientific* Nicolet iZ10 Transmission spectrometer as nujol mulls between KBr plates or as KBr pellets. Spectra in liquid phase were measured in a cuvette containing KBr windows and sealed with teflon plugs. All sample preparation was carried out in a glove box. Signal intensities are abbreviated as: w (weak), m (medium), s (strong).

UV-Vis Spectroscopy

UV-Vis absorption spectra were recorded on a *Varian* Cary 300 Scan spectrophotometer with sealed UV-Vis cuvettes under argon atmosphere.

Cyclic Voltammetry

Cyclic voltammograms were recorded on an Autolab PGSTAT101 from *Metrohm* in a glove box. Measurements were perfomed in a freshly prepared 0.1 M [nBu$_4$N][PF$_6$]-solution of either THF or DCM with glassy carbon working electrode, Ag/AgNO$_3$ reference electrode and Pt counter electrode. Original spectra were referenced against the [(C$_5$H$_5$)$_2$Fe]$^{0/+}$ couple.

Magnetic Measurements

Magnetic moments were determined in THF at room temperature by Evans' method as modified by Sur and corrected for diamagnetic contribution.[230,231] Therefore, the sample (ca. 5 mg) was weighed in a J-Young NMR tube and dissolved in a defined volume (ca. 0.500 mL) of d$_8$-THF and referenced against the signal of a sealed capillary of the same solvent. The difference in chemical shift of the residual proton resonance of the solvent and the sealed capillary was used for the calculation of the magnetic moment.

2 Reagents and starting materials

2.1 Commercially available reagents and starting materials

MeOTf and EtOTf (Alfa Aesar) were destilled and stored at -34°C over molecular sieves or MgSO$_4$. N-chlorosuccinimide (Acros), [Fe(C$_5$H$_5$)] and KOtBu (Sigma) were sublimed prior to use. PPh$_3$ (ABCR) was recrystallized out of ethanol. CN^{t}Bu (abcr) was degassed and stored over molecular sieves. Trifluoromethanesulfonic anhydride (ChemPur), Di-$tert$-butylchlorophosphine, benzylbromide (Alfa), ^{15}N$_2$, Lithium granula, [N(PPh$_3$)$_2$]Cl, KBTSA, TBD, NH$_4$PF$_6$, CoCp$_2$, CoCp$_2$*, BuLi (2.5 M in hexanes), PhMgBr (1 M in THF), MeMgCl (3 M inTHF, Sigma Aldrich), MeLi (1.6 M/Et$_2$O, Acros), KF, NaN$_3$ (Merck), AgOTf, AgPF$_6$, KReO$_4$, HCl (2 M in Et$_2$O, abcr) and HOTf (abcr) were used as purchased.

2.2 Non commercially available reagents and starting materials

Following reagents and starting materials were not obtained commercially and were synthesized according to following literature:

Compound	Literature
Re(O)(PPh$_3$)$_2$Cl$_3$ (**1**)	[194]
Re(Cl)$_3$(PPh$_3$)$_2$(NCCH$_3$) (**2**)	[195]
Di(2-chloroethyl)trimethylsilylamine	[232]
Bis(di-$tert$-butylphosphinoethyl)amine (PNP)	[233,234]
KC$_8$	[235]
Na/Hg	[236]
[N(PPh$_3$)$_2$]N$_3$ ([PPN]N$_3$)	[234,237]
2,3:5,6-Dibenzo-7-azabicyclo[2.2.1]hepta-2,5-diene (HDBABH)	[238]
2,4,6-tri-$tert$-butylphenoxyl radical	[239]
H[B{C$_6$H$_3$(CF$_3$)$_2$}$_4$] (H[BAr$^F_4$])	[240]

3 Synthesis

3.1 Re(III) platform

3.1.1 (PNP)ReCl$_2$ (3)

Published route

Re(Cl)$_3$(PPh$_3$)$_2$(NCCH$_3$) (**2**) (220 mg, 0.256 mmol, 1 eq), ^{H}PNP (92.7 mg, 0.256 mmol, 1 eq) and NEt$_3$ (71 μL, 0.513 mmol, 2 eq) are suspended in THF (30 mL) and heated to reflux for 1 h, leading to a color change from yellow to dark brown-violet. The mixture is allowed to cool to room temperature and the solvent is removed *i. vac.* The crude product is consecutively extracted with benzene (3 x 10 mL) and pentane (10 x 10 mL), filtered, and the solvent is removed *i. vac.* After lyophilization (benzene), residual PPh$_3$ is sublimed off by heating to 80°C for 3 d at 30 mTorr. The product **3** is obtained as violet powder. Yield: 126 mg, 0.204 mmol, 79%.

Improved synthesis

[Re(Cl)$_3$(PPh$_3$)$_2$(NCCH$_3$)] (**2**) (1.025 g, 1.194 mmol, 1 eq), ^{H}PNP (504.7 mg, 1.396 mmol, 1.2 eq) and NEt$_3$ (331 μL, 2.388 mmol, 2 eq) are suspended in THF (50 mL) and heated to reflux for 2.5 h, leading to a color change from yellow to dark brown-violet. The mixture is allowed to cool to room temperature and the solvent is removed *i. vac.* The crude product is extracted with benzene (3 x 10 mL) and after evaporation of the solvent, the residue is washed with pentanes until the color changes from brown to violet (ca. 4 x 5 mL). After lyophilization (benzene), residual PPh$_3$ is sublimed off by heating to 80°C for 30 h at 30 mTorr. The product **3** is obtained as violet powder. Yield: 634.7 mg, 1.028 mmol, 86%.

Spectroscopic Characterization

^{1}H NMR   (300 MHz, C$_6$D$_6$, [ppm]): δ = 1.54 (A$_{18}$XX´A´$_{18}$, N = | ^{3}J$_{HP}$ + ^{5}J$_{HP}$ | = 6.0 Hz, 36H, P(C(C*H$_3$*)$_3$)), 2.20 (A$_2$B$_2$XX´B´$_2$A´$_2$, N = | ^{3}J$_{HP}$ + ^{4}J$_{HP}$ | = 6.0 Hz, ^{3}J$_{HH}$ = 6.6 Hz, 4H, NC*H$_2$*), 2.28 (m, 4H, PC*H$_2$*).

^{13}C{^{1}H} NMR (75.5 MHz, C$_6$D$_6$, [ppm]): δ = 32.0 (A$_6$XX´A´$_6$, N = | ^{2}J$_{CP}$ + ^{4}J$_{CP}$ | = 2.0 Hz, P(C(C*H$_3$*)$_3$)), 36.7 (AXX´A´, N = | ^{1}J$_{CP}$ + ^{3}J$_{CP}$ | = 6.9 Hz, PC*H$_2$*), 52.4 (A$_2$XX´A´$_2$, N = | ^{1}J$_{CP}$ + ^{3}J$_{CP}$ | = 7.7 Hz, P(*C*(CH$_3$)$_3$)), 98.0 (AXX´A´, N = | ^{2}J$_{CP}$ + ^{3}J$_{CP}$ | = 4.1 Hz, N*C*H$_2$).

^{31}P{^{1}H} NMR (121.5 MHz, C$_6$D$_6$, [ppm]): δ = -51.5 (s, *P*^{t}Bu$_2$).

Elemental Analysis

$C_{20}H_{44}Cl_2NP_2Re$ (%) calcd.: C, 38.89; H, 7.18; N, 2.27

found: C, 39.43; H, 6.97; N, 2.13

3.1.2 Synthesis of [^{H}PNP^{iPr}ReCl$_3$] (4)

^{H}PNP^{iPr} (2.2 mg, 6.8 µmol, 1.1 eq) is dissolved in C_6D_6 and added to **2** (5.2 mg, 6.1 µmol, 1 eq) in a J-Young NMR tube. The mixture is heated to 65°C for 2 h during which the suspension clears off. The solvent is reduced to about 0.1 mL and pentane is added (0.7 mL). After filtration, the residue is again washed with pentanes (2 x 0.7 mL). The residue is extracted with benzene and filtered over Celite. NMR-spectra show formation of paramagnetic **4**.

^{1}H NMR (300 MHz, C_6D_6, [ppm]): δ = -12.1 (m, 2H), -6.7 (m, 2H), -0.1 (m, 2H), 6.7 (m, 2H), 8.2 (m, 6H), 8.6 (m, 6H), 9.0 (m, 12H), 9.7 (m, 2H), 137.2 (s, 1H).

3.1.3 Deprotonation of [HPNP^{iPr}ReCl$_3$] (4)

KO^{t}Bu or KBTSA:

To a solution of **4** (3.5 mg, 5.8 µmol, 1 eq) in d$_8$-THF (0.5 mL) the respective base, KO^{t}Bu (0.7 mg, 6.4 µmol, 1.1 eq) or KBTSA (1.2 mg, 5.8 µmol, 1 eq), is added. The solution turns dark brown immediately and the ^{31}P-NMR spectra show formation of two diamagnetic products.

^{31}P{^{1}H} NMR (121.5 MHz, C_6D_6, [ppm]): δ = -1.4 (s, 35%), -17.0 (s, 65%).

TBD (Synthesis of 5):

To a solution of **4** (3.5 mg, 5.8 µmol, 1 eq) in C_6D_6 (0.5 mL) TBD (0.8 mg, 5.8 µmol, 1 eq) is added, followed by a color change to grass green and selective formation of one compound. The solvent is evaporated and the residue is extracted with pentanes. After drying *i. vac.* the residue is dissolved in C_6D_6. Crystallization out of pentane confirmed the formation of **5**.

^{31}P{^{1}H} NMR (121.5 MHz, C_6D_6, [ppm]): δ = -6.1 (s, *P*^{i}Pr$_2$).

3.1.4   Synthesis of [(P=N=P)ReCl$_2$] (6)

3 (40.0 mg, 64.8 μmol, 1 eq) and 2,4,6-tri-*tert*-butylphenoxyl radical (101.6 mg, 388.6 μmol, 6 eq) are dissolved in benzene (5-8 mL) and warmed to 50°C until the color changes from blue to green (5 h). The reaction is then stirred for another 15 h at room temperature, before the solvent is evaporated and the residue washed with pentanes (3 x 2 mL). CoCp$_2$ (1.5 mg, 7.9 μmol, 0.12 eq) is added together with benzene (5 mL) and the reaction is stirred for 1.5 h before filtration and lyophilization. The brown powder is then heated to 85°C under reduced pressure (30mTorr) to sublime off residual CoCp$_2$. Pure **6** is obtained as brown powder. Yield: 28.0 mg, 45.6 μmol, 71%.

Spectroscopic Characterization

^{1}H NMR   (300 MHz, C$_6$D$_6$, [ppm]): δ = 0.90 (d, ^{3}J$_{HH}$ = 6.4 Hz, 2H, PC*H*CH), 2.61 (A$_{18}$XX′A′$_{18}$, N = | ^{3}J$_{HP}$ + ^{5}J$_{HP}$ | = 6.2 Hz, 36H, P(C(C*H$_3$*)$_3$), 3.65 (A$_2$B$_2$XX′B′$_2$A′$_2$, N = | ^{3}J$_{HP}$ + ^{4}J$_{HP}$ | = 16.4 Hz, ^{3}J$_{HH}$ = 6.4 Hz, 2H, NC*H*CH).

^{13}C{^{1}H} NMR (75.5 MHz, C$_6$D$_6$, [ppm]): δ = 34.7 (A$_6$XX′A′$_6$, N = | ^{2}J$_{CP}$ + ^{4}J$_{CP}$ | = 2.5 Hz, P(C(*C*H$_3$)$_3$), 77.4 (A$_2$XX′A′$_2$, N = | ^{1}J$_{CP}$ + ^{3}J$_{CP}$ | = 9.5 Hz, P(*C*(CH$_3$)$_3$), 147.6 (AXX′A′, N = | ^{1}J$_{CP}$ + ^{3}J$_{CP}$ | = 15.4 Hz, P*C*HCH), 212.4 (AXX′A′, N = | ^{2}J$_{CP}$ + ^{3}J$_{CP}$ | = 7.9 Hz, N*C*HCH).

^{31}P{^{1}H} NMR (121.5 MHz, C$_6$D$_6$, [ppm]): δ = -275.6 (s, *P*^{t}Bu$_2$).

Mass Spectrometry

LIFDI+   (toluene, m/z$^+$): 613.1 (C$_{20}$H$_{40}$Cl$_2$NP$_2$Re$^+$).

Elemental Analysis

C$_{20}$H$_{40}$Cl$_2$NP$_2$Re (%)   calcd.:   C, 39.15; H, 6.57; N, 2.28
                                         found: C, 38.81; H, 6.63; N, 2.14

3.1.5   Synthesis of [(P=N=P)ReCl$_3$] (7)

23 (5.0 mg, 7.7 μmol, 1 eq) and 2,4,6-tri-*tert*-butylphenoxyl radical (10.0 mg, 38.3 μmol, 5 eq) are dissolved in C$_6$D$_6$ (0.5 mL) and heated to 50°C for 18 h. NMR spectra show complete conversion to paramagnetic 7 together with the formation of 2,4,6-tri-*tert*-butylphenol.

Spectroscopic Characterization

1H NMR   (300 MHz, C_6D_6, [ppm]): δ = -51.3 (br), 15.1 (br).

Mass Spectrometry

LIFDI+   (toluene, m/z$^+$): 648.0 ($C_{20}H_{40}Cl_3NP_2Re^+$).

3.1.6 Synthesis of [(P=NP)ReCl$_2$] (8)

3 (5.0 mg, 8.1 µmol, 1 eq) and 2,4,6-tri-*tert*-butylphenoxyl radical (4.2 mg, 388.6 µmol, 2 eq) are dissolved in benzene (0.5 mL) and stirred for 18 h, before more 2,4,6-tri-*tert*-butylphenoxyl radical (1.1 mg, 4.2 µmol, 0.5 eq) is added. After stirring for another 5 h, the solvent is evaporated and the residue washed with pentanes until the washing solution is colorless (5 x 0.3 mL). The green product **8** is obtained in 80% spectroscopic yield (^{31}P-NMR integration) next to starting material **3** (δ_P = -54.7 ppm, 9%) and **6** (δ_P = -278.7 ppm, 11%).

Spectroscopic Characterization

1H NMR   (300 MHz, C_6D_6, [ppm]): δ = 1.68 (d, $^3J_{HP}$ = 11.8 Hz, 18H, PC(CH_3)$_3$), 1.78 (d, $^3J_{HP}$ = 11.8 Hz, 18H, PC(CH_3)$_3$), 2.36 (A$_2$B$_2$XX′B′$_2$A′$_2$, N = | $^2J_{HP}$ + $^4J_{HP}$ | = 6.8 Hz, $^3J_{HH}$ = 6.6 Hz, 4H, PCH_2), 2.63 (A$_2$B$_2$XX′B′$_2$A′$_2$, N = | $^3J_{HP}$ + $^4J_{HP}$ | = 6.7 Hz, $^3J_{HH}$ = 66 Hz, 4H, NCH_2, partially superimposed), 4.31 (d, $^3J_{HH}$ = 6.7 Hz, NCH), 6.31 (dd, $^2J_{HP}$ = 32.7 Hz, $^3J_{HH}$ = 6.7 Hz, PCH).

31P{1H} NMR (121.5 MHz, C_6D_6, [ppm]): δ = -107.3 (d, $^2J_{PP}$ = 283.3 Hz, P^tBu$_2$), -113.7 (d, $^2J_{PP}$ = 283.3 Hz, P^tBu$_2$).

Mass Spectrometry

LIFDI+   (toluene, m/z$^+$): 615.1 ($C_{20}H_{42}Cl_2NP_2Re^+$).

3.1.7 Synthesis of [(P=N=P)Re(N)Cl] (11)

[PPN]N_3 (6.5 mg, 11.2 μmol, 1.4 eq) is added to **6** (5.0 mg, 8.1 μmol, 1 eq) and the reactants are suspended in THF (0.5 mL). The mixture is stirred for 3 d at room temperature. NMR spectra show complete conversion to **11** (95%) and an undefined sideproduct (5%, ^{31}P-NMR signal at 48.1 ppm).

Spectroscopic Characterization

^{1}H NMR (300 MHz, C_6D_6, [ppm]): δ = 1.18 (A$_9$XX′A′$_9$, N = |$^3J_{HP}$ + $^5J_{HP}$| = 7.0 Hz, 18H, PC(CH_3)$_3$), 1.49 (A$_9$XX′A′$_9$, N = |$^3J_{HP}$ + $^5J_{HP}$| = 7.2 Hz, 18H, PC(CH_3)$_3$), 4.29 (A$_2$B$_2$XX′B′$_2$A′$_2$, N = | $^3J_{HP}$ + $^4J_{HP}$ | = 2.2 Hz, $^3J_{HH}$ = 6.2 Hz, 2H, PCHCH), 7.00 (m, 2H, NCHCH).

^{31}P{^{1}H} NMR (121.5 MHz, C_6D_6, [ppm]): δ = 71.8 (s, P^tBu$_2$).

Mass Spectrometry

LIFDI+ (toluene, m/z$^+$): 592.0 (C$_{20}$H$_{40}$ClN$_2$P$_2$Re$^+$).

3.2 Nitride synthesis and functionalization

3.2.1 [(PNP)Re(N)Cl] (9)

N_2-route **A**

Na/Hg (109.7 mg, 1 mol/L, 1 eq) is added to a solution of **3** (5.0 mg, 8.10 μmol, 1 eq) in d$_8$-THF (0.5 mL) in a J-Young-NMR tube under N_2-atmosphere (1 bar) and the mixture is shaken. The color changes from violet to brown-yellow over the course of about 5 minutes. ^{31}P{^{1}H}-NMR spectroscopy indicates the full conversion of the starting material and formation of Re(N)Cl(PNP) (**9**) in 86% yield besides two unidentified side-products (82.1 ppm (12%), 54.9 ppm (2%)). The ^{1}H, ^{13}C{^{1}H} and ^{31}P{^{1}H} NMR spectra of **9** are identical with an analytically pure sample obtained on the azide route (see below).

The ^{15}N-labelled isotopomer Re(^{15}N)Cl(PNP) **9^{15N}** is prepared by adding **3** (10.0 mg, 16.2 µmol, 1 eq) in d_8-THF (0.5 mL) under argon atmosphere to Na/Hg (240 mg, 1 mol/L, 1 eq) in a J-Young-NMR tube. The reaction mixture is frozen immediately and the atmosphere is replaced by $^{15}N_2$. The mixture is allowed to warm to room temperature while shaking.

Spectroscopic characterization

^{15}N NMR   (50.7 MHz, d_8-THF), [ppm]): δ = 370.6 (s, Re*N*). $^{15}N_2$ displays a signal at -70.8 ppm.

*N$_2$-route **B***:

In a J-Young-NMR tube **3** (5.0 mg, 8.10 µmol, 1 eq) and CoCp$^*_2$ (2.8 mg, 8.50 µmol, 1.05 eq) are dissolved in d_8-THF (0.5 mL) under N$_2$-atmosphere and shaken. The color changes immediately to green and a green precipitate forms. The mixture is shaken for 16 h to allow for complete conversion of the reducing agent. **9** is formed in 48% yield ($^{31}P\{1H\}$-NMR) besides one major (31.2 ppm (24%)) and several smaller (<5%) diamagnetic side products. Additionally, one paramagnetic compound (14 ppm, br) could be detected in the ^1H-NMR.

Azide route:

3 (300 mg, 0.486 mmol, 1 eq) and [N(PPh$_3$)$_2$]N$_3$ (310 mg, 0.534 mmol, 1.1 eq) are stirred in THF (20 mL) at room temperature. The color changes slowly from violet to brown and gas evolution is observed. The mixture is stirred for at least 24 h at room temperature and filtered before evaporation of the solvent. The residue is first extracted with benzene (3 x 10 mL), the solvent evaporated and the residue extracted with pentane (6 x 15 mL) and filtered over Celite. After evaporation of the solvent, the product is lyophilized out of benzene to obtain an orange solid, which is sufficiently pure for most syntheses. Yield: 182 mg, 0.305 mmol, 63%. For further purification, this product is extracted another time with pentane and acetonitrile and dried at 80°C for 1 d. Yield: 153 mg, 0.257 mmol, 53%.

An equimolar mixture of the $^{14}N/^{15}N$ isotopomers is prepared by employing [N(PPh$_3$)$_2$]$^+$[$^{15}N^{14}N_2$]$^-$, which was synthesized from [N(PPh$_3$)$_2$]Cl and Na[$^{15}N^{14}N_2$].

Spectroscopic Characterization

^1H NMR   (300 MHz, C$_6$D$_6$, [ppm]): δ = 1.22 (A$_9$XX´A´$_9$, N = | $^3J_{HP}$ + $^5J_{HP}$ = 6.6 Hz, 18H, PC(CH_3)$_3$), 1.37 (m, 2H, PCH_2, superimposed), 1.41 (A$_9$XX´A´$_9$, N = | $^3J_{HP}$ + $^5J_{HP}$ = 6.7 Hz, 18H, PC(CH_3)$_3$), 1.61 (ABCDXX´D´C´B´A´, N = | $^2J_{HP}$ + $^4J_{HP}$ | = 3.8 Hz, $^2J_{HH}$ = 14.4 Hz , $^3J_{HH}$ = 7.7 Hz, $^3J_{HH}$ = 10.8 Hz, 2H, PCH_2), 3.08 (ABCDXX´D´C´B´A´, N = | $^3J_{HP}$ + $^4J_{HP}$ | = 1.6 Hz, $^2J_{HH}$ = 10.9 Hz, $^3J_{HH}$ =

10.8 Hz, $^3J_{HH}$ = 5.4 Hz, 2H, NCH_2), 3.69 (ABCDXX′D′C′B′A′, N = | $^3J_{HP}$ + $^4J_{HP}$ | = 15.9 Hz, $^2J_{HH}$ = 10.9 Hz, $^3J_{HH}$ = 7.7 Hz, $^3J_{HH}$ = 1.8 Hz, 2H, NCH_2).

^{13}C{^{1}H} NMR (75.5 MHz, C$_6$D$_6$, [ppm]): δ = 25.7 (AXX′A′, N = | $^1J_{CP}$ + $^3J_{CP}$ | = 11.3 Hz, PCH$_2$), 28.9 (A$_3$XX′A′$_3$, N = | $^2J_{CP}$ + $^4J_{CP}$ | = 1.9 Hz, PC(CH$_3$)$_3$), 29.0 (A$_3$XX′A′$_3$, N = | $^2J_{CP}$ + $^4J_{CP}$ | = 2.0 Hz, PC(CH$_3$)$_3$), 35.5 (AXX′A′, N = |$^1J_{CP}$ + $^3J_{CP}$ | = 8.0 Hz, PC(CH$_3$)$_3$), 36.3 (AXX′A′, N = |$^1J_{CP}$ + $^3J_{CP}$ | = 10.6 Hz, PC(CH$_3$)$_3$), 72.0 (AXX′A′, N = |$^2J_{CP}$ + $^3J_{CP}$ | = 3.5 Hz, NCH$_2$).

^{31}P{^{1}H} NMR (121.5 MHz, C$_6$D$_6$, [ppm]): δ = 84.2 (s, P^{t}Bu$_2$).

^{15}N{^{1}H} NMR (50.7 MHz, C$_6$D$_6$), [ppm]): δ = 369.0 (s, ReN).

Mass Spectrometry

ESI (acetonitrile, m/z$^+$): 596.03 (C$_{20}$H$_{44}$ClN$_2$P$_2$Re$^+$), 597.03 (C$_{20}$H$_{45}$ClN$_2$P$_2$Re$^+$), 602.28 (C$_{20}$H$_{44}$ClN$_2$P$_2$Re$^+$ - CH$_3$CN).

Elemental Analysis

C$_{20}$H$_{44}$ClN$_2$P$_2$Re (%)   calcd: C, 40.29; H, 7.44; N, 4.70
                                      Found: C, 41.12; H, 7.52; N, 4.67

Li[DBABH] route
HDBABH (1.6 mg, 8.1 μmol, 1 eq) is dissolved in THF (0.3 mL) and BuLi (1.6 M in hexanes, 5 μL, 1 eq) is added dropwise at -35°C. The cold reaction mixture is transferred to **3** (5.0 mg, 8.10 μmol, 1 eq) in cold THF (0.2 mL) in a J-Young-NMR tube and shaken for 1 h upon warming to room temperature. The solvent is exchanged by d$_8$-THF and shaken for another 27 h. ^{31}P{^{1}H}-NMR spectroscopy indicates selective formation of **9** in 66% yield.

By deprotonation of **12-OTf**
12-OTf (10.0 mg, 16.2 μmol, 1 eq) is dissolved in d$_6$-benzene (0.5 mL) and KO^{t}Bu (1.8 mg, 16.2 μmol, 1 eq) in d$_8$-THF (0.1 mL) is added. The color immediately changes to yellow and **9** is formed quantitatively (^{31}P{^{1}H}-NMR).

3.2.2 [(^{H}PNP)Re(N)Cl]X (12)

12-OTf: HOTf (2.9 μL, 33.5 μmol, 1 eq) is added to a solution of **9** (20 mg, 33.5 μmol, 1 eq) in benzene (5 mL). The yellow solution immediately turns darker. After stirring for 20 h, the solution is evaporated to dryness and the residue washed with pentane (2 x 5 mL). Lyophilization out of benzene affords the product **12-OTf** as red-orange solid. Yield: 23.2 mg, 31.1 μmol, 92%.

Spectroscopic Characterization

^{1}H NMR   (300 MHz, C$_6$D$_6$, [ppm]): δ = 1.11 (A$_9$XX′A′$_9$, N = |^{3}J$_{HP}$ + ^{5}J$_{HP}$ | = 7.7 Hz, 18H, PC(CH_3)$_3$, partially superimposed), 1.15 (A$_9$XX′A′$_9$, N = |^{3}J$_{HP}$ + ^{5}J$_{HP}$ | = 7.3 Hz, 18H, PC(CH_3)$_3$, partially superimposed), 1.50 (m, 2H, PCH_2), 2.34-2.12 (m, 4H, NCH_2 and PCH_2 superimposed), 4.22 (m, 2H, NCH_2), 6.54 (br, 1H, HPNP).

^{13}C{^{1}H} NMR (75.5 MHz, C$_6$D$_6$, [ppm]): δ = 25.0 (AXX′A′, N = | ^{1}J$_{CP}$ + ^{3}J$_{CP}$ | = 11.5 Hz, PCH_2), 27.6 (A$_3$XX′A′$_3$, N = | ^{2}J$_{CP}$ + ^{4}J$_{CP}$ | = 2.3 Hz, PC(CH_3)$_3$), 28.2 (A$_3$XX′A′$_3$, N = | ^{2}J$_{CP}$ + ^{4}J$_{CP}$ | = 2.0 Hz, PC(CH_3)$_3$), 35.7 (AXX′A′, N = |^{1}J$_{CP}$ + ^{3}J$_{CP}$ | = 7.8 Hz, PC(CH$_3$)$_3$), 36.3 (AXX′A′, N = |^{1}J$_{CP}$ + ^{3}J$_{CP}$ | = 11.1 Hz, P(C(CH$_3$)$_3$), 65.3 (s, NCH_2).

^{31}P{^{1}H} NMR (121.5 MHz, C$_6$D$_6$, [ppm]): δ = 69.4 (s, PtBu$_2$).

Elemental Analysis

C$_{21}$H$_{45}$ClF$_3$N$_2$O$_3$P$_2$ReS (%)	calcd:	C, 33.80; H, 6.08; N, 3.75; S, 4.30
	found:	C, 34.26; H, 6.07; N, 3.68; S, 5.92

The deviation in the sulfur Analysis is attributed to the presence of fluorine.

12-Cl: A solution of HCl (2 M in ether, 4.1 μL, 1 eq) in THF (0.5 mL) is added to **9** (4.9 mg, 8.2 μmol, 1 eq) in a J-Young-NMR tube. The color of the solution turns from yellow to red-orange and a red precipitate forms. After removing the solvent *i. vac.* the residue is dissolved in CD$_2$Cl$_2$. The product **12**-Cl is obtained spectroscopically pure (^{1}H-NMR) in 98% yield.

Spectroscopic Characterization

^{1}H NMR   (300 MHz, CD$_2$Cl$_2$, [ppm]): δ = 1.38 (A$_9$XX′A′$_9$, N = |^{3}J $_{HP}$ + ^{5}J $_{HP}$ | = 7.5 Hz, 18H, PC(CH_3)$_3$), 1.54 (A$_9$XX′A′$_9$, N = |^{3}J$_{HP}$ + ^{5}J$_{HP}$ | = 7.2 Hz, 18H, PC(CH_3)$_3$), 2.18 (m, 2H, PCH_2), 2.68-2.54 (m, 4H, NCH_2 and PCH_2 superimposed), 4.21 (m, 2H, NCH_2), 9.17 (br, 1H, HN(CH$_2$)$_2$).

$^{31}P\{^1H\}$ NMR (121.5 MHz, CD_2Cl_2, [ppm]): δ = 71.0 (s, P^tBu_2).

12-PF_6: $AgPF_6$ (2.1 mg, 8.4 μmol, 1 eq) and **9** (5.0 mg, 8.4 μmol, 1 eq) are dissolved in CD_2Cl_2 (0.5 mL). The solution turns red-orange and a grey precipitate forms. Two broad paramagnetic signals can be detected in the ^1H NMR spectrum (5.8 ppm and 3.8 ppm) besides the formation of **12-PF_6**.

3.2.3   (PNP)Re(N)(CH$_3$) (13)

9 (24.0 mg, 40.3 μmol, 1 eq) is dissolved in benzene (10 mL) and a solution of MeLi (1.6 M in Et_2O, 50 μL, 80.5 μmol, 2 eq) is added. The mixture is filtered and the solvent evaporated before the residue is extracted with pentanes and filtered over celite. After removal of the solvent *i. vac.* the product **13** is lyophilized out of benzene. Yield: 15.8 mg, 27.4 μmol, 68%).

Spectroscopic Characterization

^1H NMR   (300 MHz, C_6D_6), [ppm]): δ = 1.05 ($A_9XX'A'_9$, N = $|^3J_{HP} + {}^5J_{HP}|$ = 6.3 Hz, 18H, PC(CH_3)$_3$), 1.45 ($A_9XX'A'_9$, N = $|^3J_{HP} + {}^5J_{HP}|$ = 6.5 Hz, 18H, PC(CH_3)$_3$), 1.77 (m, 4H, PCH_2), 2.32 (t, $^3J_{HP}$ = 4.1 Hz, 3H, ReCH_3), 3.52 (m, 2H, NCH_2, partially superimposed), 3.59 (m, 2H, NCH_2, partially superimposed).

$^{13}C\{^1H\}$ NMR (75.5 MHz, C_6D_6, [ppm]): δ = -17.4 (t, $^2J_{CP}$ = 4.7 Hz, ReCH_3), 28.0 (AXX'A', N = $|^1J_{CP} + {}^3J_{CP}|$ = 10.7 Hz, PCH_2), 29.3 ($A_3XX'A'_3$, N = $|^2J_{CP} + {}^4J_{CP}|$ = 2.1 Hz, PC(CH_3)$_3$), 29.6 ($A_3XX'A'_3$, N = $|^2J_{CP} + {}^4J_{CP}|$ = 1.7 Hz, PC(CH_3)$_3$), 35.2 (AXX'A', N = $|^1J_{CP} + {}^3J_{CP}|$ = 8.0 Hz, PC(CH$_3$)$_3$), 35.7 (AXX'A', N = $|^1J_{CP} + {}^3J_{CP}|$ = 9.9 Hz, P(C(CH$_3$)$_3$), 68.9 (AXX'A', N = $|^2J_{CP} + {}^3J_{CP}|$ = 3.8 Hz, NCH_2).

$^{31}P\{^1H\}$ NMR (121.5 MHz, C_6D_6, [ppm]): δ = 88.2 (s, P^tBu_2).

Elemental Analysis

$C_{21}H_{47}N_2P_2Re$ (%)		
	calcd:	C, 43.81; H, 8.23; N, 4.87
	Found:	C, 43.61; H, 7.96; N, 4.90

3.2.4   Reaction with isonitriles

*Reaction of **9** with CN^{t}Bu*

9 (5.0 mg, 8.4 µmol, 1 eq) is dissolved in C_6D_6 (0.5 mL) and CN^{t}Bu (1 µL, 8.8 µmol, 1 eq) is added. The reaction mixture is stirred for several days (7 d) at room temperature to observe the formation of 2 products in the NMR spectra.

^{31}P{^{1}H} NMR (121.5 MHz, C_6D_6, [ppm]): δ = 60.8 (42%, **15**), 83.2 (15%, **9**), 94.8 (43%, **14**)

*Reaction of **9** with CN^{t}Bu and base to **14***

9 (5.0 mg, 8.4 µmol, 1 eq) is dissolved in C_6D_6 (0.5 mL) and CN^{t}Bu (1 µL, 8.8 µmol, 1 eq) and DBU (1.3 µL, 8.4 µmol, 1 eq) are added. The reaction is heated to 60°C for 4 d before the solvent is evaporated and the residue washed with pentanes (3 x 0.5 mL). After extraction with benzene, the NMR spectra shows full conversion to **14**.

Spectroscopic Characterization

^{1}H NMR   (300 MHz, C_6D_6), [ppm]): δ = 1.18 (A$_9$XX´A´$_9$, N = |^{3}J$_{HP}$ + ^{5}J$_{HP}$| = 6.9 Hz, 18H, PC(CH_3)$_3$), 1.35 (A$_9$XX´A´$_9$, N = |^{3}J$_{HP}$ + ^{5}J$_{HP}$| = 6.9 Hz, 18H, PC(CH_3)$_3$), 1.49 (m, 4H, PCH_2), 3.36 (m, 2H, NCH_2), 3.63 (m, 2H, NCH_2).

^{31}P{^{1}H} NMR (121.5 MHz, C_6D_6, [ppm]): δ = 94.8 (s, *P*^{t}Bu$_2$).

*Reaction of **12-OTf** with CN^{t}Bu to **15***

12-OTf (2.5 mg, 3.5 µmol, 1 eq) is dissolved C_6D_6 and CN^{t}Bu (0.5 µL, 3.6 µmol, 1 eq) is added and the mixture is stirred for 2 d at room temperature.

Spectroscopic Characterization

^{1}H NMR   (300 MHz, C_6D_6), [ppm]): δ = 0.75 (s, 9H, CN^t*Bu*), 0.88 (A$_9$XX´A´$_9$, N = |^{3}J$_{HP}$ + ^{5}J$_{HP}$| = 5.6 Hz, 18H, PC(CH_3)$_3$), 0.93 (A$_9$XX´A´$_9$, N = |^{3}J$_{HP}$ + ^{5}J$_{HP}$| = 5.4 Hz, 18H, PC(CH_3)$_3$), 1.53 (m, 2H, PCH_2), 1.97 (m, 2H, PCH_2), 2.67 (m, 2H, NCH_2), 3.67 (m, 2H, NCH_2).

^{31}P{^{1}H} NMR (121.5 MHz, C_6D_6, [ppm]): δ = 60.0 (s, *P*^{t}Bu$_2$).

3.2.5 [(PNP)Re(NMe)Cl]OTf (16a-OTf)

9 (40.0 mg, 67.1 μmol, 1 eq) is dissolved in toluene (10 mL) and MeOTf (7.6 μL, 69.3 μmol, 1 eq) is added. The orange solution is heated to 40°C for 4 h whereupon the color changes to green. The solution is allowed to cool to room temperature, filtered, layered with pentane and crystallized at -32°C. The solid is filtered off, washed with pentane (2 x 5 mL) and dried in vacuo. **16a-OTf** is obtained as a green microcrystalline solid. Yield: 39.9 mg, 51.6 μmol, 77%.

Spectroscopic Characterization

^{1}H NMR (300 MHz, C_6D_6, [ppm]): δ = 1.01 ($A_9XX'A'_9$, N = | $^3J_{HP}$ + $^5J_{HP}$ | = 6.9 Hz, 18H, PC(CH_3)$_3$), 1.15 ($A_9XX'A'_9$, N = | $^3J_{HP}$ + $^5J_{HP}$ | = 7.2 Hz, 18H, PC(CH_3)$_3$), 2.04 (ABCDXX'D'C'B'A', N = | $^2J_{HP}$ + $^4J_{HP}$ | = 5.5 Hz, $^2J_{HH}$ = 14.9 Hz, $^3J_{HH}$ = 4.3 Hz, $^3J_{HH}$ = 6.7 Hz, 2H, PCH_2), 2.21 (ABCDXX'D'C'B'A', N = | $^2J_{HP}$ + $^4J_{HP}$ | = 3.9 Hz, $^2J_{HH}$ = 15.3 Hz, $^3J_{HH}$ = 7.8 Hz, $^3J_{HH}$ = 7.8 Hz, 2H, PCH_2), 2.64 (s, 3H, NCH_3), 3.77 (ABCDXX'D'C'B'A', N = | $^3J_{HP}$ + $^4J_{HP}$ | = 4.0 Hz, $^2J_{HH}$= 14.2 Hz, $^3J_{HH}$= 7.1 Hz, $^3J_{HH}$= 7.1 Hz, 2H, NCH_2), 4.64 (ABCDXX'D'C'B'A', N = | $^3J_{HP}$ + $^4J_{HP}$ | = 9.6 Hz, $^2J_{HH}$= 13.4 Hz, $^3J_{HH}$= 8.0 Hz, $^3J_{HH}$= 4.1 Hz, 2H, NCH_2).

^{13}C{^{1}H} NMR (75.5 MHz, C_6D_6, [ppm]): δ = 24.2 (AXX'A', N = | $^1J_{CP}$ + $^3J_{CP}$ | = 11.3 Hz, PCH_2), 29.6 ($A_3XX'A'_3$, N = | $^2J_{CP}$ + $^4J_{CP}$ | = 1.4 Hz, PC(CH_3)$_3$), 29.7 ($A_3XX'A'_3$, N = | $^2J_{CP}$ + $^4J_{CP}$ | = 1.8 Hz, PC(CH_3)$_3$), 37.7 (AXX'A', N = |$^1J_{CP}$ + $^3J_{CP}$ | = 10.8 Hz, PC(CH$_3$)$_3$), 38.4 (AXX'A', N = |$^1J_{CP}$ + $^3J_{CP}$ | = 8.8 Hz, PC(CH$_3$)$_3$), 60.4 (s, NCH_3), 76.1 (AXX'A', N = |$^2J_{CP}$ + $^3J_{CP}$ | = 2.7 Hz, NCH_2).

^{31}P{^{1}H} NMR (121.5 MHz, C_6D_6, [ppm]): δ = 90.7 (s, P^tBu_2).

^{19}F{^{1}H} NMR (282.4 MHz, C_6D_6, [ppm]): δ = -77.6 (s, CF_3).

Elemental Analysis

$C_{22}H_{47}ClF_3N_2O_3P_2ReS$ *($C_6H_5CH_3$)$_{0.5}$ (%)   calcd: C, 37.98; H, 6.38; N, 3.47

Found: C, 37.54; H, 6.38; N, 3.55

3.2.6 [(PNP)Re(NEt)Cl)]OTf (16b-OTf)

Published procedure

9 (100 mg, 168 µmol, 1 eq) is dissolved in benzene (5-10 mL) and freshly distilled EtOTf (23 µL, 177 µmol, 1.05 eq) is added. The mixture is heated to 40°C for 18h under stirring before it is allowed to cool to room temperature. The solvent is removed i. vac. and the residue washed with pentanes (3 x 5 mL), followed by extraction with benzene (2 x 5 mL), filtration and lyophilization. Complex **16b-OTf** is obtained as green powder. Yield: 126 mg, 163 µmol, 97%, often contaminated with 3-6% of **12**, based on ^{31}P NMR integration.

Improved synthesis

9 (70.5 mg, 118 µmol, 1 eq) is dissolved in benzene (5-10 mL) and EtOTf (20 µL, 150 µmol, 1.2 eq) is added. The mixture is stirred at room temperature for 24 h, filtered and the volume reduced to about 2 mL under reduced pressure, before layering with diethylether (10 mL). After 1 d at room temperature, the solvent is filtered off and the residue washed with ether (2 x 4 mL). The pure product **16b-OTf** is lyophilized (benzene) and obtained as green powder (68 mg, 87.9 µmol, 78%).

Spectroscopic Characterization

^{1}H NMR (400 MHz, C$_6$D$_6$, [ppm]): δ = 1.02 (A$_9$XX′A′$_9$, N = | ^{3}J$_{HP}$ + ^{5}J$_{HP}$| = 7.0 Hz, 18H, PC(CH$_3$)$_3$), 1.07 (t, ^{3}J$_{HH}$ = 7.1 Hz, 3H, NCH$_2$C*H$_3$*), 1.16 (A$_9$XX′A′$_9$, N = | ^{3}J$_{HP}$ + ^{5}J$_{HP}$| = 7.2 Hz, 18H, PC(CH$_3$)$_3$), 2.14 (ABCDXX′D′C′B′A′, N = | ^{2}J$_{HP}$ + ^{4}J$_{HP}$ | = 3.9 Hz, ^{2}J$_{HH}$ = 15.1 Hz , ^{3}J$_{HH}$ = 8.0 Hz, ^{3}J$_{HH}$ = 7.5 Hz, 2H, PC*H$_2$*), 2.23 (ABCDXX′D′C′B′A′, N = | ^{2}J$_{HP}$ + ^{4}J$_{HP}$ | = 5.7 Hz, ^{2}J$_{HH}$ = 15.1 Hz , ^{3}J$_{HH}$ = 4.1 Hz, ^{3}J$_{HH}$ = 7.0 Hz, 2H, PC*H$_2$*), 2.90 (q, ^{3}J$_{HH}$ = 7.1 Hz, 2H, NC*H$_2$*CH$_3$), 3.90 (ABCDXX′D′C′B′A′, N = | ^{3}J$_{HP}$ + ^{4}J$_{HP}$ | = 3.3 Hz, ^{2}J$_{HH}$ = 14.6 Hz, ^{3}J$_{HH}$ = 7.0 Hz, ^{3}J$_{HH}$ = 7.5 Hz, 2H, NC*H$_2$*CH$_2$), 4.54 (ABCDXA'B'C'D'X′, N = | ^{3}J$_{HP}$ + ^{4}J$_{HP}$ | = 9.9 Hz, ^{2}J$_{HH}$ = 14.6 Hz, ^{3}J$_{HH}$ = 4.1 Hz, ^{3}J$_{HH}$ = 8.0 Hz, 2H, NC*H$_2$*CH$_2$).

^{13}C{^{1}H} NMR (100.6 MHz, C$_6$D$_6$, [ppm]): δ = 14.0 (s, NCH$_2$*C*H$_3$), 25.0 (AXX′A′, N = | ^{1}J$_{CP}$ + ^{3}J$_{CP}$ | = 11.3 Hz, P*C*H$_2$), 29.9 (A$_3$XX′A′$_3$, N = | ^{2}J$_{CP}$ + ^{4}J$_{CP}$ | = 1.9 Hz, PC(*C*H$_3$)$_3$), 30.0 (A$_3$XX′A′$_3$, N = | ^{2}J$_{CP}$ + ^{4}J$_{CP}$ | = 1.3 Hz, PC(*C*H$_3$)$_3$), 38.3 (AXX′A′, N = |^{1}J$_{CP}$ + ^{3}J$_{CP}$ | = 10.8 Hz, P*C*(CH$_3$)$_3$), 38.4 (AXX′A′, N = |^{1}J$_{CP}$ + ^{3}J$_{CP}$ | = 8.8 Hz, P*C*(CH$_3$)$_3$), 76.8 (AXX′A′, N = |^{2}J$_{CP}$ + ^{3}J$_{CP}$ | = 2.6 Hz, N*C*H$_2$CH$_2$), 67.6 (s, N*C*H$_2$CH$_3$).

^{31}P{^{1}H} NMR (162.0 MHz, C$_6$D$_6$, [ppm]): δ = 90.1 (s, P^{t}Bu$_2$).

^{19}F{^{1}H} NMR (376.5 MHz, C$_6$D$_6$, [ppm]): δ = -77.6 (s, C*F$_3$*).

Elemental Analysis

$C_{23}H_{48}ClF_3N_2O_3P_2ReS$ (%)

calcd.: C, 35.72; H, 6.26, N, 3.62

found: C, 35.96; H, 6.53; N, 3.52

3.2.7 [(PNP)Re(NBn)Cl)]OTf (16c-OTf)

AgOTf (8.2 mg, 31.9 µmol, 1.6 eq) is dissolved in Et_2O and cooled to -34°C before benzylbromide (ex.) is added. Immediate formation of a yellow precipitate indicates conversion to benzyl triflate. DTBMP (8.5 mg, 41.4 µmol, 2 eq) is added to the cold suspension and the mixture stirred for 5 min. The cold reaction is filtered to **9** (12.5 mg, 21 µmol, 1 eq) and stirred at room temperature for 15 h. The green precipitate is filtered off, washed with Et_2O until colourless, extracted with THF, overlaid with Et_2O and crystallized at -34°C. The product is filtered off and dried *in vac.* to give **16c-OTf** as a green microcrystalline solid. Yield: 10.5 mg, 12.6 µmol, 60%.

Spectroscopic Characterization

^1H NMR (300 MHz, C_6D_6, [ppm]): δ = 1.00 ($A_9XX'A'_9$, N = | $^3J_{HP}$ + $^5J_{HP}$| = 7.0 Hz, 18H, $PC(CH_3)_3$), 1.08 ($A_9XX'A'_9$, N = | $^3J_{HP}$ + $^5J_{HP}$| = 7.2 Hz, 18H, $PC(CH_3)_3$), 2.02 (m, 2H, PCH_2), 2.28 (m, 2H, PCH_2), 3.80 (m, 2H, NCH_2CH_2), 4.61 (s, 2H, NCH_2Ph), 4.70 (m, 2H, NCH_2CH_2), 7.00 (t, $^3J_{HH}$ = 7.4 Hz, 1H, NCH_2Ph), 7.13 (m, 2H, NCH_2Ph, partially superimposed), 7.49 (d, $^3J_{HH}$ = 7.2 Hz, 2H, NCH_2Ph).

$^{13}C\{^1H\}$ NMR (100.6 MHz, C_6D_6, [ppm]): δ = 24.3 ($AXX'A'$, N = | $^1J_{CP}$ + $^3J_{CP}$ | = 11.3 Hz, PCH_2), 29.5 ($A_3XX'A'_3$, N = | $^2J_{CP}$ + $^4J_{CP}$ | = 1.9 Hz, $PC(CH_3)_3$), 29.7 ($A_3XX'A'_3$, N = | $^2J_{CP}$ + $^4J_{CP}$ | = 1.4 Hz, $PC(CH_3)_3$), 37.8 ($AXX'A'$, N = |$^1J_{CP}$ + $^3J_{CP}$ | = 10.7 Hz, $PC(CH_3)_3$), 38.1 ($AXX'A'$, N = |$^1J_{CP}$ + $^3J_{CP}$ | = 8.7 Hz, $PC(CH_3)_3$), 75.0 (s, NCH_2Ph), 76.2 ($AXX'A'$, N = |$^2J_{CP}$ + $^3J_{CP}$ | = 2.7 Hz, NCH_2CH_2), 127.0 (s, NCH_2Ph), 129.1 (s, NCH_2Ph), 134.8 (s, NCH_2Ph).

$^{31}P\{^1H\}$ NMR (162.0 MHz, C_6D_6, [ppm]): δ = 90.3 (s, P^tBu_2).

$^{19}F\{^1H\}$ NMR (376.5 MHz, d_8-THF, [ppm]): δ = -79.0(s, CF_3).

Mass Spectrometry

LIFDI+   (toluene, m/z$^+$): 687.1 ($C_{27}H_{51}ClN_2P_2Re^+$).

3.2.8   [(PNP)Re(NTf)Cl]OTf (17-OTf)

9 (25.0 mg, 41.9 μmol, 1 eq) is dissolved in benzene (5 mL) and trifluoromethanesulfonic anhydride (7.1 μL, 42.0 μmol, 1 eq) is added. The yellow solution immediately turns green. The solvent is evaporated, the residue dissolved in chlorobenzene (3 mL) and overlaid with diethylether (10 mL). After 3 d, the crystalline material is filtered off, washed with diethylether (3 x 5 mL) and dried *in vac.* to yield green **17-OTf** (19.7 mg, 22.4 μmol, 54%).

Spectroscopic Characterization

^{1}H NMR   (400 MHz, d$_8$-THF, [ppm]): δ = 1.31 (A$_9$XX′A′$_9$, N = | ^{3}J$_{HP}$ + ^{5}J$_{HP}$ | = 7.6 Hz, 18H, PC(C*H$_3$*)$_3$), 1.58 (A$_9$XX′A′$_9$, N = | ^{3}J$_{HP}$ + ^{5}J$_{HP}$ | = 7.8 Hz, 18H, PC(C*H$_3$*)$_3$), 2.37 (ABCDXX′D′C′B′A′, N = | ^{2}J$_{HP}$ + ^{4}J$_{HP}$ | = 4.0 Hz, ^{2}J$_{HH}$ = 15.3 Hz, ^{3}J$_{HH}$ = 9.3 Hz, ^{3}J$_{HH}$ = 9.2 Hz, 2H, PC*H$_2$*), 3.28 (m, 2H, PC*H$_2$*), 4.71 (m, 2H, NC*H$_2$*), 5.31 (m, 2H, NC*H$_2$*).

^{13}C{^{1}H} NMR   (100.6 MHz, C$_6$D$_6$, [ppm]): δ = 23.5 (AXX′A′, N = | ^{1}J$_{CP}$ + ^{3}J$_{CP}$ | = 10.7 Hz, P*C*H$_2$), 30.0 (A$_3$XX′A′$_3$, N = | ^{2}J$_{CP}$ + ^{4}J$_{CP}$ | = 1.1 Hz, PC(*C*H$_3$)$_3$), 30.4 (A$_3$XX′A′$_3$, N = | ^{2}J$_{CP}$ + ^{4}J$_{CP}$ | = 1.0 Hz, PC(*C*H$_3$)$_3$), 38.1 (AXX′A′, N = |^{1}J$_{CP}$ + ^{3}J$_{CP}$ | = 7.9 Hz, P*C*(CH$_3$)$_3$), 42.7 (AXX′A′, N = |^{1}J$_{CP}$ + ^{3}J$_{CP}$ | = 10.0 Hz, P*C*(CH$_3$)$_3$), 87.1 (s, N*C*H$_2$), 121.9 (q, ^{1}J$_{CF}$ = 321.2 Hz, *Tf*), 122.6 (q, ^{1}J$_{CF}$ = 322.4 Hz, *Tf*).

^{31}P{^{1}H} NMR   (162.0 MHz, d$_8$-THF, [ppm]): δ = 102.4 (s, *P*tBu$_2$).

^{19}F{^{1}H} NMR   (376.5 MHz, d$_8$-THF, [ppm]): δ = -78.9 (s, O*Tf*), -75.7 (s, N*Tf*).

Mass Spectrometry

LIFDI+   (toluene, m/z$^+$): 729.1 ($C_{21}H_{44}ClF_3N_2O_2P_2ReS^+$).

3.2.9   Reduction of 9

9 (5.0 mg, 8.4 μmol, 1 eq), KC_8 (2.8 mg, 21.0 μmol, 2.5 eq) and 18-crown-6 (4.5 mg, 16.8 μmol, 2 eq) are suspended in either C_6D_6 or THF (0.5 mL) and stirred at room temperature for 3 d. Formation of two main products and isobutene is observed by NMR spectroscopy.

^{31}P{^{1}H} NMR (121.5 MHz, C_6D_6, [ppm]): δ = 31.3 (d, J = 103.2 Hz, 45%), 107.5 (s, 9%), 113.1 (d, J = 103.2 Hz, 46%).

3.3   Reactivity of the Imido complexes

3.3.1   (PNP)Re(NCH$_2$)Cl (18a)

16a-OTf (50.0 mg, 65.7 μmol, 1 eq) and KBTSA (13.1 mg, 65.7 μmol, 1 eq) are dissolved in THF (5 mL) and stirred for 1h at room temperature. The solvent is evaporated and the residue extracted with pentanes (4 x 5 mL). After evaporation of the solvent, the product **18a** is lyophilized (benzene) and obtained as brick red powder. Yield: 20.2 mg, 33.1 μmol, 50%.

Spectroscopic Characterization

^{1}H NMR   (300 MHz, C_6D_6), [ppm]): δ = 1.27 (A$_9$XX′A′$_9$, N = | ^{3}J$_{HP}$ + ^{5}J$_{HP}$ | = 6.2 Hz, 18H, PC(C*H$_3$*)$_3$), 1.33 (A$_9$XX′A′$_9$, N = | ^{3}J$_{HP}$ + ^{5}J$_{HP}$ | = 5.9 Hz, 18H, PC(C*H$_3$*)$_3$), 1.60 (ABCDXX′D′C′B′A′, N = | ^{2}J$_{HP}$ + ^{4}J$_{HP}$ | = 3.6 Hz, ^{2}J$_{HH}$ = 13.9 Hz, ^{3}J$_{HH}$ = 7.1 Hz, ^{3}J$_{HH}$ = 7.1 Hz, 2H, PC*H$_2$*), 1.80 (ABCDXX′D′C′B′A′, N = | ^{2}J$_{HP}$ + ^{4}J$_{HP}$ | = 3.8 Hz, ^{2}J$_{HH}$ = 13.9 Hz, ^{3}J$_{HH}$ = 6.5 Hz, ^{3}J$_{HH}$ = 6.5 Hz, 2H, PC*H$_2$*), 2.16 (dt, ^{2}J$_{HH}$ = 4.8 Hz, ^{4}J$_{HP}$ = 2.4 Hz, 1H, N=C*H$_2$*), 3.41 (m, 4H, NC*H$_2$*CH$_2$, superimposed), 3.79 (dt, ^{2}J$_{HH}$ = 4.8 Hz, ^{4}J$_{HP}$ = 2.4 Hz, 1H, N=C*H$_2$*).

^{13}C{^{1}H} NMR (75.5 MHz, C_6D_6, [ppm]): δ = 27.7 (AXX′A′, N = | ^{1}J$_{CP}$ + ^{3}J$_{CP}$ | = 8.1 Hz, PC*H$_2$*), 30.8 (A$_3$XX′A′$_3$, N = | ^{2}J$_{CP}$ + ^{4}J$_{CP}$ | = 2.3 Hz, PC(C*H$_3$*)$_3$), 30.3 (A$_3$XX′A′$_3$, N = | ^{2}J$_{CP}$ + ^{4}J$_{CP}$ | = 2.1 Hz, PC(C*H$_3$*)$_3$), 38.6 (AXX′A′, N = |^{1}J$_{CP}$ + ^{3}J$_{CP}$ | = 6.9 Hz, P*C*(CH$_3$)$_3$), 39.5 (AXX′A′, N = |^{1}J$_{CP}$ + ^{3}J$_{CP}$ | = 8.3 Hz,

$PC(CH_3)_3$),74.2 (AXX′A′, N = $|^2J_{CP} + ^3J_{CP}|$ = 4.5 Hz, NCH_2CH_2), 137.8 (t, $^3J_{PC}$ = 2.4 Hz, N=CH_2).

$^{31}P\{^1H\}$ NMR (121.5 MHz, C_6D_6, [ppm]): δ = 55.0 (s, P^tBu_2).

Elemental Analysis

$C_{21}H_{46}ClN_2P_2Re$ (%)   calcd.:   C, 41.33; H, 7.60; N, 4.49
                              found: C, 42.10; H, 7.40; N, 4.36

3.3.2   [(PNP)Re(NCHCH₃)Cl)] (18b)

Published procedure
EtOTf (23 μL, 177 μmol, 1.05 eq) is added to a solution of **9** (100 mg, 168 μmol, 1 eq) in benzene (5-10 mL). The mixture is stirred at room temperature for 24 h. The solvent and residual EtOTf are removed by evaporation under reduced pressure and the residue is redissolved in benzene (5-10 mL). After deprotonation with KBTSA (33.5 mg, 168 μmol, 1 eq) and stirring for 2 h at room temperature the reaction mixture is filtered and the solvent removed *i. vac.* Extraction with pentane (4 x 3-5 mL), filtration and solvent evaporation gives a crude product with spectroscopic purity >95% and small amounts of parent **9** which is sufficient for most purposes. Full conversion is achieved by treatment of the crude product with additional EtOTf and work-up as described above. After final lyophilization from benzene analytically pure, red-brown **18b** is obtained (84.4 mg, 135 μmol, 81%). Spectroscopic Characterization reveals the formation of two stereoisomers in about 60:40 ratio. The ^{15}N-enriched sample was synthesized starting from **9**, prepared with 1-^{15}N-azide.

Improved synthesis
Synthetis of the imido complex **16b-OTf** is carried out as described earlier. After reaction with EtOTf, the solvent is reduced to 2-5 mL and layered with diethylether (10 mL). Crystallization leads to pure compound **16b-OTf** which can be filtered off and used for deprotonation with KBTSA to yield pure **18b**.

Spectroscopic Characterization

^1H NMR   (300 MHz, C_6D_6, [ppm]): δ = 1.25 ($A_9XX′A′_9$, N = $|^3J_{HP} + ^5J_{HP}|$ = 6.2 Hz, 18H, PC(CH_3)₃ isomer 2), 1.28 (m, 36H, PC(CH_3)₃ isomer 1), 1.34 ($A_9XX′A′_9$, N = $|^3J_{HP} + ^5J_{HP}|$ = 6.0 Hz, 18H, PC(CH_3)₃ isomer 2), 1.52 (m, 2H, PCH_2CH₂ isomer 1), 1.62 (m, 2H, PCH_2CH₂ isomer 2), 1.80 (m, 2H,

PCH_2 isomer 2), 1.90 (m, 2H, PCH_2 isomer 1), 2.43 (dt, $^3J_{HH}$ = 5.1 Hz, $^5J_{HP}$ = 1.3 Hz, 3H, NCHCH_3 isomer 1), 2.43 (m, 1H, NCHCH$_3$ isomer 2), 3.18 (dt, $^3J_{HH}$ = 5.3 Hz, $^5J_{HP}$ = 1.3 Hz , 3H, NCHCH_3 isomer 2), 3.40 (m, 2H, NCH_2 isomer 2), 3.50 (m, 6H, NCH_2 isomers 1+2), 4.21 (qt, $^4J_{HP}$ = 2.7 Hz, $^3J_{HH}$ = 5.1 Hz, 1H, NCHCH$_3$ isomer 1).

^{13}C{^{1}H} NMR (100.6 MHz, C$_6$D$_6$, [ppm]): δ = 11.9 (s, NCHCH_3 isomer 2), 13.2 (s, NCHCH_3 isomer 2), 28.3 (AXX′A′, N = |$^1J_{CP}$ + $^3J_{CP}$| = 8.0 Hz, PCH_2CH$_2$ isomer 2), 29.7 (AXX′A′, N = |$^1J_{CP}$ + $^3J_{CP}$| = 7.5 Hz, PCH_2CH$_2$ isomer 1), 30.7 (m, PC(CH$_3$)$_3$), 30.9 (A$_3$XX′A′$_3$, N = |$^2J_{CP}$ + $^4J_{CP}$| = 2.5 Hz, PC(CH$_3$)$_3$), 31.0 (A$_3$XX′A′$_3$, N = |$^2J_{CP}$ + $^4J_{CP}$| = 2.5 Hz, PC(CH$_3$)$_3$), 36.6 (AXX′A′, N = |$^1J_{CP}$ + $^3J_{CP}$| = 6.4 Hz, PC(CH$_3$)$_3$), 37.4 (AXX′A′, N = |$^1J_{CP}$ + $^3J_{CP}$| = 6.7 Hz, PC(CH$_3$)$_3$), 39.7 (AXX′A′, N = |$^1J_{CP}$ + $^3J_{CP}$| = 8.8 Hz, PC(CH$_3$)$_3$), 40.1 (AXX′A′, N = |$^1J_{CP}$ + $^3J_{CP}$| = 8.2 Hz, PC(CH$_3$)$_3$), 74.6 (AXX′A′, N = |$^2J_{CP}$ + $^3J_{CP}$| = 4.4 Hz, NCH_2 isomer 2), 75.5 (AXX′A′, N = |$^2J_{CP}$ + $^3J_{CP}$| = 4.3 Hz, NCH_2 isomer 1), 143.6 (, t, $^3J_{CP}$ =2.6 Hz, NCHCH$_3$ isomer 1), 147.3 (t, $^3J_{CP}$ = 2.4 Hz, NCHCH$_3$ isomer 2).

^{31}P{^{1}H} NMR (162.0 MHz, C$_6$D$_6$, [ppm]): δ = 51.66 (s, PtBu$_2$ isomer 2), 51.74 (s, PtBu$_2$ isomer 1).

^{15}N{^{1}H} NMR (50.7 MHz, C$_6$D$_6$, [ppm]): δ = 7.8 (t, $^2J_{NP}$ = 2.3 Hz, ReNCHMe), 11.1 (t, $^2J_{NP}$ = 2.0 Hz, ReNCHMe).

IR (KBr, cm^{-1}): 1594 (w, υ(C=^{14}N)), 1572 (w, υ(C=^{15}N)).

Elemental Analysis

C$_{22}$H$_{48}$ClN$_2$P$_2$Re (624.24)   calcd: C, 42.33; H, 7.75; N, 4.49
found: C, 42.90; H, 8.02; N, 4.34

3.3.3   [(PNP)Re(NCHPh)Cl)] (18c)

16c-OTf (8.8 mg, 10.5 µmol, 1 eq) and KO^{t}Bu (1.2 mg, 10.5 µmol, 1 eq) are suspended in benzene (2 mL) and stirred for 2 h at room temperature before the solvent is evaporated and the residue extracted with pentanes (3 x 2 mL). After lyophilization (benzene) the product **18c** is obtained as red powder. Yield: 4.5 mg, 6.6 µmol, 63%.

Spectroscopic Characterization

As for **18b**, two isomers are observed for **18c**. An assignment of all signals to distinct isomers was not possible.

¹H NMR   (400 MHz, C_6D_6, [ppm]): δ = 1.16 ($A_9XX'A'_9$, N = $|^3J_{HP} + {}^5J_{HP}|$ = 6.3 Hz, 18H, $PC(CH_3)_3$), 1.18 ($A_9XX'A'_9$, N = $|^3J_{HP} + {}^5J_{HP}|$ = 6.5 Hz, 18H, $PC(CH_3)_3$), 1.24 ($A_9XX'A'_9$, N = $|^3J_{HP} + {}^5J_{HP}|$ = 6.0 Hz, 18H, $PC(CH_3)_3$), 1.29 ($A_9XX'A'_9$, N = $|^3J_{HP} + {}^5J_{HP}|$ = 6.2 Hz, 18H, $PC(CH_3)_3$), 1.65 (m, 4H, PCH_2, isomer 1+2), 1.80 (m, 2H, PCH_2), 1.95 (m, 2H, PCH_2), 3.42 (m, 4H, NCH_2CH_2, isomer 1), 3.54 (ABCDXX'D'C'B'A', N = $|{}^3J_{HP} + {}^4J_{HP}|$ = 1.7 Hz, $^2J_{HH}$ = 13.1 Hz, $^3J_{HH}$ = 9.3 Hz, $^3J_{HH}$ = 6.3 Hz, 2H, NCH_2CH_2, isomer 2), 3.75 (t, $^4J_{HP}$ = 2.0 Hz, 1H, N=CHPh), 3.78 (m, 2H, NCH_2CH_2, isomer 2, partially superimposed), 5.47 (t, $^4J_{HP}$ = 2.2 Hz, 1H, N=CHPh), 6.47 (br, 2H, N=CHPh), 6.65 (tt, $^3J_{HH}$ = 7.3 Hz, $^4J_{HH}$ = 1.2 Hz, 1H, N=CHPh-*para*), 6.73 (tt, $^3J_{HH}$ = 7.2 Hz, $^4J_{HH}$ = 1.4 Hz, 1H, N=CHPh-*para*), 7.18 (m, 2H, N=CHPh, superimposed by benzene), 7.35 (m, 2H, N=CHPh), 4.44 (m, 2H, N=CHPh).

¹³C{¹H} NMR (100.6 MHz, C_6D_6, [ppm]): δ = 27.4 (AXX'A', N = $|^1J_{CP} + {}^3J_{CP}|$ = 8.3 Hz, PCH_2CH_2), 29.6 (AXX'A', N = $|^1J_{CP} + {}^3J_{CP}|$ = 7.9 Hz, PCH_2CH_2), 30.3 (m, PC$(CH_3)_3$), 30.5 (m, PC$(CH_3)_3$), 36.5 (AXX'A', N = $|^1J_{CP} + {}^3J_{CP}|$ = 7.0 Hz, P$C(CH_3)_3$), 37.2 (AXX'A', N = $|^1J_{CP} + {}^3J_{CP}|$ = 7.0 Hz, P$C(CH_3)_3$), 38.7 (AXX'A', N = $|^1J_{CP} + {}^3J_{CP}|$ = 8.9 Hz, P$C(CH_3)_3$), 39.2 (AXX'A', N = $|^1J_{CP} + {}^3J_{CP}|$ = 8.5 Hz, P$C(CH_3)_3$), 74.0 (AXX'A', N = $|^2J_{CP} + {}^3J_{CP}|$ = 4.4 Hz, NCH_2CH_2), 75.0 (AXX'A', N = $|^2J_{CP} + {}^3J_{CP}|$ = 4.1 Hz, NCH_2CH_2), 124.2 (s, Ph), 124.8 (s, Ph), 127.5 – 129.0 (Ph, superimposed by benzene), 132.3 (s, Ph), 132.8 (s, Ph), 146.8 (t, $^3J_{CP}$ = 2.4 Hz, N=CHPh), 150.6 (t, $^3J_{CP}$ = 2.3 Hz, N=CHPh).

³¹P{¹H} NMR (162.0 MHz, C_6D_6, [ppm]): δ = 54.8 (s, PtBu$_2$), 56.5 (s, PtBu$_2$).

3.3.4   Reaction of 16b-OTf with excess CNtBu (20)

16b-OTf (5.0 mg, 6.5 μmol, 1 eq) is dissolved in C_6D_6 (0.5 mL) and CN^{t}Bu (2.0 μL, 20.0 μmol, 3 eq) is added. The reaction is stirred for 2 d at room temperature. ¹H and ³¹P-NMR spectra show conversion to **20** in about 85% yield.

3.3.5   Reaction of 16b-OTf with stoichiometric CNtBu (21)

16b-OTf (25.0 mg, 32.3 μmol, 1 eq) is dissolved in benzene (3 mL) and CNtBu (3.4 μL, 32.3 μmol, 1 eq) is added. The mixture is stirred for 45 min accompanied by the formation of a blue precipitate. The solvent is removed i. vac. and the residue

extracted with THF (2 x 3 mL), concentrated and layered with pentanes. After crystallization at -34°C the product **21** is filtered off, washed with pentane and obtained as blue microcrystalline solid. Yield: 11.0 mg, 15.6 µmol, 48%.

Spectroscopic Characterization

^{1}H NMR   (400 MHz, d$_8$-THF, [ppm]): δ = 0.0 (m, 1H, N=CHCH$_3$), 1.36 (A$_9$XX′A′$_9$, N = $|^3J_{HP} + {}^5J_{HP}|$ = 6.3 Hz, 18H, PC(CH_3)$_3$), 1.49 (A$_9$XX′A′$_9$, N = $|^3J_{HP} + {}^5J_{HP}|$ = 6.6 Hz, 18H, PC(CH_3)$_3$), 1.53 (s, 9H, NC(CH_3)$_3$), 2.14 (ABCDXX′D′C′B′A′, N = $|{}^2J_{HP} + {}^4J_{HP}|$ = 2.7 Hz, $^2J_{HH}$ = 15.3 Hz, $^3J_{HH}$ = 12.0 Hz, $^3J_{HH}$ = 6.7 Hz, 2H, PCH_2), 2.33 (ABCDXX′D′C′B′A′, N = $|{}^2J_{HP} + {}^4J_{HP}|$ = 5.0 Hz, $^2J_{HH}$ = 15.3 Hz, $^3J_{HH}$ = 5.8 Hz, $^3J_{HH}$ = 2.5 Hz, 2H, PCH_2), 3.08 (m, 2H, NCH_2CH$_2$), 3.78 (m, 2H, NCH_2CH$_2$), 3.90 (d, $^3J_{HH}$ = 6.0 Hz, 3H, N=CHCH_3), 6.06 (br, 1H, HPNP).

^{13}C{^{1}H} NMR (100.6 MHz, d$_8$-THF, [ppm]): δ = -1.5 (s, N=CHCH$_3$), 24.3 (PCH$_2$, superimposed by THF), 29.8 (s, NC(CH$_3$)$_3$), 30.3 (br, PC(CH$_3$)$_3$), 31.7 (A$_3$XX′A′$_3$, N = $|{}^2J_{CP} + {}^4J_{CP}|$ = 2.2 Hz, PC(CH$_3$)$_3$), 37.3 (AXX′A′, N = $|{}^1J_{CP} + {}^3J_{CP}|$ = 8.9 Hz, PC(CH$_3$)$_3$), 40.2 (AXX′A′, N = $|{}^1J_{CP} + {}^3J_{CP}|$ = 7.2 Hz, PC(CH$_3$)$_3$), 56.1 (AXX′A′, N = $|{}^2J_{CP} + {}^3J_{CP}|$ =2.3 Hz, NCH$_2$CH$_2$), 57.9 (s, NC(CH$_3$)), 136.9 (s, N=CHCH$_3$).

^{31}P{^{1}H} NMR (162.0 MHz, d$_8$-THF, [ppm]): δ = 33.6 (s, P^{t}Bu$_2$).

Elemental Analysis

C$_{27}$H$_{57}$ClN$_3$P$_2$Re (707.38)   calcd: C, 39.22; H, 6.82; N, 4.90
                                         found: C, 39.74; H, 7.31; N, 4.83

3.3.6   (PNP)Re(NCH$_2$)(CH$_3$) (25)

16a-OTf (50.0 mg, 65.7 µmol, 1 eq) is dissolved in THF (10 mL) and MeMgCl (44 µL, 3M in THF, 132 µmol, 2.0 eq) is added. The mixture is stirred at room temperature for 18 h before the solvent is evaporated and the residue extracted with pentanes (5 x 10 mL). After evaporation of the solvent, the residue is again extracted with pentanes (3 x 5 mL) and lyophilized out of benzene. Yield: 31.2 mg, 52.9 µmol, 81%.

Spectroscopic Characterization

^{1}H NMR   (300 MHz, d$_8$-THF, [ppm]): δ = 1.22 (A$_9$XX′A′$_9$, N = $|^3J_{HP} + {}^5J_{HP}|$ = 5.8 Hz, 18H, PC(CH_3)$_3$), 1.33 (A$_9$XX′A′$_9$, N = $|^3J_{HP} + {}^5J_{HP}|$ = 5.8 Hz, 18H,

PC(CH_3)$_3$), 1.90 (m, 2H, PCH_2), 2.19 (m, 2H, PCH_2, superimposed), 2.21 (t, $^3J_{HP}$ = 4.2 Hz, 3H, ReCH_3, superimposed), 2.27 (m, $^2J_{HH}$ = 6.4 Hz, 1H, N=CH_2), 3.10 (m, 2H, NCH_2CH$_2$), 3.25 (m, 2H, NCH_2CH$_2$), 3.47 (m, $^2J_{HH}$ = 6.4 Hz, 1H, N=CH_2).

^{13}C{^{1}H} NMR (100.6 MHz, d$_8$-THF, [ppm]): δ = -10.1 (t, $^2J_{CP}$ = 2.5 Hz, ReCH$_3$), 28.0 (AXX′A′, N = |$^1J_{CP}$ + $^3J_{CP}$| = 7.7 Hz, PCH$_2$), 30.5 (A$_3$XX′A′$_3$, N = |$^2J_{CP}$ + $^4J_{CP}$| = 2.5 Hz, PC(CH$_3$)$_3$), 31.3 (A$_3$XX′A′$_3$, N = |$^2J_{CP}$ + $^4J_{CP}$| = 2.1 Hz, PC(CH$_3$)$_3$), 38.5 (AXX′A′, N = |$^1J_{CP}$ + $^3J_{CP}$| = 5.8 Hz, PC(CH$_3$)$_3$), 41.0 (AXX′A′, N = |$^1J_{CP}$ + $^3J_{CP}$| = 7.9 Hz, PC(CH$_3$)$_3$), 70.1 (AXX′A′, N = |$^2J_{CP}$ + $^3J_{CP}$| = 5.3 Hz, NCH$_2$CH$_2$), 127.7 (t, $^3J_{CP}$ = 2.2 Hz, N=CH$_2$).

^{31}P{^{1}H} NMR (162.0 MHz, d$_8$-THF, [ppm]): δ = 54.9 (s, P^tBu$_2$).

Elemental Analysis

C$_{22}$H$_{49}$N$_2$P$_2$Re (589.80) calcd: C, 44.80; H, 8.37; N, 4.75
found: C, 46.07; H, 8.67; N, 4.48

3.3.7   Deprotonation of 16a-OTf using PhMgBr

16a-OTf (5.0 mg, 6.6 μmol, 1 eq) is dissolved in C$_6$D$_6$ (0.5 mL) and phenyl magnesium bromide (1 M in THF, 6.6 μL, 6.6 μmol, 1 eq) is added. The solution is stirred for 1 h before another equivalent of PhMgBr is added and the mixture again stirred for 1 h. The solvent is evaporated and the residue extracted with pentanes (4 x 0.3 mL).

^{1}H NMR (300 MHz, C$_6$D$_6$, [ppm]): δ = 1.30 (m, 18H, PC(CH_3)$_3$, superimposed), 1.32 (m, 18H, PC(CH_3)$_3$, superimposed), 1.56 (m, 1H, N=CH_2, superimposed), 1.59 (m, 2H, PCH_2, superimposed), 1.84 (m, 2H, PCH_2), 3.20 (m, $^2J_{HH}$ = 4.1 Hz, 1H, N=CH_2), 3.40 (m, 4H, NCH_2).

^{31}P{^{1}H} NMR (162.0 MHz, C$_6$D$_6$, [ppm]): δ = 52.5 (s, P^tBu$_2$).

3.3.8   (PNP)Re(NCHR)(H) (26)

*Via 2e$^-$ reduction of **16**:*
THF (0.5 mL) is added to a mixture of **16a-OTf** (5.0 mg, 6.6 μmol, 1 eq) and KC$_8$ (2.2 mg, 16.2 μmol, 2.5 eq) and the reaction is stirred for 1 h at room temperature. The

suspension is filtered, the solvent evaporated and the residue dissolved in C_6D_6. NMR spectra show the formation of **26a** in 95% spectroscopic yield.

For **26b** the reaction is carried out similarly with a spectroscopic yield of 60%.

Via double deprotonation of **16** *under H_2 atmosphere:*

C_6H_6 (0.5 mL) is added to **16b-OTf** (5.4 mg, 7.0 μmol, 1 eq) and KO^{t}Bu (2.0 mg, 17.8 μmol, 2.5 eq) and the atmosphere is exchanged for H_2 (1.5 bar). The mixture is heated to 70°C for 15 h and stirred at room temperature for another 3 d. ^{31}P-NMR spectra show clean formation of **26b**.

Via Hydrogenation of **25**:

25a (5.0 mg, 8.5 μmol) is dissolved in d$_8$-THF, degassed and pressurized with H_2 (1 bar). After heating to 70°C for 15 h, complete conversion of **26a** is observed in the NMR spectra, together with the formation of methane (^{1}H-NMR: 0.18 ppm).

For **26b** the reaction is carried out similarly.

***Spectroscopic Characterization of* 26a**:

^{1}H NMR 	(300 MHz, C_6D_6, [ppm]): δ = -3.81 (t, $^2J_{HP}$ = 11.6 Hz, 1H, Re*H*), 1.29 ($A_9XX'A'_9$, N = $|^3J_{HP} + {}^5J_{HP}|$ = 6.0 Hz, 18H, PC(C*H₃*)₃), 1.36 ($A_9XX'A'_9$, N = $|^3J_{HP} + {}^5J_{HP}|$ = 6.1 Hz, 18H, PC(C*H₃*)₃), 1.76 (m, 4H, PC*H₂*), 2.12 (dt, $^4J_{HP}$ = 2.5 Hz, $^2J_{HH}$ = 4.7 Hz, 1H, N=C*H₂*), 2.96 (m, 2H, NC*H₂*CH₂), 3.17 (m, 2H, NC*H₂*CH₂), 3.38 (dt, $^4J_{HP}$ = 2.4 Hz, $^2J_{HH}$ = 4.6 Hz, 1H, N=C*H₂*).

^{13}C{^{1}H} NMR 	(75.5 MHz, d$_8$-THF, [ppm]): δ = 27.6 (AXX'A', N = $|^1J_{CP} + {}^3J_{CP}|$ = 7.4 Hz, P*C*H₂), 29.6 ($A_3XX'A'_3$, N = $|^2J_{CP} + {}^4J_{CP}|$ = 3.0 Hz, PC(*C*H₃)₃), 30.6 ($A_3XX'A'_3$, N = $|^2J_{CP} + {}^4J_{CP}|$ = 2.7 Hz, PC(*C*H₃)₃), 37.9 (AXX'A', N = $|^1J_{CP} + {}^3J_{CP}|$ = 8.4 Hz, P*C*(CH₃)₃), 41.0 (AXX'A', N = $|^1J_{CP} + {}^3J_{CP}|$ = 7.0 Hz, P*C*(CH₃)₃), 72.1 (AXX'A', N = $|^2J_{CP} + {}^3J_{CP}|$ = 6.6 Hz, N*C*H₂CH₂), 126.1 (t, $^3J_{CP}$ = 2.0 Hz, N=*C*H₂).

^{31}P{^{1}H} NMR 	(162.0 MHz, C_6D_6, [ppm]): δ = 79.1 (s, *P*^{t}Bu₂).

***Spectroscopic Characterization of* 26b**:

^{1}H NMR 	(300 MHz, C_6D_6, [ppm]): δ = -4.25 (t, $^2J_{HP}$ = 12.0 Hz, 1H, Re*H*, isomer 1), -3.91 (t, $^2J_{HP}$ = 11.7 Hz, 1H, Re*H*, isomer 2), 1.24 ($A_9XX'A'_9$, N = $|^3J_{HP} + {}^5J_{HP}|$ = 5.9 Hz, 18H, PC(C*H₃*)₃, isomer 2), 1.31 ($A_9XX'A'_9$, N = $|^3J_{HP} + {}^5J_{HP}|$

= 5.7 Hz, 18H, PC(CH_3)$_3$, isomer 1), 1.35 (m, PC(CH_3)$_3$, isomer 1, superimposed), 1.36 (A$_9$XX′A′$_9$, N = |$^3J_{HP}$ + $^5J_{HP}$| = 6.1 Hz, 18H, PC(CH_3)$_3$, isomer 2), 1.76 (m, 4H, PCH_2, isomer 1+2), 2.23 (qt, $^4J_{HP}$ = 2.7 Hz, $^3J_{HH}$ = 5.0 Hz, 1H, N=CHCH$_3$ isomer 2), 2.83 (dt, $^3J_{HH}$ = 5.0 Hz, $^5J_{HP}$ = 1.1 Hz, 3H, N=CHCH_3 isomer 2), 2.90 (dt, $^3J_{HH}$ = 5.3 Hz, $^5J_{HP}$ = 1.0 Hz, 3H, N=CHCH_3 isomer 1), 3.00 (m, 2H, NCH_2CH$_2$, isomer 1+2), 3.21 (m, 2H, NCH_2CH$_2$, isomer 1+2), 3.44 (m, $^3J_{HH}$ = 5.3 Hz, 1H, N=CHCH$_3$, isomer 1).

^{31}P{^{1}H} NMR (121.5 MHz, C$_6$D$_6$, [ppm]): δ = 79.3 (s, PtBu$_2$, isomer 2)., 75.0 (s, PtBu$_2$, isomer 1).

3.3.9   Reaction of 16a with H$_2$ to 27a

27a-OTf:

16a-OTf (5.0 mg, 6.6 µmol, 1 eq) and MeOTf (cat.) are dissolved in C$_6$D$_6$, before the atmosphere is exchanged for H$_2$ gas (1 bar). Without MeOTf no reaction is observed. The mixture is heated to 80°C for 3 d to give clean conversion to **27a-OTf.** The solvent is evaporated and the residue washed with pentanes.

Spectroscopic Characterization

^{1}H NMR (300 MHz, C$_6$D$_6$, [ppm]): δ = 1.13 (s, 3H, NCH_3), 1.22 (A$_9$XX′A′$_9$, N = |$^3J_{HP}$ + $^5J_{HP}$| = 6.8 Hz, 18H, PC(CH_3)$_3$), 1.35 (A$_9$XX′A′$_9$, N = |$^3J_{HP}$ + $^5J_{HP}$| = 6.8 Hz, 18H, PC(CH_3)$_3$), 1.63 (m, 2H, PCH_2), 2.32 (m, 4H, PCH_2, NCH_2, superimposed), 3.08 (m, 2H, NCH_2, partially superimposed), 3.16 (t, ReH, partiall superimposed), 4.76 (br, 1H, HPNP).

^{31}P{^{1}H} NMR (121.5 MHz, C$_6$D$_6$, [ppm]): δ = 66.7 (s, PtBu$_2$).

27a-Cl:

16a-Cl, prepared *in situ* from **18a** and HCl (2 M in Et$_2$O), is dissolved in THF and heated to 65°C under an atmosphere of H$_2$ (1 bar) for 18 h. The solvent is evaporated and the residue washed with pentanes and benzene. The spectroscopically pure blue residue **27a-Cl** is dried *in vac.* and dissolved in CD$_2$Cl$_2$.

Spectroscopic Characterization

^{1}H NMR (300 MHz, CD$_2$Cl$_2$, [ppm]): δ = 1.53 (A$_9$XX′A′$_9$, N = |$^3J_{HP}$ + $^5J_{HP}$| = 6.9 Hz, 18H, PC(CH_3)$_3$), 1.65 (A$_9$XX′A′$_9$, N = |$^3J_{HP}$ + $^5J_{HP}$| = 6.9 Hz, 18H,

PC(CH_3)$_3$), 2.10 (s, 3H, NCH_3), 2.21 (m, 2H, PCH_2), 2.47 (m, 4H, PCH_2, NCH_2, superimposed), 3.03 (m, 2H, NCH_2), 3.57 (t, $^2J_{HP}$ = 18.2 Hz, 1H, ReH).

^{31}P{^{1}H} NMR (121.5 MHz, CD$_2$Cl$_2$, [ppm]): δ = 67.6 (s, P^tBu_2).

3.3.10 Hydrogenation of 28

Freshly prepared **28b** (ca. 7 μmol) in CD$_2$Cl$_2$ solution (0.5 mL), still containing traces of acid, is pressurized with H$_2$ (1.5 bar). The color of the solution changes within 5-10 min from green to rose. ^{31}P-NMR spectra display conversion into a single compound in 93% yield. ^{1}H-NMR spectra are due to residual solvent and signal overlap not significant. No signals below 0 ppm in the ^{1}H-NMR spectra are detected.

^{31}P{^{1}H} NMR (121.5 MHz, CD$_2$Cl$_2$, [ppm]): δ = 77.8 (s, P^tBu_2).

3.4 Reactivity of ketimido complexes

3.4.1 Protonation to imido complexes (16 and 28)

Azavinylidene complexes **18** and **26** can be quantitatively (spectroscopically) protonated back to the respective imido complexes by dissolving the complex in benzene, Et$_2$O or DCM and adding 1 eq of acid (HOTf, HBAr$^F_4$ or NH$_4$PF$_6$). Excess of a strong acid leads to degradation of the complexes.

Spectroscopic Characterization for 28b-BAr$^F_4$

^{1}H NMR (300 MHz, CD$_2$Cl$_2$, [ppm]): δ = -6.18 (t, $^2J_{HP}$ = 14.3 Hz, 1H, ReH), 1.28 (t, $^3J_{HH}$ = 7.1 Hz, 3H, NCH$_2$CH_3), 1.42 (m, 36H, PC(CH_3)$_3$), 2.34 (m, 4H, PCH_2), 2.52 (m, 2H, NCH_2CH$_3$), 3.15 (m, 2H, NCH_2), 3.39 (m, 2H, NCH_2), 7.57 (s, 4H, BAr^F_4), 7.73 (s, 8H, BAr^F_4).

^{31}P{^{1}H} NMR (121.5 MHz, CD$_2$Cl$_2$, [ppm]): δ = 96.5 (s, P^tBu_2).

3.4.2 Release of NCMe upon treatment with isonitriles (Synthesis of 20)

CN^{t}Bu (2.5 μL, 24 μmol, 3 eq) is added to a solution of **18b** (5.0 mg, 8.0 μmol, 1 eq) in C$_6$D$_6$ (0.5 mL) and the mixture is stirred for 10 d at room temperature. Heating (2 d, 60°C) leads to partial degradation. Spectroscopic yield to **20** is about 85% based on NMR spectra. The solvent is evaporated and the green residue washed with pentanes until colorless and dried in vacuo.

3.4.3 Release of NCMe upon deprotonation of 18b (Synthesis of 19)

18b (30.0 mg, 48.1 μmol, 1 eq), KBTSA (9.6 mg, 48.1 μmol, 1 eq) and CN^{t}Bu (11 μL, 105 μmol, 2.2 eq) are dissolved in THF (5 mL) at room temperature. The solution immediately turns bright orange and the ^{1}H-NMR spectrum shows clean formation of **19** under release of acetonitrile. After evaporation of the solvent under reduced pressure, the product is extracted with pentanes and the solvent removed *in vacuo.* Lyophilization from benzene yields the **19** as orange powder (33.0 mg, 46.3 μmol, 96%).

Spectroscopic Characterization

^{1}H NMR
(400 MHz, C$_6$D$_6$, [ppm]): δ = 1.42 (A$_{18}$XX′A′$_{18}$ = N = $|^3J_{HP}$ + $^5J_{HP}|$ = 5.9 Hz, 36H, PC(C*H$_3$*)$_3$), 1.43 (s, 18H, CNC(C*H$_3$*)$_3$), 1.96 (A$_2$B$_2$XX′B′$_2$A′$_2$, N = $|^2J_{HP}$ + $^4J_{HP}|$ = 3.4 Hz, ^{3}J$_{HH}$ = 6.5 Hz, 4H, PC*H$_2$*), 3.26 (A$_2$B$_2$XX′B′$_2$A′$_2$, N = $|^3J_{HP}$ + $^4J_{HP}|$ = 6.5 Hz, ^{3}J$_{HH}$ = 6.5 Hz, 4H, NC*H$_2$*).

^{13}C{^{1}H} NMR
(100.6 MHz, C$_6$D$_6$, [ppm]): δ = 28.0 (AXX′A′, N = $|^1J_{CP}$ + $^3J_{CP}|$ = 7.9 Hz, PC*H$_2$*), 30.9 (A$_6$XX′A′$_6$, N = $|^2J_{CP}$ + $^4J_{CP}|$ = 2.6 Hz, PC(*C*H$_3$)$_3$), 33.4 (s, NC(*C*H$_3$)$_3$), 37.5 (A$_2$XX′A′$_2$, N = $|^1J_{CP}$ + $^3J_{CP}|$ = 8.1 Hz, P*C*(CH$_3$)$_3$), 54.8 (s, N*C*(CH$_3$)$_3$), 67.2 (AXX′A′, N = $|^2J_{CP}$ + $^3J_{CP}|$ = 7.1 Hz, N*C*H$_2$), 194.8 (t, ^{2}J$_{CP}$ = 5.1 Hz, *C*NC(CH$_3$)$_3$).

^{31}P{^{1}H} NMR
(162.0 MHz, C$_6$D$_6$, [ppm]): δ = 90.2 (s, *P*^{t}Bu$_2$).

IR
(KBr, cm^{-1}): 1975 (m, ν(C≡N)), 1957 (m, ν(C≡N)), 1797 (s, ν(C≡N)), 1769 (s, ν(C≡N)).

IR (liq.)
(DCM, cm^{-1}): 1974 (br, ν(C≡N)), 1955 (br, ν(C≡N)), 1778 (s, ν(C≡N)), 1742 (s, ν(C≡N)).

Elemental Analysis

C$_{30}$H$_{62}$N$_3$P$_2$Re (%)   calcd.:   C, 50.54; H, 8.77; N, 5.89

found: C, 50.61; H, 8.73; N, 5.56

3.4.4   Oxidation of 18a or 25a with Ag$^+$ (Synthesis of 24)

25a (3.8 mg, 6.5 µmol, 1 eq) is dissolved in C$_6$D$_6$ and AgOTf (1.7 mg, 6.5 µmol, 1 eq) is added. The solution turns dark immediately and Ag precipitates. After stirring for 1h, the mixture is filtered, the residue washed with benzene and THF and extracted with DCM. After crystallization out of DCM/pentane, pure **24** is obtained according to NMR data. The reaction can be carried out similarly using **18a**, however the spectroscopic the product was not obtained pure (78% spectroscopic yield).

3.4.5   Oxidation of 18a with [CPh$_3$][PF$_6$] (Synthesis of 16d-PF$_6$)

18a (5.0 mg, 8.2 µmol, 1 eq) is dissolved in C$_6$D$_6$ and [CPh$_3$][PF$_6$] (3.2 mg, 8.2 µmol, 1 eq) is added. The color of the solution immediately turns deep red. The solvent is evaporated and the residue washed with pentanes. After drying i. vac., the residual is dissolved in d$_8$-THF to observe formation of **16a-PF$_6$** and **16d-PF$_6$** in an about equimolar ratio.

Spectroscopic Characterization for **16d-PF$_6$**

^{1}H NMR   (300 MHz, d$_8$-THF, [ppm]): δ = 1.01 (A$_{18}$XX′A′$_{18}$ = N = |$^3J_{HP}$ + $^5J_{HP}$| = 7.3 Hz, 36H, PC(CH_3)$_3$), 1.23 (A$_{18}$XX′A′$_{18}$ = N = |$^3J_{HP}$ + $^5J_{HP}$| = 6.9 Hz, 36H, PC(CH_3)$_3$), 2.3 (m, 2H, PCH_2), 2.4 (m, 2H, PCH_2), 4.1 (m, 2H, NCH_2), 4.3 (m, 2H, NCH_2), 4.52 (s, 2H, NCH_2CPh$_3$), 7.2 (m, 15H, CPh_3).

^{31}P{^{1}H} NMR (121.5 MHz, d$_8$-THF, [ppm]): δ = 87.6 (s, P^{t}Bu$_2$).

Addition of KBTSA (1.0 mg, 8.2 µmol, 1 eq) yields a mixture of **18a** and **18d** in a clean reaction.

^{31}P{^{1}H} NMR of **18d** (121.5 MHz, d$_8$-THF, [ppm]): δ = 45.9 (s, P^{t}Bu$_2$).

^{31}P{^{1}H} NMR of **18d** (121.5 MHz, C$_6$D$_6$, [ppm]): δ = 44.9 (s, P^{t}Bu$_2$), 41.9 (s, P^{t}Bu$_2$).

3.4.6 Oxidation of 18b with Ag⁺

CD_2Cl_2 (0.5 mL) is trap-to-trap transferred to a J-Young NMR tube charged with **18b** (5.0 mg, 8.0 µmol, 1 eq) and $AgPF_6$ (2.0 mg, 8.0 µmol, 1 eq). The mixture is warmed to -70°C and shaken for 10 min. The ^{31}P and ^1H NMR spectra at room temperature show the complete consumption of **18b** and formation of a paramagnetic compound (δ_H(300 MHz, ppm) = 23.1 (br), 7.1 (br), 6.8 (br), 0.0 (br), -3.6 (br), -31.7 (br)), which slowly decomposes at room temperature to a mixture of diamagnetic compounds that was not further characterized.

3.4.7 [(PNP)Re(NCHCH₂)Cl]OTf (22)

18b (5.0 mg, 8.0 µmol, 1 eq) and AgOTf (2.1 mg, 8.0 µmol, 1 eq) are dissolved in d_2-DCM at -34°C. The color of the reaction immediately turns deep red and a grey precipitate is formed. 2,4,6-Tri-*tert*-butyl phenoxyl radical (2.6 mg, 9.9 µmol, 1.2 eq) is added to the cold suspension and the reaction is allowed to warm to room temperature. After filtration, the product is precipitated by pentane addition (2 mL), filtered off and dried *in vacuo* as a greenish black solid.

Spectroscopic Characterization

^1H NMR
(300 MHz, C_6D_6, [ppm]): δ = 1.02 ($A_9XX'A'_9$, N = $|^3J_{HP} + {}^5J_{HP}|$ = 6.9 Hz, 18H, PC(CH_3)$_3$), 1.16 ($A_9XX'A'_9$, N = $|^3J_{HP} + {}^5J_{HP}|$ = 7.2 Hz, 18H, PC(CH_3)$_3$), 2.12 (ABCDXX'D'C'B'A', N = $|^2J_{HP} + {}^4J_{HP}|$ = 2.8 Hz, $^2J_{HH}$ = 14.9 Hz, $^3J_{HH}$ = 6.4 Hz, $^3J_{HH}$ = 3.0 Hz, 2H, PCH_2), 2.30 (ABCDXX'D'C'B'A', N = $|^2J_{HP} + {}^4J_{HP}|$ = 3.8 Hz, $^2J_{HH}$ = 14.9 Hz, $^3J_{HH}$ = 8.5 Hz, $^3J_{HH}$ = 8.7 Hz, 2H, PCH_2), 3.66 (ABCDXX'D'C'B'A', N = $|^3J_{HP} + {}^4J_{HP}|$ = 2.4 Hz, $^2J_{HH}$ = 14.8 Hz, $^3J_{HH}$ = 8.7 Hz, $^3J_{HH}$ = 6.4 Hz, 2H, NCH_2CH₂), 4.87 (ABCDXX'D'C'B'A', N = $|^3J_{HP} + {}^4J_{HP}|$ = 12.2 Hz, $^2J_{HH}$ = 14.8 Hz, $^3J_{HH}$ = 3.0 Hz, $^3J_{HH}$ = 8.5 Hz, 2H, NCH_2CH₂), 5.08 (d, $^3J_{HH}$ = 8.0 Hz, 1H, ReNCHCH_2), 5.23 (d, $^3J_{HH}$ = 15.3 Hz, 1H, ReNCHCH_2), 7.08 (dd, $^3J_{HH}$ = 15.3 Hz, $^3J_{HH}$ = 8.0 Hz, 1H, ReNCHCH₂).

$^{31}P\{^1H\}$ NMR (121.5 MHz, C_6D_6, [ppm]): δ = 89.2 (s, P^tBu_2).

Mass Spectrometry

LIFDI+
(toluene, m/z⁺): 623.1 ($C_{22}H_{47}ClN_2P_2Re^+$).

3.4.8 Release of NCMe from 22 (Synthesis of [(PNP)ReCl$_2$] (3))

22 (5.0 mg, 6.5 µmol, 1 eq), 12-crown-4 (3.1 µL, 20 µmol, 3 eq), LiCl (2.8 mg, 65 µmol, 10 eq), DBU (0.5 µL, 3.5 µmol, 0.5 eq) and naphthalene (0.8 mg, 6.5 µmol, 1 eq) as internal standard are dissolved in d$_8$-THF in a J-Young-NMR tube and shaken for 12 h. ^{1}H and ^{31}P NMR spectra show the formation of **3** and acetonitrile in about 30% yield.

3.4.9 Release of NCMe from 18b with CuCl$_2$ and base

18b (5.0 mg, 8.0 µmol, 1 eq), CuCl$_2$ (1.1 mg, 8.0 µmol, 1 eq) and DBU (1.2 µL, 8.0 µmol, 1 eq) are suspended in d$_8$-THF at -34°C and stirred for 2 d at room temperature before another equivalent of CuCl$_2$ and DBU are added. The ^{31}P NMR spectrum shows the formation of **3** in about 25% yield.

3.4.10 Oxidation of 18b with N-chlorosuccinimide (Synthesis of 23)

A mixture of **18b** (20.0 mg, 32.0 µmol, 1 eq) and N-chlorosuccinimide (8.6 mg, 64.0 µmol, 2 eq) is dissolved in benzene (5 mL) and stirred at room temperature for 18 h. The formation of acetonitrile is confirmed by ^{1}H (spectroscopic yield about 80%, hexamethylbenzene (1 eq) as internal standard), ^{15}N and ^{1}H-^{15}N-HMBC NMR spectroscopy. The mixture is worked up by evaporation of the solvent under reduced pressure, washing with pentane (2 x 5 mL) and extraction with benzene (2 x 3 mL). After filtration and solvent evaporation residual succinimide is sublimed off over 18 h (80°C @ 10 mTorr) to obtain **23** as a green powder (19.5 mg, 29.9 µmol, 93%), which was identified by comparison of ^{1}H NMR, UV-vis and LIFDI-MS data with an original sample.

3.4.11 Oxidation of 18a with NCS

18a (5.0 mg, 8.1 µmol, 1 eq) and NCS (2.2 mg, 16.4 µmol, 2 eq) are dissolved in C$_6$D$_6$. Formation of four diamagnetic signals in the ^{31}P-NMR spectra is observed, besides the signal corresponding to **23** in the ^{1}H-NMR spectrum.

^{1}H NMR (300 MHz, C_6D_6, [ppm]): δ = 10.8 (s, **23**).

^{31}P{^{1}H} NMR (121.5 MHz, C_6D_6, [ppm]): δ = 91.4 (s, 65%), 71.1 (s, 29%), 47.7 (s, 1%), 42.8 (s, 5%).

LIFDI+(toluene, m/z$^+$): 682.5 (unknown); 652.1 (unknown); 596.2 (**23**$^+$).

IR (KBr, cm^{-1}): 2258 (w, ν(C≡N)), 2223 (w, ν(C≡N)).

3.4.12 [(PNP)ReCl$_3$] (23)

N-chlorosuccinimide (8.6 mg, 64.8 µmol, 1 eq) is added to a frozen solution of **3** (40.0 mg, 64.8 µmol, 1 eq) in benzene (5-10 mL) and warmed to room temperature. Upon melting the color changes from violet to dark green. After stirring for 2 h, the volume is reduced to about 3 mL and the product is precipitated with pentanes (10 mL). After filtration, the green powder is washed with pentanes (2 x 5 mL), dissolved in benzene (3 x 5 mL), filtered and lyophilized. The crude product is heated to 80°C (30 mTorr) for 18 h to sublime off residual succinimide. Yield: 32.0 mg, 49.0 µmol, 76%.

Spectroscopic Characterization

^{1}H NMR (300 MHz, d_8-THF, [ppm]): δ = -15.8 (br), 10.7 (br).

Magnetic Properties

Evans method μ_{eff}^{298K}: 1.54 μ_B.

Elemental Analysis

$C_{20}H_{44}Cl_3NP_2Re$ (%) calcd.: C, 36.78; H, 6.79; N, 2.14
found: C, 37.26; H, 7.22; N, 2.51

Mass Spectrometry

LIFDI+ (toluene, m/z$^+$): 652.2 ($C_{20}H_{44}Cl_3NP_2Re^+$).

3.4.13 Reduction of 23 (Synthesis of [(PNP)ReCl$_2$] (3))

23 (5.0 mg, 7.7 µmol, 1 eq) and CoCp$_2^*$ (2.5 mg, 7.7 µmol, 1 eq) are dissolved in d$_8$-THF (0.5 mL) in a J-Young NMR tube. Upon shaking the color of the solution turns from green to red-brown and a yellow precipitate is formed. Examination by ^{1}H and ^{31}P NMR spectroscopy reveals clean formation of **3**.

3.4.14 Reduction of 23 under N$_2$ (Synthesis of [(PNP)Re(N)Cl] (9))

Na/Hg (209 mg, 1 M, 15.4 µmol, 2 eq) is added to a solution of **23** (5.0 mg, 7.7 µmol, 1 eq) in d$_8$-THF (0.5 mL) at room temperature and stirred under N$_2$ atmosphere for 15 h. Examination by ^{1}H and ^{31}P NMR spectroscopy reveals formation of **9** in about 70% spectroscopic yield.

3.4.15 Hydrogenation of 18

In the presence of HCl

To **18a** (5.0 mg, 8.1 µmol, 1 eq) a solution of HCl (8 µL, 2 M in Et$_2$O, 1 eq) in THF is added and the reaction mixture is pressurized with H$_2$ (1 bar). The solution is heated to 65°C for 18 h to observe formation of **27** in 70% spectroscopic yield.

In the presence of KO^{t}Bu
18b (4.4 mg, 7.0 µmol, 1 eq) and KO^{t}Bu (0.8 mg, 7.0 µmol, 1 eq) are suspended in benzene (0.5 mL) and pressurized with H$_2$ (1.5 bar). The mixture is heated to 70°C for 2 d and then stirred for 2 d at room temperature to observe conversion to **26b** in 95% spectroscopic yield.

V   Literature

Bibliography

[1] M. M. Georgiadis, H. Komiya, P. Chakrabarti, D. Woo, J. J. Kornuc, D. C. Rees, *Chem. Rev.* **1992**, *257*, 1653–1659.

[2] O. Einsle, F. A. Tezcan, S. L. A. Andrade, B. Schmid, M. Yoshida, J. B. Howard, D. C. Rees, *Science* **2002**, *297*, 1696–1700.

[3] K. M. Lancaster, M. Roemelt, P. Ettenhuber, Y. Hu, M. W. Ribbe, F. Neese, U. Bergmann, S. DeBeer, *Science* **2011**, *334*, 974–977.

[4] T. Spatzal, M. Aksoyoglu, L. Zhang, S. L. a. Andrade, E. Schleicher, S. Weber, D. C. Rees, O. Einsle, *Science* **2011**, *334*, 940–940.

[5] B. M. Hoffman, D. R. Dean, L. C. Seefeldt, *Acc. Chem. Res.* **2009**, *42*, 609–619.

[6] B. M. Hoffman, D. Lukoyanov, Z. Y. Yang, D. R. Dean, L. C. Seefeldt, *Chem. Rev.* **2014**, *114*, 4041–4062.

[7] F. Haber, *Zeitschrift für Elektrochem. und Angew. Phys. Chemie* **1910**, *16*, 244–246.

[8] G. Ertl, *Angew. Chem. Int. Ed.* **2008**, *47*, 3524–3535.

[9] C. J. M. van der Ham, M. T. M. Koper, D. G. H. Hetterscheid, *Chem. Soc. Rev.* **2014**, *43*, 5183.

[10] M. Ali, F. Zhou, K. Chen, C. Kotzur, C. Xiao, L. Bourgeois, X. Zhang, D. R. MacFarlane, *Nat. Commun.* **2016**, *7*, 1–5.

[11] U.S. Governement Printing Office, *Nitrogen (Fixed) - Ammonia*, U.S. Geological Survey, Mineral Commodity Summaries, Washington DC, **2016**.

[12] International Energy Agency, *Tracking Industrial Energy Efficiency and CO2 Emissions*, OECD, Paris, **2007**.

[13] M. Hidai, *Coord. Chem. Rev.* **1999**, *185–186*, 99–108.

[14] M. J. Bezdek, P. J. Chirik, *Angew. Chem. Int. Ed.* **2016**, *55*, 7892–7896.

[15] M. E. Vol'pin, V. B. Shur, *Nature* **1966**, *209*, 1236–1236.

[16] E. E. Van Tamelen, W. Cretney, N. Klaentschi, J. S. Miller, *J. Chem. Soc. Chem. Commun.* **1972**, 481.

[17] J. E. Bercaw, R. H. Marvich, L. G. Bell, H. H. Brintzinger, *J. Am. Chem. Soc.* **1972**, *94*, 1219–1238.

[18] E. E. Van Tamelen, *Acc. Chem. Res.* **1970**, *3*, 361–367.

[19] A. D. Allen, C. V. Senoff, *Chem. Commun.* **1965**, *24*, 621–622.

[20] A. D. Allen, R. O. Harris, B. R. Loescher, J. R. Stevens, R. N. Whiteley, *Chem. Rev.*

1973, *73*, 11–20.

[21] D. Sellmann, *Angew. Chem. Int. Ed. Engl.* **1974**, *13*, 639–649.

[22] J. Chatt, G. A. Heath, R. L. Richards, *J. Chem. Soc. Chem. Commun.* **1972**, 1010.

[23] J. Chatt, G. A. Heath, G. J. Leigh, *J. Chem. Soc. Chem. Commun.* **1972**, 444–445.

[24] J. Chatt, G. A. Heath, N. E. Hooper, G. J. Leigh, *J. Organomet. Chem.* **1973**, *57*, 67–68.

[25] J. Chatt, R. L. Richards, *J. Organomet. Chem.* **1982**, *239*, 65–77.

[26] J. Chatt, A. J. Pearman, R. L. Richards, *J. Chem. Soc. Dalt. Trans.* **1977**, 1852–1860.

[27] J. Chatt, J. R. Dilworth, R. L. Richards, *Chem. Rev.* **1978**, *78*, 589–625.

[28] B. S. N. Anderson, M. E. Fakley, R. Richards, J. Chatt, *J.C.S. Dalt. Trans.* **1981**, 1973–1979.

[29] J. Chatt, A. J. Pearman, R. L. Richards, *J. Organomet. Chem.* **1975**, *101*, C45–C47.

[30] G. C. Stephan, C. Sivasankar, F. Studt, F. Tuczek, *Chem. - A Eur. J.* **2008**, *14*, 644–652.

[31] D. V Yandulov, R. R. Schrock, *Science* **2003**, *301*, 76–78.

[32] R. R. Schrock, *Acc. Chem. Res.* **2005**, *38*, 955–962.

[33] D. V. Yandulov, R. R. Schrock, *Inorg. Chem.* **2005**, *44*, 1103–1117.

[34] D. V. Yandulov, R. R. Schrock, A. L. Rheingold, C. Ceccarelli, W. M. Davis, *Inorg. Chem.* **2003**, *42*, 796–813.

[35] V. Ritleng, D. V. Yandulov, W. W. Weare, R. R. Schrock, A. S. Hock, W. M. Davis, *J. Am. Chem. Soc.* **2004**, *126*, 6150–6163.

[36] K. Arashiba, Y. Miyake, Y. Nishibayashi, *Nat. Chem.* **2011**, *3*, 120–125.

[37] Y. Nishibayashi, *Inorg. Chem.* **2015**, *54*, 9234–9247.

[38] S. Kuriyama, K. Arashiba, K. Nakajima, H. Tanaka, N. Kamaru, K. Yoshizawa, Y. Nishibayashi, *J. Am. Chem. Soc.* **2014**, *136*, 9719–9731.

[39] Y. Nishibayashi, *Nat. Chem.* **2011**, *3*, 502–504.

[40] E. Kinoshita, K. Arashiba, S. Kuriyama, Y. Miyake, R. Shimazaki, H. Nakanishi, Y. Nishibayashi, *Organometallics* **2012**, *31*, 8437–8443.

[41] Y. H. Tian, A. W. Pierpont, E. R. Batista, *Inorg. Chem.* **2014**, *53*, 4177–4183.

[42] H. Tanaka, K. Arashiba, S. Kuriyama, A. Sasada, K. Nakajima, K. Yoshizawa, Y. Nishibayashi, *Nat. Commun.* **2014**, *5*, 3737.

[43] K. Arashiba, E. Kinoshita, S. Kuriyama, A. Eizawa, K. Nakajima, H. Tanaka, K. Yoshizawa, Y. Nishibayashi, *J. Am. Chem. Soc.* **2015**, *137*, 5666–5669.

[44] J. S. Anderson, J. Rittle, J. C. Peters, *Nature* **2013**, *501*, 84–87.

[45] H. Fong, M. E. Moret, Y. Lee, J. C. Peters, *Organometallics* **2013**, *32*, 3053–3062.

[46] N. Khoenkhoen, B. de Bruin, J. N. H. Reek, W. I. Dzik, *Eur. J. Inorg. Chem.* **2015**, 567–598.

[47] T. A. Bazhenova, A. E. Shilov, *Coord. Chem. Rev.* **1995**, *144*, 69–145.

[48] H.-P. Jia, E. A. Quadrelli, *Chem. Soc. Rev.* **2014**, *43*, 547–564.

[49] A. E. Shilov, *Russ. Chem. Bull.* **2003**, *52*, 2555–2562.

[50] M. D. Fryzuk, S. A. Johnson, *Coord. Chem. Rev.* **2000**, *200–202*, 379–409.

[51] B. A. MacKay, M. D. Fryzuk, *Chem. Rev.* **2004**, *104*, 385–401.

[52] M. P. Shaver, M. D. Fryzuk, *Adv. Synth. Catal.* **2003**, *345*, 1061–1076.

[53] F. Studt, F. Tuczek, *J. Comput. Chem.* **2006**, *27*, 1278–1291.

[54] I. M. Treitel, M. T. Flood, R. E. Marsh, H. B. Gray, *J. Am. Chem. Soc.* **1969**, *91*, 6512–6513.

[55] J. Chatt, R. C. Fay, R. L. Richards, *J. Chem. Soc. A* **1971**, 702–704.

[56] R. Duchateau, S. Gambarotta, N. Beydoun, C. Bensimon, *J. Am. Chem. Soc.* **1991**, *113*, 8986–8988.

[57] F. Studt, N. Lehnert, B. E. Wiesler, A. Scherer, R. Beckhaus, F. Tuczek, *Eur. J. Inorg.Chem.* **2006**, 291–297.

[58] A. Scherer, K. Kollak, A. Lützen, M. Friedemann, D. Haase, W. Saak, R. Beckhaus, *Eur. J. Inorg. Chem.* **2005**, 1003–1010.

[59] R. D. Sanner, D. M. Duggan, T. C. McKenzie, R. E. Marsh, J. E. Bercaw, *J. Am. Chem. Soc.* **1976**, *98*, 8358–8365.

[60] M. J. Bezdek, S. Guo, P. J. Chirik, *Inorg. Chem.* **2016**, *55*, 3117–3127.

[61] M. Hirotsu, P. P. Fontaine, A. Epshteyn, P. Y. Zavalij, L. R. Sita, *J. Am. Chem. Soc.* **2007**, *129*, 9284–9285.

[62] P. P. Fontaine, B. L. Yonke, P. Y. Zavalij, L. R. Sita, *J. Am. Chem. Soc* **2010**, *132*, 12273–12285.

[63] A. J. Keane, B. L. Yonke, M. Hirotsu, P. Y. Zavalij, L. R. Sita, *J. Am. Chem. Soc.* **2014**, *136*, 9906–9909.

[64] M. Hirotsu, P. P. Fontaine, P. Y. Zavalij, L. R. Sita, *J. Am. Chem. Soc.* **2007**, *129*, 12690–12692.

[65]   B. Peigné, J. Cano, G. Aullón, *Eur. J. Inorg. Chem.* **2012**, 797–806.

[66]   E. A. Maclachlan, M. D. Fryzuk, *Organometallics* **2006**, *25*, 1530–1543.

[67]   M. D. Fryzuk, T. S. Haddad, M. Mylvaganam, D. H. McConville, S. J. Rettig, *J. Am. Chem. Soc.* **1993**, *115*, 2782–2792.

[68]   J. N. Armor, H. Taube, *J. Am. Chem. Soc.* **1970**, *92*, 2560–2562.

[69]   K. Jonas, *Angew. Chem. Int. Ed. Engl.* **1973**, *12*, 997–998.

[70]   C. Krüger, Y.-H. Tsay, *Angew. Chem. Int. Ed. Engl.* **1973**, *12*, 998–99.

[71]   W. Evans, T. Ulibarri, J. Ziller, *J. Am. Chem. Soc.* **1988**, *110*, 6877–6879.

[72]   M. D. Fryzuk, T. S. Haddad, S. J. Rettig, *J. Am. Chem. Soc.* **1990**, *112*, 8185–8186.

[73]   C. B. Powell, M. B. Hall, *Inorg. Chem.* **1984**, *23*, 4619–4627.

[74]   R. D. Archer, R. O. Day, M. L. Illingsworth, *Inorg. Chem.* **1979**, *18*, 2908–2916.

[75]   E. J. Peterson, R. B. Dreele, T. M. Brown, *Inorg. Chem.* **1976**, *15*, 309–315.

[76]   J. M. Manriquez, J. E. Bercaw, *J. Am. Chem. Soc.* **1974**, *96*, 6229–6230.

[77]   J. A. Pool, E. Lobkovsky, P. J. Chirik, *Nature* **2004**, *427*, 527–530.

[78]   J. A. Pool, W. H. Bernskoetter, P. J. Chirik, *J. Am. Chem. Soc.* **2004**, *126*, 14326–14327.

[79]   P. Bobadova-Parvanova, Q. Wang, K. Morokuma, D. G. Musaev, *Angew. Chem. Int. Ed. Engl.* **2005**, *44*, 7101–3.

[80]   P. J. Chirik, *Organometallics* **2010**, *29*, 1500–1517.

[81]   M. D. Fryzuk, S. A. Johnson, S. J. Rettig, *J. Am. Chem. Soc* **1998**, *120*, 11024–11025.

[82]   M. D. Fryzuk, S. A. Johnson, B. O. Patrick, A. Albinati, S. A. Mason, T. F. Koetzle, *J. Am. Chem. Soc.* **2001**, *123*, 3960–3973.

[83]   C. E. Laplaza, C. C. Cummins, *Science* **1995**, *268*, 861–863.

[84]   C. E. Laplaza, M. J. A. Johnson, J. C. Peters, A. L. Odom, E. Kim, C. C. Cummins, G. N. George, I. J. Pickering, *J. Am. Chem. Soc.* **1996**, *118*, 8623–8638.

[85]   J. J. Curley, T. R. Cook, S. Y. Reece, P. Müller, C. C. Cummins, *J. Am. Chem. Soc.* **2008**, *130*, 9394–9405.

[86]   Q. Cui, D. G. Musaev, M. Svensson, S. Sieber, K. Morokuma, *J. Am. Chem. Soc* **1995**, *117*, 12366–12367.

[87]   J. C. Peters, J. P. F. Cherry, J. C. Thomas, L. Baraldo, D. J. Mindiola, W. M. Davis, C. C. Cummins, *J. Am. Chem. Soc.* **1999**, *121*, 10053–10067.

[88]   M. H. Chisholm, F. A. Cotton, B. A. Frenz, W. W. Reichert, L. W. Shive, B. R. Stults, *J. Am. Chem. Soc.* **1976**, *98*, 4469–4476.

[89]   J. Hahn, C. R. Landis, V. A. Nasluzov, K. M. Neyman, N. Rosch, *Inorg. Chem.* **1997**, *36*, 3947–3951.

[90]   C. C. Cummins, *Chem. Commun.* **1998**, *7*, 1777–1786.

[91]   C. E. Laplaza, A. R. Johnson, C. C. Cummins, R. V October, *J. Am. Chem. Soc.* **1996**, *118*, 709–710.

[92]   M. J. A. Johnson, P. M. Lee, A. L. Odom, W. M. Davis, C. C. Cummins, *Angew. Chem. Int. Ed. Engl.* **1997**, *36*, 87–91.

[93]   Y. C. Tsai, M. J. A. Johnson, D. J. Mindiola, C. C. Cummins, W. T. Klooster, T. F. Koetzle, *J. Am. Chem. Soc.* **1999**, *121*, 10426–10427.

[94]   G. Christian, R. Stranger, B. F. Yates, C. C. Cummins, *Dalton Trans.* **2007**, 1939–1947.

[95]   M. Kol, R. R. Schrock, R. Kempe, W. M. Davis, *J. Am. Chem. Soc.* **1994**, *116*, 4382–4390.

[96]   K.-Y. Shih, R. R. Schrock, R. Kempe, *J. Am. Chem. Soc.* **1994**, *116*, 8804–8805.

[97]   G. Christian, J. Driver, R. Stranger, *Faraday Discuss.* **2003**, *124*, 331.

[98]   G. Christian, R. Stranger, B. F. Yates, D. C. Graham, *Dalton Trans.* **2005**, 962–968.

[99]   E. Solari, C. Da Silva, B. Iacono, J. Hesschenbrouck, C. Rizzoli, R. Scopelliti, C. Floriani, *Angew. Chem. Int. Ed.* **2001**, *40*, 3907–3909.

[100] A. S. Huss, J. J. Curley, C. C. Cummins, D. A. Blank, *J. Phys. Chem. B* **2013**, *117*, 1429–1436.

[101] M. Reiher, B. Kirchner, J. Hutter, D. Sellmann, B. A. Hess, *Chem. - A Eur. J.* **2004**, *10*, 4443–4453.

[102] M. B. O'Donoghue, N. C. Zanetti, W. M. Davis, R. R. Schrock, *J. Am. Chem. Soc.* **1997**, *119*, 2753–2754.

[103] M. B. O'Donoghue, W. M. Davis, R. R. Schrock, *Inorg. Chem.* **1998**, *37*, 5149–5158.

[104] E. L. Sceats, J. S. Figueroa, C. C. Cummins, N. M. Loening, P. Van der Wel, R. G. Griffin, *Polyhedron* **2004**, *23*, 2751–2768.

[105] R. A. Eikey, M. M. Abu-Omar, *Coord. Chem. Rev.* **2003**, *243*, 83–124.

[106] H. Henderickx, G. Kwakkenbos, A. Peters, J. van der Spoel, K. de Vries, *Chem. Commun.* **2003**, *897*, 2050–1.

[107] A. F. Cozzolino, J. S. Silvia, N. Lopez, C. C. Cummins, *Dalton Trans.* **2014**, *43*, 4639–52.

[108] J. S. Silvia, C. C. Cummins, *J. Am. Chem. Soc.* **2009**, *131*, 446–447.

[109] B. L. Tran, M. Pink, X. Gao, H. Park, D. J. Mindiola, *J. Am. Chem. Soc.* **2010**, *132*, 1458–1459.

[110] J. J. Curley, E. L. Sceats, C. C. Cummins, *J. Am. Chem. Soc.* **2006**, *128*, 14036–14037.

[111] S. W. Benson, *J. Chem. Educ.* **1965**, *42*, 502–518.

[112] J. J. Curley, A. F. Cozzolino, C. C. Cummins, *Dalton Trans.* **2011**, *40*, 2429–2432.

[113] G. K. B. Clentsmith, V. M. E. Bates, P. B. Hitchcock, F. G. N. Cloke, *J. Am. Chem. Soc.* **1999**, *121*, 10444.

[114] F. Studt, V. M. E. Lamarche, G. K. B. Clentsmith, F. G. N. Cloke, F. Tuczek, *Dalton Trans.* **2005**, 1052–1057.

[115] V. M. E. Bates, G. K. B. Clentsmith, F. G. N. Cloke, J. C. Green, H. D. L. Jenkin, *Chem. Commun.* **2000**, 927–928.

[116] I. Korobkov, S. Gambarotta, G. P. A. Yap, *Angew. Chem. Int. Ed.* **2002**, *41*, 3433–3436.

[117] I. Korobkov, S. Gambarotta, G. P. A. Yap, *Angew. Chem. Int. Ed.* **2003**, *42*, 4958–4961.

[118] G. B. Nikiforov, I. Vidyaratne, S. Gambarotta, I. Korobkov, *Angew. Chem. Int. Ed.* **2009**, *48*, 7415–7419.

[119] T. Shima, S. Hu, G. Luo, X. Kang, Y. Luo, Z. Hou, *Science* **2013**, *340*, 1549–52.

[120] Z. Hou, T. Shima, S. Hu, Y. Endo, *Patent* **2014**, WO2014080939, US20150291635 A1.

[121] S. Hu, T. Shima, Y. Luo, Z. Hou, *Organometallics* **2013**, *32*, 2145–2151.

[122] M. M. Guru, T. Shima, Z. Hou, *Angew. Chem. Int. Ed.* **2016**, DOI 10.1002/anie.201607426.

[123] D. J. Knobloch, E. Lobkovsky, P. J. Chirik, *Nat. Chem.* **2010**, *2*, 30–35.

[124] P. Berno, S. Gambarotta, *Angew. Chem. Int. Ed.* **1995**, *34*, 822–824.

[125] J. Jubb, L. Scoles, H. Jenkins, S. Gambarotta, *Chem. - A Eur. J.* **1996**, *2*, 767–771.

[126] I. Vidyaratne, P. Crewdson, E. Lefebvre, S. Gambarotta, *Inorg. Chem.* **2007**, *46*, 8836–8842.

[127] Y. Ishida, H. Kawaguchi, *J. Am. Chem. Soc.* **2014**, *136*, 16990–16993.

[128] B. L. Tran, B. Pinter, A. J. Nichols, F. T. Konopka, R. Thompson, C. H. Chen, J. Krzystek, A. Ozarowski, J. Telser, M. H. Baik, et al., *J. Am. Chem. Soc.* **2012**, *134*, 13035–13045.

[129] A. Zanotti-Gerosa, E. Solari, L. Giannini, C. Floriani, A. Chiesi-Villa, C. Rizzoli, *J. Am. Chem. Soc.* **1998**, *120*, 437–438.

[130] A. Caselli, E. Solari, R. Scopelliti, C. Floriani, N. Re, C. Rizzoli, A. Chiesi-Villa, *J. Am. Chem. Soc.* **2000**, *122*, 3652–3670.

[131] D. J. Mindiola, K. Meyer, J. P. F. Cherry, T. A. Baker, C. C. Cummins, *Organometallics* **2000**, *19*, 1622–1624.

[132] J. S. Figueroa, N. A. Piro, C. R. Clough, C. C. Cummins, *J. Am. Chem. Soc.* **2006**, *128*, 940–950.

[133] M. D. Fryzuk, C. M. Kozak, M. R. Bowdridge, B. O. Patrick, S. J. Rettig, *J. Am. Chem. Soc.* **2002**, *124*, 8389–8397.

[134] G. J. Christian, R. N. L. Terrett, R. Stranger, G. Cavigliasso, B. F. Yates, *Chem. - A Eur. J.* **2009**, *15*, 11373–11383.

[135] H. Kawaguchi, T. Matsuo, *Angew. Chem. Int. Ed.* **2002**, *41*, 2792–2794.

[136] F. Akagi, T. Matsuo, H. Kawaguchi, *Angew. Chem. Int. Ed.* **2007**, *46*, 8778–8781.

[137] F. Akagi, S. Suzuki, Y. Ishida, T. Hatanaka, T. Matsuo, H. Kawaguchi, *Eur. J. Inorg. Chem.* **2013**, 3930–3936.

[138] K. Searles, P. J. Carroll, C. Chen, M. Pink, D. J. Mindiola, *Chem. Commun.* **2015**, *51*, 3526–3528.

[139] M. D. Fryzuk, B. A. MacKay, S. A. Johnson, B. O. Patrick, *Angew. Chem. Int. Ed.* **2002**, *41*, 3709–3712.

[140] M. D. Fryzuk, B. A. MacKay, B. O. Patrick, *J. Am. Chem. Soc.* **2003**, *125*, 3234–3235.

[141] B. A. MacKay, R. F. Munha, M. D. Fryzuk, *J. Am. Chem. Soc.* **2006**, *128*, 9472–9483.

[142] A. Yeo, M. P. Shaver, M. D. Fryzuk, *Zeitschrift fur Anorg. und Allg. Chemie* **2015**, *641*, 123–127.

[143] B. A. MacKay, B. O. Patrick, M. D. Fryzuk, *Organometallics* **2005**, *24*, 3836–3841.

[144] L. P. Spencer, B. A. MacKay, B. O. Patrick, M. D. Fryzuk, *Proc. Natl. Acad. Sci. U. S. A.* **2006**, *103*, 17094–17098.

[145] J. Ballmann, A. Yeo, B. O. Patrick, M. D. Fryzuk, *Angew. Chem. Int. Ed.* **2011**, *50*, 507–510.

[146] P. Avenier, M. Taoufik, A. Lesage, X. Solans-Monfort, A. Baudouin, A. de Mallmann, L. Veyre, J.-M. Basset, O. Eisenstein, L. Emsley, et al., *Science* **2007**, *317*, 1056–1060.

[147] C. Chow, M. Taoufik, E. A. Quadrelli, *Eur. J. Inorg. Chem.* **2011**, 1349–1359.

[148] H. P. Jia, E. Gouré, X. Solans-Monfort, J. Llop Castelbou, C. Chow, M. Taoufik, O. Eisenstein, E. A. Quadrelli, *Inorg. Chem.* **2015**, *54*, 11648–11659.

[149] X. Solans-Monfort, C. Chow, E. Gouré, Y. Kaya, J. M. Basset, M. Taoufik, E. A. Quadrelli, O. Eisenstein, *Inorg. Chem.* **2012**, *51*, 7237–7249.

[150] W. Zhang, Y. Tang, M. Lei, K. Morokuma, D. G. Musaev, *Inorg. Chem.* **2011**, *250*, 9481–9490.

[151] T. J. Hebden, R. R. Schrock, M. K. Takase, P. Müller, *Chem. Commun.* **2012**, *48*, 1851–1853.

[152] Q. Liao, A. Cavaillé, N. Saffon-Merceron, N. Mézailles, *Angew. Chem. Int. Ed.* **2016**, DOI 10.1002/anie.201604812.

[153] Q. Liao, N. Saffon-Merceron, N. Mézailles, *ACS Catal.* **2015**, *5*, 6902–6906.

[154] T. Miyazaki, H. Tanaka, Y. Tanabe, M. Yuki, K. Nakajima, K. Yoshizawa, Y. Nishibayashi, *Angew. Chem. Int. Ed.* **2014**, *53*, 11488–11492.

[155] C. Rebreyend, B. De Bruin, *Angew. Chem. Int. Ed.* **2015**, *54*, 42–44.

[156] M. G. Scheibel, B. Askevold, F. W. Heinemann, E. J. Reijerse, B. de Bruin, S. Schneider, *Nat. Chem.* **2012**, *4*, 552–558.

[157] M. G. Scheibel, Y. Wu, A. C. Stueckl, L. Krause, E. Carl, D. Stalke, B. De Bruin, S. Schneider, *J. Am. Chem. Soc.* **2013**, *135*, 17719–17722.

[158] A. J. Keane, W. S. Farrell, B. L. Yonke, P. Y. Zavalij, L. R. Sita, *Angew. Chem. Int. Ed.* **2015**, *54*, 10220–10224.

[159] B. L. Yonke, J. P. Reeds, P. P. Fontaine, P. Y. Zavalij, L. R. Sita, *Organometallics* **2014**, *33*, 3239–3242.

[160] N. C. Smythe, R. R. Schrock, P. Müller, W. W. Weare, *Inorg. Chem.* **2006**, *45*, 7111–7118.

[161] I. Vidyaratne, J. Scott, S. Gambarotta, P. H. M. Budzelaar, *Inorg. Chem.* **2007**, *46*, 7040–7049.

[162] M. T. Mock, S. Chen, M. O'Hagan, R. Rousseau, W. G. Dougherty, W. Scott Kassel, R. Morris Bullock, *J. Am. Chem. Soc.* **2013**, *135*, 11493–11496.

[163] D. Sellmann, W. Weiss, *Angew. Chem.* **1978**, *17*, 269–270.

[164] J. L. Crossland, D. R. Tyler, *Coord. Chem. Rev.* **2010**, *254*, 1883–1894.

[165] S. F. McWilliams, P. L. Holland, *Acc. Chem. Res.* **2015**, *48*, 2059–2065.

[166] N. Hazari, *Chem. Soc. Rev.* **2010**, *39*, 4044–4056.

[167] K. C. MacLeod, P. L. Holland, *Nat. Chem.* **2013**, *5*, 559–565.

[168] J. J. Scepaniak, J. A. Young, R. P. Bontchev, J. M. Smith, *Angew. Chem. Int. Ed.*

2009, *48*, 3158–3160.

[169] J. J. Scepaniak, R. P. Bontchev, D. L. Johnson, J. M. Smith, *Angew. Chem. Int. Ed.* **2011**, *50*, 6630–6633.

[170] M. M. Rodriguez, E. Bill, W. W. Brennessel, P. L. Holland, *Science* **2011**, *334*, 780–783.

[171] J. M. Smith, R. J. Lachicotte, K. A. Pittard, T. R. Cundari, G. Lukat-Rodgers, K. R. Rodgers, P. L. Holland, *J. Am. Chem. Soc.* **2001**, *123*, 9222–9223.

[172] T. M. Figg, P. L. Holland, T. R. Cundari, *Inorg. Chem.* **2012**, *51*, 7546–7550.

[173] K. Grubel, W. W. Brennessel, B. Q. Mercado, P. L. Holland, *J. Am. Chem. Soc* **2014**, *136*, 16807–16816.

[174] K. C. MacLeod, D. J. Vinyard, P. L. Holland, *J. Am. Chem. Soc.* **2014**, *136*, 10226–10229.

[175] Y. Lee, F. T. Sloane, G. Blondin, K. A. Abboud, R. Garc??a-Serres, L. J. Murray, *Angew. Chem. Int. Ed.* **2015**, *54*, 1499–1503.

[176] B. Askevold, T. Nieto, S. Tussupbayev, M. Diefenbach, E. Herdweck, M. C. Holthausen, S. Schneider, *Nat. Chem.* **2011**, *3*, 532–537.

[177] M. Jahncke, A. Neels, H. Stoeckli-Evans, G. Süss-Fink, *J. Organomet. Chem.* **1998**, *565*, 97–103.

[178] Y. Nakajima, H. Suzuki, *Organometallics* **2003**, *22*, 959–969.

[179] M. Hölscher, M. H. G. Prechtl, W. Leitner, *Chem. - A Eur. J.* **2007**, *13*, 6636–6643.

[180] H. Kunkely, A. Vogler, *Angew. Chem. Int. Ed.* **2010**, *49*, 1591–1593.

[181] A. Vogler, H. Kunkely, *Inorg. Chem. Commun.* **2012**, *18*, 73–74.

[182] J. F. Harrison, *Chem. Rev.* **2000**, *100*, 679–716.

[183] J. F. Berry, E. Bill, E. Bothe, S. DeBeer George, B. Meinert, F. Neese, K. Wieghardt, *Science* **2006**, *312*, 1937–1941.

[184] T. A. Betley, J. C. Peters, *J. Am. Chem. Soc.* **2004**, *126*, 6252–6254.

[185] C. Vogel, F. W. Heinemann, J. Sutter, C. Anthon, K. Meyer, *Angew. Chem. Int. Ed.* **2008**, *47*, 2681–2684.

[186] J. J. Scepaniak, M. D. Fulton, R. P. Bontchev, E. N. Duesler, M. L. Kirk, J. M. Smith, *J. Am. Chem. Soc.* **2008**, *130*, 10515–10517.

[187] J. J. Scepaniak, C. S. Vogel, M. M. Khusniyarov, F. W. Heinemann, K. Meyer, J. M. Smith, *Science* **2011**, *331*, 1049–1052.

[188] A. Walstrom, M. Pink, X. Yang, J. Tomaszewski, M. H. Baik, K. G. Caulton, *J. Am. Chem. Soc.* **2005**, *127*, 5330–5331.
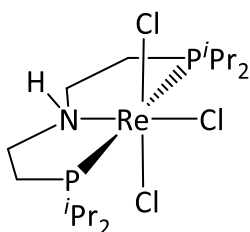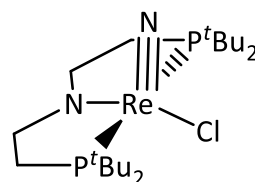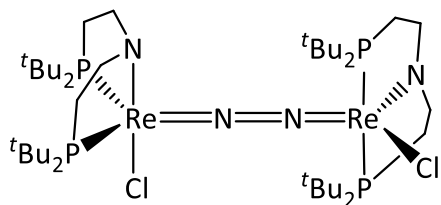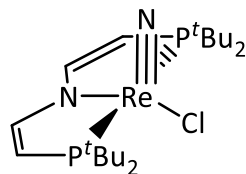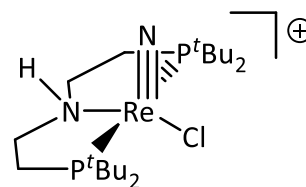
[189] F. S. Schendzielorz, M. Finger, C. Volkmann, C. Würtele, S. Schneider, *Angew. Chem. Int. Ed.* **2016**, *55*, 11417–11420.

[190] J. Schöffel, N. Šušnjar, S. Nückel, D. Sieh, P. Burger, *Eur. J. Inorg. Chem.* **2010**, 4911–4915.

[191] J. Schöffel, A. Y. Rogachev, S. D. George, P. Burger, *Angew. Chem. Int. Ed.* **2009**, *48*, 4734–4738.

[192] C. Sivasankar, F. Tuczek, *Dalton Trans.* **2006**, 3396–3398.

[193] I. Klopsch, M. Finger, C. Würtele, B. Milde, D. B. Werz, S. Schneider, *J. Am. Chem. Soc.* **2014**, *136*, 6881–6883.

[194] G. W. Parshall, L. W. Shive, F. A. Cotton, *Inorg. Synth.* **1977**, *17*, 110–111.

[195] G. Rouschias, G. Wilkinson, *J. Chem. Soc.* **1967**, 993–1000.

[196] L. E. Sutton, *Tables of Interatomic Distances and Configuration in Moleclues and Ions*, The Chemical Society, London, **1958**.

[197] A. N. Marziale, A. Friedrich, I. Klopsch, M. Drees, V. R. Celinski, J. Schmedt Auf Der Günne, S. Schneider, *J. Am. Chem. Soc.* **2013**, *135*, 13342–13355.

[198] A. Glüer, M. Förster, V. R. Celinski, J. Schmedt Auf Der Günne, M. C. Holthausen, S. Schneider, *ACS Catal.* **2015**, *5*, 7214–7217.

[199] S. Chakraborty, P. O. Lagaditis, M. Förster, E. A. Bielinski, N. Hazari, M. C. Holthausen, W. D. Jones, S. Schneider, *ACS Catal.* **2014**, *4*, 3994–4003.

[200] E. A. Bielinski, P. O. Lagaditis, Y. Zhang, B. Q. Mercado, C. Würtele, W. H. Bernskoetter, N. Hazari, S. Schneider, *J. Am. Chem. Soc.* **2014**, *136*, 10234–10237.

[201] S. Schneider, J. Meiners, B. Askevold, *Eur. J. Inorg. Chem.* **2012**, 412–429.

[202] P. O. Lagaditis, B. Schluschaß, S. Demeshko, C. Würtele, S. Schneider, *Inorg. Chem.* **2016**, *55*, 4529–4536.

[203] J. Meiners, M. G. Scheibel, M. H. Lemée-Cailleau, S. A. Mason, M. B. Boeddinghaus, T. F. Fässler, E. Herdtweck, M. M. Khusniyarov, S. Schneider, *Angew. Chem. Int. Ed.* **2011**, *50*, 8184–8187.

[204] J. Chatt, G. J. Leigh, D. M. P. Mingos, *J. Chem. Soc.* **1969**, 1674–1680.

[205] R. Grinter, J. Mason, *J. Chem. Soc.* **1970**, 2196–2199.

[206] K. M. Neyman, V. A. Nasluzov, J. Hahn, C. R. Landis, N. Rosch, *Organometallics* **1997**, *16*, 995–1000.

[207] I. Klopsch, M. Kinauer, M. Finger, C. Würtele, S. Schneider, *Angew. Chem. Int. Ed.* **2016**, *55*, 4786–4789.

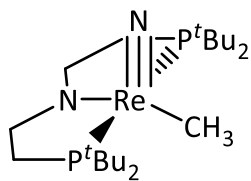[208] C. L. Tennent, W. D. Jones, *Can. J. Chem.* **2005**, *83*, 626–633.

[209] Z. D. Brown, P. Vasko, J. C. Fettinger, H. M. Tuononen, P. P. Power, *J. Am. Chem. Soc.* **2012**, *134*, 4045–4048.

[210] A. Walstrom, H. Fan, M. Pink, K. G. Caulton, *Inorganica Chim. Acta* **2010**, *363*, 633–636.

[211] C. Beard, K. Baum, *J. Org. Chem.* **1974**, *39*, 3875–3877.

[212] C. D. Beard, K. Baum, V. Grakauskas, *J. Org. Chem.* **1973**, *38*, 3673–3677.

[213] P. J. Stang, M. Hanack, L. R. Subramanian, *Synthesis (Stuttg).* **1982**, *2*, 85–126.

[214] F. J. Weigert, *J. Org. Chem.* **1980**, *45*, 3476–3483.

[215] D. Naumann, J. Kischkewitz, *J. Fluor. Chem.* **1990**, *47*, 283–299.

[216] O. A. Tomashenko, V. V. Grushin, *Chem. Rev.* **2011**, *111*, 4475–4521.

[217] C. Alonso, E. Martínez De Marigorta, G. Rubiales, F. Palacios, *Chem. Rev.* **2015**, *115*, 1847–1935.

[218] L. Chu, F. L. Qing, *Acc. Chem. Res.* **2014**, *47*, 1513–1522.

[219] N. Shibata, A. Matsnev, D. Cahard, *Beilstein J. Org. Chem.* **2010**, *6*, DOI 10.3762/bjoc.6.65.

[220] B. R. Langlois, E. Laurent, N. Roidot, *Tetrahedron Lett.* **1991**, *32*, 7525–7528.

[221] J.-A. Ma, D. Cahard, *J. Fluor. Chem.* **2007**, *128*, 975–996.

[222] D. A. Nagib, D. W. C. MacMillan, *Nature* **2011**, *480*, 224–228.

[223] L. Li, X. Mu, W. Liu, Y. Wang, Z. Mi, C. J. Li, *J. Am. Chem. Soc.* **2016**, *138*, 5809–5812.

[224] V. Y. Kukushkin, A. J. L. Pombeiro, *Chem. Rev.* **2002**, *102*, 1771–1802.

[225] M. F. C. Guedes da Silva, J. J. R. Fraústo da Silva, A. J. L. Pombeiro, *Inorg. Chem.* **2002**, *41*, 219–228.

[226] S. P. Semproni, W. S. McNeil, R. A. Baillie, B. O. Patrick, C. F. Campana, P. Legzdins, *Organometallics* **2010**, *29*, 867–875.

[227] N. G. Connelly, W. E. Geiger, *Chem. Rev.* **1996**, *96*, 877–910.

[228] W. Preetz, A. Franken, M. Rath, *Z. Naturforschung, B Chem. Sci.* **1993**, *48*, 598–602.

[229] M. Finze, E. Bernhardt, H. Willner, C. W. Lehmann, *J. Am. Chem. Soc.* **2005**, *127*, 10712–10722.

[230] D. F. Evans, *J. Chem. Soc.* **1959**, 2003.

[231] S. K. Sur, *J. Magn. Res.* **1989**, *82*, 169.

[232] Z. E. Clarke, P. T. Maragh, T. P. Dasgupta, D. G. Gusev, A. J. Lough, K. Abdur-Rashid, *Organometallics* **2006**, *25*, 4113–4117.

[233] J. Meiners, A. Friedrich, E. Herdtweck, S. Schneider, *Organometallics* **2009**, *28*, 6331–6338.

[234] M. G. Scheibel, PhD Thesis, Georg August University Göttingen, **2014**.

[235] J.-M. Lalancette, G. Rollin, P. Dumas, *Can. J. Chem.* **1972**, *50*, 3058–3062.

[236] S. H. Babcock, H. O. Lankelma, E. Vopicka, *Inorg. Synth.* **2007**, 10–11.

[237] A. Martinsen, J. Songstad, *Acta Chem. Scand. A* **1977**, *31*, 645–650.

[238] L. A. Carpino, R. E. Padykula, D. E. Barr, F. H. Hall, J. G. Krause, R. F. Dufresne, C. J. Thoman, *J. Org. Chem.* **1988**, *53*, 2565–2572.

[239] V. W. Manner, T. F. Markle, J. H. Freudenthal, J. P. Roth, J. M. Mayer, *Chem. Comm.* **2008**, *246*, 256–258.

[240] M. Brookhart, B. Grant, A. F. Volpe Jr., *Organometallics* **1992**, *11*, 3920–3922.

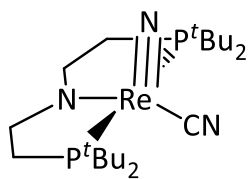# VI Appendix

1 Index of all numerated compounds
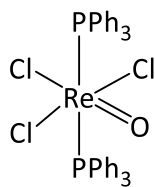
1
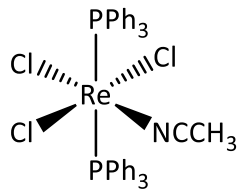
2
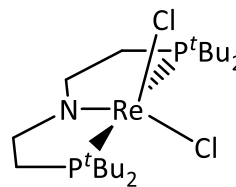
3

4
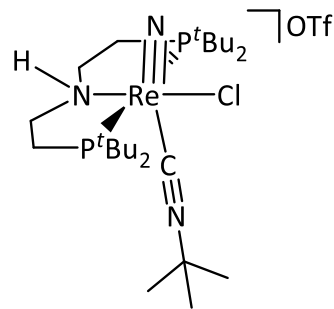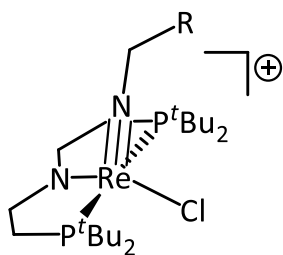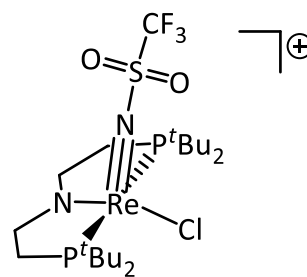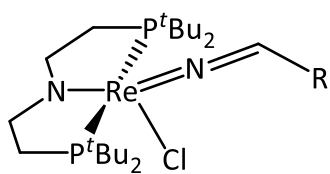
5

6

7

8

9

10

11

12

13

14

15

a: R = H

b: R = Me

c: R = Ph

d: R = CPh₃

16

17

18

19

20

185

21

22

23

24

25

26

27

28

29
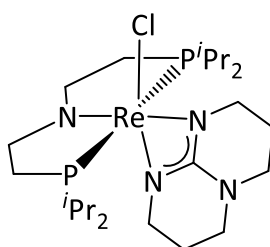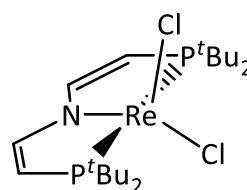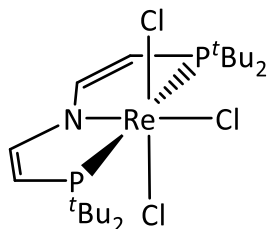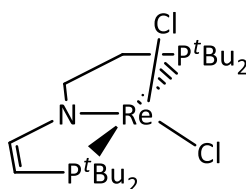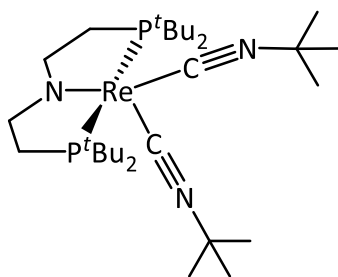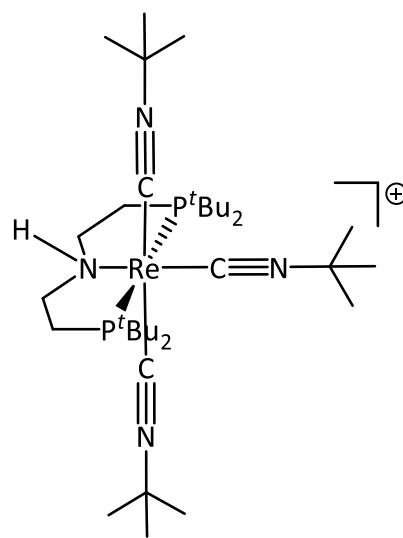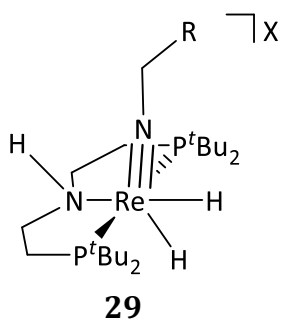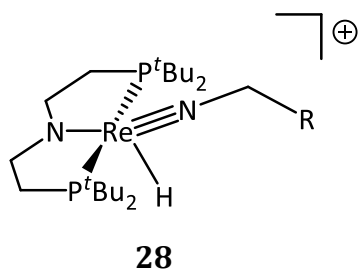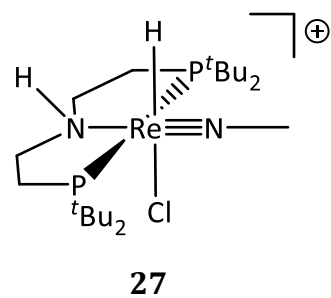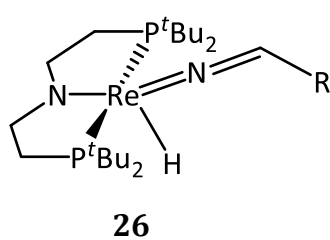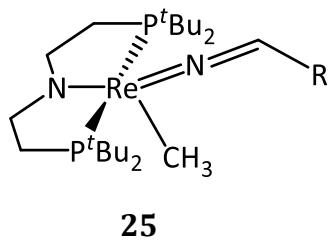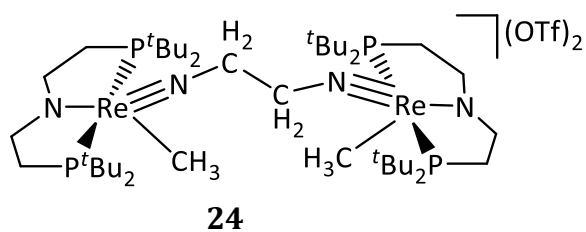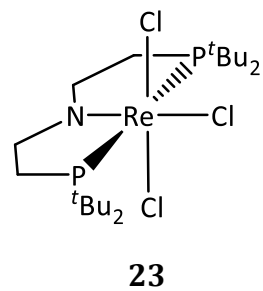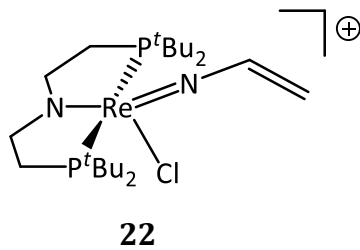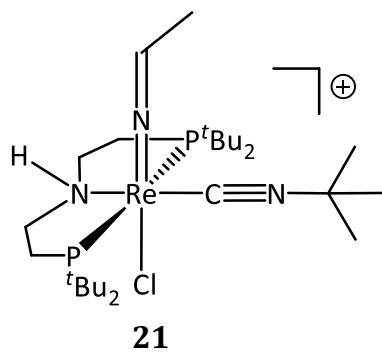
2   List of abbreviations

$\{MNNM\}^{x^{\pi}y^{\delta}}$	x = number of electrons in π-symmetric orbitals; y = number of electrons in δ-symmetric orbitals of a $\{MNNM\}$ unit
δ	chemical shift [ppm]
υ	wave number [cm^{-1}]
μ_{eff}	effective magnetization
atm	standard atmosphere
BAr$^F_4$	$[B\{C_6H_3(CF_3)_2\}_4]^-$
BDE	bond dissociation energy
br	broad
^{t}Bu	*tert*–butyl
Bn	benzyl
calcd.	calculated
Cp	cyclopentadienyl
Cp*	(penta-methyl)cyclopentadienyl
CV	cyclic voltammetry
d	doublet
DCM	dichloromethane
DFT	density functional theory
Et	ethyl
equiv.	equivalents
ESI	electron spray ionization
exp	experimental
Fc	ferrocene
Fc$^+$	ferrocenium cation
FT	fourrier transform
h	hour
hpp	hexahydroprymidinopyrimidine (deprotonated TBD)
HOMO	highest occupied molecular orbital

*i*Pr	*iso*-propyl
IR	infrared
i. vac.	in vacuo
LUMO	lowest unoccupied molecular orbital
m	multiplet (NMR) or medium (IR)
Me	methyl
MO	molecular orbital
M	molar
NMR	nuclear magnetic resonance
OTf	trifluoromethanesulfonate
Ph	phenyl
PhO·	2,4,6-tri-*tert*-butylphenoxyl radical
PNP	bis(di-*tert*–butylphosphinoethylene)amide
HPNP	bis(di-*tert*–butylphosphinoethylene)amine
P=N=P	bis(di-*tert*–butylphosphinoethylidene)amide
PNPiPr	bis(di-*iso*-propylphosphinoethylene)amide
ppm	parts per million
q	quartet
RT	room temperature
S	spin
t	triplet
TBD	1,3,5-Triazabicyclo[4.4.0]dec-5-ene, Hhpp
THF	tetrahydrofurane
TIP	temperature independent paramagnetism
vs	versus
w	weak

3 Crystallographic details

3.1 [(PNP)ReCl$_2$] (3)

Empirical formula	C$_{20}$H$_{44}$Cl$_2$NP$_2$Re
Formula weight	617.60
Temperature	100(2) K
Wavelength	0.56086 Å
Crystal system, space group	Orthorhombic, P2$_1$2$_1$2$_1$
Unit cell dimensions	a = 12.1991(13) Å α = 90°
	b = 12.3901(14) Å β = 90°
	c = 16.5297(18) Åγ = 90°
Volume	2498.4(5) Å^3
Z, Density (calculated)	4, 1.642 Mg/m^3
Absorption coefficient	2.799 mm^{-1}
F(000)	1240
Crystal shape and color	Block, blue
Crystal size	0.407 x 0.217 x 0.188 mm^3
θ range for data collection	1.297 to 23.674°
Index ranges	-17<=h<=17, -17<=k<=17, -23<=l<=23
Reflections collected / independent	36601 / 7624 [R(int) = 0.0539]
Completeness to θ = 19.665°	99.4 %
Absorption correction	Numerical
Max. and min. transmission	0.7295 and 0.5455
Refinement method	Full-matrix least-squares on F^2
Data / restraints / parameters	7624 / 240 / 250
Goodness-of-fit on F^2	1.137
Final R indices [I>2σ(I)]	R1 = 0.0380, wR2 = 0.0935
R indices (all data)	R1 = 0.0405, wR2 = 0.0966
Largest diff. peak and hole	4.211 and -2.383 eÅ^{-3}

3.2 [(PNP)Re(NCMe)Cl$_2$]

Empirical formula	C$_{22}$H$_{47}$Cl$_2$N$_2$P$_2$Re
Formula weight	658.65
Temperature	298(2) K
Wavelength	0.71073 Å
Crystal system, space group	Triclinic, P-1
Unit cell dimensions	a = 7.4049(3) Å α = 93.800(2)°
	b = 12.4480(5) Å β = 101.613(2)°
	c = 15.8353(7) Å γ = 105.263(2)°
Volume	1368.30(10) Å^3
Z, Density (calculated)	2, 1.599 Mg/m^3
Absorption coefficient	4.765 mm^{-1}
F(000)	664
Crystal shape and color	Plate, clear intense green
Crystal size	0.109 x 0.073 x 0.053 mm^3
θ range for data collection	2.290 to 30.659°
Index ranges	-10<=h<=10, -17<=k<=17, -22<=l<=22
Reflections collected / independent	70775 / 8447 [R(int) = 0.0732]
Completeness to θ = 25.242°	99.9%
Refinement method	Full-matrix least-squares on F^2
Data / restraints / parameters	8447 / 0 / 275
Goodness-of-fit on F^2	1.048
Final R indices [I>2σ(I)]	R1 = 0.0313, wR2 = 0.0432
R indices (all data)	R1 = 0.0485, wR2 = 0.0462
Largest diff. peak and hole	0.597 and -0.748 eÅ^{-3}

3.3   [(PNP^iPr)Re(hpp)Cl] (5)

Empirical formula	$C_{23}H_{48}ClN_4P_2Re$
Formula weight	664.24
Temperature	100(2) K
Wavelength	0.56086 Å
Crystal system, space group	Triclinic, P-1
Unit cell dimensions	a = 7.9189(3) Å α = 85.3520(10)°
	b = 9.5438(4) Å β = 83.0080(10)°
	c = 18.8217(7) Å γ = 76.5260(10)°
Volume	1370.99(9) Å^3
Z, Density (calculated)	2, 1.609 Mg/m^3
Absorption coefficient	2.509 mm^{-1}
F(000)	672
Crystal shape and color	Block, green
Crystal size	0.184 x 0.155 x 0.150 mm^3
θ range for data collection	0.861 to 22.198°
Index ranges	-10<=h<=10, -12<=k<=12, -25<=l<=25
Reflections collected / independent	91475 / 7000 [R(int) = 0.0442]
Completeness to θ = 19.665°	100.0%
Absorption correction	Semi-empirical from equivalents
Max. and min. transmission	0.462 and 0.3938
Refinement method	Full-matrix least-squares on F^2
Data / restraints / parameters	7000 / 60 / 468
Goodness-of-fit on F^2	1.098
Final R indices [I>2σ(I)]	R1 = 0.0164, wR2 = 0.0339
R indices (all data)	R1 = 0.0189, wR2 = 0.0347
Largest diff. peak and hole	0.928 and -1.237 eÅ^{-3}

3.4 [(^{H}PNP)Re(N)Cl][Cl] (12)

Empirical formula	$C_{20}H_{45}Cl_2N_2P_2Re$
Formula weight	632.62
Temperature	100(2) K
Wavelength	0.56086 Å
Crystal system, space group	Orthorhombic, Pbca
Unit cell dimensions	a = 15.1843(12) Å α = 90°
	b = 12.3918(9) Å β = 90°
	c = 27.434(2) Å γ = 90°
Volume	5162.0(7) Å^3
Z, Density (calculated)	8, 1.628 Mg/m^3
Absorption coefficient	2.711 mm^{-1}
F(000)	2544
Crystal shape and color	Plate, yellow
Crystal size	0.092 x 0.064 x 0.058 mm^3
θ range for data collection	1.579 to 20.596°
Index ranges	-19<=h<=18, -15<=k<=15, -34<=l<=34
Reflections collected / independent	116371 / 5313 [R(int) = 0.1613]
Completeness to θ = 19.665°	100.0%
Absorption correction	Numerical
Max. and min. transmission	0.7445 and 0.6445
Refinement method	Full-matrix least-squares on F^2
Data / restraints / parameters	5313 / 0 / 260
Goodness-of-fit on F^2	1.050
Final R indices [I>2σ(I)]	R1 = 0.0329, wR2 = 0.0518
R indices (all data)	R1 = 0.0604, wR2 = 0.0593
Largest diff. peak and hole	0.980 and -1.461 eÅ^{-3}

3.5 [(PNP)Re(N)(CH$_3$)] (13)

Empirical formula	C$_{21}$H$_{47}$N$_2$P$_2$Re
Formula weight	575.74
Temperature	100(2) K
Wavelength	0.56086 Å
Crystal system, space group	Orthorhombic, Pbca
Unit cell dimensions	a = 11.9638(4) Å α = 90°
	b = 15.5451(5) Å β = 90°
	c = 26.4482(8) Å γ = 90°
Volume	4918.8(3) Å^3
Z, Density (calculated)	8, 1.555 Mg/m^3
Absorption coefficient	2.736 mm^{-1}
F(000)	2336
Crystal shape and color	Plate, yellow
Crystal size	0.207 x 0.190 x 0.078 mm^3
θ range for data collection	1.215 to 22.317°
Index ranges	-16<=h<=12, -20<=k<=21, -35<=l<=35
Reflections collected / independent	50947 / 6396 [R(int) = 0.0634]
Completeness to θ = 19.665°	100.0%
Absorption correction	Numerical
Max. and min. transmission	0.8532 and 0.6696
Refinement method	Full-matrix least-squares on F^2
Data / restraints / parameters	6396 / 0 / 248
Goodness-of-fit on F^2	1.173
Final R indices [I>2σ(I)]	R1 = 0.0412, wR2 = 0.0692
R indices (all data)	R1 = 0.0617, wR2 = 0.0753
Largest diff. peak and hole	2.927 and -3.149 eÅ^{-3}

3.6   [(PNP)Re(NMe)Cl][OTf] (16a)

Empirical formula	$C_{26}H_{55}ClF_3N_2O_4P_2ReS$
Formula weight	832.37
Temperature	100(2) K
Wavelength	0.56086 Å
Crystal system, space group	Monoclinic, $P2_{1/c}$
Unit cell dimensions	a = 14.9341(6) Å α = 90°
	b = 17.4589(7) Å β = 115.5100(17)°
	c = 14.5106(6) Å γ = 90°
Volume	3414.5(2) Å^3
Z, Density (calculated)	4, 1.619 Mg/m^3
Absorption coefficient	2.065 mm^{-1}
F(000)	1688
Crystal shape and color	Plate, yellow
Crystal size	0.219 x 0.083 x 0.076 mm^3
θ range for data collection	1.192 to 20.583°
Index ranges	-18<=h<=18, -21<=k<=21, -18<=l<=18
Reflections collected / independent	73633 / 7039 [R(int) = 0.0418]
Completeness to θ = 19.665°	100.0%
Absorption correction	Numerical
Max. and min. transmission	0.9489 and 0.8097
Refinement method	Full-matrix least-squares on F^2
Data / restraints / parameters	7039 / 0 / 374
Goodness-of-fit on F^2	1.138
Final R indices [I>2σ(I)]	R1 = 0.0159, wR2 = 0.0320
R indices (all data)	R1 = 0.0229, wR2 = 0.0376
Largest diff. peak and hole	1.043 and -0.558 eÅ^{-3}

3.7   [(PNP)Re(NCHCH$_3$)Cl] (18b)

Empirical formula	C$_{22}$H$_{48}$ClN$_2$P$_2$Re
Formula weight	624.21
Temperature	173(2) K
Wavelength	0.71073 Å
Crystal system, space group	Monoclinic, P2$_1$/n
Unit cell dimensions	a = 12.1123(5) Å α = 90°
	b = 14.6857(6) Å β = 97.492(2)°
	c = 15.2552(6) Å γ = 90°
Volume	2690.39(19) Å^3
Z, Density (calculated)	4, 1.541 Mg/m^3
Absorption coefficient	4.746 mm^{-1}
F(000)	1264
Crystal size	0.317 x 0.086 x 0.074 mm^3
θ range for data collection	1.933 to 27.564°
Index ranges	-15<=h<=15, -19<=k<=19, -19<=l<=19
Reflections collected / independent	71062 / 6200 [R(int) = 0.0593]
Completeness to θ = 25.242°	100.0%
Absorption correction	Semi empirical from equivalents
Max. and min. transmission	0.7456 and 0.4758
Refinement method	Full-matrix least-squares on F^2
Data / restraints / parameters	6200 / 0 / 266
Goodness-of-fit on F^2	1.409
Final R indices [I>2σ(I)]	R1 = 0.0341, wR2 = 0.0872
R indices (all data)	R1 = 0.0392, wR2 = 0.0900
Largest diff. peak and hole	1.540 and -1.740 eÅ^{-3}

3.8 [(PNP)Re(CNtBu)$_2$] (19)

Empirical formula	C$_{30}$H$_{62}$N$_3$P$_2$Re
Formula weight	712.96
Temperature	173(2) K
Wavelength	0.71073 Å
Crystal system, space group	Monoclinic, P2$_1$/n
Unit cell dimensions	a = 10.8645(5) Å α = 90°
	b = 30.8758(14) Å β = 116.691(2)°
	c = 11.2147(5) Å γ = 90°
Volume	3361.1(3) Å^3
Z, Density (calculated)	4, 1.409 Mg/m^3
Absorption coefficient	3.732 mm^{-1}
F(000)	1472
Crystal size	0.214 x 0.165 x 0.032 mm^3
θ range for data collection	2.137 to 26.370°
Index ranges	-13<=h<=12, -38<=k<=38, -13<=l<=14
Reflections collected / independent	36525 / 6857 [R(int) = 0.0383]
Completeness to θ = 25.242°	99.8%
Absorption correction	Semi empirical from equivalents
Max. and min. transmission	0.7457 and 0.6143
Refinement method	Full-matrix least-squares on F^2
Data / restraints / parameters	6857 / 21 / 356
Goodness-of-fit on F^2	1.222
Final R indices [I>2σ(I)]	R1 = 0.0325, wR2 = 0.0626
R indices (all data)	R1 = 0.0418, wR2 = 0.0648
Largest diff. peak and hole	2.174 and -2.995 eÅ^{-3}

3.9   [(^{H}PNP)Re(NCHCH$_3$)(CN^{t}Bu)Cl][OTf] (21)

Empirical formula	C$_{28}$H$_{58}$ClF$_3$N$_3$O$_3$P$_2$ReS
Formula weight	857.42
Temperature	100(2) K
Wavelength	0.71073 Å
Crystal system, space group	Monoclinic, P2$_1$/n
Unit cell dimensions	a = 14.0330(8) Å $\quad$ α = 90°
	b = 12.2246(7) Å $\quad$ β = 106.820(2)°
	c = 22.0602(13) Å $\quad$ γ = 90°
Volume	3622.5(4) Å^3
Z, Density (calculated)	4, 1.572 Mg/m^3
Absorption coefficient	3.622 mm^{-1}
F(000)	1744
Crystal size	0.298 x 0.292 x 0.092 mm^3
Crystal shape and color	Plate, clear intense blue
θ range for data collection	2.253 to 36.448°
Index ranges	-23<=h<=22, -20<=k<=20, -36<=l<=36
Reflections collected / independent	267200 / 17692 [R(int) = 0.0428]
Completeness to θ = 25.242°	99.9%
Max. and min. transmission	0.7471 and 0.5121
Refinement method	Full-matrix least-squares on F^2
Data / restraints / parameters	17692 / 0 / 395
Goodness-of-fit on F^2	1.069
Final R indices [I>2σ(I)]	R1 = 0.0215, wR2 = 0.0438
R indices (all data)	R1 = 0.0288, wR2 = 0.0462
Largest diff. peak and hole	1.835 and -1.478 eÅ^{-3}

3.10 [(PNP)ReCl$_3$] (23)

Empirical formula	C$_{20}$H$_{44}$Cl$_3$NP$_2$Re
Formula weight	653.05
Temperature	100(2) K
Wavelength	0.71073 Å
Crystal system, space group	Orthorhombic, Pbca
Unit cell dimensions	a = 13.0596(8) Å α = 90°
	b = 14.2366(8) Å β = 90°
	c = 28.2239(16) Å γ = 90°
Volume	5247.5(5) Å^3
Z, Density (calculated)	8, 1.653 Mg/m^3
Absorption coefficient	5.066 mm^{-1}
F(000)	2616
Crystal size	0.153x 0.138 x 0.119 mm^3
θ range for data collection	2.236 to 30.119°
Index ranges	-18<=h<=18, -20<=k<=20, -39<=l<=39
Reflections collected / independent	195808 / 7721 [R(int) = 0.0420]
Completeness to θ = 25.242°	100.0%
Refinement method	Semi-empirical from equivalents
Max. and min. transmission	0.7460and 0.6254
Refinement method	Full-matrix least-squares on F^2
Data / restraints / parameters	7721 / 0 / 256
Goodness-of-fit on F^2	1.097
Final R indices [I>2σ(I)]	R1 = 0.0187, wR2 = 0.0386
R indices (all data)	R1 = 0.0244, wR2 = 0.0402
Largest diff. peak and hole	1.462 and -0.849 eÅ^{-3}

3.11 [(PNP)Re(NCHPh)Cl] (18c)

Empirical formula	$C_{29.50}H_{56}ClN_2P_2Re$
Formula weight	722.35
Temperature	100(2) K
Wavelength	0.71073 Å
Crystal system, space group	Triclinic, P-1
Unit cell dimensions	a = 12.8449(5) Å α = 82.388(2)°
	b = 14.3234(7) Å β = 88.031(2)°
	c = 19.6479(9) Å γ = 67.417(2)°
Volume	3307.8(3) Å^3
Z, Density (calculated)	4, 1.451 Mg/m^3
Absorption coefficient	3.871 mm^{-1}
F(000)	1476
Crystal size	0.279 x 0.066 x 0.034 mm^3
Crystal color and shape	Plate, clear light orange-brown
θ range for data collection	1.981 to 28.431°
Index ranges	-17<=h<=17, -19<=k<=19, -26<=l<=26
Reflections collected / independent	195920 / 16588 [R(int) = 0.0715]
Completeness to θ = 25.242°	100.0%
Refinement method	Semi-empirical from equivalents
Max. and min. transmission	0.7457 and 0.5777
Refinement method	Full-matrix least-squares on F^2
Data / restraints / parameters	16588 / 70 / 763
Goodness-of-fit on F^2	1.017
Final R indices [I>2σ(I)]	R1 = 0.0235, wR2 = 0.0406
R indices (all data)	R1 = 0.0394, wR2 = 0.0445
Largest diff. peak and hole	0.817 and -0.764 eÅ^{-3}

3.12 [(PNP)Re(NCH$_2$)Cl] (18a)

Empirical formula	C$_{21}$H$_{46}$ClN$_2$P$_2$Re
Formula weight	610.19
Temperature	100(2) K
Wavelength	0.71073 Å
Crystal system, space group	Monoclinic, P2$_1$/n
Unit cell dimensions	a = 12.3076(4) Å a= 90°.
	b = 14.8267(5) Å b= 103.222(2)°.
	c = 14.0218(5) Å g = 90°.
Volume	2490.88(15) Å^3
Z, Density (calculated)	4, 1.627 Mg/m^3
Absorption coefficient	5.124 mm^{-1}
F(000)	1232
Crystal size	0.276 x 0.232 x 0.094 mm^3
θ range for data collection	2.185 to 33.140°.
Index ranges	-18<=h<=18, -22<=k<=22, -21<=l<=21
Reflections collected / independent	191147 / 9491 [R(int) = 0.0536]
Completeness to θ = 25.242°	100.0 %
Refinement method	Full-matrix least-squares on F^2
Data / restraints / parameters	9491 / 0 / 256
Goodness-of-fit on F^2	1.051
Final R indices [I>2σ(I)]	R1 = 0.0198, wR2 = 0.0385
R indices (all data)	R1 = 0.0278, wR2 = 0.0406
Largest diff. peak and hole	2.194 and -1.177 eÅ^{-3}

3.13 [(PNP)Re(NCHCPh₃)Cl] (18d)

Empirical formula	$C_{40}H_{60}ClN_2P_2Re$
Formula weight	852.49
Temperature	100(2) K
Wavelength	0.71073 Å
Crystal system, space group	Monoclinic, $P2_1/n$
Unit cell dimensions	a = 11.3915(6) Å a= 90°.
	b = 19.8542(10) Å b= 104.449(2)°
	c = 17.6702(9) Å g = 90°.
Volume	3870.0(3) Å³
Z, Density (calculated)	4, 1.463 Mg/m³
Absorption coefficient	3.321 mm⁻¹
F(000)	1744
Crystal size	0.371 x 0.239 x 0.216 mm³
Crystal shape and color	Block, metallic dark brown
θ range for data collection	2.186 to 30.507°.
Index ranges	-16<=h<=16, -28<=k<=28, -25<=l<=25
Reflections collected / independent	176840 / 11810 [R(int) = 0.0460]
Completeness to θ = 25.242°	99.9%
Max. and min. transmission	0.7479 and 0.6131
Refinement method	Full-matrix least-squares on F^2
Data / restraints / parameters	11810 / 0 / 515
Goodness-of-fit on F^2	1.044
Final R indices [I>2σ(I)]	R1 = 0.0210, wR2 = 0.0473
R indices (all data)	R1 = 0.0288, wR2 = 0.0509
Largest diff. peak and hole	1.904 and -0.746 eÅ⁻³

3.14 [(PNP)Re(NCH$_2$)(CH$_3$)] (25)

Empirical formula	C$_{22}$H$_{49}$N$_2$P$_2$Re
Formula weight	589.77
Temperature	100(2) K
Wavelength	0.56086 Å
Crystal system, space group	Monoclinic, P2$_1$/n
Unit cell dimensions	a = 12.2290(18) Å a= 90°.
	b = 14.940(2) Å b= 102.731(3)°
	c = 14.118(2) Å g = 90°.
Volume	2516.0(6) Å^3
Z, Density (calculated)	4, 1.557 Mg/m^3
Absorption coefficient	2.676 mm^{-1}
F(000)	1200
Crystal size	0.333 x 0.291 x 0.164 mm^3
Crystal shape and color	Block, brown
θ range for data collection	1.576 to 21.428°.
Index ranges	-15<=h<=15, -19<=k<=19, -18<=l<=18
Reflections collected / independent	86472 / 5815 [R(int) = 0.0308]
Completeness to θ = 19.665°	100.0%
Absorption coefficient	Numerical
Max. and min. transmission	0.5336 and 0.4305
Refinement method	Full-matrix least-squares on F^2
Data / restraints / parameters	5815 / 0 / 257
Goodness-of-fit on F^2	1.075
Final R indices [I>2σ(I)]	R1 = 0.0131, wR2 = 0.0294
R indices (all data)	R1 = 0.0147, wR2 = 0.0302
Largest diff. peak and hole	1.513 and -0.454 eÅ^{-3}

4   List of scientific contributions

Publications in scientific journals

1. M. G. Scheibel, I. Klopsch, H. Wolf, P. Stollberg, D. Stalke, S. Schneider, *Eur. J. Inorg. Chem.* **2013**, 3453-3457.

2. A. N. Marziale, A. Friedrich, I. Klopsch, M. Drees, V. R. Celinski, J. Schmedt auf der Günne, S. Schneider*, J. Am. Chem. Soc.* **2013**, *135*, 13342-13355.

3. I. Klopsch, M. Finger, C. Würtele, B. Milde, D. B. Werz, S. Schneider, *J. Am. Chem. Soc.* **2014**, *136*, 6881-6883.

4. I. Klopsch, M. Finger, C. Würtele, S. Schneider, *Angew. Chem. Int. Ed.* **2016**, *55*, 4786-4789.

5. I. Klopsch, S. Schneider, *Topics in Organometallic Chemistry*, in progress.

Oral contributions to conferences

1. I. Klopsch, M. Finger, C. Würtele, S. Schneider, "N_2-Splitting in the Coordination Sphere of Rhenium", 10th Coordination Chemistry Conference, Kaiserslautern/Germany, 2014.

2. I. Klopsch, M. G. Scheibel, M. Finger, C. Würtele, S. Schneider, "Electronic Structure-Reactivity Relationsships for N_2 Fixation and NR Group Transfer", Catalytic Routines for Small Molecule Activation (CARISMA), COST Meeting, Venice/Italy, 2014.

3. I. Klopsch, M. Finger, C. Würtele, S. Schneider, "N_2-Splitting and Functionalization in the Coordination Sphere of Rhenium", 16th International Seminar of PhD Students on Organometallic and Coordination Chemistry, Lichtenfels/Germany, 2015.

4. I. Klopsch, M. Finger, C. Würtele, S. Schneider, "N_2-Splitting and Functionalization in the Coordination Sphere of Rhenium", Pacifichem, Honolulu/Hawaii/USA, 2015.

5. I. Klopsch, J. Abbenseth, M. Finger, C. Würtele, S. Schneider, "N_2-Splitting and Functionalization in the Coordination Sphere of Rhenium", Catalytic Routines for Small Molecule Activation (CARISMA), COST Meeting, Ljubljana/Slovenia, 2016.

Poster presentations on conferences

1. I. Klopsch, M. Finger, C. Würtele, S. Schneider, "N_2-Splitting in the Coordination Sphere of Rhenium", 17. Conference on Inorganic Chemistry of the Wöhler Foundation, Saarbrücken/Germany, 2014.

2. I. Klopsch, M. Finger, C. Würtele, S. Schneider, "N_2-Splitting in the Coordination Sphere of Rhenium", Lower Saxony Catalysis Symposium (NiKaS), Göttingen/Germany, 2014, awarded.

3. I. Klopsch, M. Finger, C. Würtele, S. Schneider, "N_2-Splitting in the Coordination Sphere of Rhenium", 11th Coordination Chemistry Conference, Paderborn/Germany, 2015.

4. I. Klopsch, M. Finger, C. Würtele, S. Schneider, "N_2-Splitting in the Coordination Sphere of Rhenium", 18. Norddeutsches Doktorandenkolloquium, Goslar/Germany, 2015.

5   Curriculum vitae

Personal data

Name: Isabel Klopsch

Date of birth: 26.12.1987

Place of birth: Erlangen, Germany

Citizenship: German

Adress: Friedrichstraße 1
                 37073 Göttingen
                 Germany

Education

1998-2007   Ohm-Gymnasium Erlangen

2004-2005   School year abroad in Deux-Montagnes, Québec, Canada

2007   School Graduation: Abitur

2007-2010   Studies Bachelor of Science in Chemistry
             Friedrich-Alexander University Erlangen-Nürnberg

2010   Bachelor Degree in Chemistry
             Thesis: "Photocatalytic Oxidation of Alcohols"
             Advisor: Prof. Dr. Sven Rau

2010-2012   Studies Master of Science in Chemistry
             Friedrich-Alexander University Erlangen-Nürnberg

2012   Master Degree in Chemistry
             Thesis: "Modified activation concepts for the chromium-based
                      selective oligomerization of ethylene"
             Advisor: Prof. Dr. Peter Wasserscheid

| JAN 2013-
OCT 2016 | PhD Thesis at the Georg August University Göttingen in the group of Prof. Dr. Sven Schneider
Thesis: "N_2 Splitting and Functionalization in the coordination sphere of rhenium" |

Languages

German (native), English (very good), French (good)